

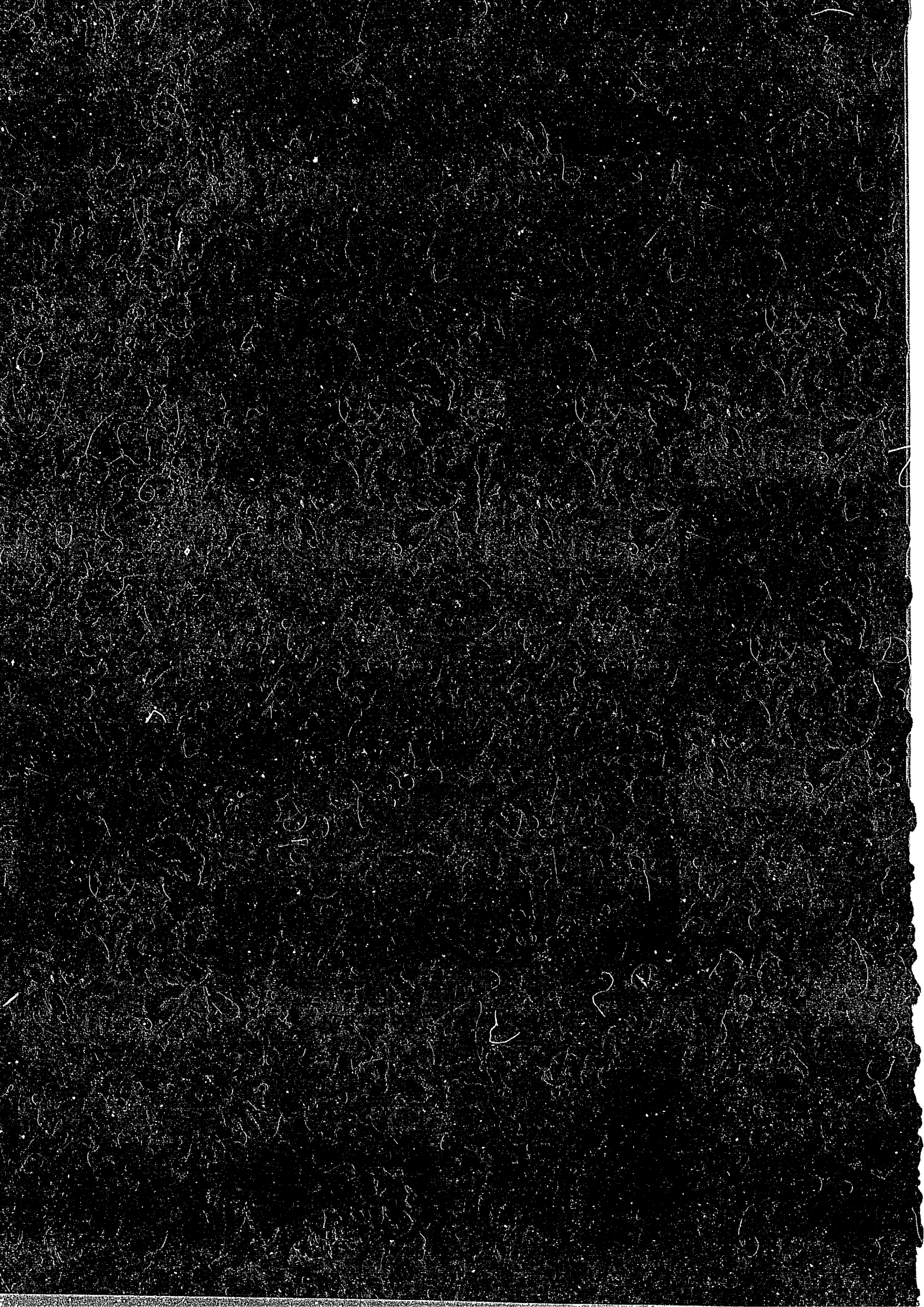
IPPJ-AM-47

● RESONANCE EFFECTS  
IN  
ELECTRON-ION COLLISIONS

EDITED BY H. TAWARA AND G. H. DUNN

INSTITUTE OF PLASMA PHYSICS  
NAGOYA UNIVERSITY

NAGOYA, JAPAN



IPPJ-AM-47

**RESONANCE EFFECTS IN ELECTRON-ION COLLISIONS**

Edited by  
Hiroyuki Tawara and Gordon H. Dunn

Institute of Plasma Physics, Nagoya University  
Chikusa-ku, Nagoya 464, Japan

October 1986

This document is prepared as a preprint of compilation of atomic data for fusion research sponsored fully or partly by the IPP/Nagoya University. This is intended for future publication in a journal or will be included in a data book after some evaluations or rearrangements of its contents. This document should not be referred without the agreement of the authors. Enquiries about copyright and reproduction should be addressed to Research Information Center, IPP/Nagoya University, Nagoya, Japan.

## PREFACE

This volume contains the proceedings of a workshop entitled "Roles of Atomic and Molecular Processes in Plasma Modelling and Diagnostics: Resonance Effects in Electron-Ion Collisions". The workshop was held under the auspices of the U.S. - Japan Fusion Collaboration Program at the Institute of Plasma Physics, Nagoya University, Nagoya, Japan, on September 1-2, 1986, with 7 U.S. and 29 Japanese participants. The meeting was intended to bring together scientists both in atomic collision and fusion plasma disciplines in order to convey recent advances in atomic collisions as pertains to plasma physics and to describe the modelling and diagnostics of fusion plasmas and the needs for A and M data in these activities. As the workshop title states, particular emphasis was placed on the effects of resonances in electron-ion collisions: ionization, excitation, and recombination.

Included in the workshop were sessions on:

1. Plasma modelling, diagnostics and A and M data needs in large plasma machines.
2. Atomic and molecular processes: Theory.
3. Atomic and molecular processes: Experiment.
4. Laboratory plasma experiments.
5. Future collaboration of U.S. and Japanese scientists in these areas.

The talks presented in these sessions are summarized in these proceedings, and the program and participants list are given at the end.

Dielectronic resonances occur in electron-ion collisions when an incoming electron excites a core electron(s) and then is left with insufficient energy to escape, so it is captured into an excited state, thus resulting in a multiply excited state. The excess energy can then be redistributed into ejected electrons (resonant-excitation-double-autoionization [REDA]) so that one has a contribution to ionization, into an ejected electron and redistribution of energy in the core (resonant excitation) so that one has a contribution to excitation, or into a stabilizing photon (dielectronic recombination [DR]) so that one has recombination of the electron and ion.

It has been recognized for a number of years now that indirect processes such as excitation-autoionization can dominate the direct process of ionization - sometimes by more than an order of magnitude - so that popular and convenient formulae (such as the Lotz formula) may drastically underestimate ionization rates. It was also hypothesized that the resonant REDA and other related

resonant processes might contribute significantly, but it is only recently that experiments have been able to conclusively demonstrate the presence of these processes. In excitation, dielectronic resonances are theoretically predicted to change the excitation rates by factors of several times. Experimental evidence for these excitation effects is sparse, and technological capability is just coming on line for getting more deterministic evidence. Dielectronic recombination has been recognized for some twenty years as the dominant recombination process in hot plasmas, but this has been based - until the past few years - on purely theoretical evidence. Recent experiments and theory have shown this process to be very sensitive to such variables in the environment as external fields, plasma microfields, and collisions. The presentations in these proceedings highlight these resonant processes.

There remain many needs in understanding the processes, in generating more data, in communicating the data and nature of the processes to the plasma user community, and in making adequate compilations of the data in a form that can - and will - be used by the user community. An important outcome of discussions on collaboration was that some cooperation - ranging from a simple agreement on division of work so as to avoid duplication to direct collaborative efforts involving travel and working with each other - was agreed to as important in order to hasten the work and to conserve limited resources of manpower and funds. Several specific cooperative efforts were suggested, but they will require working out of details by the individual scientists and institutions involved. Emphasis was placed on greater coordination and communication with the diagnostic and modelling programs of the two countries.

Finally, the editors acknowledge and give thanks for support for the workshop through the U.S.-JAPAN Fusion Collaboration Program.

H. Tawara (IPP/Nagoya University)  
G. H. Dunn (JILA-NBS/Univ. Colorado)

Co-chairpersons of the Workshop

## Contents

1. H. Tawara:  
Introduction to the Workshop-some aspect of the status  
in electron-ion collision research .....p. 1
2. T. Sugie, A. Sakasai, H. Kubo, Y. Koide, N. Akaoka,  
T. Hirayama and H. Takeuchi:  
Diagnostics of JT-60 and impurity measurement .....p. 9
3. S. Morita:  
Some Comments on Atomic Cross sections used in analysis  
of X-Ray Spectra from Tokamak Plasmas .....p. 28
4. M. Nakai, H. Azechi, N. Miyanaga, M. Itoh, T. Yabe,  
K. Miya, T. Yamanaka and C. Yamanaka:  
Spectroscopic measurement of non-local heat transport  
in laser produced plasma .....p. 35
5. R.A. Phaneuf and D.C. Gregory:  
Indirect mechanisms in electron-impact ionization of  
multiply charged ions .....p. 53
6. H. Suzuki:  
Recent activities of electron-ion collision experiments  
in IPP/Nagoya and Sophia University .....p. 69
7. Y. Itikawa and K. Sakimoto:  
Distorted-wave-method calculation of innershell  
excitation .....p. 89
8. R.J.W. Henry:  
Resonance effects in electron ion excitation .....p.100
9. S. Nakazaki:  
Cross sections for electron impact excitation of O IV ...p.109

10. T. Fujimoto and T. Kato:  
Decrease and disappearance of the resonance contribution  
to the excitation cross section of ions in dense plasma .p.116
11. Y. Hahn:  
Resonance effects on electron capture and ionization ....p.125
12. Y. Kim:  
Relativistic effects in electron-ion excitation .....p.130
13. T. Kagawa and S. Kiyokawa:  
Energy levels and transition probabilities for multiply  
charged ions .....p.139
14. G.H. Dunn:  
Tuneable resonances: dielectronic recombination .....p.148
15. K. Sakimoto:  
Effects of electric fields on dielectronic recombination  
---MQDT treatment--- .....p.154
16. H.R. Griem:  
Electron-ion collisional rate coefficients from  
time-dependent plasmas .....p.165
17. T. Kawamura and T. Ono:  
Evaluation and assessment of atomic data for plasma  
modelling .....p.196
18. Program of the Workshop .....p.210
19. List of participants .....p.212

## Introduction to the Workshop

- Some aspect of the status in electron-ion collision research -

H. Tawara

Institute of Plasma Physics

Nagoya University

I would like to welcome all of you to this Workshop, one of a series of the workshops under U.S.- Japan Fusion Collaboration Program. This is the second workshop involving atomic and molecular data necessary for fusion studies. The first workshop was held in 1980 at JILA, under the chairmanship of Dr. D. Crandall, then ORNL, and Dr. Y. Itikawa, then IPP, with the help by JILA staff in particular Dr. G. Dunn. As the title of that workshop "U.S.- Japan Workshop on Atomic Collision Data for Fusion" indicated, that workshop covered a wide range of topics ranging from basic problems in ionization, charge transfer, atomic structures and surfaces to critical discussion on needs of AM data for fusion plasmas and there we discussed what kind of AM data should be compiled and evaluated under U.S.- Japan collaboration. Since then, our close collaboration began to work efficiently. One of the important results which came out of such collaboration is the critical evaluation of excitation data of ions by electron impact. In addition to a number of the letters exchanged, Dr. Crandall and Dr. Pindzolla came to Nagoya before finishing the evaluation of excitation data. Finally, that was published in Atomic Data and Nuclear Data Tables in 1985 and was appreciated very much by a number of scientists the world over. Also we regularly exchange the compiled and evaluated data and

other important information involving AM data among various laboratories of two sides of the Pacific.

In the past few years, we tried to have a similar workshop and to exchange scientists. Unfortunately we could not get support to our proposal so far. After discussing a possible workshop with Dr. Dunn, we both realized that it was the time to organize the second workshop and tried to get support. This year, with strong support of IPP/Nagoya, DOE and others, we are able to have this workshop here in Nagoya. After exchange of several letters with Dr. Dunn and also discussion with Dr. Crandall who happened to be in Nagoya early this year, we decided to convene the workshop around the time of ICAP (International Conference on Atomic Physics) in Tokyo. We know of course a wide range of AM data should be covered in fusion research. One of the reasons why we have chosen AM problems involving electron + ion collision processes is the fact that these electron + ion collision processes are one of the most critical parameters which influence very much the balance of particles and of energies in plasmas and the techniques for plasma diagnostics and, more importantly, the design of fusion apparatus. And another is the fact that AM physicists have recently succeeded in achieving fairly good understanding of electron + ion collision phenomena not only qualitatively but also quantitatively and theoretically as well as experimentally. For example, significant contribution to ionization of ions by electron impact has been found to originate not only from direct ionization but from indirect ionization processes such as excitation-autoionization. Some times, this contribution of the indirect ionization processes is found to be far dominant over that of the direct ionization, in particular in multiply charged ions. On the other hand,

in the present-day plasma modelling, the ionization rates of ions are still calculated using the so-called Lotz formula which is based totally on the direct ionization mechanism and is found to be seriously in error in many cases.

Here in this workshop we would like to emphasize some need of the modifications in atomic calculations in such plasma modellings and of changing their old formula into new formula based on new findings. Similar effects can be seen in the ionization balance of ions if you take into account multiple ionization which is usually neglected but is found to be significant in some cases (see Fig.1). Also, another important collision process involving multiply charged ions, the dielectronic recombination (DR) process, which is known to play a key role in energy loss from high temperature plasmas, has been recently investigated experimentally with the advance of various experimental techniques and of understanding of various processes associated and, accordingly, extensive theoretical investigations of DR are being made at various laboratories. Furthermore, it has been recently realized that these atomic processes are significantly modified under the influence of hot/dense plasmas where nuclear fusion reaction can be maintained and the understanding of these is being obtained rapidly. Some of these processes behave like resonances where, at particular energies, their cross sections are significantly enhanced. So, this is why we in this workshop emphasize the resonance effects in electron + ion collisions. In Figures 2 (a) and (b), I would like to summarize how far our present experimental and theoretical findings are extended in cross section measurements of electron + ion collisions. I feel there are too many unknown, compared with the known which is really too little.

In this workshop we have arranged the talks as follows: First we, AM physicists, would like to hear about the present status in investigations of big tokamak and laser plasmas and what kinds of AM data are critically needed for their diagnostics and modelling and ultimately for achieving high temperature plasma fusion. Then, bearing these in mind, we concentrate ourselves to what we have recently achieved in electron + ion collision studies and what we should do for more detailed understanding of collision processes involving electrons and ions, particularly highly charged ions and furthermore what we could do helping modelling and diagnostics of high temperature plasmas. Then we are going to discuss how our understanding of plasma behaviors and diagnostics is influenced through AM data used and how accurate the AM data should be for plasma research. Finally we would like to discuss the possibilities of our future collaboration among laboratories in U.S. and Japan. Various laboratories both in U.S. and Japan have different facilities with their own features. For example, ORNL has very good facilities and extended experience in studying and measuring total cross sections of ionization, in particular of highly charged ions, by electron impact, meanwhile IPP is now building a new facility where we can measure differential cross sections in electron + ion collisions and get more detailed understanding on such collisions. Other examples are good facilities for investigating DR at JILA and ORNL, whereas we in Japan have just started some experiments on DR for which we urgently need to know a number of technical and experimental know-hows. The exchange of our experience and information should enhance our activities in this particular field. So I hope that, after listening a series of

the talks to be presented here, you will be able to join discussion on our future collaboration and give us your suggestions and comments.

Finally I hope you enjoy this workshop.

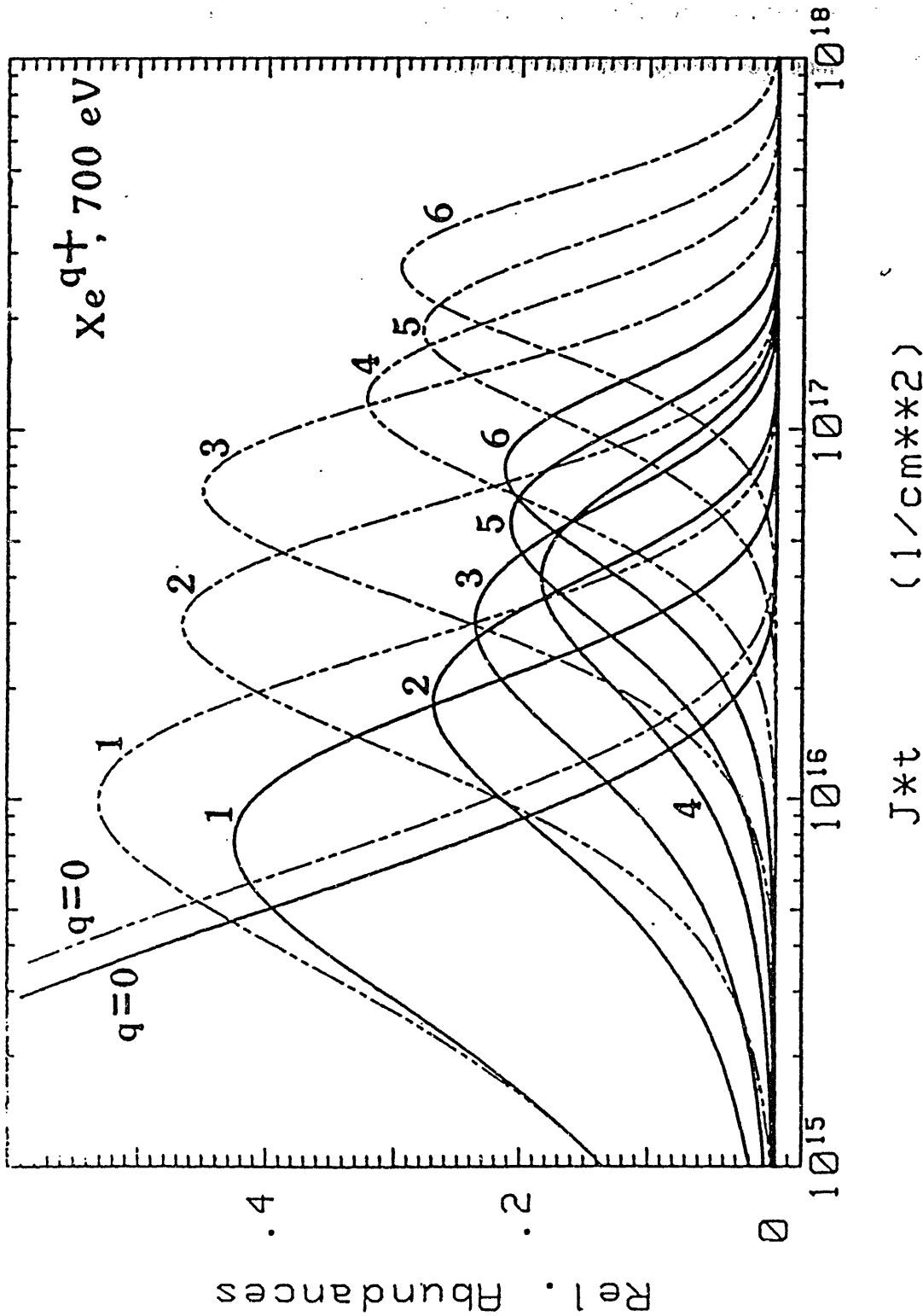


Fig.1

Fig. 3. Relative abundances of Xe<sup>q+</sup> ions ( $q = 0, 1, \dots, 6$ ) as a function of the product of electron flux density and ion containment time at 700 eV electron energy. The solid lines are calculated including multiple ionization, the dot-dot-dashed lines are based on single ionization cross sections from the Lotz formula [16] only.

taken from A.Muller, Phys. Letters 113A (1986) 415.

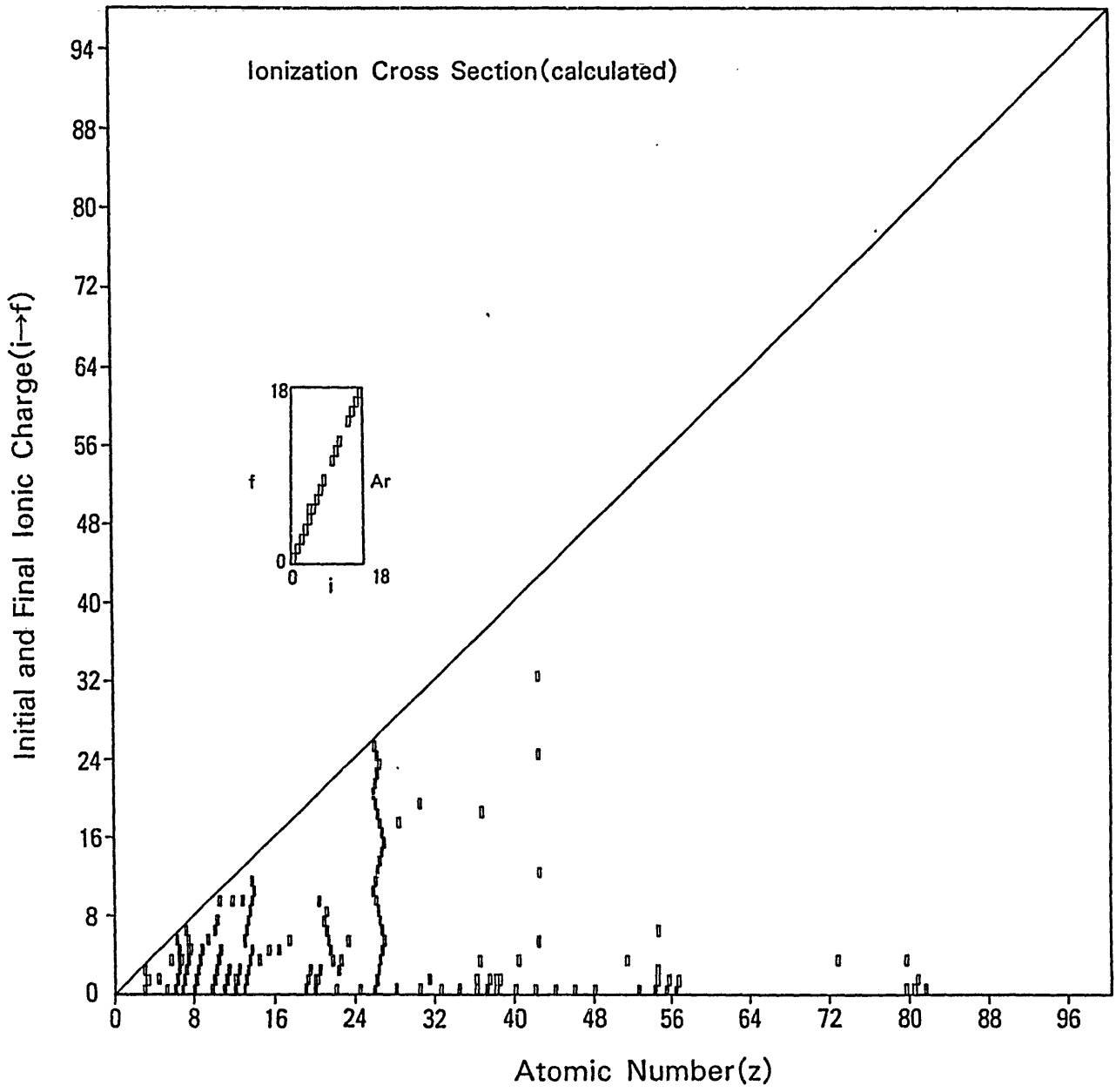


Fig.2(a)

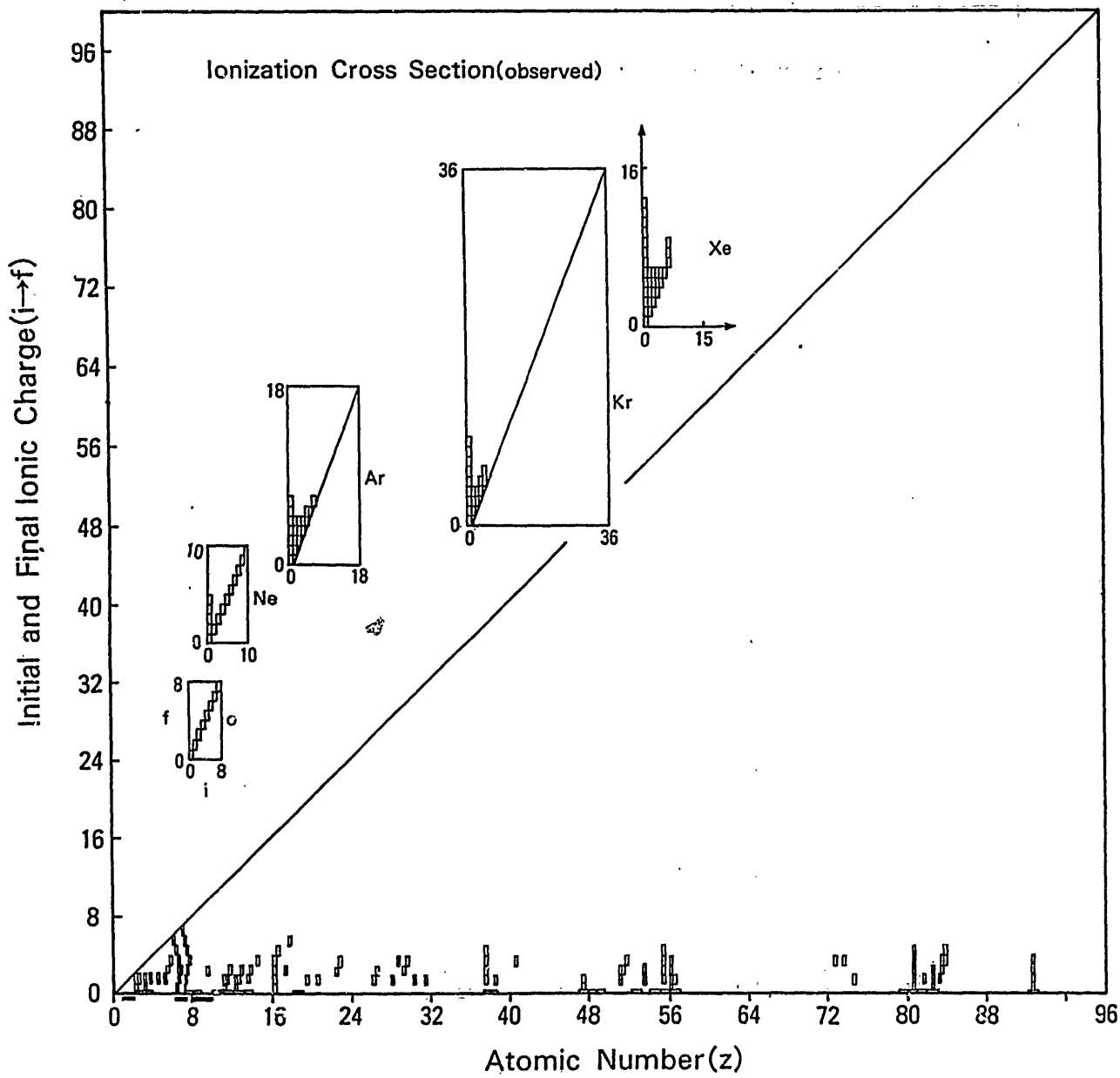


Fig.2(b)

## Diagnositics of JT-60 and Impurity Measurement

Tatsuo SUGIE, Akira SAKASAI, Hirotaka KUBO,  
Yoshihiko KOIDE, Nobuo AKAOKA, Toshio HIRAYAMA  
and Hiroshi TAKEUCHI

Department of Large Tokamak Research  
Naka Fusion Research Establishment  
Japan Atomic Energy Research Institute  
Naka-machi, Naka-gun, Ibaraki-ken

Spectroscopic measurement system of the JT-60 is composed by a visible spectrometers, a normal incidence spectrometer, grazing incidence spectrometers and a crystal specrometer. Unit type grazing incidence spectrometers have been developed for the measurements of spatial behaviors of impurity lines with in one shot of plasma. The oxygen, carbon, titanium and nickel lines were observed. When the titanium contamination was occured, the time behaviors of TiXX and TiXIII lines were analyzed with 1D-impurity transport code. The ion temperature was preliminarily obtained from the Doppler broadening of TiXXI resonance line with the crystal spectrometer.

## Diagnosics of JT-60 and Impurity Measurement

### 1. Introduction

JT-60 is a Tokamak type fusion experimental facility aiming at achieving a break-even plasma condition. The bird's-eye view of the JT-60 is shown in Fig. 1-1. The major and minor radii of the plasma produced in the vacuum vessel are 3.0 meters, 0.95 meters, respectively. The toroidal field up to 4.5 Tesla is produced by eighteen toroidal field coils, and plasma current up to 2.7 MA is induced by the poloidal field coils.

The temperature and the electron density of the JT-60 plasma are shown in Fig. 1-2. The temperature of the plasma is 1-2 keV with joule heating and will be reached to 10-20 keV with additional heating (NBI, LH, ICRF).

The overview of the diagnostics system of the JT-60 is shown in table 1-1.

The electron density is measured by mm and sub-mm wave interferometers, and electron temperature by a Fourier spectrometer and a multipulse laser for Thomson scattering.

The ion temperature is measured by a neutral particle analysers, an active beam probing apparatus and neutron counters.

The impurities are measured with various spectrometers.

The radiation flux is measured with a germanium detector, a PIN diode array and a bolometer array.

The peripheral plasma and wall surface are measured with probes, thermocouples, TV. and so on. Here, we describe the impurity measurement system with spectroscopic methods.

## 2. Impurity measurement system of the JT-60 (Spectroscopic measurement)

Fig. 2-1 shows a cross section of the vacuum vessel of the JT-60. The vacuum vessel is made of inconel 625. Its inner surface is covered with molybdenum limiters and molybdenum and inconel liners, which are coated with TiC. So, it is expected that impurities in the plasma are Ni, Ti, Mo, C and O. These impurities have a bad influence on the plasma confinement. JT-60 has a divertor (magnetic limiter: Fig. 2-1) in order to reduce the quantity of impurities. For these reasons, it is important to know the behavior of impurity ions in the plasma. The impurity ions in the plasma radiate spectral lines and continuum over wide wavelength range from infrared to X-ray.

The purposes of the spectroscopic measurement of the JT-60 as follows.

- 1) Diagnostics of impurity behavior in the plasma.
- 2) Measurement of plasma parameters (ion temperature).
- 3) Basic measurement of the impurity lines.

Spectrometers are installed in the JT-60 as shown in Fig. 2-2. Wavelength ranges of these spectrometers are shown in Fig. 2-3.

In addition, we have the beam injection spectroscopic measurement system, which is shown in Fig. 2-4, to obtain information of fully stripped ions and ion temperature profile.

### 2.1 Diagnostics of the impurity behaviors

In order to diagnose impurity behavior, it is necessary to measure spatial profiles with the time behavior of impurity lines in the plasma. And, spatial profiles must be obtained with in one discharge of plasma, because the reproducibility of the plasma with additional heating (for

example, NBI, LH, ICRF) will be not expected.

For these reasons, unit type flat field grazing incidence spectrometers with holographic grating and multichannel detector have been developed. Fig. 2.1-1 shows the unit type flat field grazing incidence spectrometer and the apparatus for spatial measurement, which can contain 17 unit type spectrometers. Now, we have two unit type spectrometers. The wavelength ranges of these spectrometers are from 0.5 nm to 5 nm and for 0.5 nm to 50 nm.

Spectral lines measured with these unit type spectrometers on JT-60 plasma are shown in Fig. 2.1-2 and 2.1-3. The optical axes of these spectrometers go through near the plasma center. Fig. 2.1-2(a) is the spectrum between 300 and 320 msec of discharge, (b) is the time behavior of OVIII (1.897 nm) line and (c) is CVI (3.374 nm) line measured with the spectrometer which wavelength range is from 0.5 nm to 5 nm. Fig. 2.1-3 (a) is the spectrum between 300 and 320 msec of discharge, and (b) is the time behavior of TiXX (25.93 nm) line measured with the spectrometer which wavelength range is from 0.5 nm to 50 nm. Sensitivity calibration and measurement of the spatial profile of impurity lines have not been done. These works are now in progress.

Next, Fig. 2.1-4 shows the signal measured with the PIN diode in rare case of discharge, where the radiation of the soft X-ray increased at 4.6 sec and 6.3 sec of the discharge. The spectra at 4.5 sec, 5.0 sec and 6.4 sec measured with the spectrometer are shown in Fig. 2.1-5(a), (b) and (c) where the Cu lines appeared at 5.0 sec and Ti lines appeared at 6.4 sec. Fig. 2.1-6(a) and (b) show the time behavior of CuXXI (7.905 nm), and TiXX (25.93 nm) lines.

In this shot, it seems that the increase of the radiation was caused by the contamination of the impurities at those times. It is

very interesting shot for the study of the impurity transport in the plasma. Now, the analysis is in progress with 1D-impurity transport code\* when the titanium contamination occurred. The preliminary results are shown in Fig. 2.1-7 (a) and (b) with dotted lines, where  $D_A$  is a radial diffusion coefficient and  $C_V$  is a shape parameter. The shape parameter  $C_V$  is related to a convection velocity  $V_A$  as  $V_A = -C_V D_A 2r/a^2$ .

And, these shots are very useful for the identification of the impurity lines.

Another unit type spectrometers observe the divertor side of the peripheral plasma, as shown in Fig. 2.1-8. For the wavelength range of these spectrometers, one is from 2 nm to 50 nm and the other is from 50 nm to 120 nm. Fig. 2.1-9 shows the time behaviors of the oxygen and carbon lines. The intensities of these lines increased from 300 msec of discharge when the divertor (magnetic limiter) operation started. It seems that the radiation near the divertor region increased in the divertor operation.

## 2.2 Measurement of plasma parameters (ion temperature)

In the spectroscopic measurement, the ion temperature of plasma is determined from the Doppler broadenings of impurity lines, assuming the thermal equilibrium between impurity ions and plasma ions (for example proton).

In the JT-60, the ion temperature of the plasma is measured with the 1.2 m normal incidence vacuum spectrometer for the peripheral region and with the 2.5 m Johann type crystal spectrometer for the center region.

---

\* T. Hirayama et al.; the 7th international conference on plasma surface interactions in controlled fusion device. (Princeton, 1986).

Fig. 2.2-1 shows the 2.5 m Johann type crystal spectrometer which has two crystals. One is Si (220) for the Ti  $k_{\alpha}$  line and the other is  $\text{SiO}_2$  (2 2  $\bar{4}$   $\bar{3}$ ) for the Ni  $k_{\alpha}$  line. The line profiles are detected with multichannel detector which is composed by MCP (micro channel plate), PCD (plasma coupled device) linear image sensor and electrical circuit.

Spectrogram measured with the crystal spectrometer is shown in Fig. 2.2-2, where the resonance line of TiXXI  $1s^{21}S_0 - 1s2p^1P_1$  and satellite lines were observed. The time behavior of the intensity of the TiXXI resonance line is shown in Fig. 2.2-3 and the profiles measured with the multichannel detector is shown in Fig. 2.2-4. In Fig. 2.2-4, the average values per 400 msec are dotted with squares. From these profiles, the ion temperatures were preliminarily obtained, which are shown in Fig. 2.2-5. The electron temperature of plasma center measured with the laser scattering method was about 2 ~ 2.2 keV.

So, it seems that the ion temperature determined from the TiXXI resonance line indicate the ion temperature of the center region of plasma until the additional heating, because the electron temperature will be more higher and the energy transport process will be complicated.

### 2.3 Basic measurement of the impurity lines

We have the 3-m grazing incidence spectrometer and the 0.5-m visible spectrometer for the basic measurement of the impurity lines. These spectrometers are used for intensity calibration with the atomic branching ratio method, and for the identification of the impurity lines. Now, these works are in progress. Untill now, titanium, nickel carbon and oxygen lines has been identified with the spectrograms.

Unidentified lines will be observed in the JT-60 plasma. It is very useful for the atomic physics and the plasma diagnostics to

analyze these lines.

### 3. Summary

In this report, we describe the present status of the impurity measurement system with spectroscopic methods. The analysis of the data is now in progress.

We summarize our results until now as follows:

- (1) The spectra of impurity ions were measured with in one shot of discharge by the unit type grazing incidence spectrometer in VUV region.
- (2) Ion temperature of the plasma was measured from the Doppler broadening of the TiXXI resonance line with the 2.5 m Johann type crystal spectrometer.
- (3) Impurities of the JT-60 plasma were mainly oxygen, carbon and titanium, from the spectrograms measured with the 3 m grazing incidence spectrometer.
- (4) The impurity transport was analyzed by the 1D-impurity transport code when the titanium contamination occurred.

Next phase of the JT-60, when the additional heatings with the full power, it seems that the atomic process of the impurity ions is very important for the study of impurity behavior in the plasma.

Table 1-1

Diagnostic System of JT-60

System	Plasma Parameter	Diagnostic Instruments
1	Electron Density	Sub-MM Wave & MM Wave Interferometers
2	Electron Temp.	Thomson Scattering, Far Infrared Spectrometer
3	Ion Temperature	Charge Exchange Neutral Analyzer, Active Beam Probe, Neutron Counter
4	Impurity	Spectrometer ( Grazing Incidence, Crystal & Holographic Grating )
5	Radiation Flux	High Speed PHA, PIN Diode, Bolometer
6	Peripheral Plasma	IR & Visible TV, Probes
7	Data Processing System	Inter Shot & Real time Processor, CAMAC System
8	Diagnostic Support System	Diagnostic Stage, Carrier, Cabling & Piping, Vacuum Connecting Instrument, Shielding

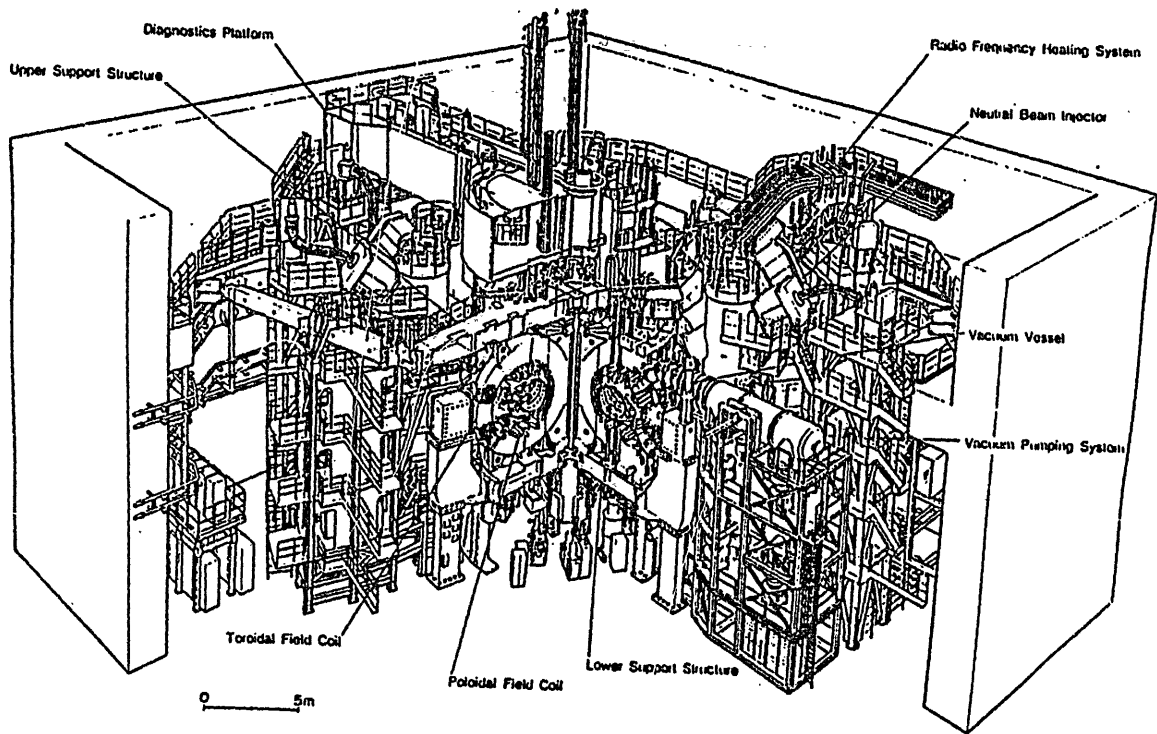


Fig.1-1 The bird's-eye view of the JT-60.

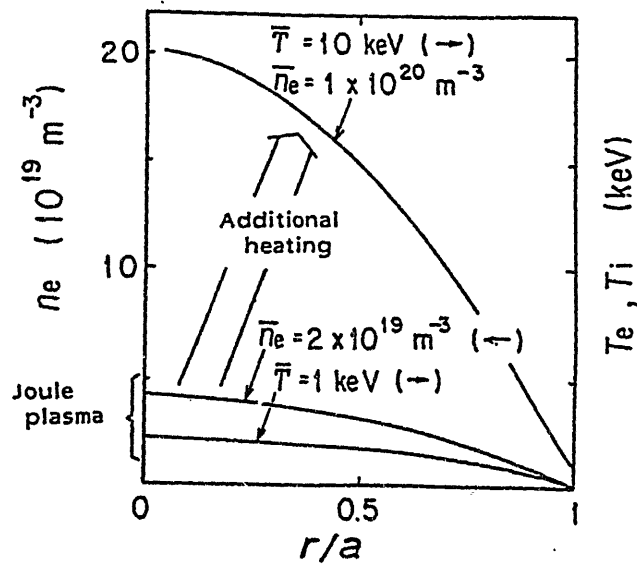


Fig.1-2 Temperature and electron density of the JT-60.

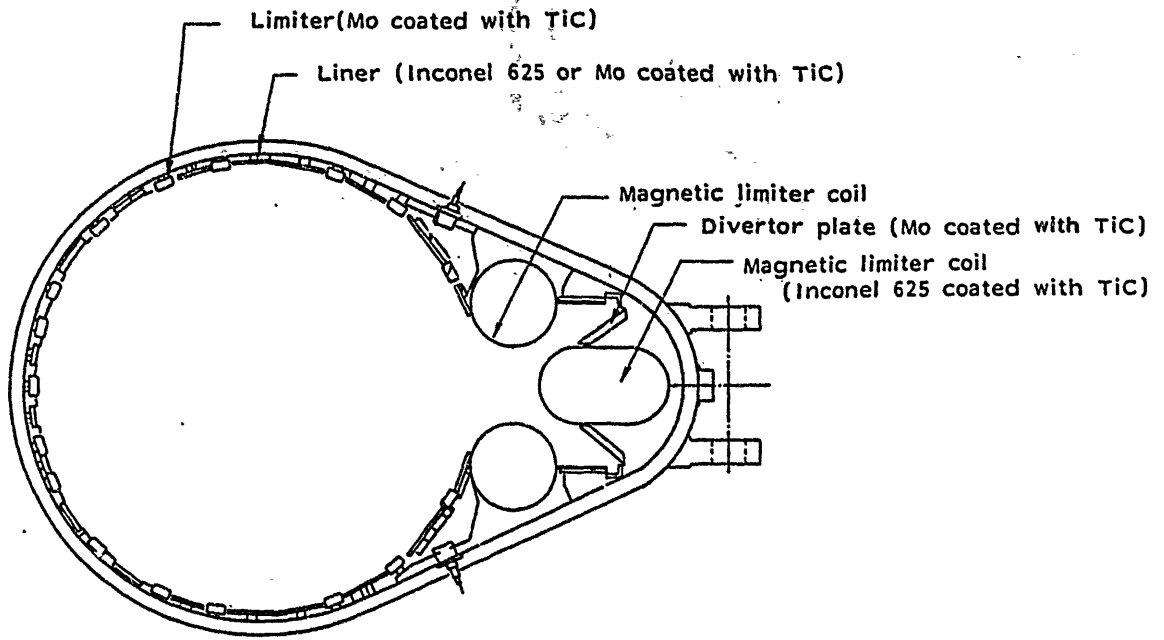


Fig.2-1 Cross section of the vacuum vessel of the JT-60.

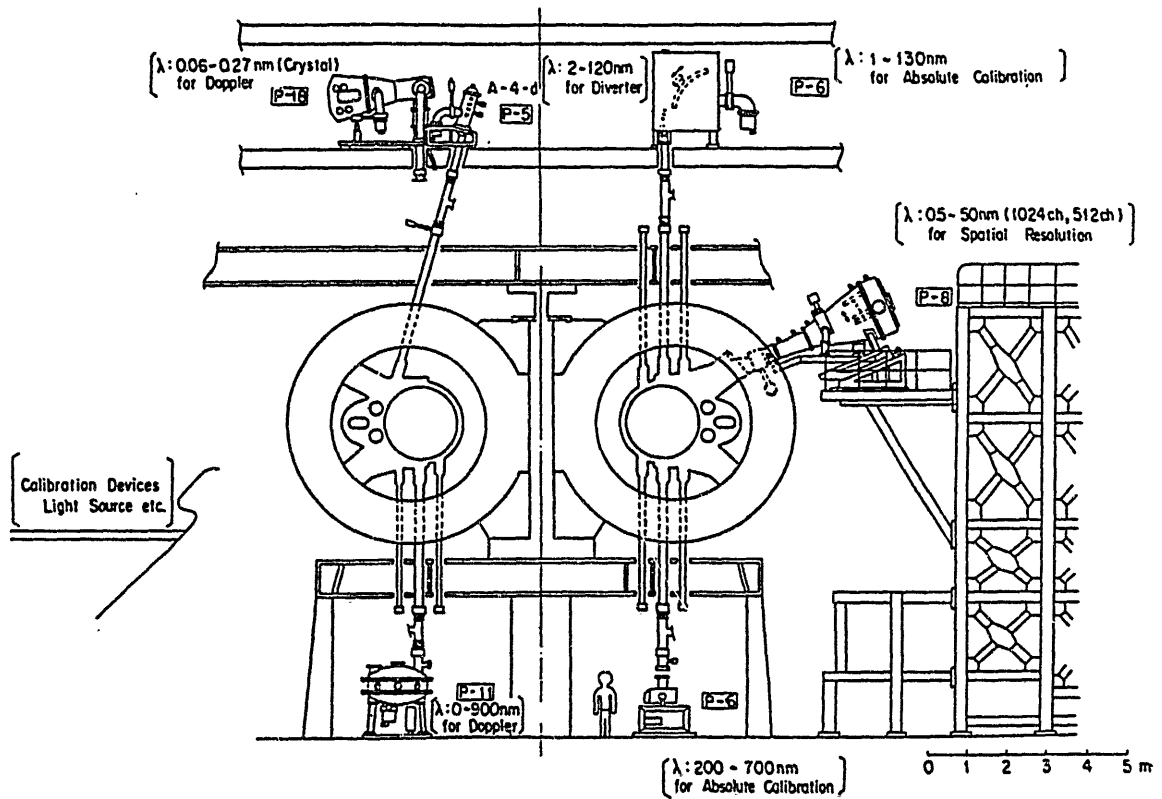


Fig.2-2 Arrangement of spectrometers

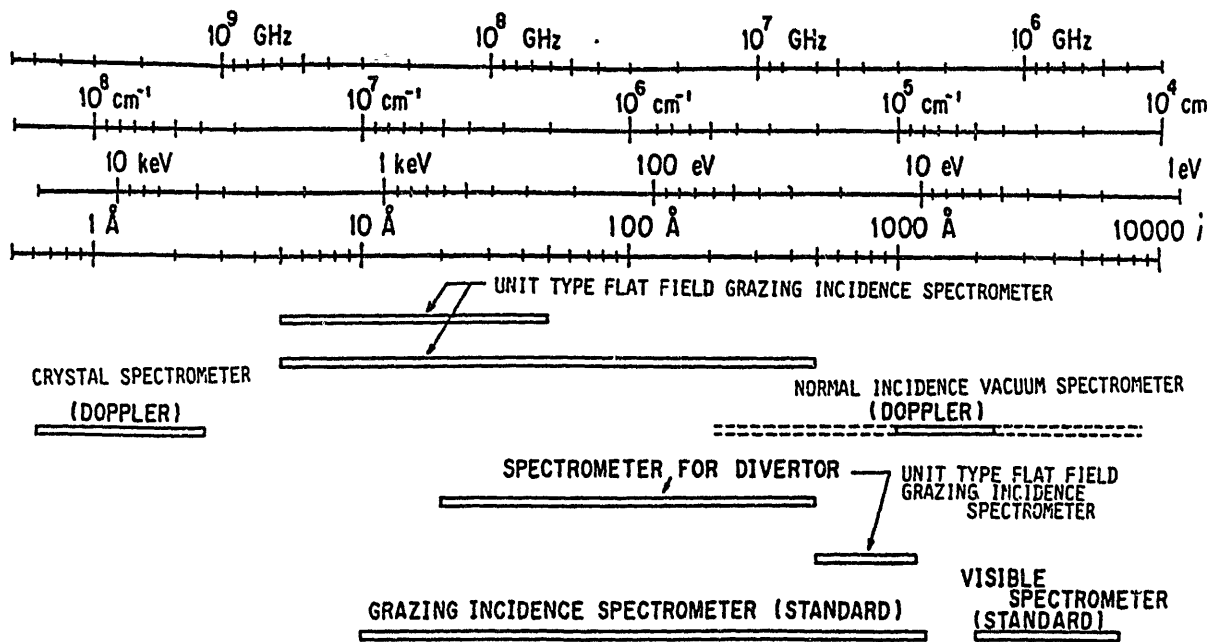


Fig.2-3 Wavelength ranges of spectrometers of the JT-60.

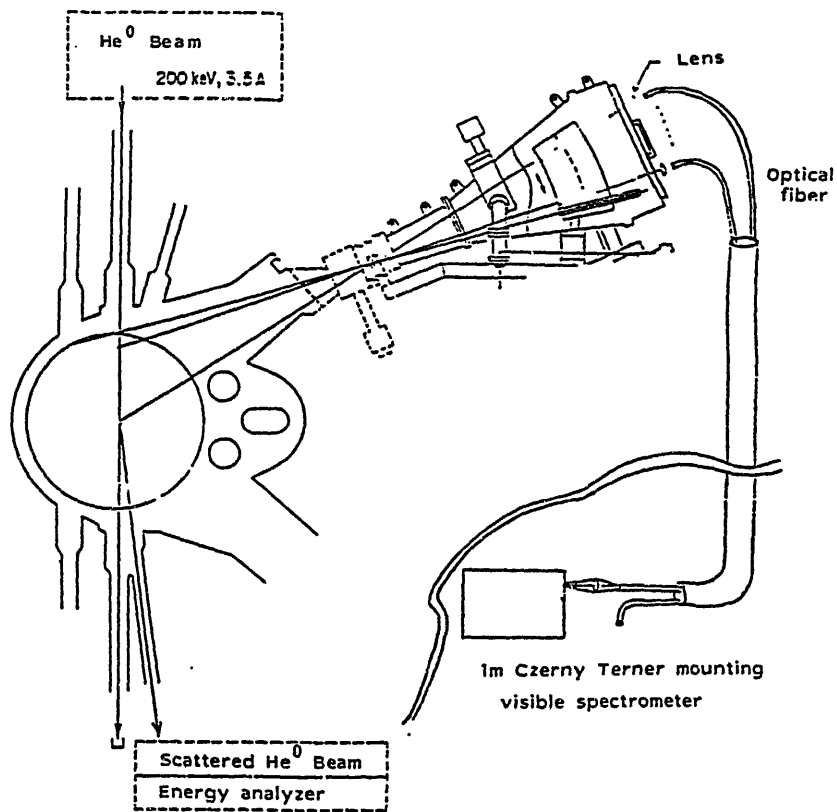


Fig.2-4 Spectroscopic measurement system with He<sup>0</sup> beam injection.

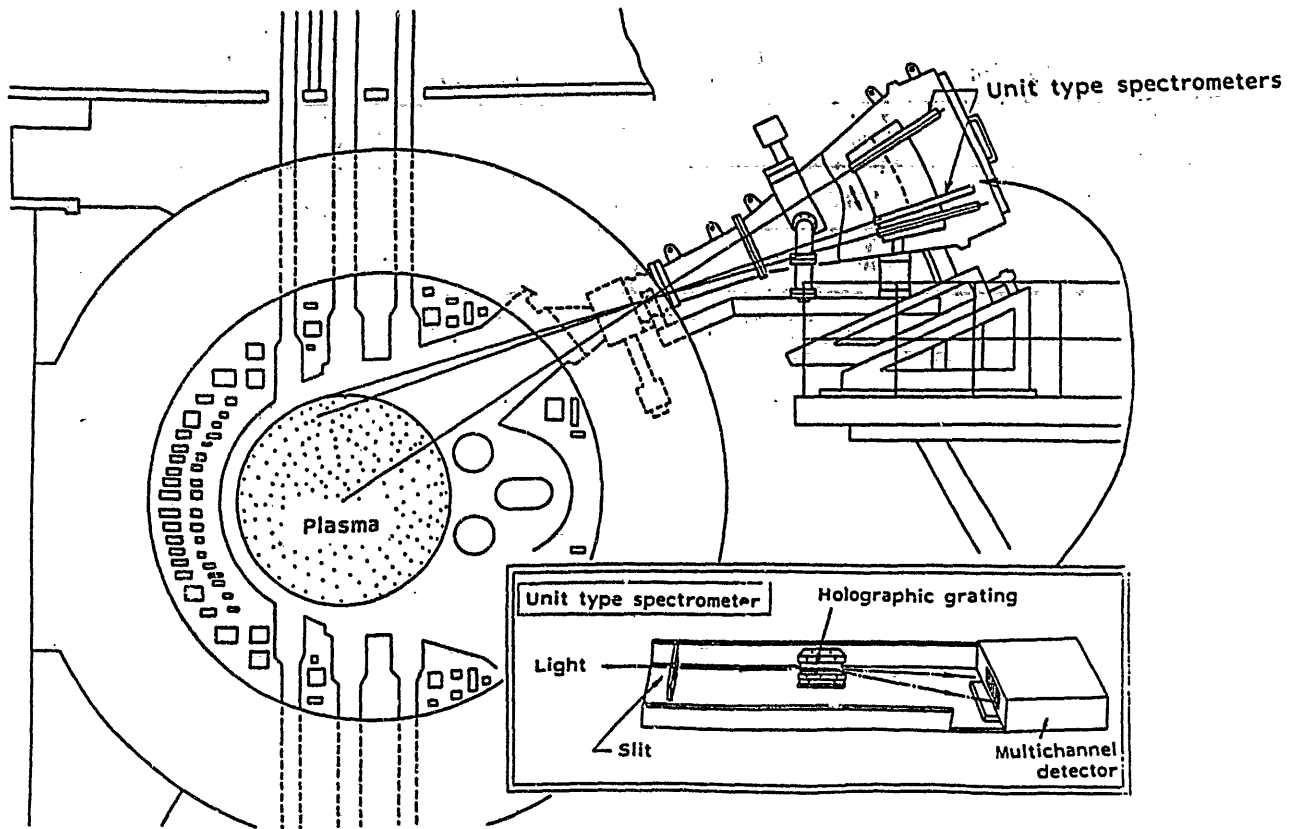


Fig.2.1-1 Unit type flat field grazing incidence spectrometer and apparatus for spatial profile measurement of impurity lines.

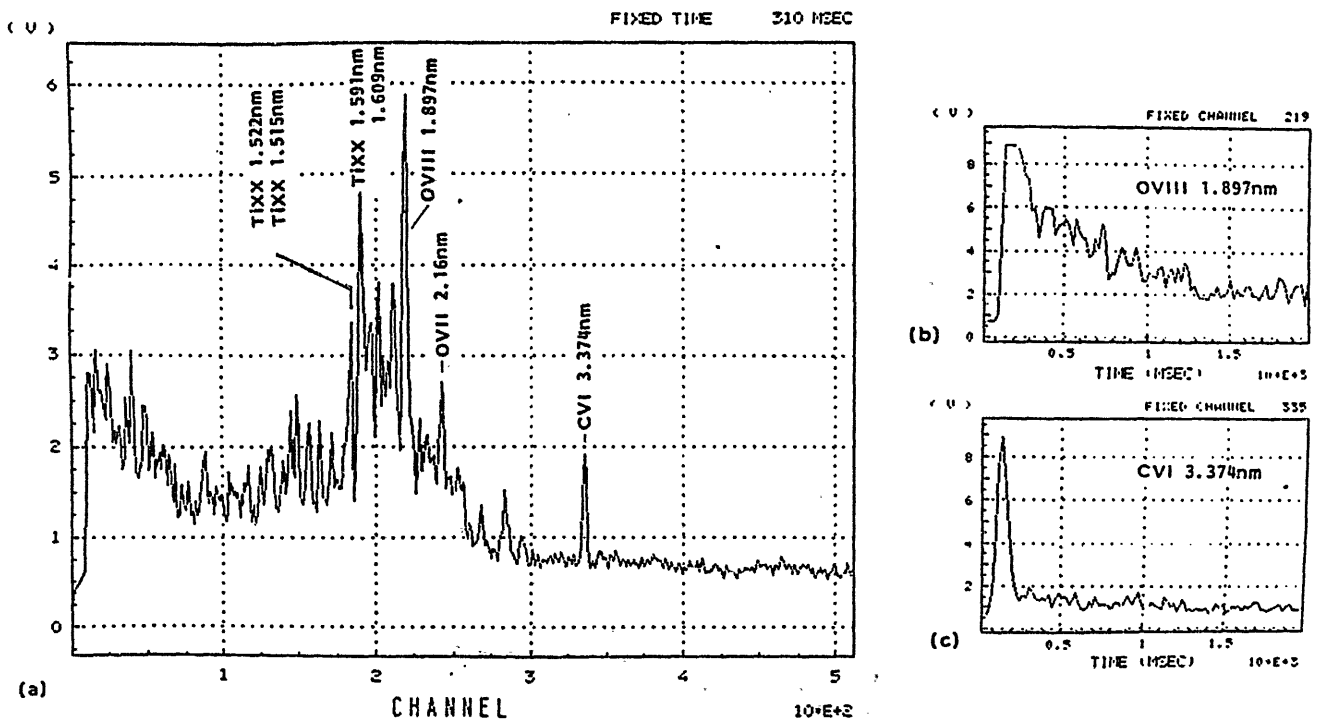


Fig.2.1-2 Spectral lines measured with the unit type spectrometer. The wavelength range is 0.5-5.0 nm. (b) and (c) are the time behaviors of OVIII and CVI lines respectively.

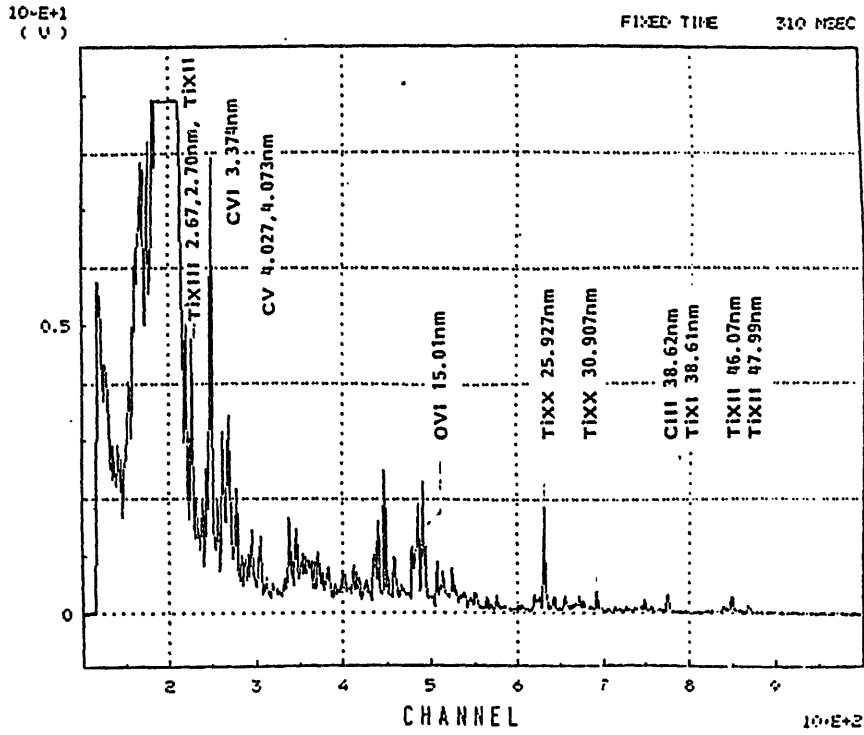


Fig.2.1-3(a) Spectral lines measured with the unit type spectrometer. The wavelength range is 0.5-50 nm.

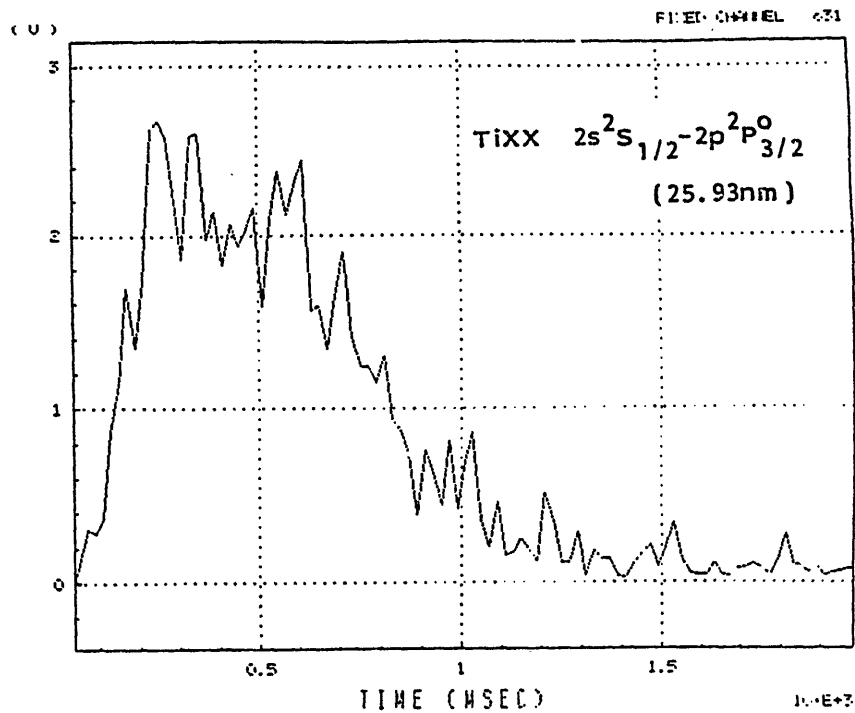


Fig.2.1-3(b) Time behavior of TiXX(25.93nm) line

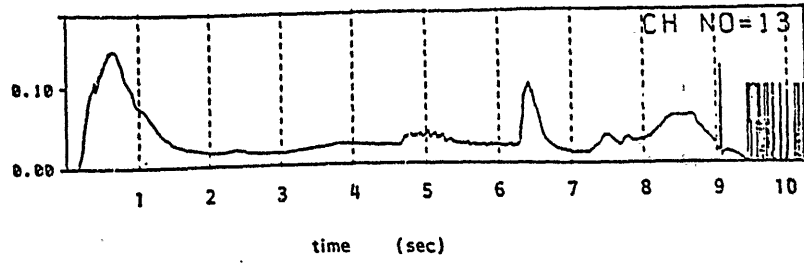


Fig.2.1-4 Time behavior of the soft x-ray radiation with PIN diode.

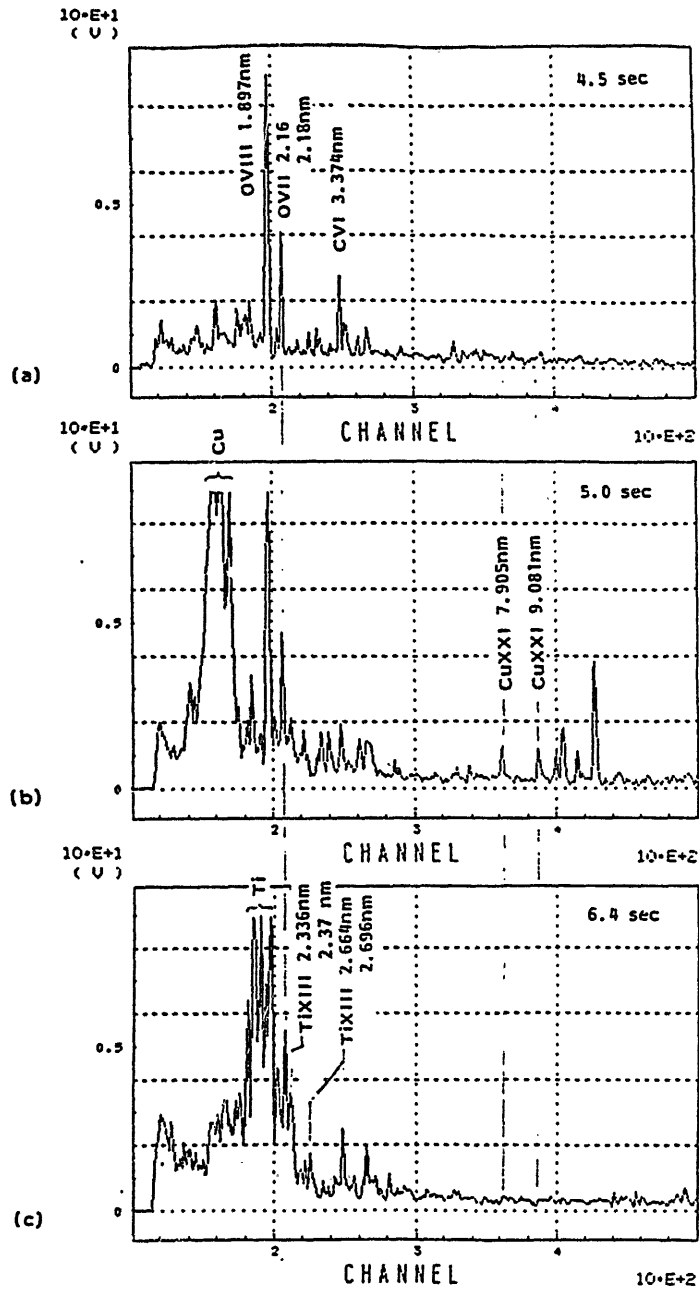


Fig.2.1-5 Spectra at 4.5 sec , 5.0 sec and 6.0 sec.

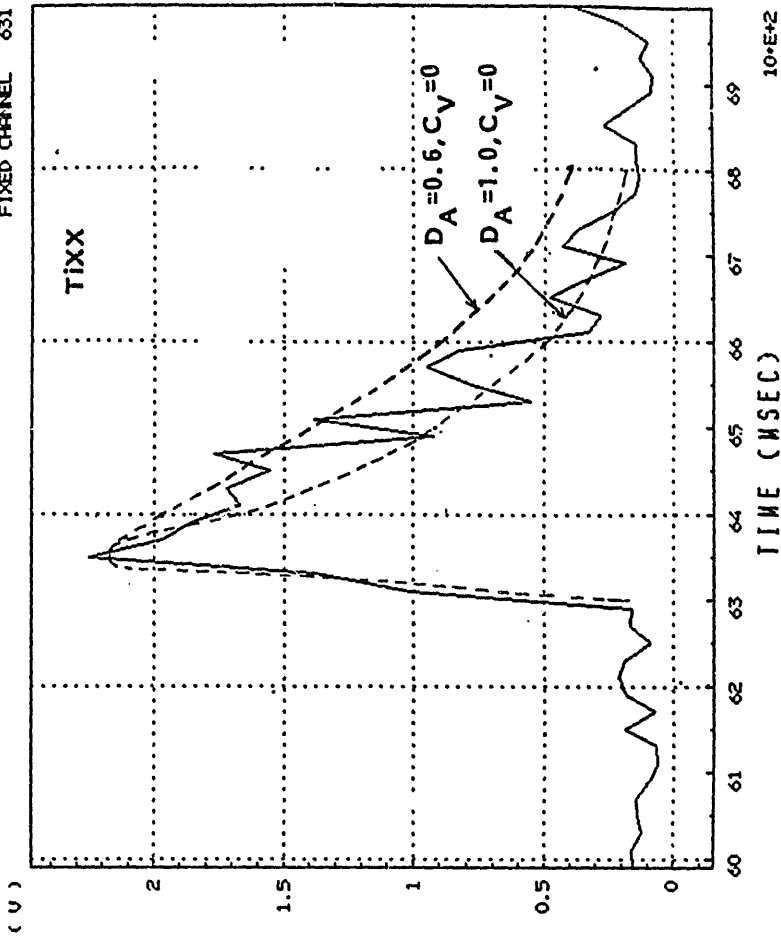


Fig.2.1-7(a) Calculated results given by the 1D-impurity transport code are shown with dotted lines for the various  $D_A$  and  $C_V$ .  $D_A$  is a radial diffusion coefficient and  $C_V$  is a shape parameter related to a convection velocity  $V_A$  as  $V_A = -C_V D_A / 2r/a^2$ .

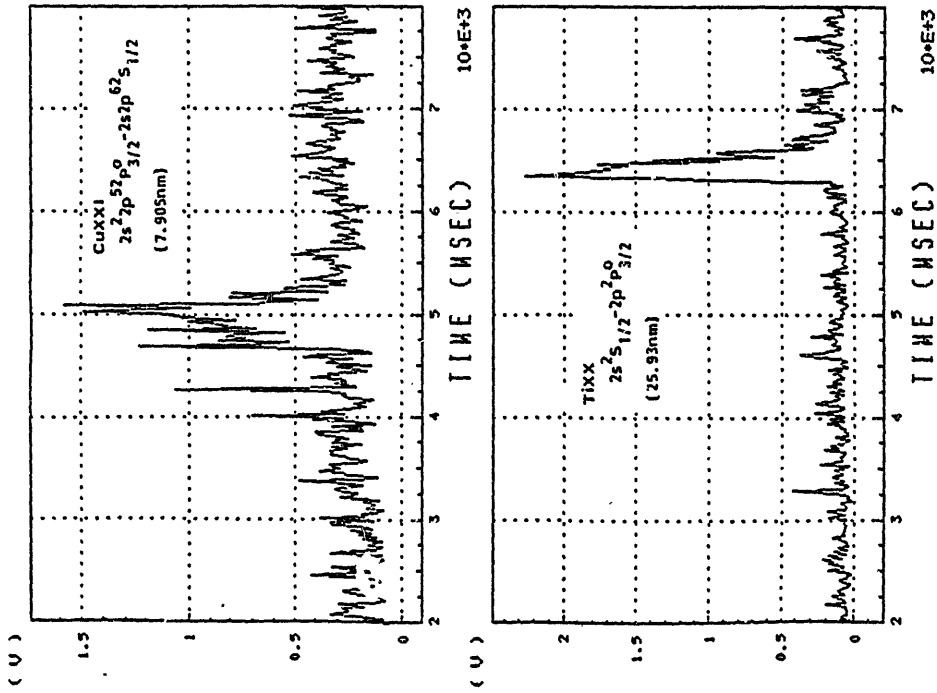


Fig.2.1-6 Time behavior of CuXXI and TiXX lines.

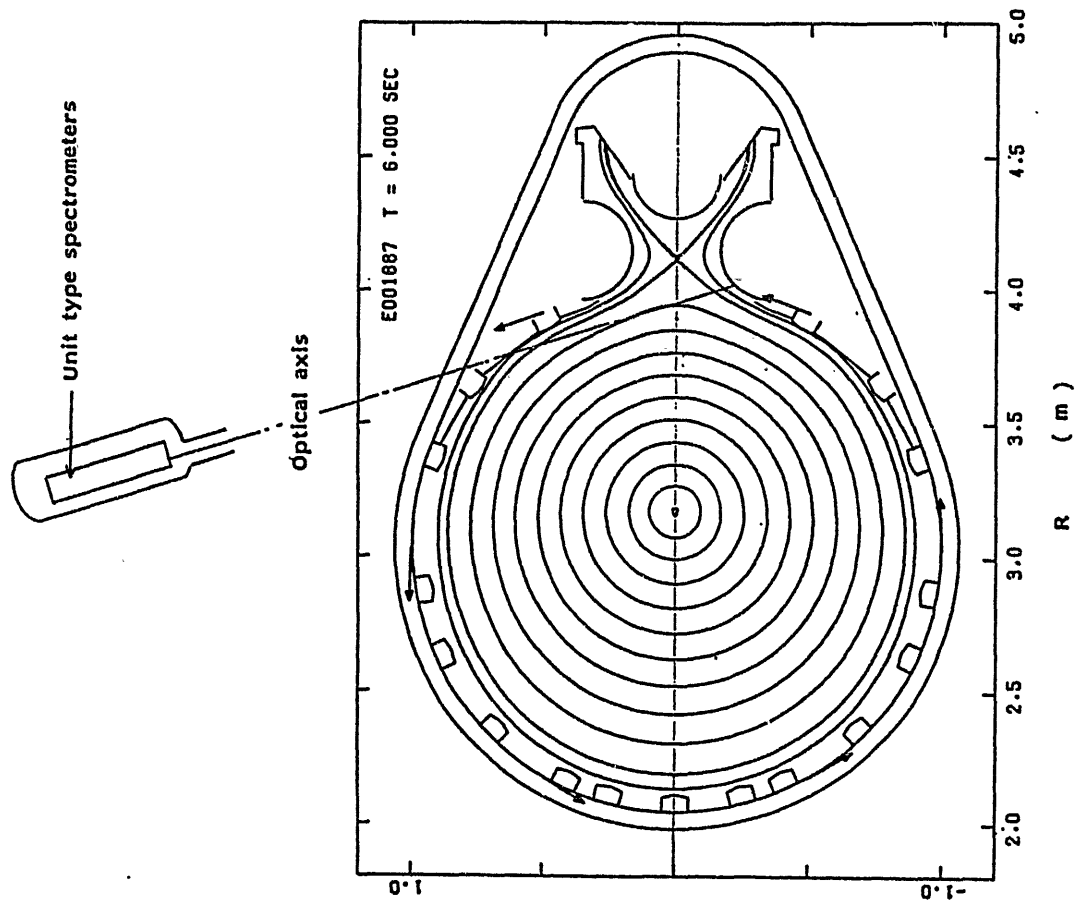


Fig.2.1-8 Unit type spectrometers observing the divertor side of the peripheral plasma.

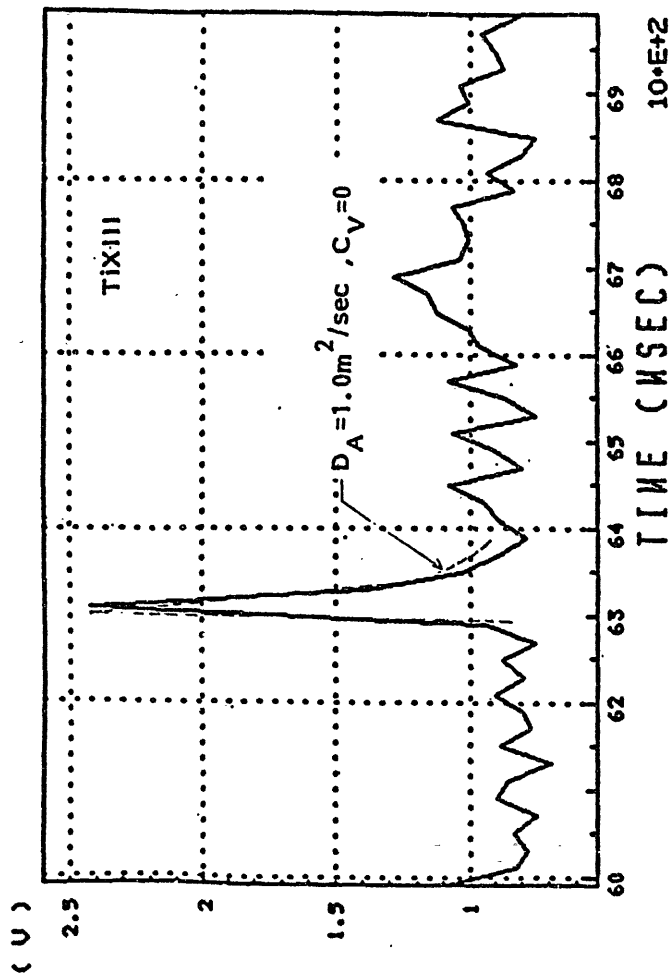


Fig.2.1-7(b) Calculated results given by the 1D-impurity transport code.

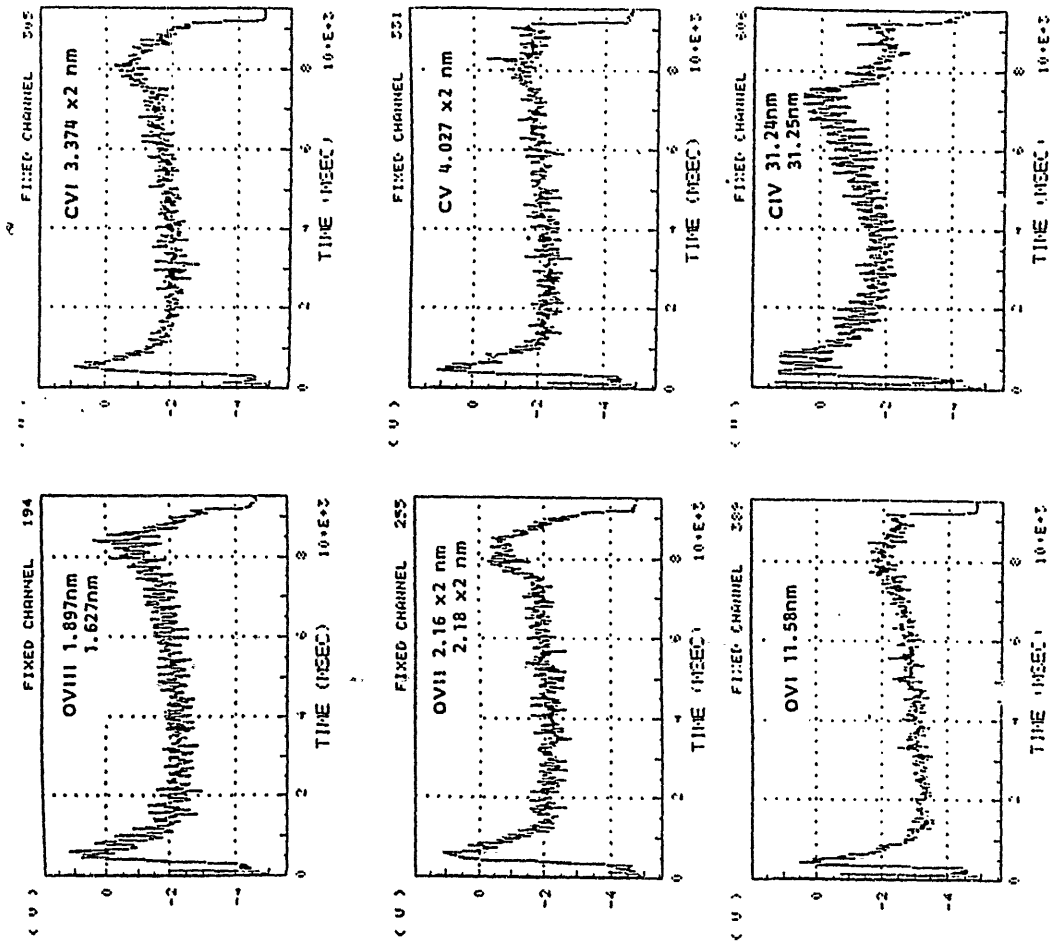


fig.2.1-9 Time behaviors of the oxygen and carbon lines measured with the spectrometers observing the divertor side of the peripheral plasma.

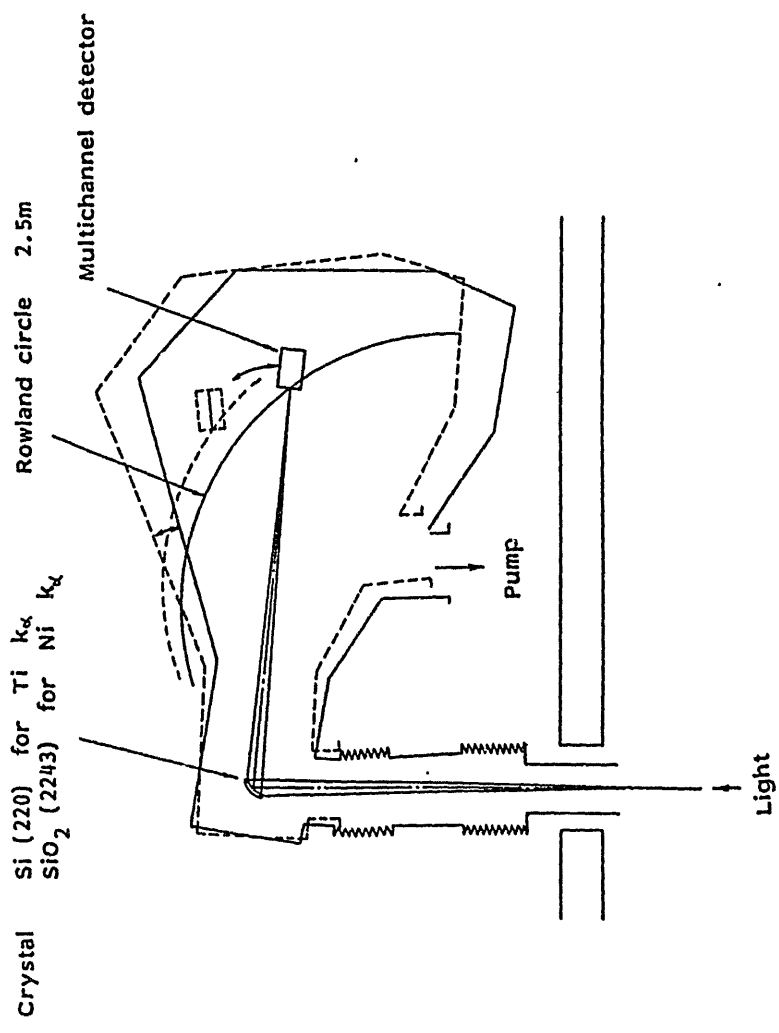


Fig.2.2-1 2.5m Johann type crystal spectrometer.

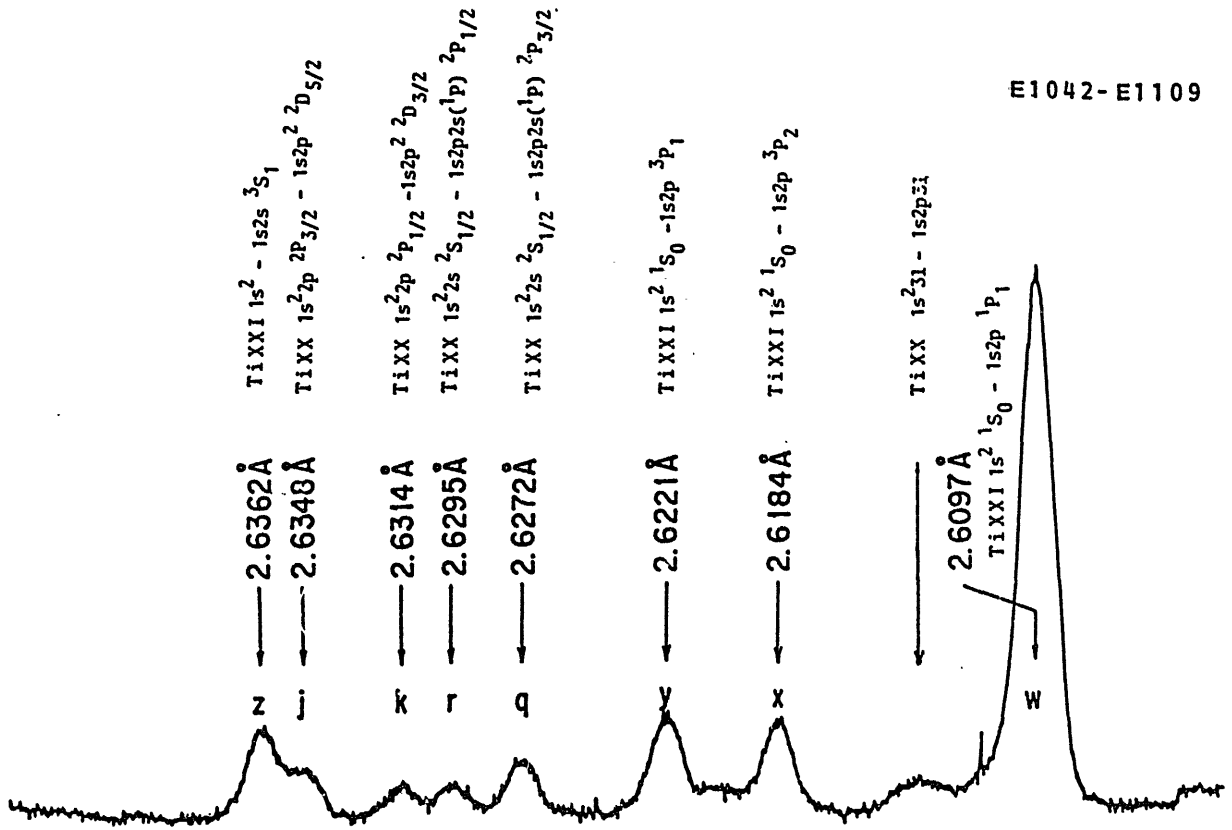


Fig. 2.2-2 Spectrogram of TiXXI resonance line and satellite lines measured with the crystal spectrometer.

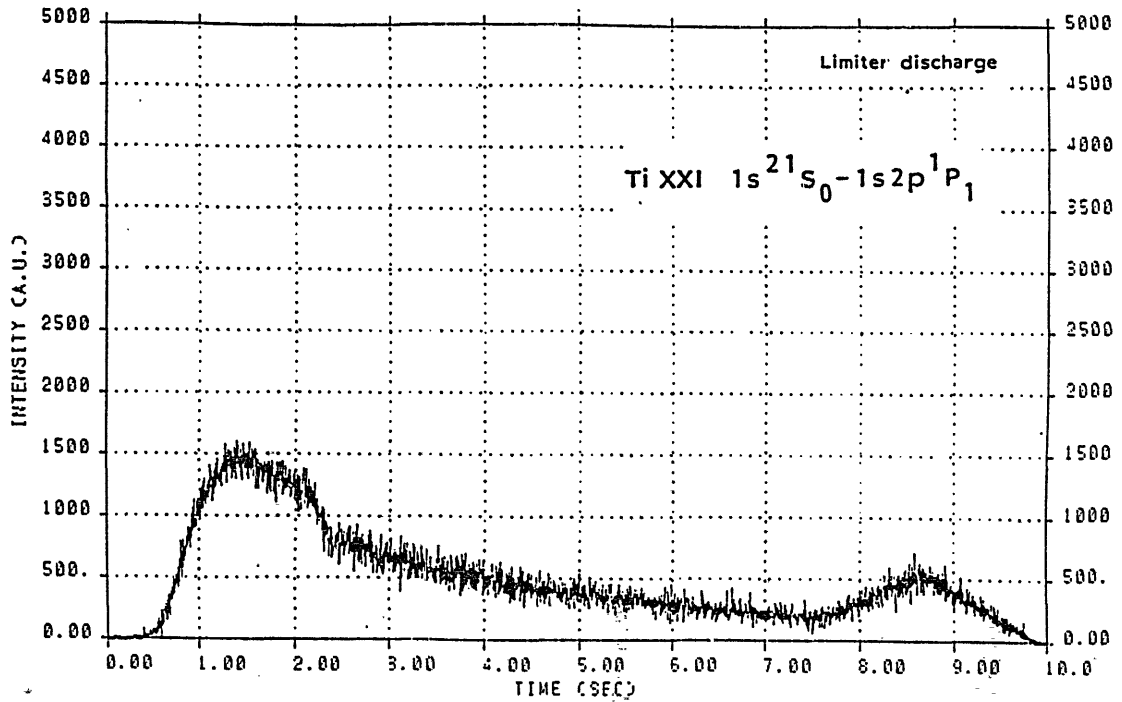


Fig.2.2-3 Time behavior of the total intensity of the TiXXI resonance line.

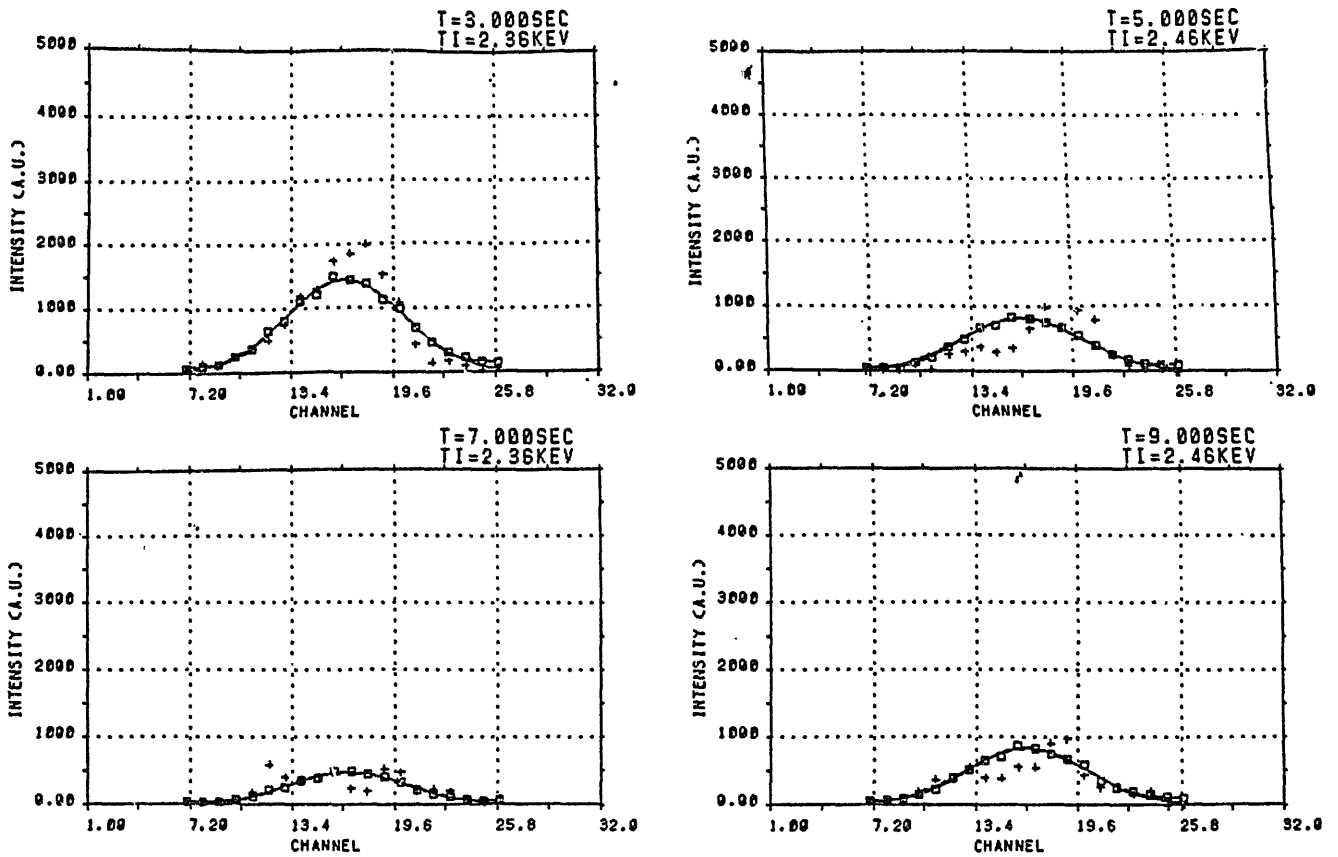


Fig.2.2-4 Profiles of TiXXI resonance line, where the average values per 400 msec are dotted with squares.

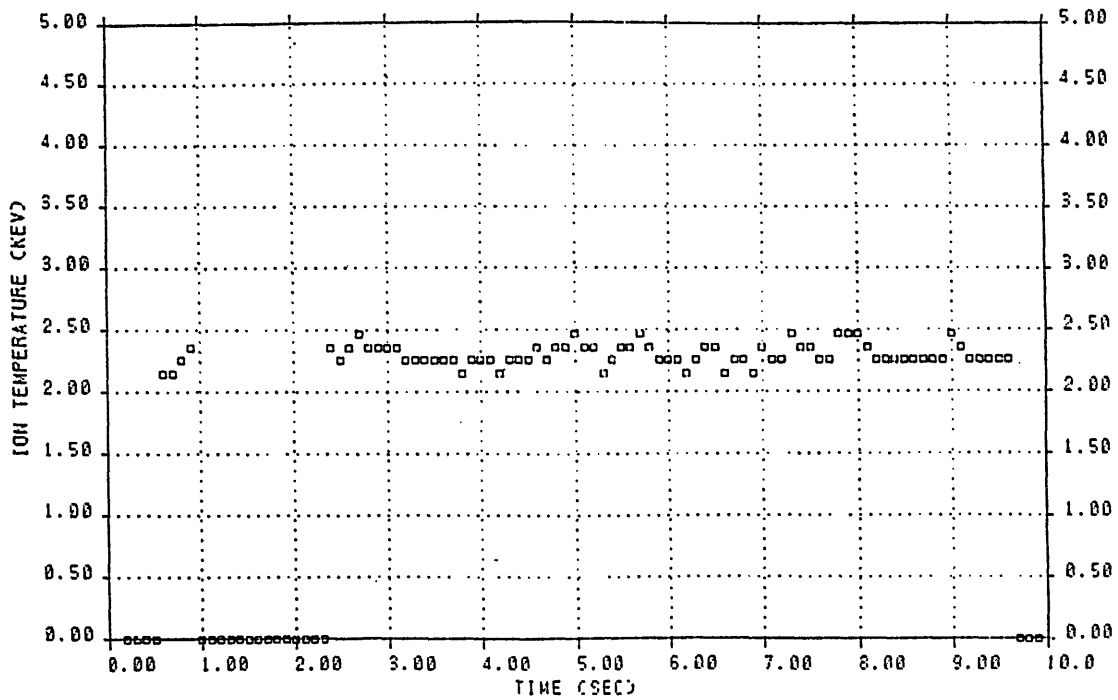


Fig2.2-5 Ion temperature measured with the Doppler broadening of the TiXXI resonance line.

Some Comments on Atomic Cross sections used in analysis  
of X-Ray Spectra from Tokamak Plasmas

Shigeru MORITA

Institute of Plasma Physics, Nagoya University, Nagoya 464

<1> Thermal spectra

Charge state distributions of Ti(Z=22), Cr(24), Fe(26) and Ni(28) ions were measured with time interval of 10ms before and during ICRF heating (40 MHz - 1 MW) using a crystal spectrometer. Most abundant charge states of the four metal impurity ions in the central plasma column of JIPP T-IIU were determined. The experimental spectra were compared with calculated ones as a function of ion transport parameters, especially ion diffusion coefficient.

As an array of  $K\alpha$  spectral lines directly displays informations of the ion abundance in the central plasma column<sup>1)</sup>, the charge state distributions of the ions can be easily obtained from it. The experimental spectra are shown in Fig.1. No emissions of H-like ions were observed. Most abundant charge states of the impurity ions shift toward lower isoelectronic sequences with increasing nuclear charge of the ions<sup>2)</sup>. The experimental charge state distributions were not largely affected by ICRF heating, although the total emissions drastically increase.

Figure 2 shows calculated  $K\alpha$  emissions of iron ions as a function of diffusion coefficient  $D$ . They strongly depend on the diffusion coefficients. As a result of comparison between the experiment and the calculation, it is found that the diffusion coefficient is roughly constant around  $7 \times 10^3 \text{ cm}^2/\text{s}$ . However, second current rise during ICRF heating gives a smaller diffusion coefficient.

## ② Nonthermal spectra

Current drive experiment by lower-hybrid waves (800 MHz - 100 kW) was carried out with electron densities of  $2 - 10 \times 10^{12} \text{ cm}^{-3}$  and electron temperatures of 0.3 - 1.0 keV. Titanium  $K\alpha$  emissions from the non-thermal plasma including suprathermal electrons were measured using a crystal spectrometer and extremely flat  $K\alpha$  spectral distributions were found over a wide range of charge states of the titanium ions. The flat distributions can be explained with enhanced excitation rates due to the suprathermal electrons.

The  $K\alpha$  x-ray lines are mainly emitted through three atomic processes in low-density and high-temperature laboratory plasmas shown in Fig.3. Since the electron temperature during the current drive is less than 1 keV, every rate coefficient in three cases is less than  $\sim 3 \times 10^{-15} \text{ cm}^3 \text{ s}^{-1}$ . But the rate coefficient of the inner-shell ionization by electron impact has a maximum value of  $\sim 10^{-12} \text{ cm}^3 \text{ s}^{-1}$  at the electron temperature higher than 10 keV. It indicates that the  $K\alpha$  spectral feature strongly depends on the amount of the suprathermal electrons with energies above  $\sim 10$  keV.

Figure 4 shows raw data of titanium  $K\alpha$  emissions. Intense  $K\alpha$  lines from partially M-shell-ionized ions<sup>3)</sup> are also emitted. However, it is mainly emitted only by the inner-shell ionization. These spectral features during LHCD strongly suggest the existence of the suprathermal electrons.

Total counts of the  $K\alpha$  emissions are plotted in Fig.5 as a function of the electron density at the same electron temperature of about 600 eV. This figure clearly shows the growth of the suprathermal electrons at  $n_e < 10^{13} \text{ cm}^{-3}$ , while the similar increase of the total counts at higher densities is due to increasing thermal emissions.

### <3> High-resolution heliumlike titanium spectra

A high-resolution Johann type crystal spectrometer has been developed to observe a Doppler broadened feature of x-ray lines emitted from highly ionized metallic impurity ions in JIPP T-IIU. This instrument offers the informations of ion temperature and electron temperature in the central column of the plasma.<sup>4)</sup>

Experimental setup of the spectrometer constructed is shown in Fig.6. The spectrometer is set tangential to the toroidal axis to raise photon intensities coming to it and to measure a toroidal rotation velocity. The spatial resolution of a position-sensitive proportional counter used as an x-ray detector is less than 200  $\mu\text{m}$ . The accuracy of the cylindrical surface of the bent crystal, which is pasted with an epoxy resin on a blue glass cut to a radius of about 300 cm with the accuracy less than 0.1  $\mu\text{m}$ , is less than 1  $\mu\text{m}$  in radius. The total resolving power of the spectrometer is  $\lambda/\Delta\lambda > 2 \times 10^4$  at 2.61Å of Ti XXI He-like resonance line. It enables us to diagnose the ion temperature of several hundreds of eV. At present the lower limit of the ion temperature measurement is roughly estimated to be 300 eV.

Typical example of the ion temperature measurement in JIPP T-IIU is shown in Fig.7. The data are fitted with Voigt function, which is the convolution of Gaussian and Lorentzian. Unresolved dielectronic satellites are also considered. The electron temperature is determined from the ratio of n=3 dielectronic satellites to w line in the range of electron densities higher than  $5 \times 10^{13} \text{ cm}^{-3}$ .

### <4> Comments

Needed data for analysis of charge state distributions are inner-shell excitation, inner-shell ionization and dielectronic recombination. Data used are by Mewe and Merts et al. The experimental spectra can be roughly explained using these data.

Needed data for analysis of non-thermal x-ray spectra are inner-shell ionization rate coefficients or cross sections by electrons with energies more than several tens of keV, fluorescence yields and polarization of x-ray emissions. But these data are very few. Theoretical works to calculate above mentioned coefficients are intensively needed.

Needed data for analysis of high-resolution heliumlike titanium spectra are line wavelengths, excitation and recombination coefficients and dielectronic recombination rate coefficients. Data used are by Bely-Dubau and Safronova. These are enough for temperature determination of tokamak plasma. However, full understanding of spectra is not yet. Many experimental data should be compared with many theoretical ones. AS an alternative process, ion-ion collisions may be taken into account.

Finally, as a new approach of collisional experiments and calculations,

- (1) ion-ion collisions including charge exchanges
- (2) energetic electron-ion collisions
- (3) polarization of x-ray emissions

are recommended.

#### References

- 1) K. W. Hill et al. : Phys. Rev. A 19(1979)1770.
- 2) S. Morita and J. Fujita : Nucl. Instrum. Methods B9(1985)713.
- 3) S. Morita and J. Fujita : Phys. Rev. A 31(1985)3299.
- 4) M. Bitter et al. : Phys. Rev. Lett. 42(1979)304.

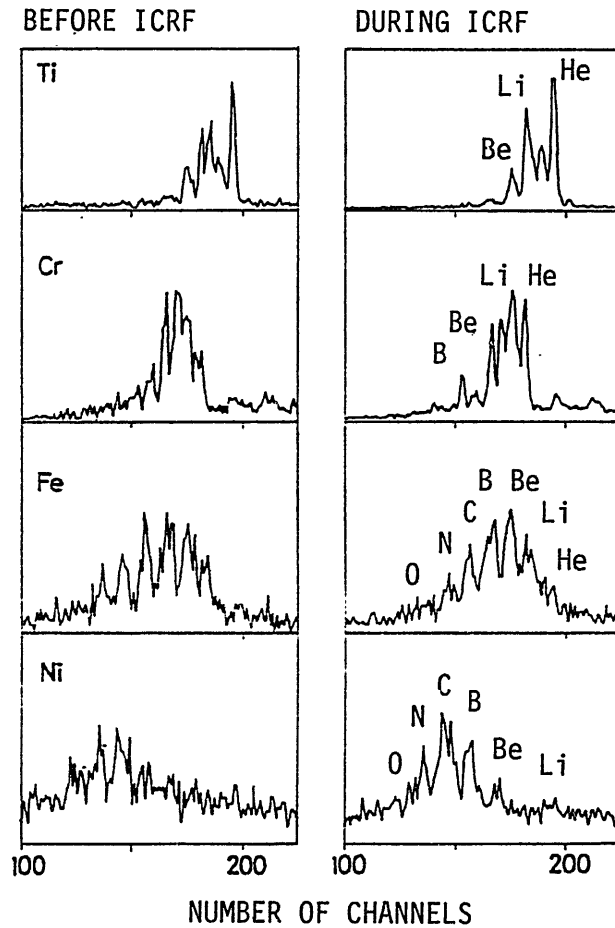


Fig.1 Experimental  $K\alpha$  x-ray line emissions showing charge state distributions in the central plasma column of JIPPT-IIU.

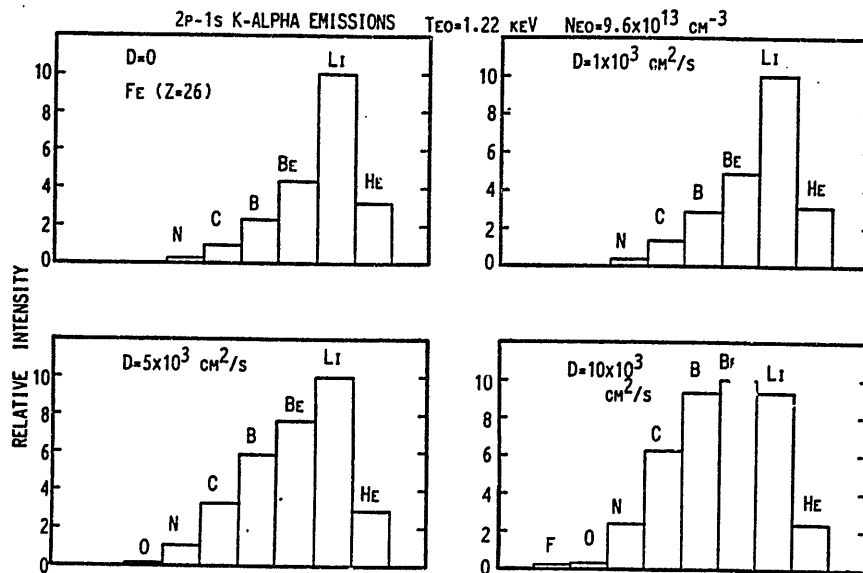


Fig.2 Calculated  $K\alpha$  x-ray line emissions as a function of diffusion coefficients. The calculation can be compared with the spectrum during ICRF in Fig.1.

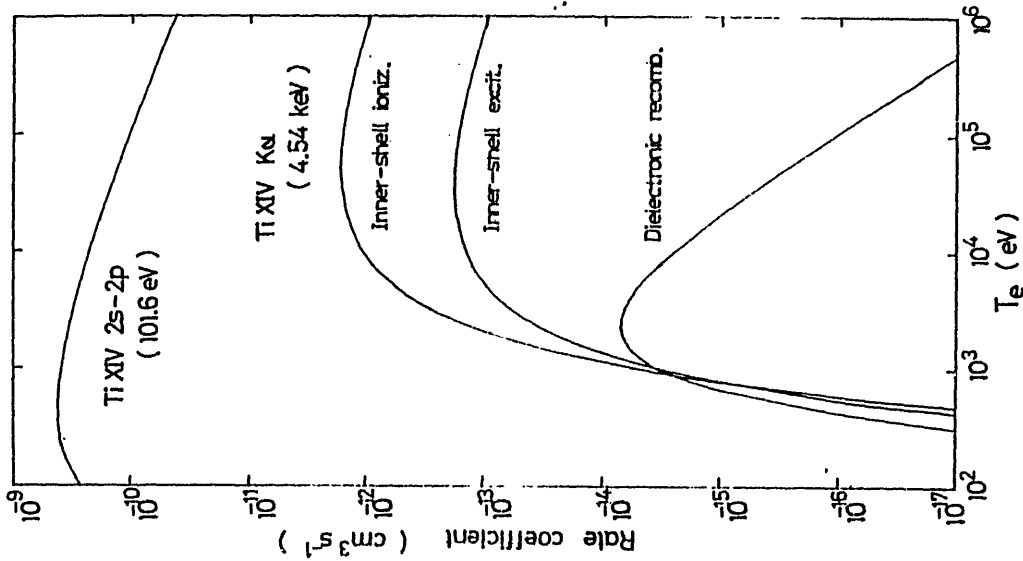


Fig.3 Excitation rate coefficients of TiXIV.

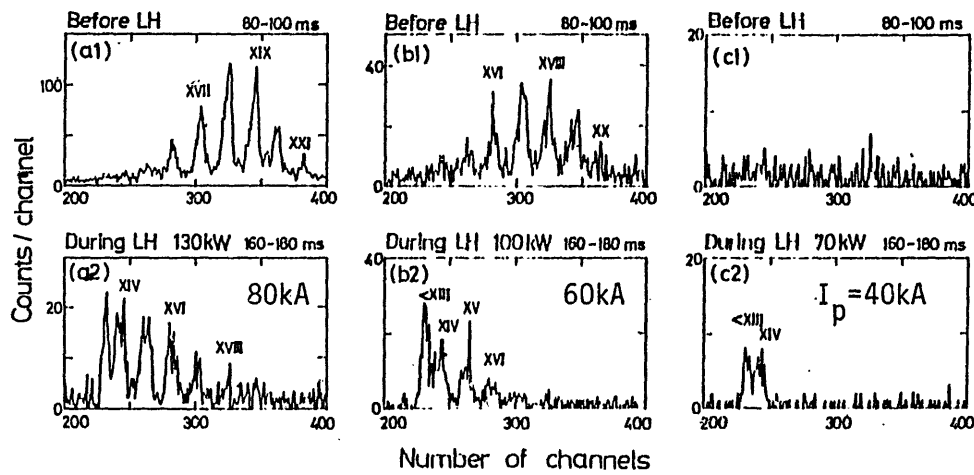


Fig.4 Experimental features of Ti  $K\alpha$  spectra before and during LHCD as a function of plasma current  $I_p$

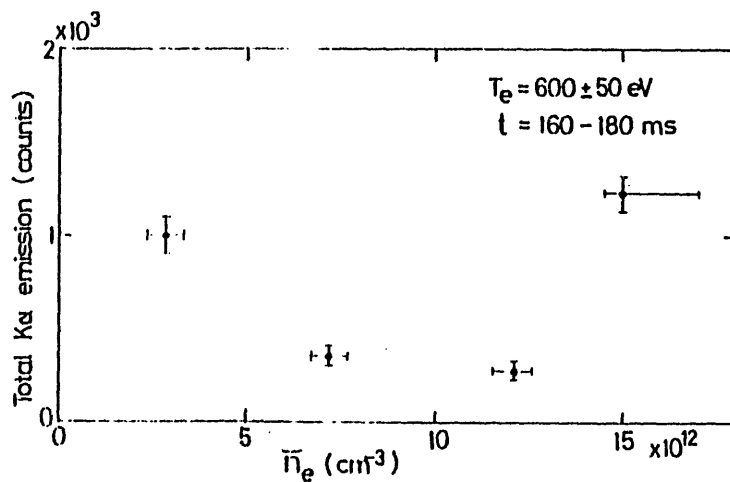


Fig.5 Electron density dependence of total  $K\alpha$  emissions.

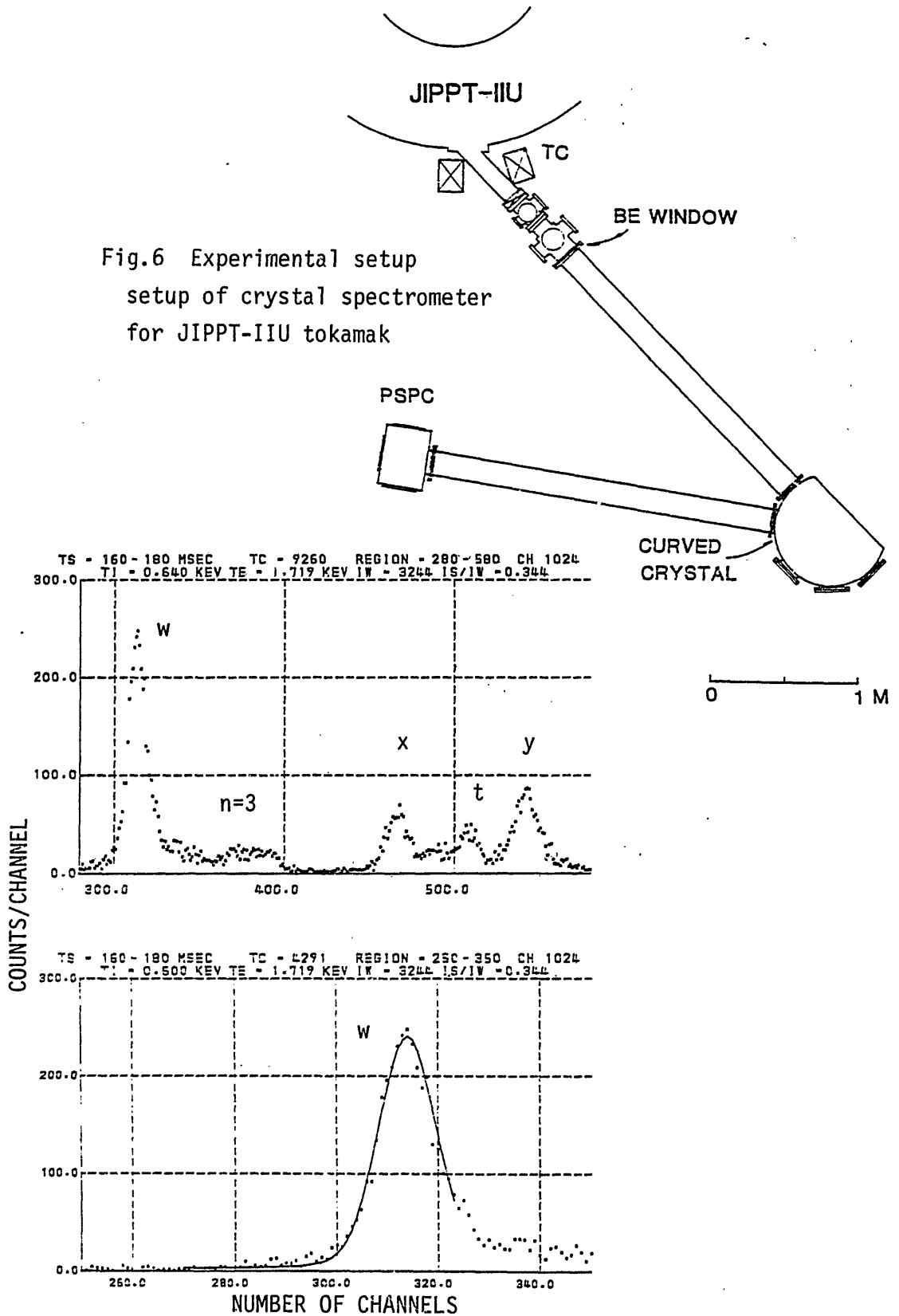


Fig.7 Typical example of ion temperature measurements. Upper display shows high-resolution titanium heliumlike spectrum. Lower display shows line fitting of w. The fitting curve indicates  $T_i$  of 600eV.

Spectroscopic measurement of non-local heat  
transport in laser produced plasma

by

M. Nakai, H. Azechi, N. Miyanaga, M. Itoh, T. Yabe,  
K. Mima, T. Yamanaka, and C. Yamanaka

Institute of Laser Engineering

Osaka University

Electron thermal flux in an ablation plasma was measured by using the x-ray spectroscopic technique. At the largest temperature gradient region, where the temperature scale-length was 25-70 times electron mean-free-path, the flux decreased to be 1/3 of the classical value. A temperature precursor due to non-local heat transport was observed in a high density region. These experimental features are in agreement with the theoretical predictions of the heat flux in the steep temperature gradient.

## Introduction

In the study of the inertial confinement fusion, the investigation of the heat transport is of great importance. Because the heat transport in the ablation region determines the structure of the ablation and, therefore, the absorption rate and the hydrodynamic efficiency of the pellet target. In the previous experimental works, results of measurements of ablation pressure, ablation mass rate and also the electron temperature profile ~~were compared~~ with predictions from hydrodynamic code simulations.<sup>6,8~10)</sup> And the heat flux was shown to be less than the classical value given by the Spitzer and Harm.<sup>1~5,7)</sup> Several mechanisms of this flux limitation are considered, e.g. 1) DC-magnetic field, 2) ion acoustic turbulence, 3) Weibel instability, 4) non-local heat transport. In order to clarify the mechanism of the flux limitation, we performed the experiment to measure the heat flux using the x-ray spectroscopic techniques. Under the experimental conditions, the mechanisms 2) and 3) may have negligible contribution, since the effective collision frequencies due to those mechanisms are estimated to be much smaller than the electron-ion collision frequency ( $\nu_{ei}$ ). In this paper, we present a direct measurement of heat flux and a comparison with the ratio of the temperature scale-length ( $L_T$ ) to the electron mean-free-path ( $\lambda_e$ ). It is shown that at the largest temperature gradient region (where the temperature scale-length was 25-70 times electron mean-free-path), the flux decreased to be one third of the classical value. Moreover, some problems about the spectroscopic measurement in this experiment and the CR model developed by one of the authors are also discussed.

## Experiment

### A. Experimental method and set-up

In 1-dimension and quasi-steady state ablation, the heat flux  $q$  is given by the following equation,<sup>11)</sup>

$$q = \frac{5}{2} \rho u c^2 + \frac{1}{2} \rho u^3 \quad (1)$$

Here  $\rho$  is the mass density,  $u$  is the flow velocity and  $c$  is the sound velocity. Therefore, to determine the heat flux, time and space resolved measurements of the electron temperature, density and flow velocity are required.

Figure 1 shows the diagnostic method. A plane target was irradiated by the one arm of the Gekko IV laser facility in Osaka university. The laser light with wavelength of  $1.05\mu\text{m}$  and gaussian shaped pulse width of 1.0 nsec was focused normal to the target surface through an (F/8) aspheric lens. The focal spot diameter was  $130\mu\text{m}$  and the laser energy was  $45\pm 5$  J. Absorbed laser intensity was  $(1.4\pm 0.3)\times 10^{14}$  w/cm<sup>2</sup>.

The x-ray emission of 1.5-5. keV was imaged on the x-ray streak camera with overall resolutions of  $20\mu\text{m}$  and 60 psec. The TLAP crystal spectrometer with  $20\mu\text{m}$  slit for spatial resolution was used to measure the spectra from 1. to 3. keV. In order to monitor the position of the cut-off density region, the second harmonic emission from the target was also imaged on a visible streak camera through a microscope objective with a 10 nm band width filter centered at 530 nm. The observation axes of these measurements are all perpendicular to the target normal. The direction of the spatial resolution are all parallel to the target normal.

Tracers, magnesium, aluminum and silicon, inbeded in plastic are irradiated by laser and ablated one by one. Since the x-ray intensity

is much stronger in tracers than in C-H, the flow diagram of the tracer can be observed by a x-ray streak camera with the spatial resolution parallel to the target normal. This enables us to measure the flow velocity along the flow line. As the tracer flows away, the spatially resolved x-ray line from such tracers is actually a time resolved one, from which density and temperature are determined. The relation between the position and the time of the tracer can be known through the streak image. The electron mean-free-path  $\lambda_e$  is obtained from the observed electron temperature and density. The temperature scale-length  $L_T$  is determined from the observed temperature profile along the tracer expansion.

#### B. Experimental results

Figure 2(a) is the picture of the x-ray streak camera. By separate shots with one and two out of the three tracers, we verified that each of the bright regions corresponds, in order, to silicon, aluminum and magnesium, respectively. Figure 2(b) is the corresponding x-ray spectrum. Figure 3 shows successive profiles of flow velocity, electron temperature and density along the flow of aluminum tracer. The results of Duston's CRE model<sup>13)</sup> were used to deduce the electron temperature from the line ratios of the aluminum lines:  $1s-2p/1s^2-1s2p$  and  $1s-2p/1s^2-1s4p$ . We used the Gabriel's formulae<sup>14)</sup> of the dielectronic satellite lines and the intercombination lines to the resonance line in order to determine the electron density. The value of electron density is also obtained by assuming a quasi-steady state flow and knowing the flow velocity, shown in Fig. 3 as closed circles. It is seen in Fig.3 that the plasma is heated up to 1.3 keV at the cut-off region and a thermal wave is formed in the observed region. A relatively flat precursor is observed ahead of the thermal front. The energy flux required to make such precursor region is

estimated to be 7% of the absorbed laser energy. This is too large to be explained solely by preheating due to hot electrons and/or soft x-rays.

In Fig. 4, The temperature scale-length divided by the electron mean-free-path(a), heat flux divided by the classical value(b) and divided by the free streaming heat flux(c) are plotted as a function of the position. For the peak temperature gradient( at  $x=70 \mu\text{m}$ ), the flux is considerably lower than the classical heat flux. The flux tends to be close to the classical value at the cut-off region and somewhat exceeds it at the high density region. The flux limit factor at the peak gradient region is 0.08. This value is in good agreement with the independent estimation obtained from the comparison of the experimental ablation mass rate with that from the computer simulation.<sup>12)</sup>

### C. Discussion

The experimental results can be explained by the non-local heat transport. Since heat is carried mainly by electrons with the velocity of 2-3 times larger than the electron thermal velocity, the range of those electrons can be much longer than the electron mean-free-path. At the large temperature-gradient region, those electrons respond not only to the local gradient but also to the gentle gradient at the top and the base of the heat front. The net flux is, therefore, reduced from the locally determined "classical value  $q_{S-H}$ ". At the top and the base, the flux can reach or exceed  $q_{S-H}$ . The excess of  $q$  is more pronounced in the base than in the top, since the tail of the electron distribution in the top streams into the base and increases the flux there. Thus the observed flux reduction at the smallest  $L_T/\lambda_e$ , the increase of  $q$  towards  $q_{S-H}$  at cut-off region and qualitatively explained by the non-local heat

transport. Figure 5 shows the experimental data of the heat flux normalized by the free streaming heat flux with the calculation by Y. Kishimoto for the uniform stationary plasma flow. Fairly good agreement is shown.

In conclusion, electron thermal flux in an ablation plasma was measured by using the x-ray spectroscopy. At the largest temperature gradient region, the heat flux decreased to be 1/3 of the classical value. A temperature precursor due to non-local heat transport was observed in a high density region. These experimental features are in agreement with the theoretical prediction of the heat flux in the steep temperature gradient.

#### Some problems about the spectroscopy in the experiment

In order to interpret the x-ray spectra, we used the results of the Duston's calculation. But, the use of x-ray line ratios is complicated by radiation transport to the extent that results will always have some uncertainty. Moreover the time-scales of this experiment might be too short to make the equilibrium assumption. Therefore, in order to investigate the problems such as follow, we are developing the collisional-radiative model similar to that of Duston.

#### Problems:

- 1) How does the accuracies of the atomic data affect the results?
- 2) How much is the plasma different from the equilibrium?
- 3) How much is the unaccuracy due to the finite spatial resolution?
- 4) How are the satellite lines and the intercombination lines affected by the redistribution of the populations by absorption?

The collisional-radiative model employed is similar to that of Duston. A general set of time-dependent atomic rate equations are

solved for a volume element of uniform plasma, homogeneous in temperature and total ion density. The CR model currently includes the following atomic processes: Collisional ionization, collisional, radiative, and dielectronic recombination, collisional excitation, collisional and spontaneous radiative de-excitation. The collisional ionization rates were calculated using a prescription suggested by Seaton<sup>15)</sup> and/or using that by Landshoff<sup>20)</sup>, and the radiative recombination rate coefficients were calculated by the detailed balance of photoionization rates.<sup>16)</sup> The dielectronic recombination rate coefficients are those calculated by Burgess,<sup>21)</sup> while the spontaneous decay rates were taken from the NBS tables<sup>17)</sup> or from oscillator strength extrapolations. The electron collision-excitation rate coefficients were those calculated by D.E.Post by semi-classical impact parameter method.<sup>18)</sup> The rates for the collisional processes from higher to lower energy states were calculated by the detailed balance of the corresponding upward collision rate coefficients. The processes of photoexcitation and stimulated emission are taken into account by a phenomenological transport model which allows photons to escape from an optically thick plasma by scattering into the optically thin wings of the absorption line profile, modifying the spontaneous emission rates by the optical depth of the plasma.<sup>19)</sup>

Figure 6. shows the line ratio of the aluminum H-like Ly- $\beta$  to He-like Ly- $\gamma$  as a function of the electron temperature at the ion density of  $10^{20}$  1/cc. The thickness of the plasma is assumed to be 60  $\mu\text{m}$ . We calculated using two different prescriptions for collisional ionization rates. Solid line is the result using the Seaton's and dashed line is using the Landshoff's prescription. Temperatures deduced from the line ratios show the difference about a factor of two.

In order to check the equilibrium assumption, the time-developed equations along the flow were solved. Figure 7 shows the comparison

between the line ratios at equilibrium and those obtained from the time-depending rate equations. Plasma parameter were given from the results of the computer simulation by 1-dimensional hydrodynamic code (HIMICO).<sup>12)</sup> The temperature peak indicated in the Fig.7 corresponds to the critical surface. In both of two graphs in Fig.7, differences are not so severe inside of the ablation region.

Figure 8 shows the effect of the spatial resolution of our x-ray spectrometer. Solid lines are the original plasma parameters given by the simulation results. Dashed and dotted lines are the electron temperatures calculated from the line ratios, locally averaging the line intensities by slit width of the spectrometer. At the highest region, the deviation up to 50 % was shown.

Figure 9 is the level structure of our model. The levels of the principal quantum number up to 5 are considered. And the population of each level in the same principal quantum number is distributed by statistical weights. We haven't included the doubly excited states and also the dielectronic recombination to the higher excited levels. Therefore, we must improve our code to investigate the last problem. Moreover, in order to take account of the plasma structure, we must carry out the ray-tracing frequency by frequency.

### References

- 1) D.R. Gray and J.D. Kirkenny, Plasma Phys. 22, 81(1980).
- 2) L. Spitzer and R. Harm, Phys. Rev. 89, 977(1953).
- 3) A.R. Bell, R.G. Evans and D.J. Nicholas, Phys. Rev. Lett. 46,243(1981).
- 4) D. Shvarts, J. Dettrez, R.L. McCrory and C.P. Verdon, Phys. Rev. Lett. 47,247(1981); Y. Kishimoto and K. Mima, J. Phys. Soc. Jpn. 52,2389(1983).

- 5) Albritton, Phys. Rev. Lett. 50, 2078(1983).
- 6) R.J. Mason, Phys. Rev. Lett. 47, 652(1981); J.P. Matte and J. Virmont, Phys. Rev. Lett. 49, 1936(1982); J.P. Matte, T.W. Johnston, J. Deletterz and R.L. McCrory, Phys. Rev. Lett. 53, 1961(1984).
- 7) J.E. Luciani, P. More and J. Virmont, Phys. Rev. Lett. 51, 1664 (1983).
- 8) W.C. Mead et al., Phys. Fluids, 27, 1301(1984).
- 9) B. Yaakkobi et al., Phys. Fluids, 27, 516(1984).
- 10) A. Hauer, W.C. Mead, O. Willi, J.D. Kilkenny, D.K. Bradley, S.D. Tabatabaei and C. Hooker, Phys. Rev. Lett. 53, 2563(1984).
- 11) C.E. Max, C.F. Mckee and W.C. Mead, Phys. Fluids, 23, 620(1980).
- 12) T. Yabe, K. Mima, K. Yoshikawa, H. Takabe, and M. Hamano, Nucl. Fusion, 21, 803(1981).
- 13) D. Duston, J. Davis, Phys. Rev. A21, 1664(1980), & A24, 1505(1981).
- 14) A.H. Gabriel, J. Phys. B5, 673(1972); Not. R. Astr. Soc, 160, 99 (1972).
- 15) M.J. Seaton, Proc. Phys. Soc. London 79, 1105(1962).
- 16) V.L. Jacobs, J. Davis, P.C. Kepple, and M. Blaha, Astrophys. J. 211, 605(1977).
- 17) W. Wiese, M. Smith, and B. Miles, Atomic Transition Probabilities (U.S.GPO, Wadhington, D.C., 1969), Vol. II.
- 18) D.E. Post, A. D. N. D. 20, 434(1977).
- 19) D. Duston and J. Davis, NRL Memorandum Report No. 3846, 1978.
- 20) R.K. Landshoff and J.D. Perez, Phys. Rev. A13, 1619(1976).
- 21) A. Burgess and H.P. Summers, Mon. Not. R. Astron. Soc. 174, 345(1976).

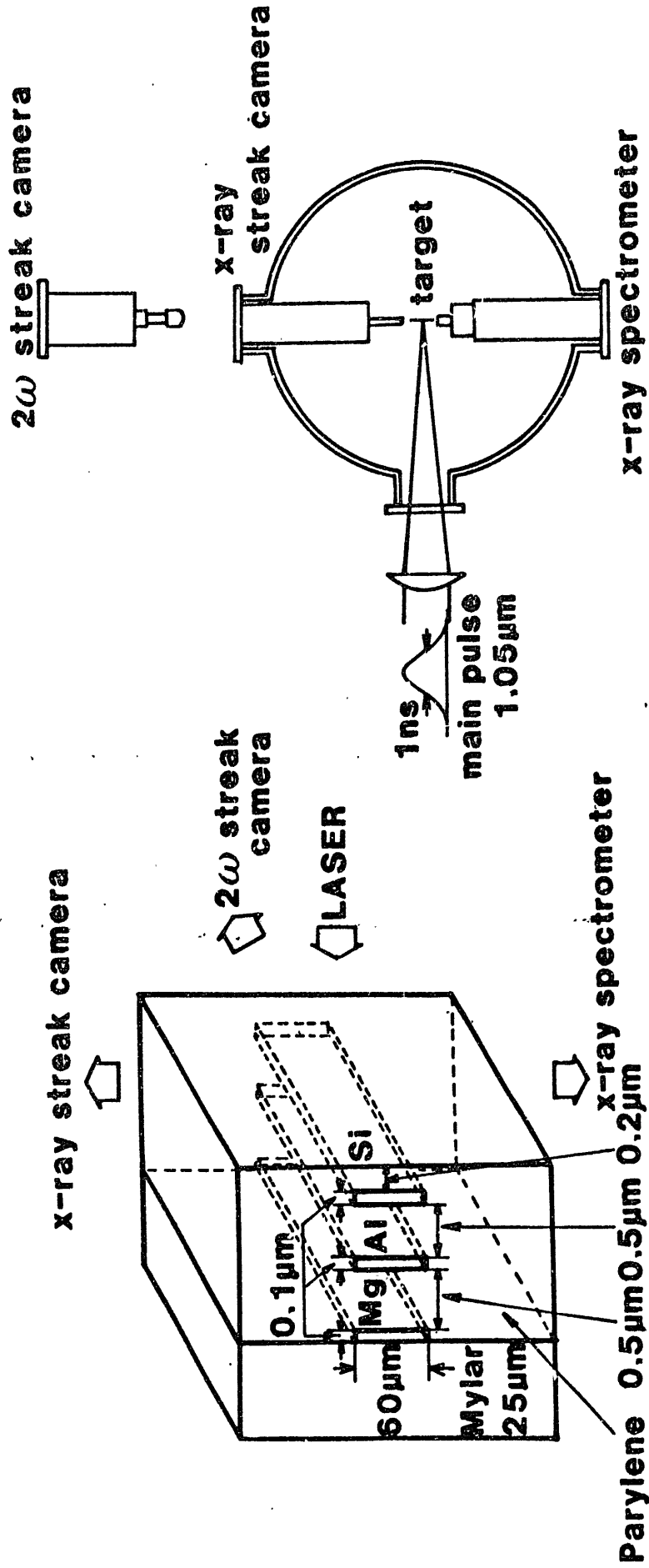
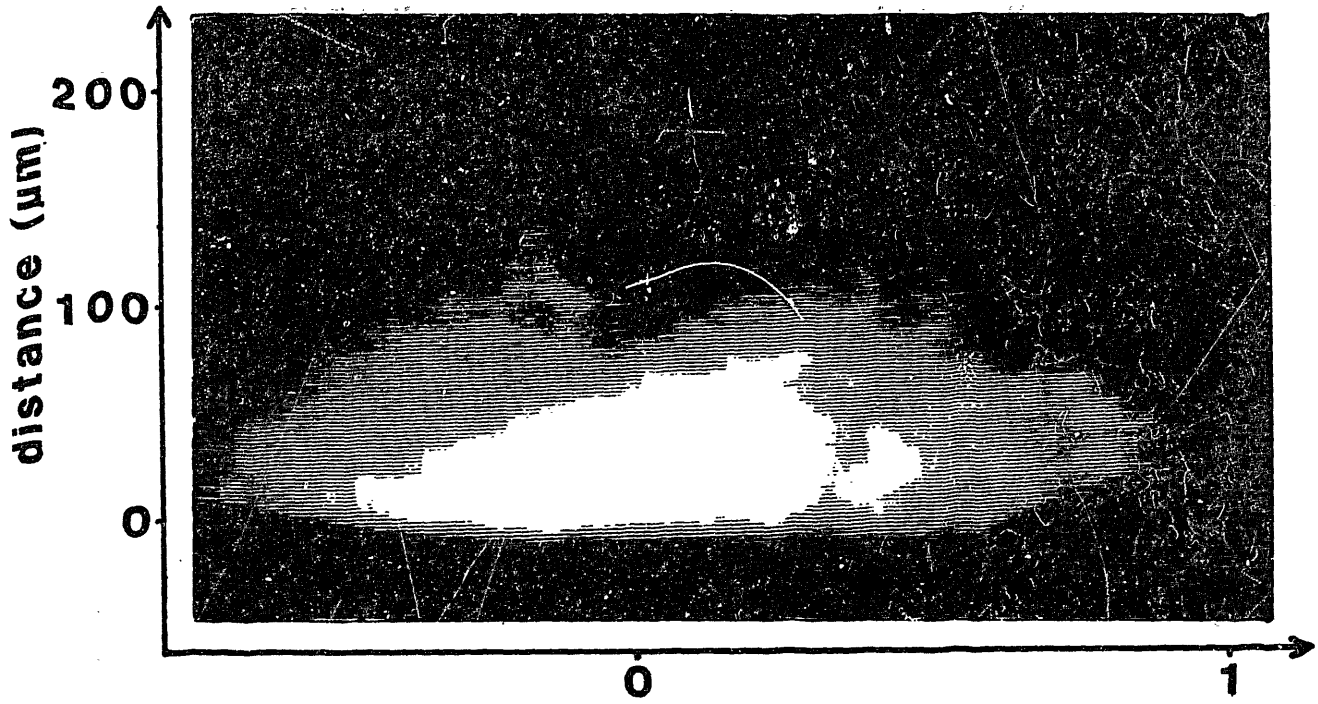


Fig. 1 Schematics of a target and diagnostics.

(a)

**X-RAY STREAK  
PHOTOGRAPH**



(b)

**X-Ray  
Spectroscopy**

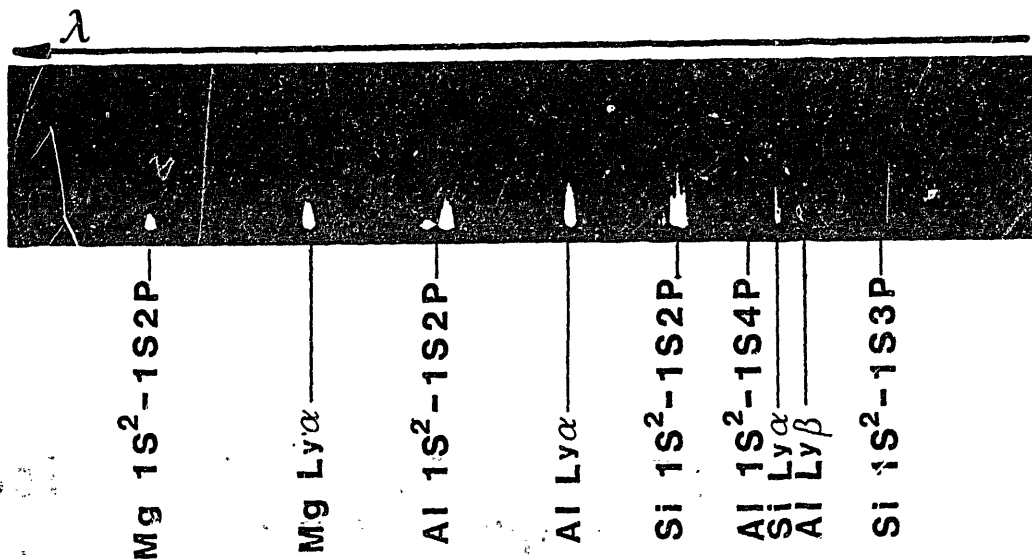


Fig. 2 Experimental data. The top(a) is a picture from the x-ray streak camera and the bottom(b) is the x-ray spectrum taken by the crystal spectrometer.

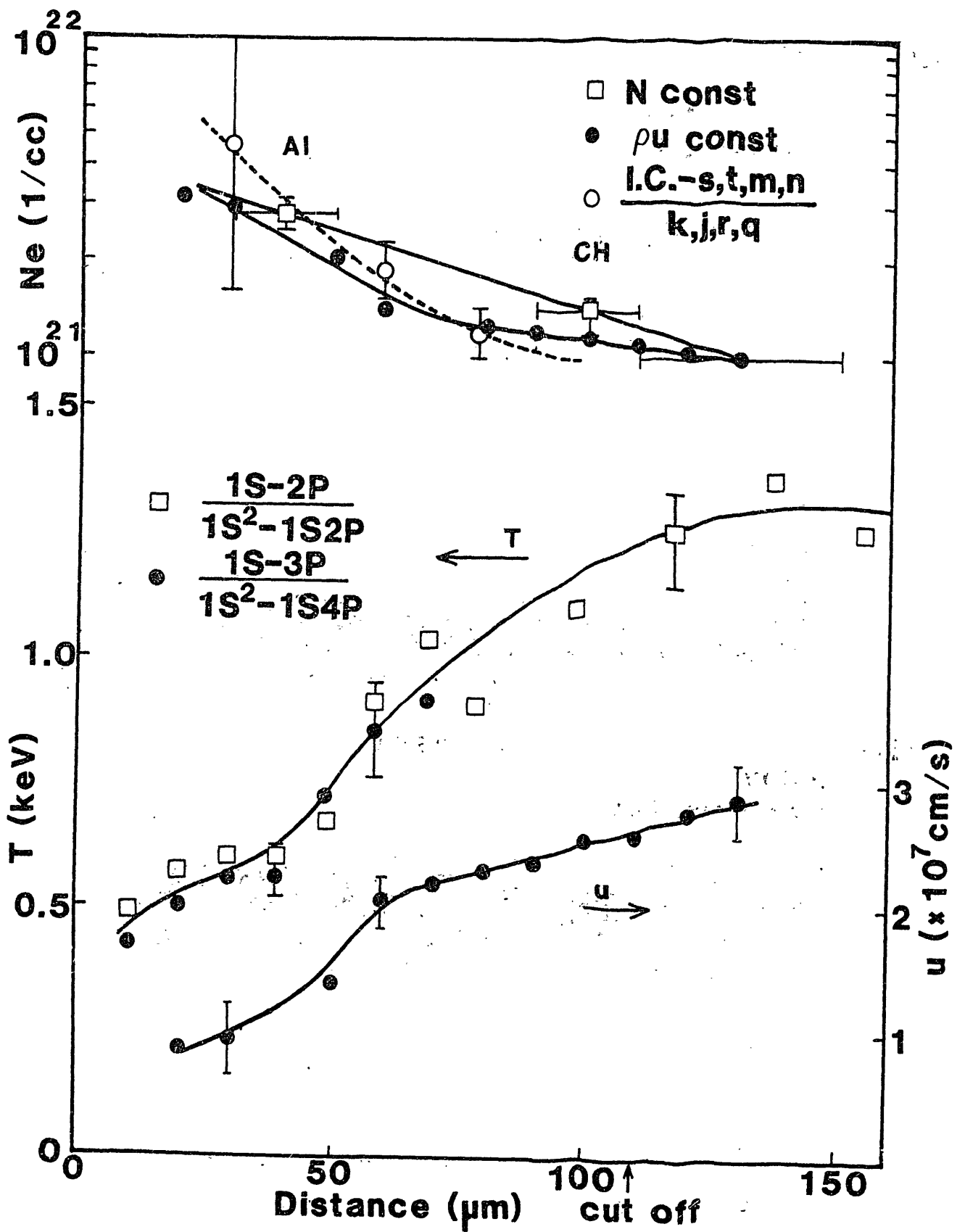


Fig. 3 Profiles of flow velocity, electron temperature and density along Al tracer.

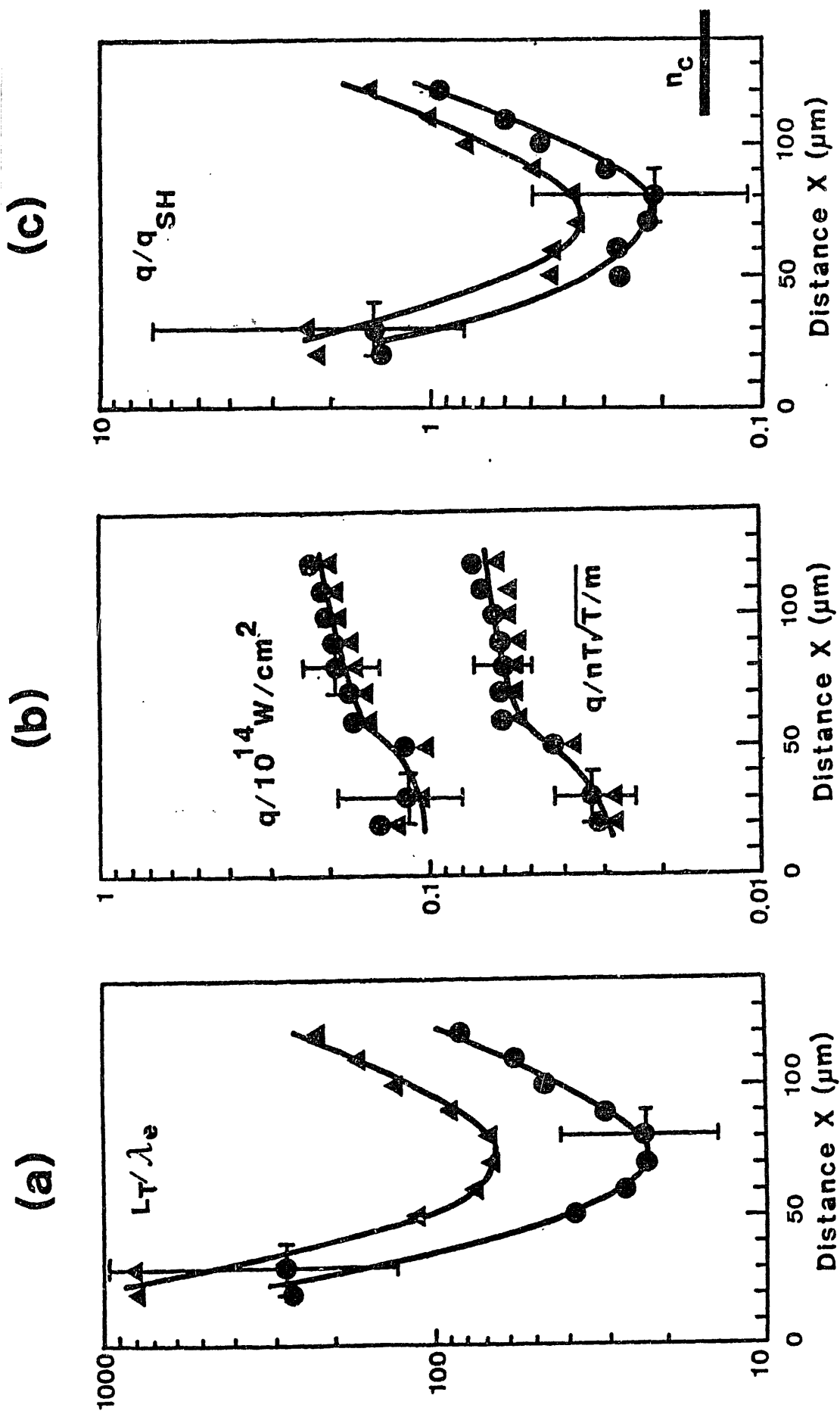


Fig. 4 (a) Temperature scale-length  $L_T$  normalized by electron mean-free-path  $\lambda_e$ , (b) heat flux  $q$  normalized by the free streaming value  $nT/\sqrt{T/m}$ . (c)  $q$  normalized by the classical value  $q_{S-H}$ . Plots are calculated as both  $Z=3.5$ ,  $A=6.5$  ( $\bullet$ ) and  $Z=12$ ,  $A=27$  ( $\blacktriangle$ ).

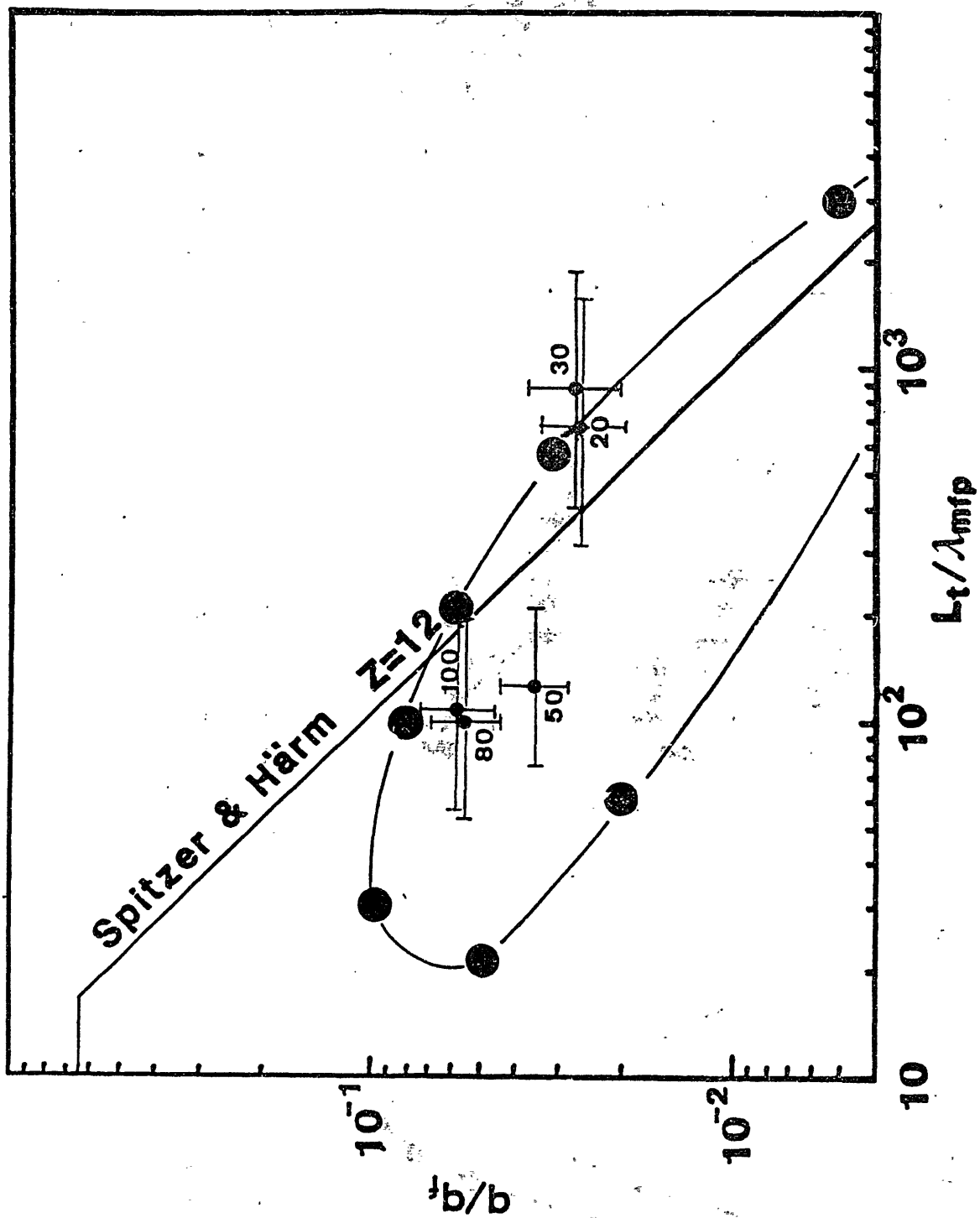


Fig. 5 Heat flux as a function of temperature scale-length.

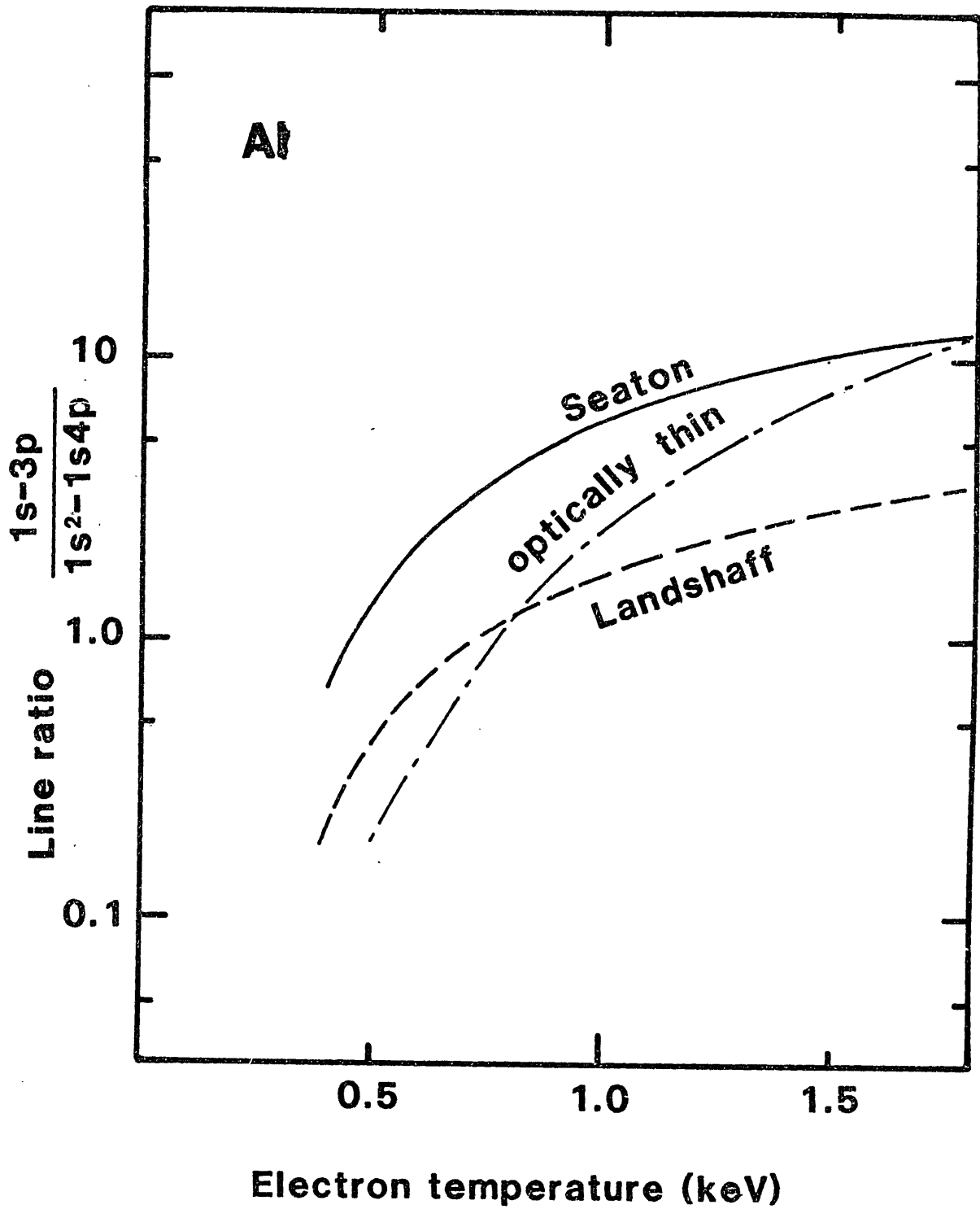


Fig 6 Comparison of two prescriptions of collisional ionization rates. One is after M.J. Seaton<sup>15)</sup> and the other after R.K. Landshoff.<sup>20)</sup>

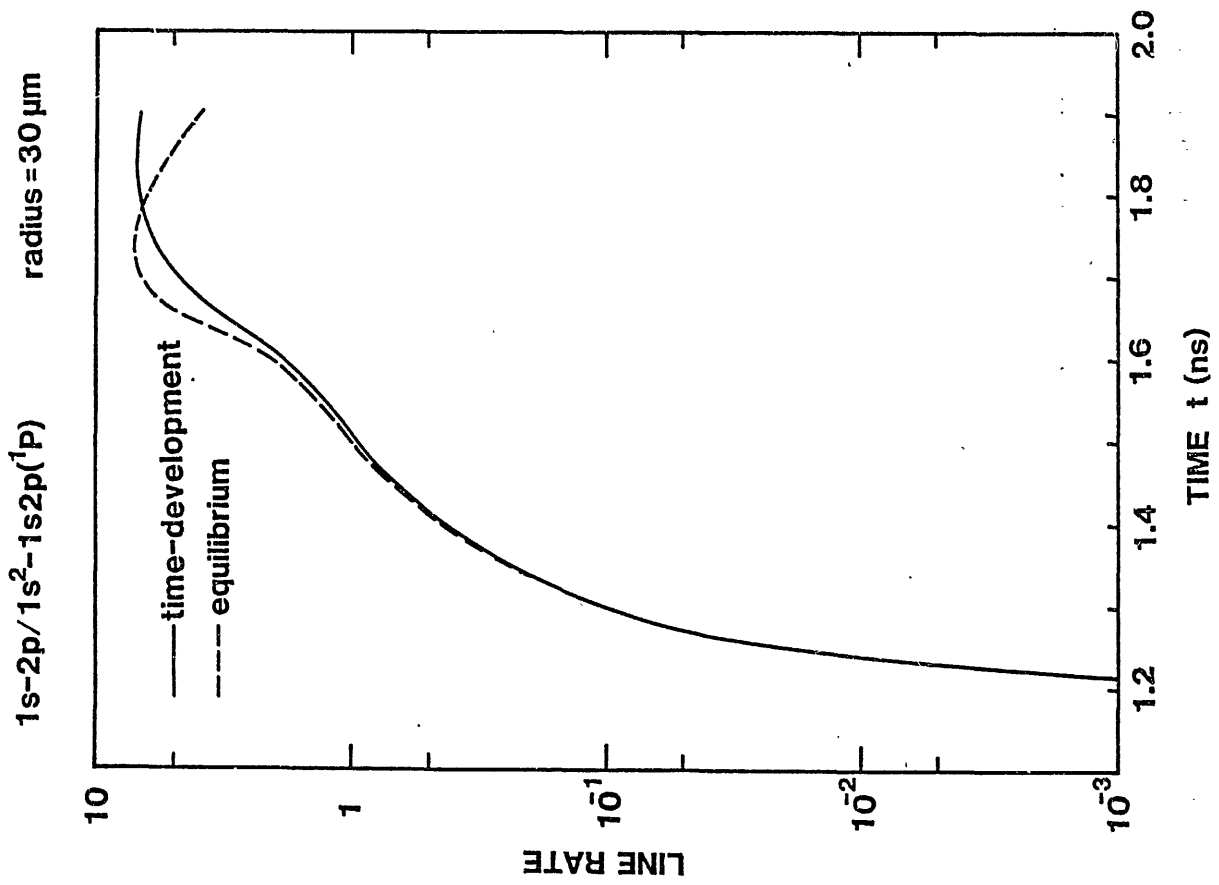
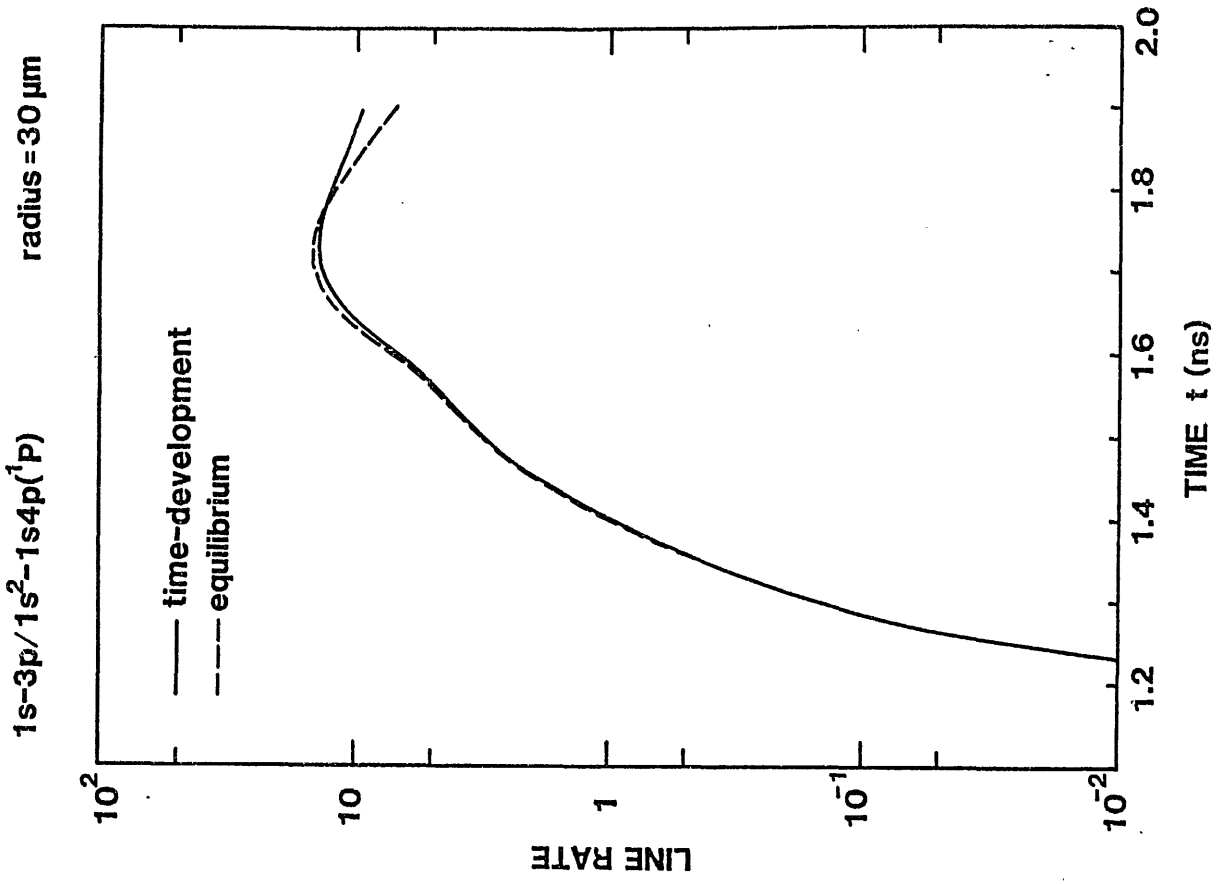


Fig. 7 Time-development of line ratios.

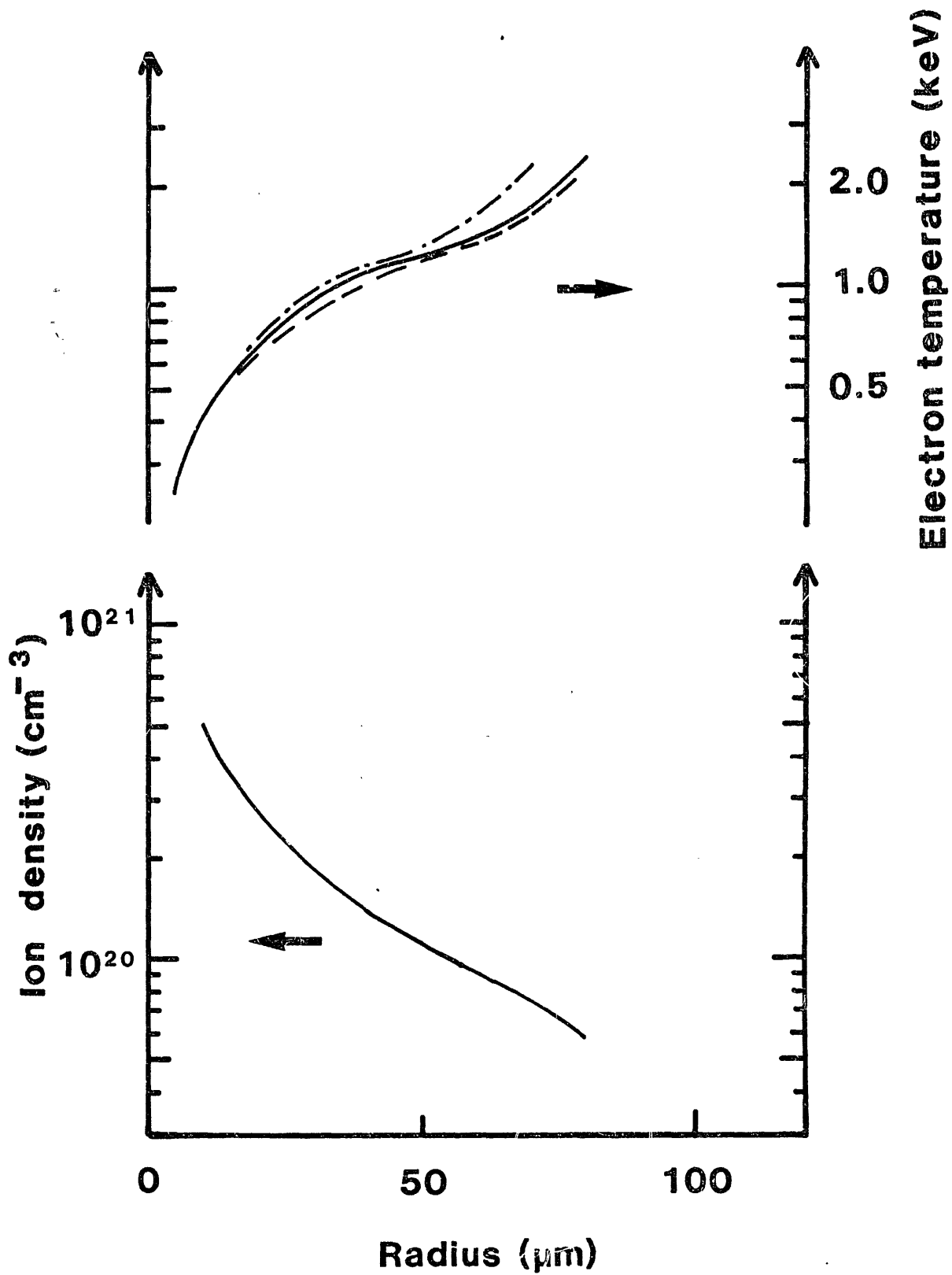


Fig. 8 Influence of the finite spatial resolution of spectroscopy. Spatial resolution of  $20 \mu\text{m}$  and  $25 \mu\text{m}$  are assumed for dashed and dotted line, respectively.

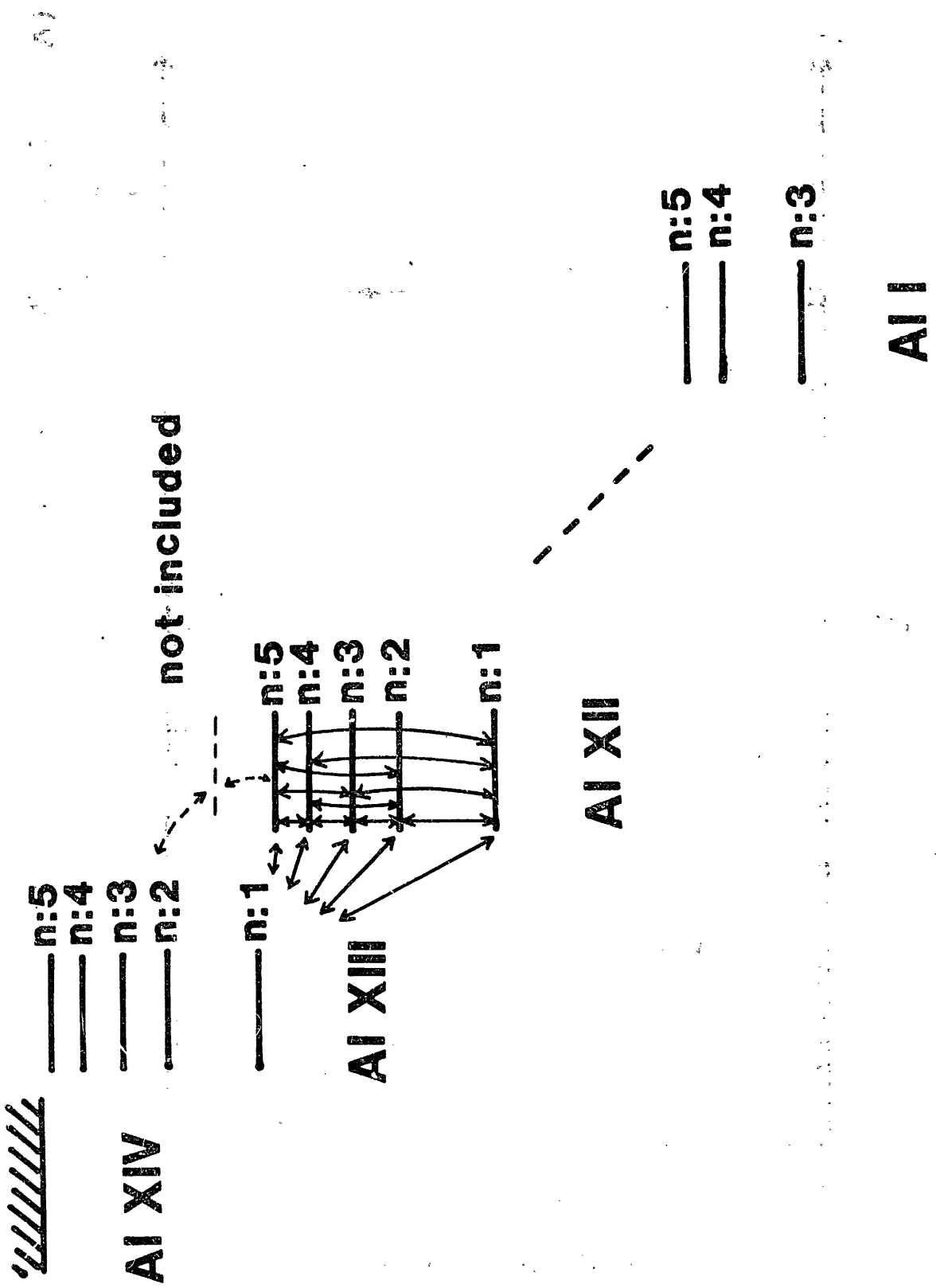


Fig. 9 Level structure of the CR model.

INDIRECT MECHANISMS IN ELECTRON-IMPACT IONIZATION  
OF MULTIPLY CHARGED IONS

Ronald A. Phaneuf and Donald C. Gregory  
Physics Division  
Oak Ridge National Laboratory  
Oak Ridge, Tennessee 37831, USA

The important role of indirect-ionization mechanisms in electron-impact ionization of multiply charged ions has been emphasized by some recent experiments conducted with the ORNL-ECR multicharged ion source. Illustrative examples of investigations of the Mg-isoelectronic and Fe-isonuclear sequences are presented and compared with the results of detailed theoretical calculations. New experimental data is also presented concerning the role of resonance effects in the ionization of Li-like  $O^{5+}$  and Na-like  $Fe^{15+}$  ions.

I. INTRODUCTION

Ionization by electron impact is a complex process, since a large number of mechanisms can cause the ejection of electrons from bound states of atomic systems. As an atom becomes more highly ionized, fewer electrons remain to screen the nucleus, and its binding energy increases. Since the direct or "knock-out" ionization cross section scales roughly as the inverse square of the binding energy, the direct ionization cross section becomes progressively smaller as the charge state of a given ionized atom increases. Indirect pathways to ionization begin to compete with direct ionization and even to dominate the ionization of many highly charged ions. Mechanisms which involve resonances and which may appear at first consideration to be exotic pathways to ionization have been predicted to make measurable contributions to the ionization of some highly charged ions.

## II. IONIZATION MECHANISMS

The most important indirect ionization mechanism is the so-called excitation-autoionization process. The incoming electron excites an inner-shell electron, leaving the ion in a core-excited state which can subsequently decay by autoionization, resulting in a net ionization process. Depending on the excitation energy of the core-excited state and the branching ratio for its decay, the ejection of more than one electron may be likely, leading to a net multiple ionization process. The cross section for excitation of an ion has the distinguishing characteristic of being finite and often largest at its threshold energy. Thus a particular inner-shell excitation can produce an abrupt jump in the ionization cross section at the threshold for the excitation process. Careful measurements of the energy dependence of the ionization cross section can thus provide quantitative information about excitation processes as well.

A core-excited state may also be produced by the direct ejection of an inner-shell electron from an ion. Subsequent release of another electron by autoionization then leads to a net double ionization event. If the collisionally-ejected core electron is from a more deeply-lying shell, the decay of the vacancy state may result in the ejection of several electrons via the Auger process. This ionization-autoionization process is the most important multiple-ionization mechanism for most ions. It is generally not considered to be an indirect ionization mechanism, since the collisional process just involves the direct ejection of an inner-shell electron.

A somewhat more exotic indirect-ionization pathway has as its first step the same resonant process that leads to dielectronic recombination. In this case, an incident electron approaches the ion with just slightly less than the minimum energy required to excite an inner-shell electron, but due to acceleration in the ionic Coulomb field, gains enough energy to

excite the transition. In so doing, it becomes captured into a doubly excited state of the ion which can decay by a number of pathways, including single Auger emission, double Auger emission, or radiative decay. The first leads to a scattering resonance, the second to ionization and the third to dielectronic recombination. This is a highly resonant process which can occur only for certain values of the electron energy, since there must exist a doubly-excited state of the ion into which the incoming electron can be captured. The process leading to a net ionization event has been called resonant-excitation-double-autoionization (REDA), and was first postulated by LaGattuta and Hahn<sup>1</sup> in 1981 as playing an important role in the electron-impact ionization of Na-like Fe<sup>15+</sup>.

The mechanisms of direct single ionization, excitation-autoionization, ionization-autoionization and resonant-excitation-double-autoionization are all generally considered to be first-order collisional processes. In each case, the incident electron interacts through the two-body Coulomb interaction to promote a single target electron during the collision.

### III. EXPERIMENTAL METHOD

Cross sections for electron-impact ionization of multiply charged ions have been measured using the intersecting-beams technique by a number of groups<sup>2-5</sup>, and a schematic of the apparatus currently in use at Oak Ridge<sup>2</sup> for such experiments is shown in Figure 1. A mass/charge analyzed beam of multiply charged ions is directed into an ultra-high vacuum chamber, deflected through 90 degrees to remove ions which may have changed charge in flight from the ion source, and intersected by an electron beam of variable energy. The emerging ion beam then enters a double-focusing magnetic spectrometer which separates the ionized ions from the parent beam. The ionized ion "signal" is further deflected and counted by a particle multiplier, while the parent-ion and electron beams are collected in

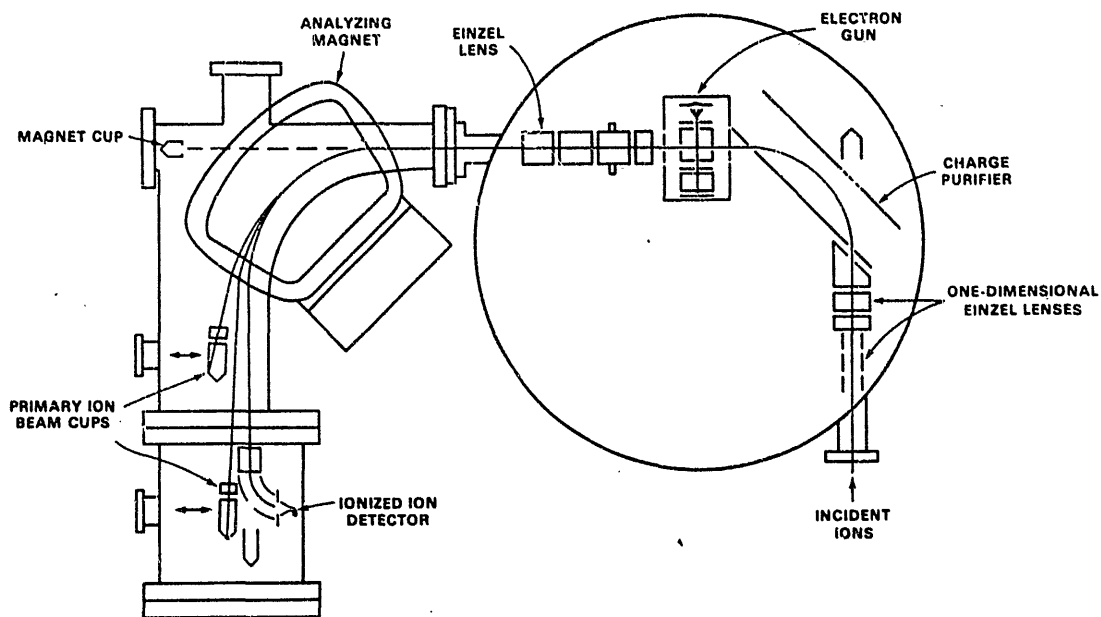


Figure 1. Schematic of electron-ion crossed-beams apparatus used to study electron-impact ionization of multiply charged ions at ORNL.

Faraday cups. The recently implemented magnetic charge analyzer system has permitted the resolution of initial/final charge ratios ranging from 4/5 to 15/16.

#### IV. EXCITATION-AUTOIONIZATION OF MAGNESIUM-LIKE IONS

A recent series of ORNL-JILA collaborative experiments<sup>6</sup> and a parallel theoretical investigation<sup>7</sup> has focused on electron-impact single ionization of Mg-like ions. In Figure 2, the experimental cross-section data for ionization of  $S^{4+}$ ,  $Cl^{5+}$  and  $Ar^{6+}$  are compared to theoretical and semiempirical predictions for direct 3s outer-shell ionization. The cross-section measurements show abrupt changes in slope near 150, 200 and 250 eV for  $S^{4+}$ ,  $Cl^{5+}$  and  $Ar^{6+}$ , respectively. These are signatures of the onset of 2p-nl inner-shell excitation-autoionization, which may be seen to increase in importance relative to the direct 3s outer-shell ionization as the ionic charge increases along the sequence.

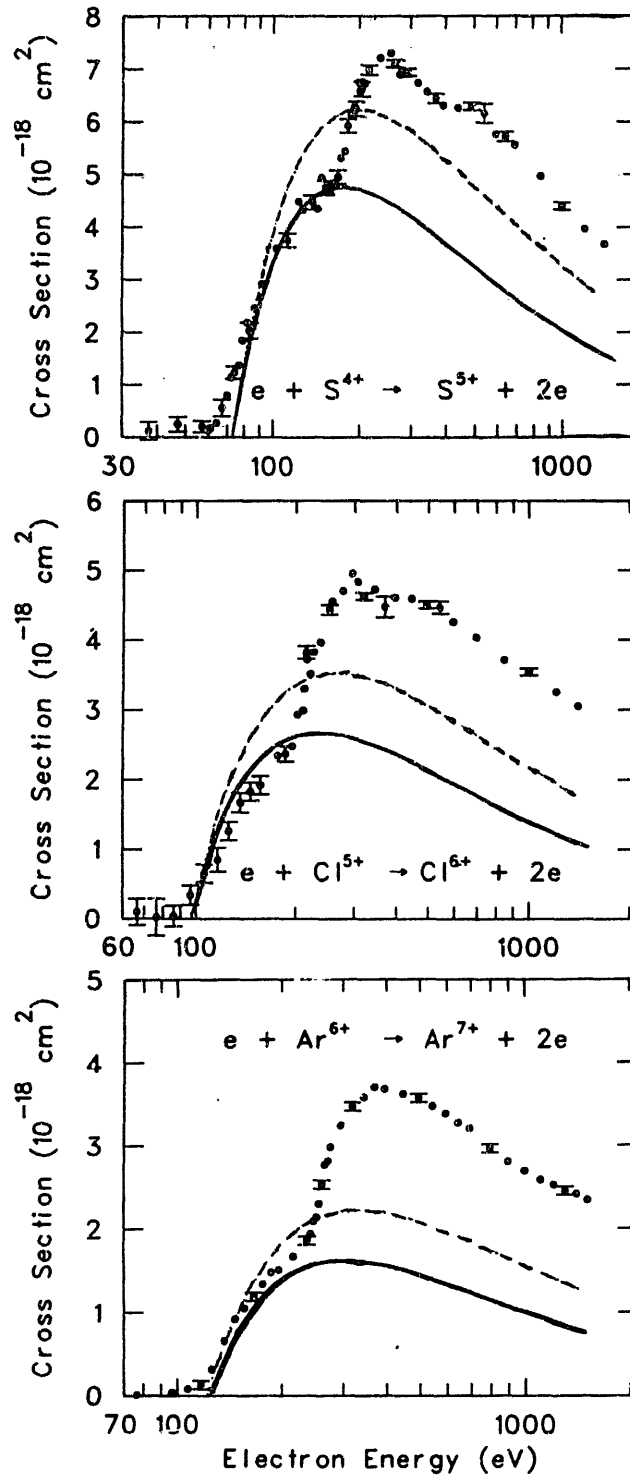


Figure 2. Comparison of experimental cross sections of Howald et al.<sup>6</sup> for electron-impact ionization of Mg-like ions with semiempirical Lotz formula (dashed curves) and scaled theoretical distorted-wave calculations (solid curves) for direct 3s outer-shell ionization. The abrupt changes in slope signify the onset of 2p inner-shell excitation-autoionization.

A closer inspection of the data for this sequence reveals that the cross-section measurements onset at energies which are about 10 eV below the threshold energies for excitation from the  $2p^63s^2$  ground state, suggesting the presence of  $2p^63s3p$  metastable ions in the experimental reactant beams. The measured cross sections also do not fall off as rapidly as expected after the peak in the cross section, suggesting that another process besides excitation-autoionization is contributing to the ionization cross section at higher energies.

The situation may be more easily understood by referring to Figure 3, which shows the relevant energy levels and transitions for  $S^{4+}$ . The only additional process which could be contributing at energies near 200 eV is direct 2p inner-shell ionization, but this should lead via subsequent Auger decay to a net double ionization, and not contribute to the single-ionization measurement. The answer to this puzzle is that while 2p inner-shell ionization from the  $2p^63s^2$  ground state will result in autoionization to yield  $S^{6+}$ , the same process from the metastable  $2p^63s3p$  state of  $S^{4+}$  will yield Na-like  $2p^53s3p$ , many levels of which are known to be metastable against autoionization with microsecond and longer lifetimes<sup>8</sup> — long enough to survive the experiment. These same levels have been identified as having potential importance in X-ray laser development.

Figure 4 shows a comparison between experiment and detailed distorted-wave theoretical calculations by Pindzola and coworkers<sup>7</sup> for ionization of metastable  $2p^63s3p$   $S^{4+}$  ions. These calculations include contributions from direct 3s and 3p ionization, 2p-nl excitation-autoionization, and direct 2p ionization. The level of agreement suggests that the metastable levels are playing a significant role in the ionization of Mg-like ions. On the basis of statistical weights alone, one would have expected a significant fraction of Mg-like ions in the experimental reactant beam to be in metastable

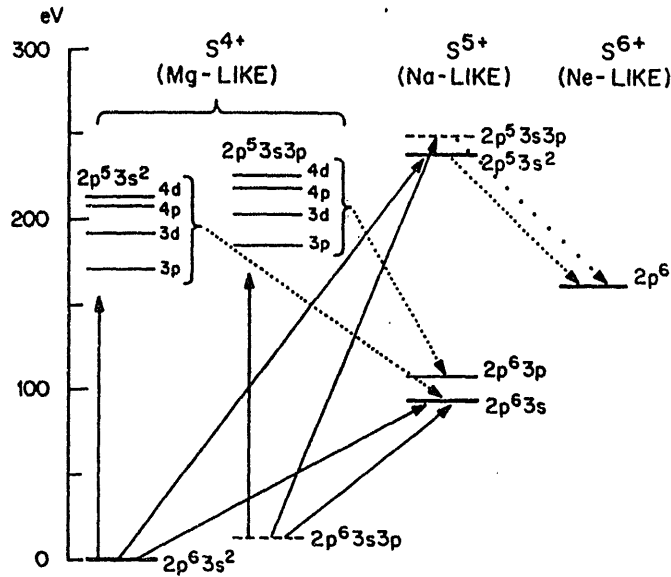


Figure 3. Energy levels and important transitions in the electron-impact ionization of Mg-like  $S^{4+}$ , from Ref. 6. Vertical arrows denote excitation processes, inclined solid arrows denote direct ionization, and dotted arrows denote autoionization pathways. Dashed energy levels indicate metastability against radiative or Auger decay.

states. Subsequent studies of electron-impact ionization of multiply charged iron ions suggest that metastable levels play an important role in the ionization balance in the plasmas where they are created.

#### V. THE IRON ISONUCLEAR SEQUENCE

Atomic processes involving iron and its ions are of considerable current interest because of its importance as an impurity in magnetically-confined fusion plasmas. Recently, a series of experiments on electron-impact ionization of Fe ions was completed using the ORNL-ECR multicharged ion source. This investigation included cross-section measurements for ion charge states 5, 6, 9, 11, 13 and 15. A parallel theoretical study was also carried out, with the goal of establishing the validity of a configuration-average model for these partially-stripped ions with complex

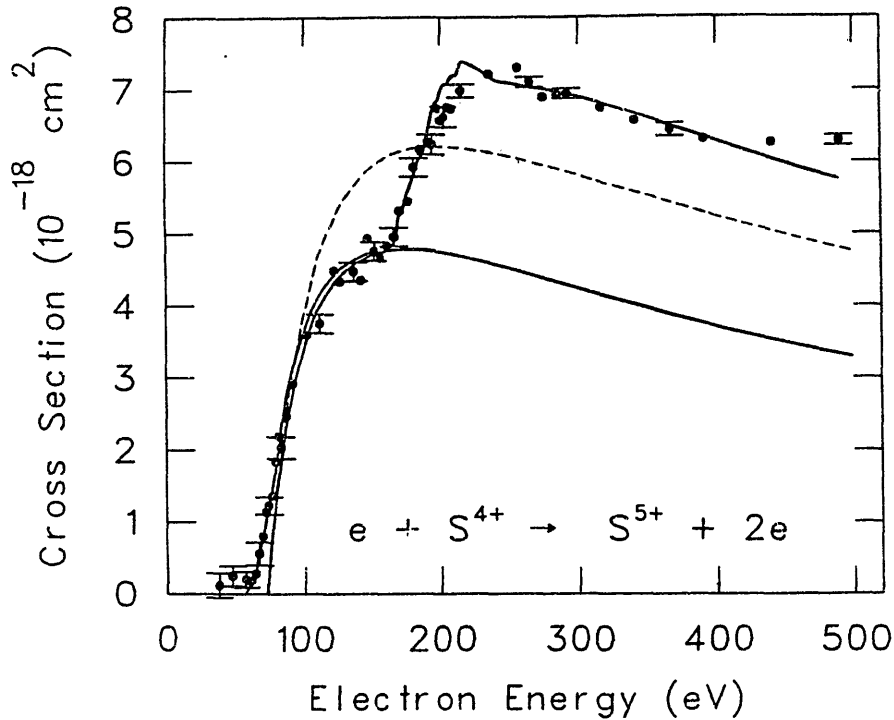
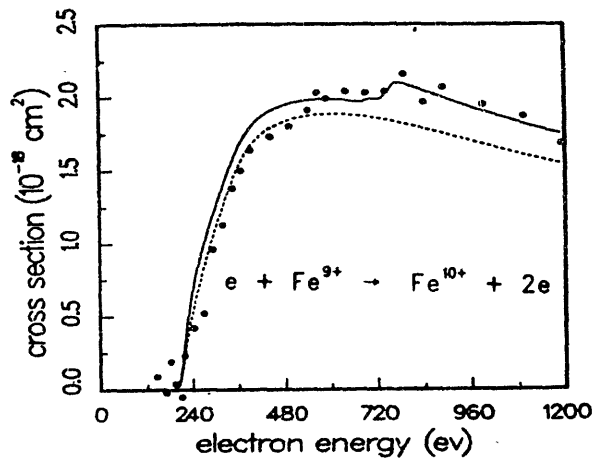


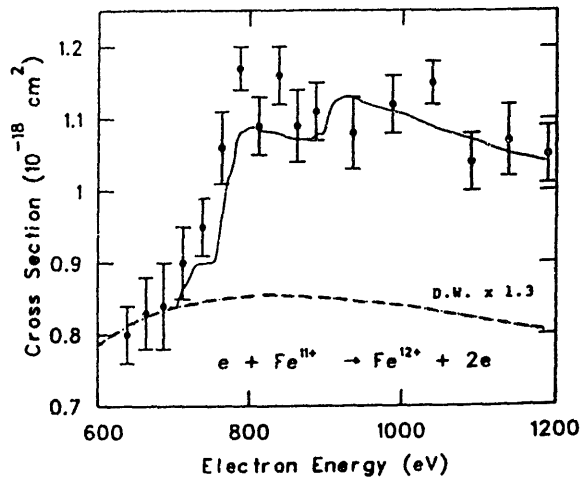
Figure 4. Comparison of theoretical and experimental results for electron-impact ionization of  $S^{4+}$ , from Ref. 7. The calculation represents ionization from the  $2p^6 3s 3p$  metastable levels. The dashed curve represents direct ionization only, while the solid curve includes contributions due to  $2p-nl$  excitation-autoionization.

electronic structures. A primary objective of these investigations was to quantify the role of excitation-autoionization processes along the iron sequence. Reports have been prepared for publication on the experimental results<sup>2</sup> for charge states 5, 6 and 9 and on the calculations<sup>9</sup> for charges 5, 6, 9, 11 and 13.

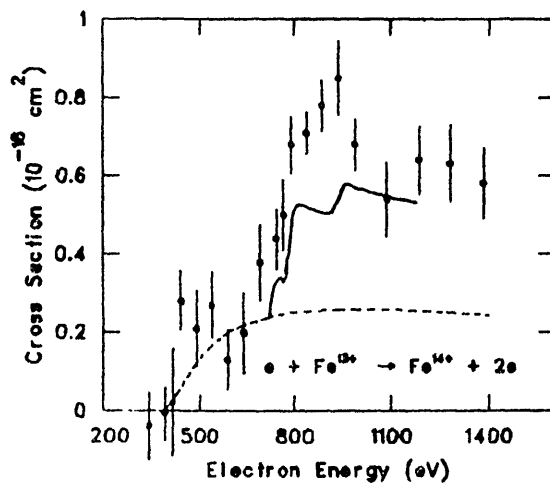
Experimental cross-section data and theoretical calculations for electron-impact ionization of  $Fe^{9+}$ ,  $Fe^{11+}$  and  $Fe^{13+}$  are compared in Figure 5. The calculations are based on the configuration-average-distorted-wave-statistical model, and include contributions of indirect  $2p-nl$  inner-shell



$\text{Fe}^{9+}$



$\text{Fe}^{11+}$



$\text{Fe}^{13+}$

Figure 5. Comparison of experimental<sup>2</sup> and theoretical<sup>9</sup> cross sections for electron-impact ionization of three members of the Fe-isonuclear sequence. Dashed curves represent distorted-wave calculations for direct ionization only, and solid curves represent the total ionization cross section, which includes contributions due to indirect excitation-autoionization calculated in the average-configuration-distorted-wave-statistical model.

excitation-autoionization channels. The determination of these contributions is based on the assumption of a statistical distribution of the excitation collision strength among the various levels, and on the calculated fraction of excited levels which are autoionizing.

The theoretical calculations for these ions are in generally good agreement with experiment, and provide some additional information about the measurements. For  $\text{Fe}^{9+}$ , the theoretical result shown is for ionization from  $3s^23p^43d$  metastable configuration only, and suggests that predominantly metastable  $\text{Fe}^{9+}$  ions are produced by the ECR source, as was found to be the case for Mg-like ions. Statistical weights and calculations of decay lifetimes of the levels in the  $3s^23p^43d$  configuration suggest that a significant fraction of the incident ion beam would be expected to be in metastable states. The fractional contribution of excitation-autoionization ( $2p-nl$ ,  $3s-nl$ ) in this case is only 10-15%.

The situations for  $\text{Fe}^{11+}$  and  $\text{Fe}^{13+}$  are somewhat different. The comparison between theory and experiment suggests that the  $\text{Fe}^{11+}$  and  $\text{Fe}^{13+}$  ion beams are predominantly in their respective ground  $3s^23p^3$  and  $3s^23p$  configurations. The fractional contributions of excitation-autoionization ( $2s-3d$ ,  $2p-nl$ ) are also larger than for  $\text{Fe}^{9+}$ , about 30% for  $\text{Fe}^{11+}$  and 60% for  $\text{Fe}^{13+}$ .

Similar comparisons between experiment and theory for the other members of the Fe-isonuclear sequence which have been investigated show that there is no clear pattern in the relative magnitudes of excitation-autoionization contributions along the sequence. The configuration-average-distorted-wave calculations in general give relatively accurate predictions of these indirect-ionization contributions. However, a careful analysis must be made to determine which of the hundreds of individual excited levels are autoionizing, and which are bound. Each ionization stage must be considered individually in order to obtain accurate predictions of ionization cross

sections for ions with such complex electronic structures. Experiments currently under way for  $\text{Ni}^{9+}$  and  $\text{Cr}^{9+}$  will establish whether the information gained from the Fe-isonuclear sequence may be reliably extended to neighboring ions of different charge which are isoelectronic to the  $\text{Fe}^{9+}$  cases studied.

## VI. RESONANCES IN ELECTRON-IMPACT IONIZATION

Substantial resonance contributions to the cross section for electron-impact ionization were first predicted by LaGattuta and Hahn<sup>1</sup> in 1981. In a series of electron-impact ionization measurements in the Xe-isonuclear sequence<sup>10</sup>, some evidence may have been obtained for this so-called resonant-excitation-double-autoionization (REDA) process, although no individual resonances could be resolved. The experimental data were characterized by an apparent smearing of calculated 4d-n1 excitation-autoionization contributions<sup>10</sup> to energies some tens of eV below the calculated threshold energies, which was suggestive of the REDA process. Such a broad feature would be expected for these ions because of the number of individual 4d-n1 level excitations involved would cause the associated resonances to overlap. The calculations could not however account for the observed magnitudes of this effect, and thus this study remains inconclusive as to whether or not the REDA mechanism is responsible.

In an effort to better characterize the role of the REDA process in ionization, the measurements at ORNL of cross sections for electron-impact ionization along the Fe-isonuclear sequence have very recently been extended to the Na-like  $\text{Fe}^{15+}$  case.<sup>11</sup> The results of this experiment are compared to the predictions of LaGattuta and Hahn<sup>1</sup> for this ion in Figure 6. The theory includes direct ionization, 2p-n1 excitation-autoionization and also the REDA process (indicated by the hatched region). The electron energy resolution of the crossed-beams experiment is less than 2 eV, while the calculated

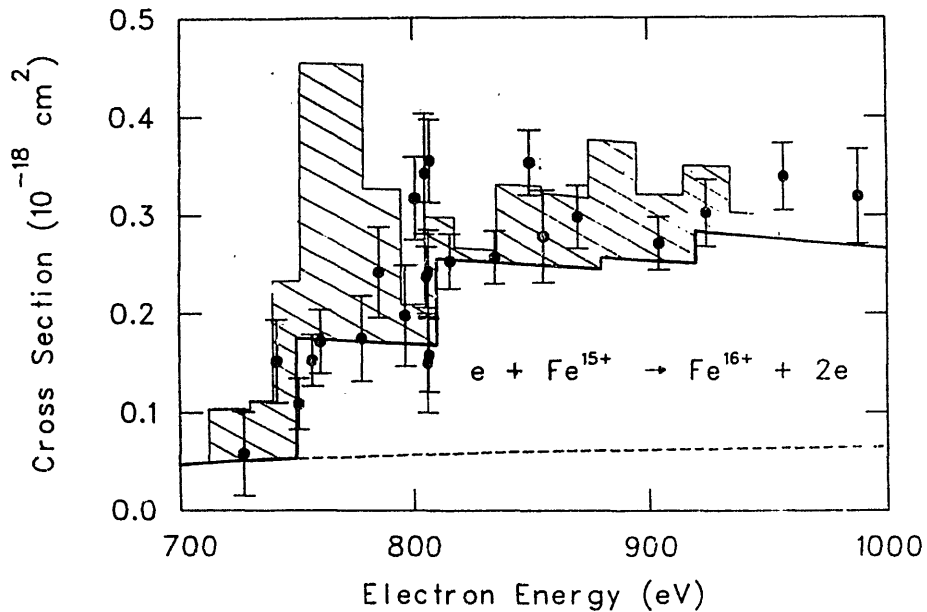


Figure 6. Comparison of predicted<sup>1</sup> and measured<sup>11</sup> cross sections for electron-impact ionization of Na-like  $\text{Fe}^{15+}$ . The dashed curve is the calculated direct-ionization cross section, to which the calculated contributions of 2p-nl excitation-autoionization and the REDA process have been added. The cross-hatched region indicates the predicted resonance contributions, which have been averaged over 20-eV energy bins. The experimental energy resolution is estimated to be 2 eV.

resonances have been averaged over 20-eV energy bins. Thus the experiment would have been expected to show even larger effects due to resonances than shown in Figure 6. The precision of the measurements was limited by the available ion beam intensity, but they suggest that while the excitation-autoionization contributions have been calculated quite reliably, the REDA contributions are smaller than predicted. The measurements do however strongly suggest a resonance feature near 800 eV electron energy, which is close to the calculated series limit for the  $2p^5 3pnl$  resonances.

It is possible that other resonances may not have been distinguished as clearly in these measurements because of the 2-eV energy resolution in the experiment, and the fact that the resonances are expected to be distributed over a 250-eV energy range. Since each of the experimental points shown represents at least several hours of data-taking time, calculations of the exact positions of the individual resonances would have been extremely helpful in the experimental search for resonance structure in the ionization cross section. It would be instructive to repeat the experiment with such information in hand.

Considerable experimental and theoretical attention has been paid to the accurate determination of  $1s-nl$  excitation-autoionization contributions to electron-impact ionization of Li-like ions<sup>12</sup>. This indirect process is now quite well understood for ions of B through Ne in the Li-isoelectronic sequence. These most recent measurements<sup>12</sup> of the cross section for electron-impact ionization of  $O^{5+}$  showed some possible indication of structure in the cross section about 40-50 eV below the  $1s-2s$  excitation threshold. Ionization cross-section measurements for  $O^{5+}$  were repeated<sup>13</sup> recently at ORNL with a fine energy grid in the electron-energy interval between 430 and 460 eV. The experimental results are shown in Figure 7, along with the theoretical direct-ionization cross section. Calculated energies<sup>12</sup> for the  $1s2s^22p$  and  $1s2s2p^2$  resonances are also indicated. The resonance structure is resolved in the experiment, and the correlation with the predicted energies is well within the combined accuracies of the calculations<sup>12</sup> and experiment (approximately 1 eV each).

The observation of these particular resonances in electron-impact ionization is especially significant, since they must involve a simultaneous double Auger process, which Henry and Msezane<sup>14</sup> have termed "auto-double ionization." There are no successive single-step Auger pathways for decay

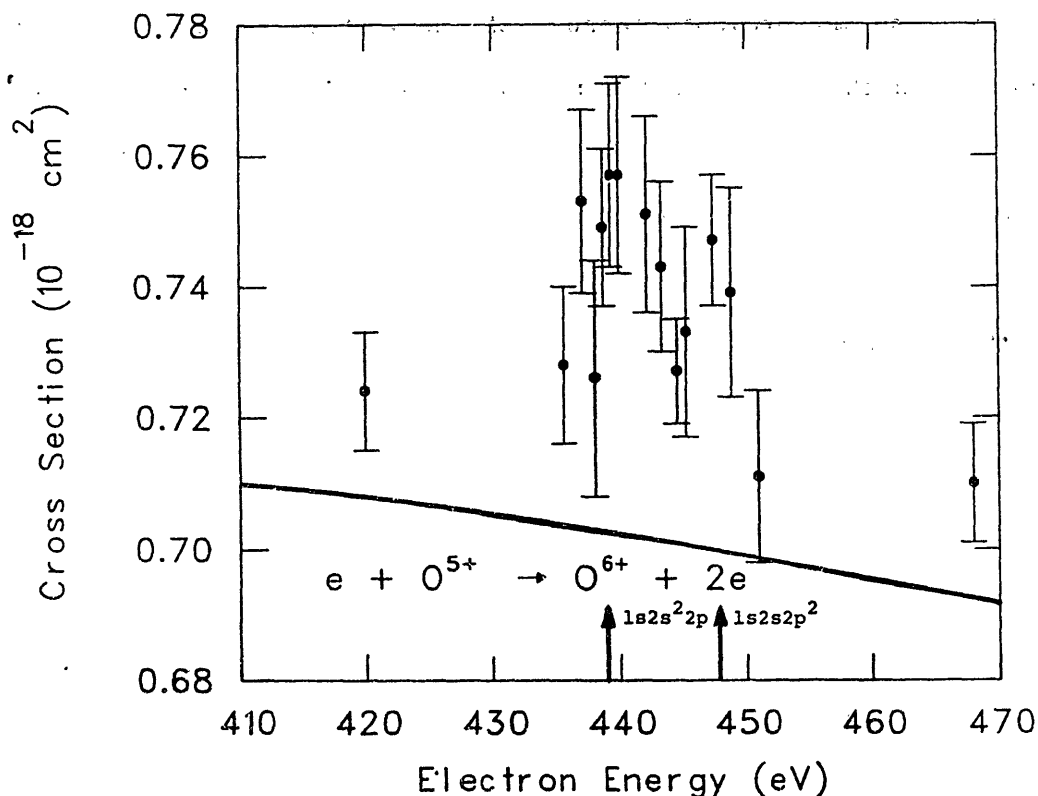


Figure 7. High-resolution measurements by Rinn and coworkers<sup>13</sup> of total cross section for electron-impact ionization of Li-like  $O^{5+}$  in the 420-470 eV electron-energy range. The solid curve is a distorted-wave direct ionization cross-section calculation and the vertical arrows at 439 and 448 eV indicate the calculated energies of the  $1s2s^2 2p$  and  $1s2s2p^2$  resonances<sup>12</sup>. Error bars represent one standard deviation on counting statistics, and are indicative of relative uncertainties.

of the  $1s2s^2$  and  $1s2s2p$  resonances which result in the release of two electrons, and thus would cause a contribution to the measured cross section for single ionization of  $O^{5+}$ . Efforts are currently under way to calculate branching ratios for the decay of these doubly excited states<sup>15</sup>. These require the development of new theoretical methods to calculate the autoionization rate and branching ratio for the auto-double channel.

Further experiments are also planned to investigate other members of the Li-sequence in finer detail in the energy regions where these resonances are expected to be.

## VII. SUMMARY

We have seen that indirect ionization mechanisms such as inner-shell excitation-autoionization can play an important role in the electron-impact ionization of multiply charged ions. Even for ions with complex electronic structures, this role has been shown to be quite accurately quantified by average-configuration-distorted-wave theoretical methods. Detailed comparisons between theory and experiment have also pointed to the potentially important role of metastable levels for some ionization stages in the ionization balance of high-temperature plasmas.

Definitive experimental evidence has also been presented for the first time for the contribution of individual resonances to the total cross section for electron-impact ionization of Li-like  $O^{5+}$ . In addition, experimental evidence has been presented for resonance structure in the cross section for electron-impact ionization of Na-like  $Fe^{15+}$ .

## ACKNOWLEDGMENTS

The authors are grateful to many coworkers who have contributed significantly to this research, and whose names are included in the references to specific work. A number of the experiments were conducted in continuing collaboration with G.H. Dunn and members of his JILA research group. C. Bottcher, D.C. Griffin and M.S. Pindzola continue to provide the theoretical background and much of the inspiration for this research.

This work was supported by the Office of Fusion Energy of the United States Department of Energy under Contract No. DE-AC05-84OR21400 with Martin Marietta Energy Systems, Inc.

#### REFERENCES

- 1) K.J. LaGattutta and Y. Hahn, Phys. Rev. A 24 (1981) 2273.
- 2) D.C. Gregory, F.W. Meyer, A. Muller and P. Defrance, Phys. Rev. A 34 (1986) in press.
- 3) A. Muller, K. Huber, K. Tinschert, R. Becker and E. Salzbom, J. Phys. B 18 (1985) 2993; J. Phys. B 18 (1985) 3011.
- 4) P. Defrance, S. Chantrenne, F. Brouillard and S. Rachafi, Nucl. Instrum. Methods. Phys. Res. B9 (1985) 400.
- 5) A. Danjo, A. Matsumoto, S. Ohtani, H. Suzuki, H. Tawara, K. Wakiya and M. Yoshino, J. Phys. Soc. Jpn. 53 (1984) 4091.
- 6) A. M. Howald, D.C. Gregory, F.W. Meyer, R.A. Phaneuf, A. Muller, N. Djuric and G.H. Dunn, Phys. Rev. A 33 (1986) 3779.
- 7) M.S. Pindzola, D.C. Griffin and C. Bottcher, Phys. Rev. A 33 (1986) 3787.
- 8) S.E. Harris, D.J. Walker, R.G. Caro, A.J. Mendelsohn and R.D. Cowan, Opt. Lett. 9 (1984) 168.
- 9) M.S. Pindzola, D.C. Griffin and C. Bottcher, Phys. Rev. A 34 (1986) in press.
- 10) D.C. Griffin, C. Bottcher, M.S. Pindzola, S.M. Younger, D.C. Gregory and D.H. Crandall, Phys. Rev. A 29 (1984) 1729.
- 11) D.C. Gregory, L.-J. Wang, K. Rinn and F.W. Meyer, unpublished data (ORNL, 1986).
- 12) D.H. Crandall, R.A. Phaneuf, D.C. Gregory, A.M. Howald, D.W. Mueller, T.J. Morgan, G.H. Dunn, D.C. Griffin and R.J.W. Henry, Phys. Rev. A 34 (1986) in press, and references contained therein.
- 13) K. Rinn, L.-J. Wang and D.C. Gregory, unpublished data (ORNL, 1986).
- 14) R.J.W. Henry and A.Z. Msezane, Phys. Rev. A 26 (1982) 2545.
- 15) D.C. Griffin and M.S. Pindzola, private communication (1986).

Recent Activities of Electron-Ion Collision Experiments  
in IPP/Nagoya and Sophia University

Hirosi Suzuki

Department of Physics, Sophia University  
Chiyoda-ku, Tokyo 102 Japan

Resonance processes in electron-ion collisions attract special attention of atomic physicists not only for their intrinsic academic interests but for their importance in atomic data which are applicable to simulations and diagnostics of high temperature plasmas aimed for CTR.

Although we had already recognized primary importance of the electron-ion collision studies, it was not until 1979 that we started the practical program to realize the modern crossed electron-ion beams experiment. It is only a short time since we have reached the present condition of data production after a few years needed for design and construction of the equipments. Although we have dealt with only a limited number of case studies, we have encountered really many interesting subjects to be solved.

In this paper, we describe activities in electron-ion collision experiments by our group at IPP, Nagoya University and at Sophia University, with particular emphasis on the resonant effects in electron impact ionization.

1. Measurements of ionization cross sections of multiply ionized rare-gas ions at Institute of Plasma Physics, Nagoya University.

This project is in progress by a joint research group consists of investigators from different institutes and universities.<sup>1)</sup>

Figure 1 illustrates schematically the main part of a crossed beam apparatus. A beam of multicharged ions extracted from an ion source of electron cyclotron resonance (ECR) type, which is named TPM-1, is analyzed according to its  $e/m$  ratio by an electromagnet and transported to a collision chamber. The ECR ion source, driven with a microwave of 2.45 GHz and a few kW, supplies a typical ion current of 150 nA for  $\text{Ar}^{2+}$  at the collision region. The beam is regulated into a desired shape with a set of electrostatic lenses, and is chopped into a group of square pulses. The beam is transported into the collision domain, and is crossed at right angles with a chopped electron beam with a squared profile produced in an electron gun. After the collision, the ion beam is led into a charge-state analyzer of the parallel-plate electrostatic type, where the product ions are separated from the primary ions and are counted with a micro-channel plate (MCP) after an appropriate acceleration. The counting efficiencies of the MCP are experimentally determined for triply charged rare gas ions. Primary ion current is measured with a Faraday cup and a vibrating-reed electrometer.

A pressure in the collision chamber is kept lower than  $1 \times 10^{-7}$  Pa during the operation of both beams. A fine slit system, which is movable very precisely by an operation from the outside of the vacuum chamber, is used in order to measure the spatial intensity distribution in the respective beam at the crossing region.

Ionization cross sections  $\sigma$  for ions of charge  $qe$  are calculated from the quantities measured using the expression

$$\sigma = \frac{q \cdot e^2 \cdot v_i \cdot v_e}{I_i \cdot I_e \cdot (v_i^2 + v_e^2)^{1/2}} \frac{S \cdot F}{\eta},$$

where

$$F = \frac{\int I_i(z) dz \cdot \int I_e(z) dz}{\int I_i(z) I_e(z) dz}.$$

In these expressions,  $S$  is the count rate of the product ions,  $\eta$  is the counting efficiency of the product-ion counter,  $I_i$  and  $I_e$  are the ion and electron beam currents respectively,  $v_i$  and  $v_e$  are the respective beam velocities. The form factor  $F$  is expressed by the integral of the beam overlapping  $I_i(z)I_e(z)$ , where  $I_i(z)$  and  $I_e(z)$  are the spatial distribution functions of the ion and electron beams along the vertical axis.

The pressure in the collision chamber must be kept lower than  $1 \times 10^{-7}$  Pa, in order to suppress the background noises below the signal levels. The double chopping technique plays an essential role in order to separate the true signals from the variety of background noises.<sup>2-6)</sup>

A part of results of single ionization cross sections of doubly ionized rare-gas ions  $\text{Ne}^{2+}$ ,  $\text{Ar}^{2+}$ ,  $\text{Kr}^{2+}$  and  $\text{Xe}^{2+}$  have been recently published by this group.<sup>7)</sup>

The ionization cross sections for  $\text{Ne}^{2+}$  through  $\text{Xe}^{2+}$  ions are shown in Fig.2 as functions of electron energies. For  $\text{Ne}^{2+}$  and  $\text{Kr}^{2+}$ , these data are the first observation by the crossed beam experiment. A systematic trend is seen from the curves. A rapid increase in cross sections is observed generally just above the threshold except for the case of  $\text{Ne}^{2+}$ . The measured cross sections become larger than those of the Lotz calculation at around the curve maximums as the atomic number increases. Cross section curves show more complicated features as the atomic number of the ions increases. For  $\text{Kr}^{2+}$  and  $\text{Xe}^{2+}$ , it is considered that the inner d-electron

contributes to the enhancement of the total ionization through indirect processes such as the excitation-autoionization. The observed finite values of cross sections below the threshold of the ground triple ion state for  $\text{Ar}^{2+}$ ,  $\text{Kr}^{2+}$  and  $\text{Xe}^{2+}$  ions are due to metastables in the primary ion beams.

In order to look into a detail, ionization cross sections for  $\text{Ar}^{2+}$  are shown in Fig.3, together with experimental data of Mueller et al.<sup>8)</sup> and with the Lotz calculation. A rapid rise from the threshold in the cross section curve is expected to be attributed to the excitation of 3s electrons followed by autoionization.

A distinct bump observed at around 160eV has been a kind of puzzle, because it can be referred to neither the 2p ionization threshold nor doubly excited autoionizing states. We may accept a strong suggestion for an interpretation of this structure, if we look at an energy dependence curve for the 3s-ionization in Ar in Fig.4.<sup>9)</sup> A rapid rise in the cross section just above the threshold is observed overlapping a slowly rising broad maximum. It is suggested that the most probable cause of the bump in the  $\text{Ar}^{2+}$  ionization curve originates from a contribution from the peculiar structure in the partial cross section curve for the 3s ionization. A comparison of the  $\text{Kr}^{2+}$  ionization curve in Fig.5 with the 4s-ionization curve in Kr in Fig.6 also is expected to support the same idea.<sup>9)</sup>

Recent results for the ionization curve of  $\text{S}^{2+}$  are shown in Fig.7. A rapid rise in the cross section near the threshold region and a clear bump at around 160eV in the curve are expected to add a further evidence for the above idea.

Experimental or theoretical efforts are desired to estimate the behavior of the partial cross sections for the outer subshell s-ionization in isonuclear sequences with the different outer most p electron numbers.

## 2. Measurements of single and double ionization cross sections of alkali-metal and alkaline earth ions at Sophia University.

Schematic diagram of the apparatus is shown in Fig.8. Ion sources of the thermionic emission type and the surface ionization type are used to obtain the alkali and alkaline earth ions.

The ions are crossed with an electron beam and selected according to their charge state, and finally the ionized ions are detected by single counting technique in a similar way that is described in the preceding section. Method to deduce the absolute cross section is also essentially the same with preceding one except for that the primary ion has a single charge, charge states of the product ions being double and triple.

Recent results of cross sections for single ionization of  $\text{Na}^+$  and  $\text{K}^+$  ions are shown in Fig.9 and Fig.10, respectively, as functions of impact energies of electrons. Experimental data of Hooper et al.<sup>10)</sup> and Peart and Dolder<sup>11)</sup> are also plotted for comparison. Curves calculated using the semiempirical formula of Lotz<sup>12)</sup> are also drawn in the respective figures. In the case of  $\text{Na}^+$ , the experimental cross sections show good agreement with the Lotz calculation, which suggests that the process is simply the direct ionization, namely the direct knock-out of the outermost electron. On the other hand, for the  $\text{K}^+$  ionization, cross sections increase abruptly from the threshold with the impact energy, and a considerable discrepancy is observed between the experimental results and the Lotz calculation especially in the lower impact energy region. The discrepancy is attributed to the contribution from the excitation-autoionization processes. A number of the core excited states which range from about 5.3 eV ( $\text{K}^+$   $3s3p^64s^1$   $^1S$ ) to 10.8 eV above the ground  $\text{K}^{2+}$  state, and a number of the doubly excited states which range from 11.3 eV ( $\text{K}^+$   $3p^4(1D)4s^2$   $^1D$ ) to 12.6 eV are identified in a literature.<sup>13)</sup> Excitation to these states, followed

by autoionization, is attributable for the main cause of the sharp increase of the cross sections near the threshold.

Results of the double ionization cross sections of  $\text{Na}^+$  and  $\text{K}^+$  ions, which are the first experimental observation, are shown in Fig.11, together with the experimental data for other alkali-metal ions,  $\text{Li}^+$  <sup>14)</sup>,  $\text{Rb}^+$  <sup>15)</sup> and  $\text{Cs}^+$  <sup>16)</sup>. One can find a systematic in which the cross section increases with atomic number of the ion. <sup>17)</sup>

Recent results of single ionization cross sections for  $\text{Ba}^+$  ion are shown in Fig.12, as a function of impact energy. <sup>19)</sup> The energy dependence of cross sections show a good agreement with the published data of Peart and Dolder <sup>18)</sup> including the structures due to the 4d excitation-autoionization. Absolute values of our results are, however, about ten per cent smaller than the data of Peart and Dolder.

Double ionization cross sections in  $\text{Ba}^+$  ion are recently measured by Hirayama et al. <sup>19)</sup> As shown in Fig.13, a modest onset of cross sections above the threshold is followed by their remarkable rise at about 90 eV of impact energy, forming a steep maximum ranging to about 200eV, which is mainly attributable to the 4d ionization-autoionization ( $N_{4,5}^{00}$  Auger) processes. An experimental cross section curve for the 4d ionization shown in Fig.14 <sup>20)</sup> suggests a decisive proof for the contribution from the 4d-ionization-autoionization to the great peak ranging from 90 eV to 200 eV in the double ionization curve of  $\text{Ba}^+$ .

### 3. Electron spectroscopic study of the electron-ion collisions.

One of the most general and useful method for measurements of the differential cross sections for inelastic collision of electrons with atoms and molecules is the electron-impact spectroscopy, which is based on measurements of the energy-loss spectra of scattered electrons resulting

from the transfer of electron kinetic energies to excitation energies of target atoms and molecules. In addition to this, the ejected-electron spectroscopy is also a useful method to study the autoionization or Auger-effect in atoms and molecules. A somewhat ambitious project which attempt to apply the electron spectroscopy technique to the electron-ion collision experiments is in progress at the Institute of Plasma Physics, Nagoya University. A schematic drawing showing a concept of our aim and a sketching diagram of the apparatus is shown in Fig.15 and Fig.16, respectively. A brief description of the plan will be presented in the seminar.

#### REFERENCES

- 1) Members of the group are as follows:  
A.Danjo (Niigata Univ.), T.Hirayama (Sophia Univ.), A.Matsumoto (Hiroshima Inst.Tech.) S.Ohtani (IPP), H.Suzuki (Sophia Univ. and IPP), T.Takayanagi (Sophia Univ.), H.Tawara (IPP), K.Wakiya (Sophia Univ.), I.Yamada (IPP) and M.Yoshino (Shibaura Inst.Tech.)
- 2) M.F.A.Harrison:"Methods of Experimental Physics" Vol.7B, ed. W.L.Fite and B.Bederson (Academic Press, 1968) pp.95-115.
- 3) K.T.Dolder:"Case Studies in Atomic Collision Physics" Vol.1, ed. E.W.McDaniel and M.R.McDowell (North-Holland, 1969) pp.249-334.
- 4) K.T.Dolder and B.Peart: Rep.Prog.Phys. 39 697 (1976).
- 5) G.H.Dunn:"Physics of Ionized Gases" ed. M.Matic and Boris Kidric (Institute of Nuclear Sciences, Beograd, 1981) pp.49-95.
- 6) D.H.Crandall:"Physics of Ion-Ion and Electron-Ion Collisions" ed. F.Brouillard and J.W.McGowan (Plenum Press, 1981) pp.201-238.
- 7) A.Danjo, A.Matsumoto, S.Ohtani, H.Suzuki, H.Tawara, K.Wakiya and M.Yoshino: J.Phys.Soc.Jpn. 53 4091 (1984).
- 8) A.Mueller, E.Salzborn, R.Becher, H.Klein and H.Winter:J.Phys.B:At.

- Mol.Phys: 13 1877 (1980).
- 9) G.P.Li et al.: J.Phys.Soc.Jpn. to be published (1986).
  - 10) J.W.Hooper, W.C.Lineberger and F.M.Bacon: Phys.Rev.141 165 (1966).
  - 11) B.Peart and K.T.Dolder: J.Phys.B:At.Mol.Phys. 1 240 (1968).
  - 12) W.Lotz: Z.Phys. 216 241 (1968).
  - 13) H.Aizawa, K.Wakiya, H.Suzuki, F.Koike and F.Sasaki:  
J.Phys.B:At.Mol.Phys. 18 289 (1985).
  - 14) B.Peart and K.T.Dolder: J.Phys.B:At.Mol.Phys. 2 1169 (1969).
  - 15) D.W.Hughes and R.K.Feeney: Phys.Rev. A23 2241 (1981).
  - 16) D.R.Hertling, R.K.Feeney, D.W.Hughes and W.E.Sayle: J.Appl.Phys. 53  
5427 (1982).
  - 17) T.Hirayama, K.Oda, Y.Morikawa, T.Ono, Y.Ikezaki, T.Takayanagi,  
K.Wakiya and H.Suzuki: J.Phys.Soc.Jpn. 55 1411 (1986).
  - 18) B.Peart and K.T.Dolder: J.Phys.B:At.Mol.Phys. 6 L359 (1973).
  - 19) T.Hirayama et al.:J.Phys.Soc.Jpn. to be published (1986).
  - 20) T.Takayanagi et al.:J.Phys.B:At.Mol.Phys. to be submitted (1986).

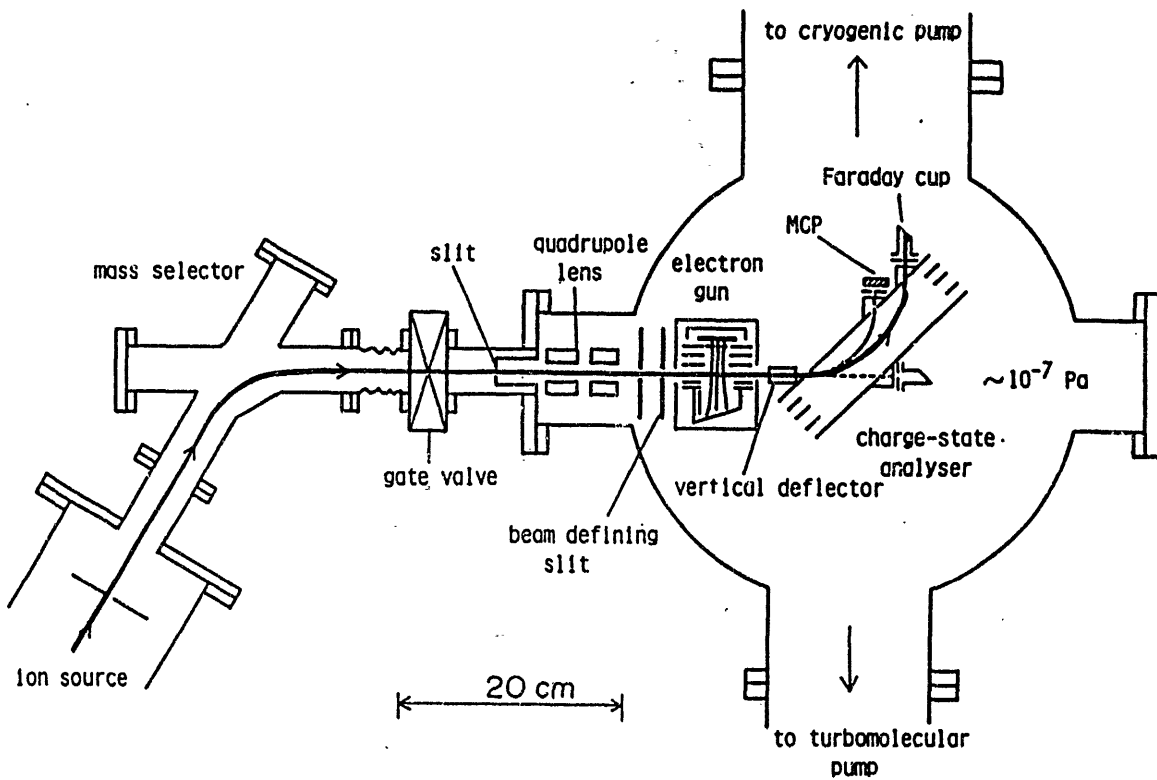


Fig.1. Schematic diagram of the crossed beams apparatus equipped to the ECR ion source (IPP/Nagoya).

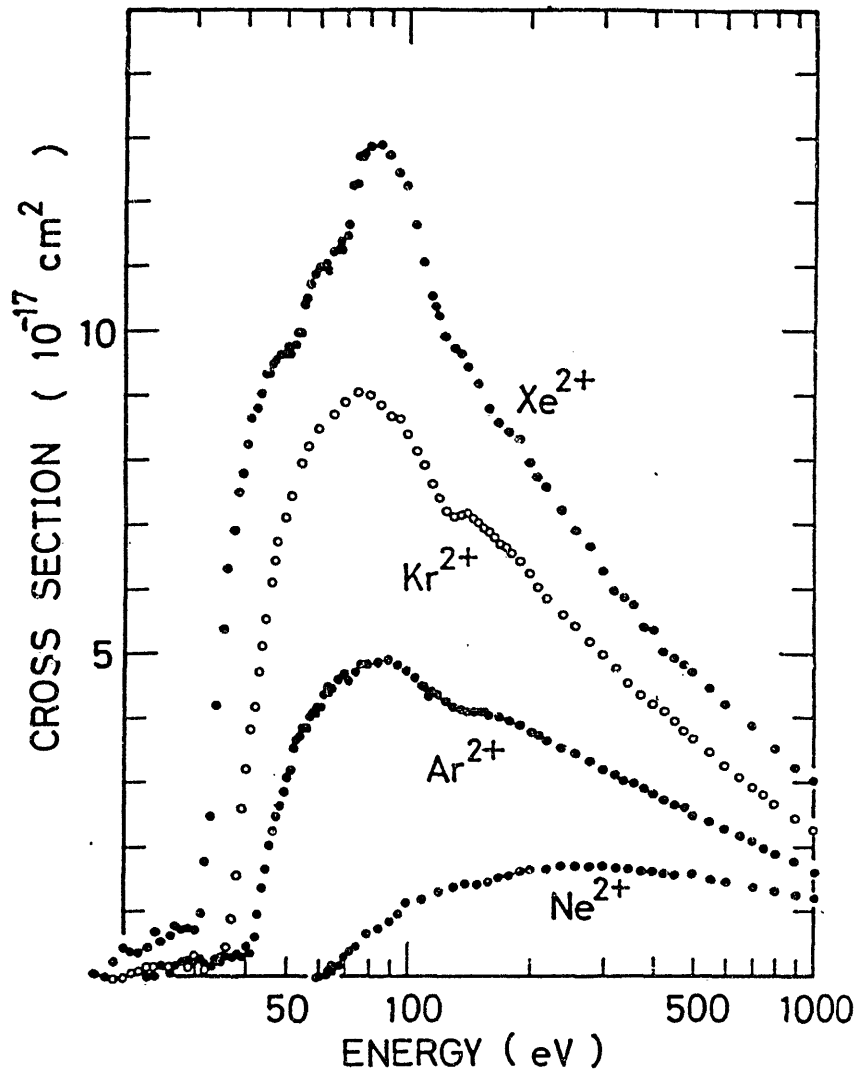


Fig.2. Single ionization cross sections for Ne<sup>2+</sup> through Xe<sup>2+</sup>. For Ne<sup>2+</sup> and Kr<sup>2+</sup>, the data are the first measurements.

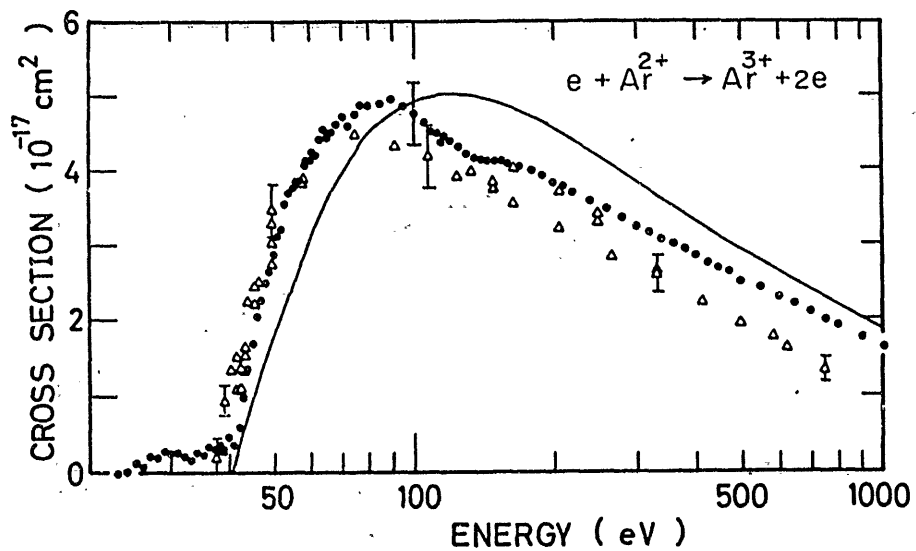


Fig.3. Ionization cross sections of  $\text{Ar}^{2+}$ .  
 Present results (solid line), Mueller et al.  
 (triangle). Solid curve is the Lotz calculation.

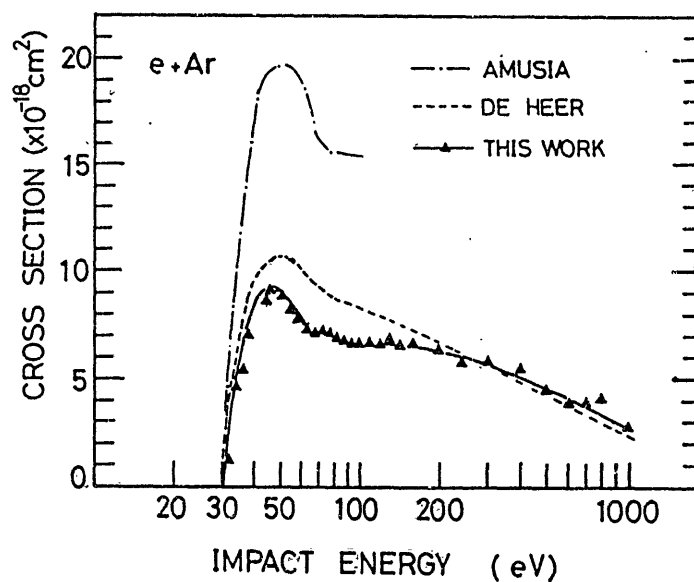


Fig.4. The 3s-ionization cross sections for Ar.  
 G.P.Li et al.<sup>9)</sup>

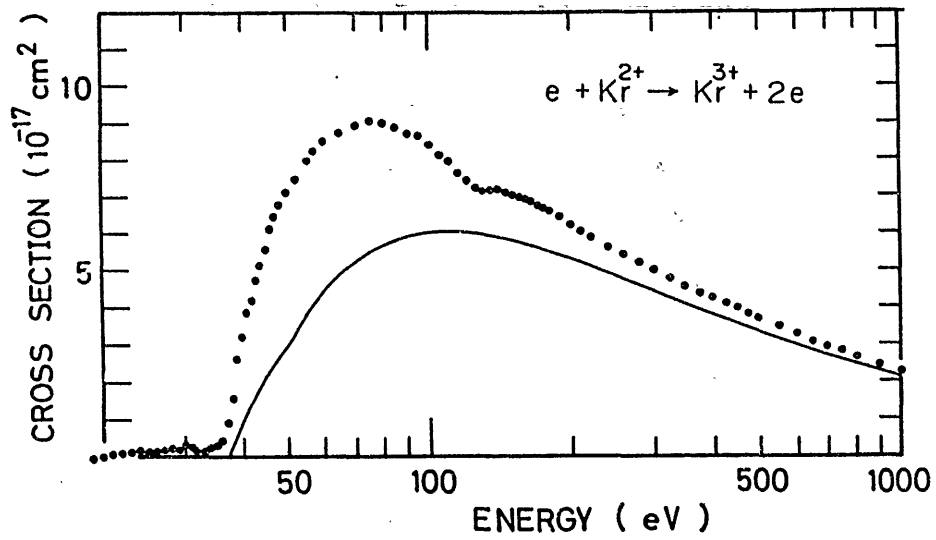


Fig.5. Ionization cross sections of  $\text{Kr}^{2+}$ .

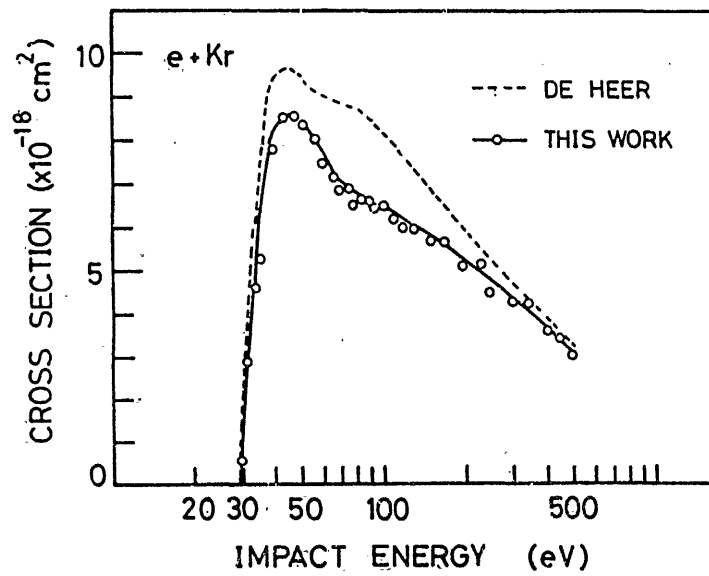


Fig.6. The 4s-ionization cross sections for Kr.  
G.P.Li et al.<sup>9)</sup>

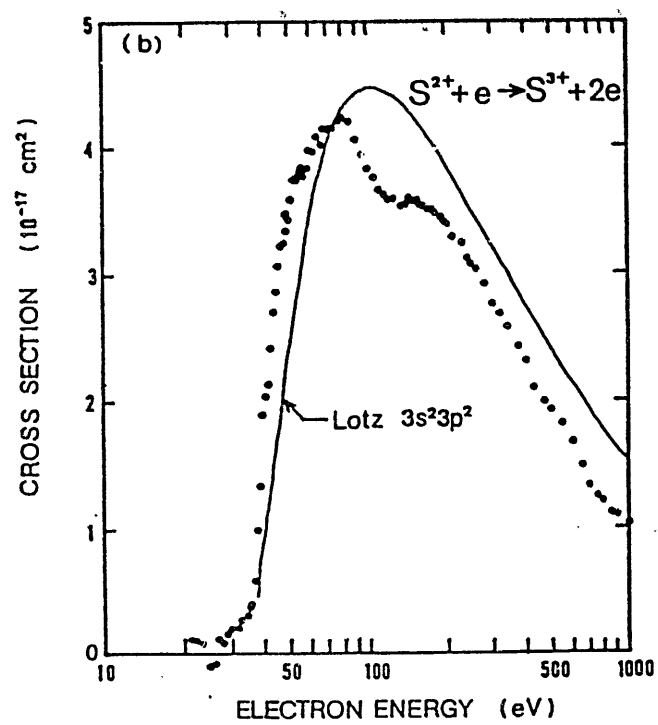


Fig.7. Ionization cross sections of  $S^{2+}$ .

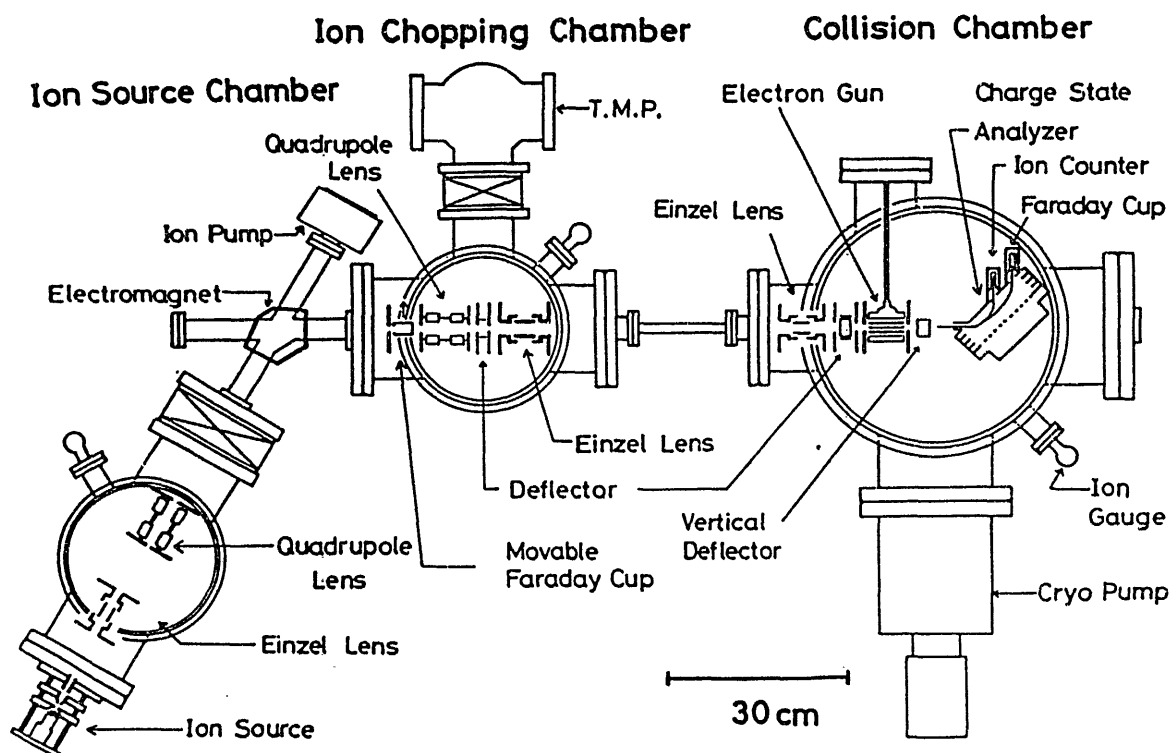


Fig.8. Schematic diagram of the crossed beams apparatus at Sophia University.

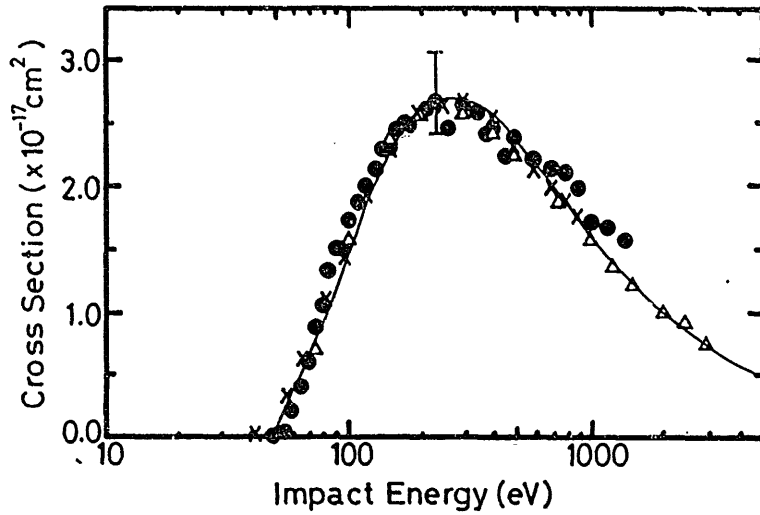


Fig.9. Single ionization cross sections of  $\text{Na}^+$  ions. Present results (open circle), Hooper et al. (cross), Peart and Dolder (triangle). Solid curve is the Lotz calculation.

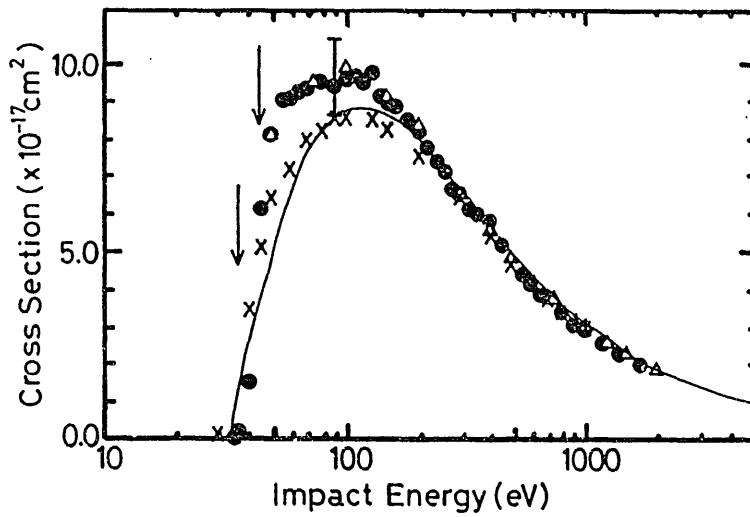


Fig.10. Single ionization cross sections of  $\text{K}^+$  ions. Symbols are same as those of Fig.9.

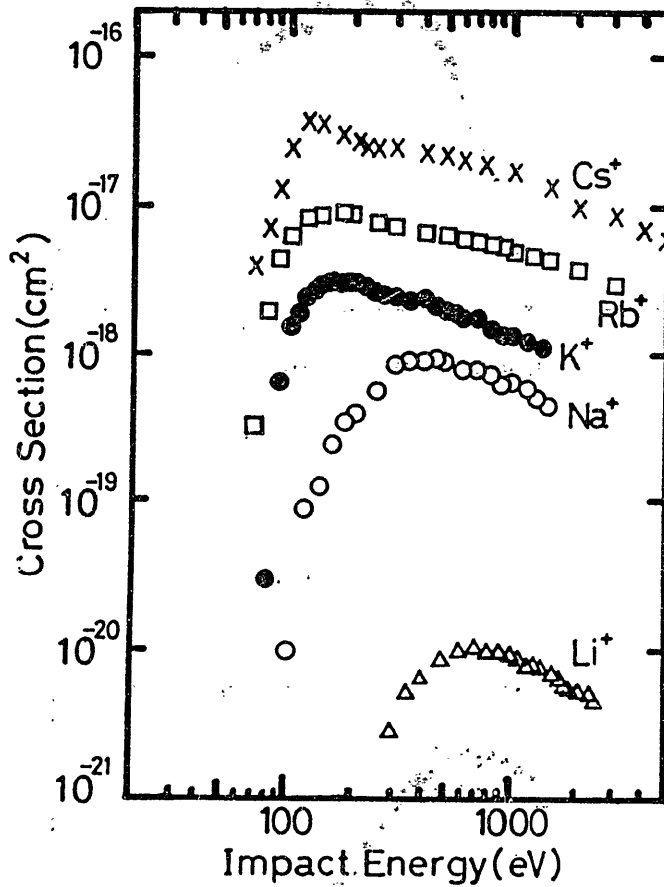


Fig.11. Double ionization cross sections of alkali-metal ions. Those for  $\text{Na}^+$  and  $\text{K}^+$  are the present results.

- $\text{Li}^+$  - Peart and Dolder, 14)
- $\text{Rb}^+$  - Hughes and Feeney, 15)
- $\text{Cs}^+$  - Hertling et al. 16)

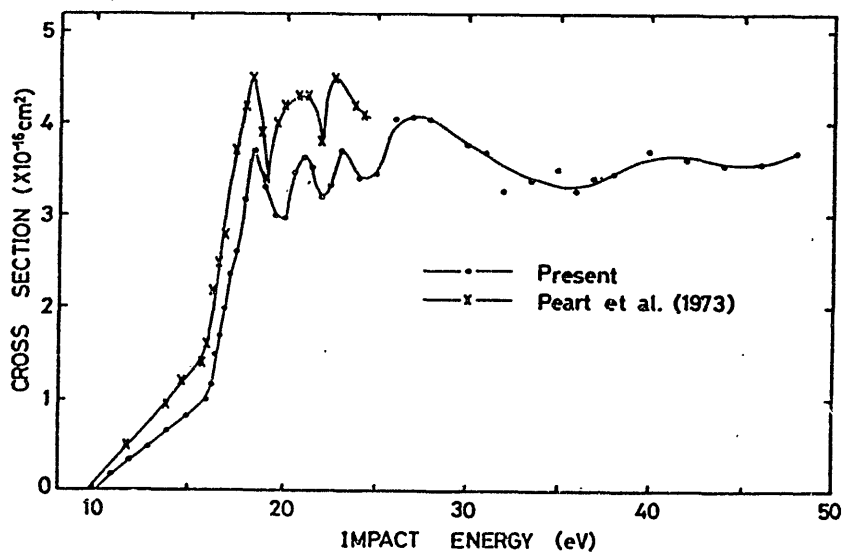


Fig.12. Single ionization cross sections of Ba<sup>+</sup>. Present results (solid circle), Peart and Dolder (x).

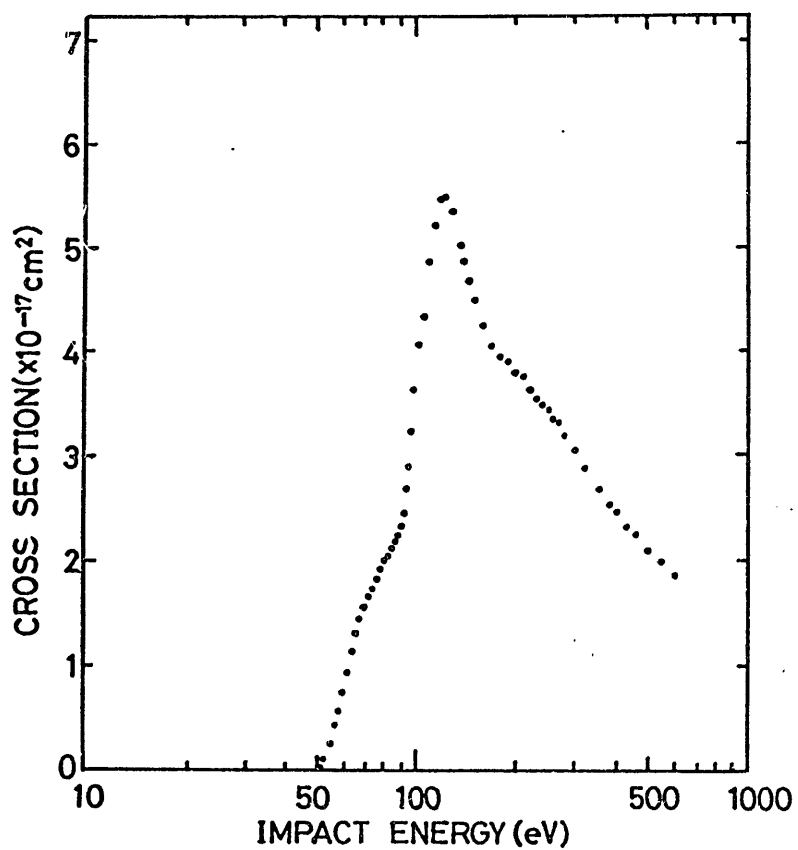


Fig.13. Double ionization cross sections of  $Ba^+$ .  
Hirayama et al. <sup>19)</sup>

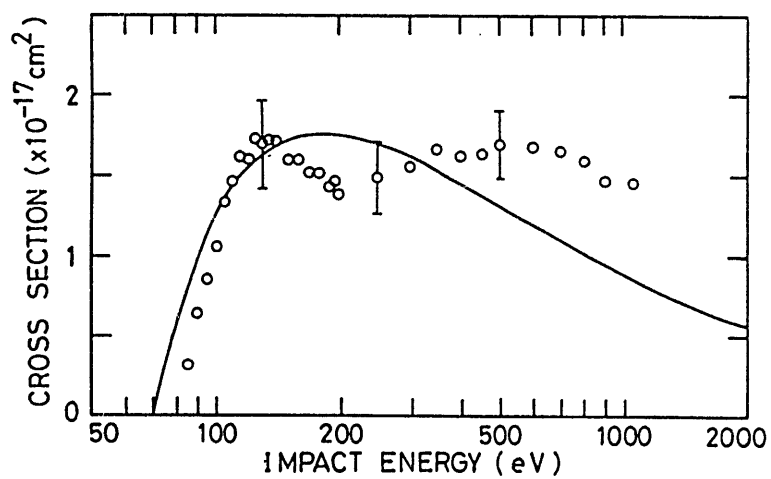


Fig.14. The 4d-ionization cross sections of Xe.  
Takayanagi et al. <sup>20)</sup>

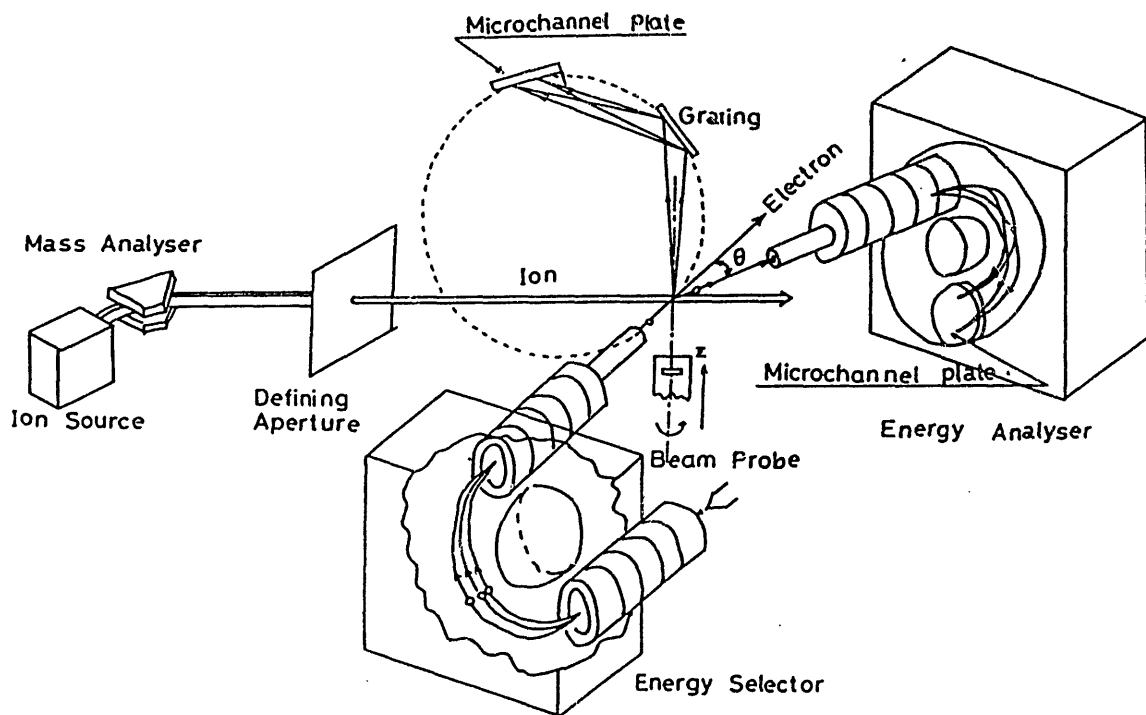


Fig.15. Schematic drawing of a possible experimental setup for electron spectroscopy in the crossed beams technique.

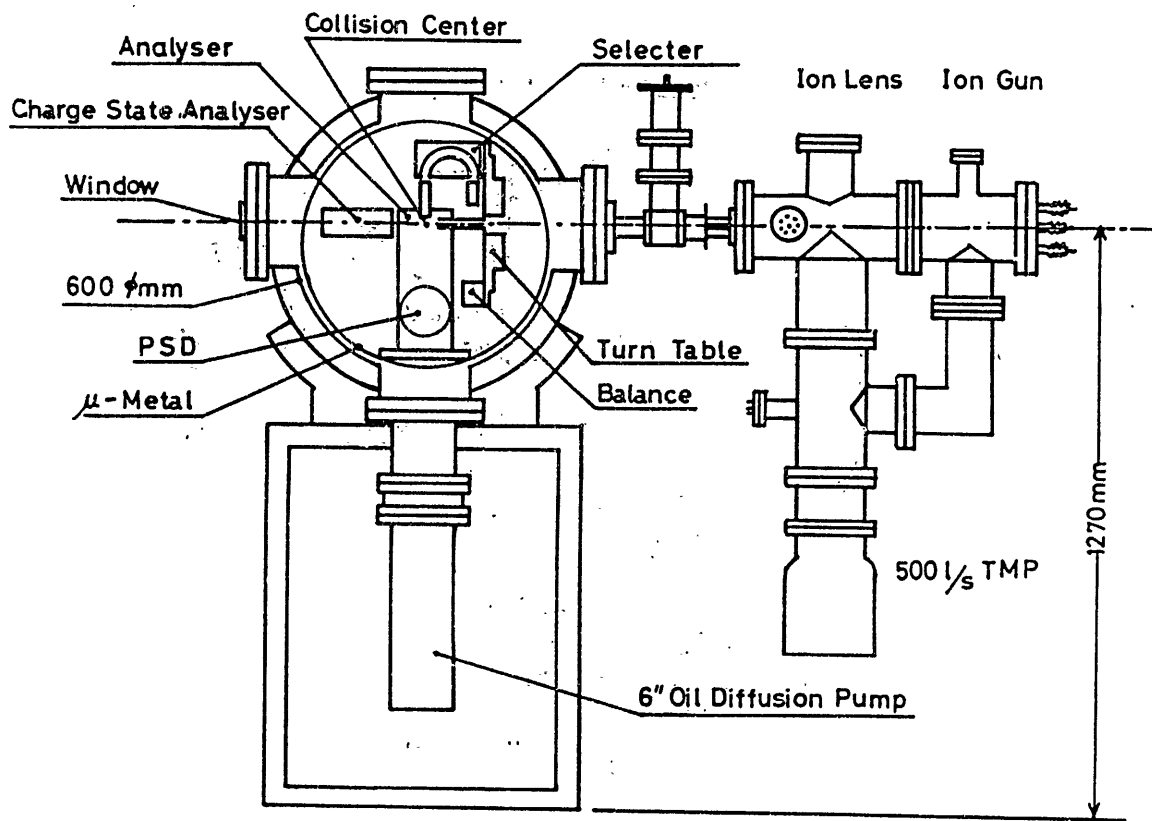


Fig.16 Schematic diagram of the electron spectrometer at IPP/Nagoya (ACE-IT).

## Distorted-Wave-Method Calculation of Innershell Excitation

Yukikazu ITIKAWA and Kazuhiro SAKIMOTO

Institute of Space and Astronautical Science

Komaba, Meguroku, Tokyo 153, Japan

In the electron-impact ionization of atomic ions, an innershell excitation followed by autoionization often has a large contribution.<sup>1</sup> To estimate the contribution, cross sections for the innershell excitation have been calculated for a number of ions.<sup>2</sup> For the sake of simplicity, many of the calculations reported so far are based on the distorted wave method (DWM). Though the distorted wave method is generally reliable in the calculation of outershell excitations of ions,<sup>3</sup> its validity for innershell excitations has not been tested extensively.

In the case of Na-like ions ( $Mg^+$ ,  $Al^{2+}$  and  $Si^{3+}$ ), Henry and Msezane<sup>4</sup> calculated the innershell cross section by the close-coupling (CC) method. When comparing their results with those of DWM, they conclude that the DWM gives a much larger cross section than the CC method. The same conclusion has been reached recently by a similar study for Mg-like ions.<sup>5</sup> It should be noted, however, that those DWM and CC calculations employ different wavefunctions for the same target ion. In the calculation

of electron-ion collisions, the resulting cross section is often much more sensitive to the target wavefunction than to the scattering approximation used. It is desirable to compare different calculations under the condition of the same target wavefunctions. Here we calculate innershell cross sections for Li-like ions with the distorted-wave method proposed recently by the present authors.<sup>6,7</sup> The result is compared with that obtained by a close-coupling calculation.<sup>8</sup> The same (CI type) target wavefunctions are used in the present DWM calculation as in the CC one.

The present DW method (called DWXA) is based on the assumptions: (1) The same distortion potential (i.e., a spherical average of the electrostatic potential formed by the target ion in its initial state) is used to calculate the distorted waves both for the initial and for the final states; (2) Electron exchange is taken into account only between the interacting two electrons and the possibility of the ejection of the third one is ignored; (3) Use is made of the wavefunctions of CI type for target states, which are given independently at the outset. This method has been successfully applied to the (outershell) excitations of He-, Be- and C-like ions.<sup>6,7</sup>

Now we apply the DWXA to the calculation of the cross sections for the excitations from the ground ( $1s^2 2s^2 S$ ) to  $1s 2s^2 2S$ ,  $1s 2s(3S) 2p^4 P^0$ ,  $1s 2s(1S) 2p^2 P^0$ , and  $1s 2s(3S) 2p^2 P^0$

of the Li-like ions ( $C^{3+}$ ,  $N^{4+}$ , and  $O^{5+}$ ). We adopt in the present calculation the same CI wavefunctions as used by Henry in his CC calculation.<sup>8</sup> Figures 1-4 show the collision strengths calculated for  $O^{5+}$  as a function of the electron energy in threshold units (X). In all the cases, the DWXA gives the cross section in close agreement with the CC one. Even at the threshold of each excitation, the DWXA result agrees with CC cross section within about 20%.

For the analysis of satellite spectra of oxygen ions, Bely-Dubau et al.<sup>9</sup> calculated the innershell cross sections for  $O^{5+}$  with the use of a DW method. They employed the computer code developed at the University College London (called hereafter DWUCL).<sup>3</sup> Their results are compared in Figs 1-4 with the present calculation and the CC one. As is seen in the figures, the result of the DWUCL is more deviated from the CC one than the DWXA. The DWUCL is not much different from the DWXA in the method of cross section calculation, but uses different target wavefunctions. Most part of the discrepancy between the DWUCL and the CC results, therefore, can be attributed to the difference in the target wavefunctions. Usually the target wavefunction used in the DWUCL calculation is generated with the same distortion potential as for the continuum electrons. On the other hand the present DWM (i.e., DWXA) assumes that the best wavefunction

is given independently and can incorporate any type of CI wavefunction into the cross section calculation. The wavefunction of Bely-Dubau et al. gives the oscillator strengths for the transitions  $1s^2 2s^2 2S - 1s2s(1S)2p^2 P^0$  and  $1s^2 2s^2 2S - 1s2s(3S)2p^2 P^0$  to be 0.681 and 0.0415, respectively. The wavefunction adopted by Henry (and in the present DW calculation) gives the corresponding values of 0.532 and 0.0649. These differences in the oscillator strengths can easily explain the difference in the energy dependence of the collision strengths at higher energies of the two dipole-allowed transitions (see Figs 3 and 4). The present study thus confirms the conclusion that the electron-impact excitation cross section is very sensitive to the target wavefunction and a comparison of different calculations should be made on the basis of the same target wavefunction.

Another conclusion drawn from the figures is that the perturbation theory can produce well the innershell cross section, once an accurate target wavefunction is provided. The Coulomb-Born approximation, i.e., the simpler perturbation method than the DWM, also can give fairly good results at higher energies, but it fails completely at lower energies (say,  $X \lesssim 2$ ). Figure 5 shows one example:  $1s^2 2s^2 2S - 1s2s(3S)2p^2 P^0$  transition in  $C^{3+}$ . The CBXA in Fig. 5 is obtained by simply replacing the distorted waves in the DWXA calculation with the corresponding Coulomb waves. Collision strengths for other ions and/or other

transitions have a similar trend. Only an exception is the transition  $1s^2 2s^2 S - 1s2s(1S)2p^2 P^0$ , for which the Coulomb-Born calculation is very close to the DWXA at the collision energy as low as the threshold. Thus the distortion due to the presence of target (other than the simple ionic charge) should be taken into account in the study of electron-impact excitation of ions at least at lower energies.

The present work will be extended to other isoelectronic sequences.

## References

1. For a recent review, D.C. Gregory, in: *Electronic and Atomic Collisions*, ed. by D.C. Lorents, W.E. Meyerhof and J.R. Peterson (North-Holland, 1986) p. 205.
2. For a bibliography on electron-ion collisions, Y. Itikawa, K. Takayanagi and T. Iwai, *At. Data Nucl. Data Tables* 31, 215 (1984).
3. For a general review of distorted-wave methods, Y. Itikawa, *Phys. Reports* (1986) (in press).
4. R.J.W. Henry and A.Z. Msezane, *Phys. Rev. A* 26, 2545 (1982).
5. S.S. Tayal and R.J.W. Henry, *Phys. Rev. A* 33, 3825 (1986).
6. Y. Itikawa and K. Sakimoto, *Phys. Rev. A* 31, 1319 (1985).
7. Y. Itikawa and K. Sakimoto, *Phys. Rev. A* 33, 2320 (1986).
8. R.J.W. Henry, *J. Phys. B* 12, L309 (1979).
9. F. Bely-Dubau, J. Dubau, P. Faucher and L. Steenman-Clark, *J. Phys. B* 14, 3313 (1981).

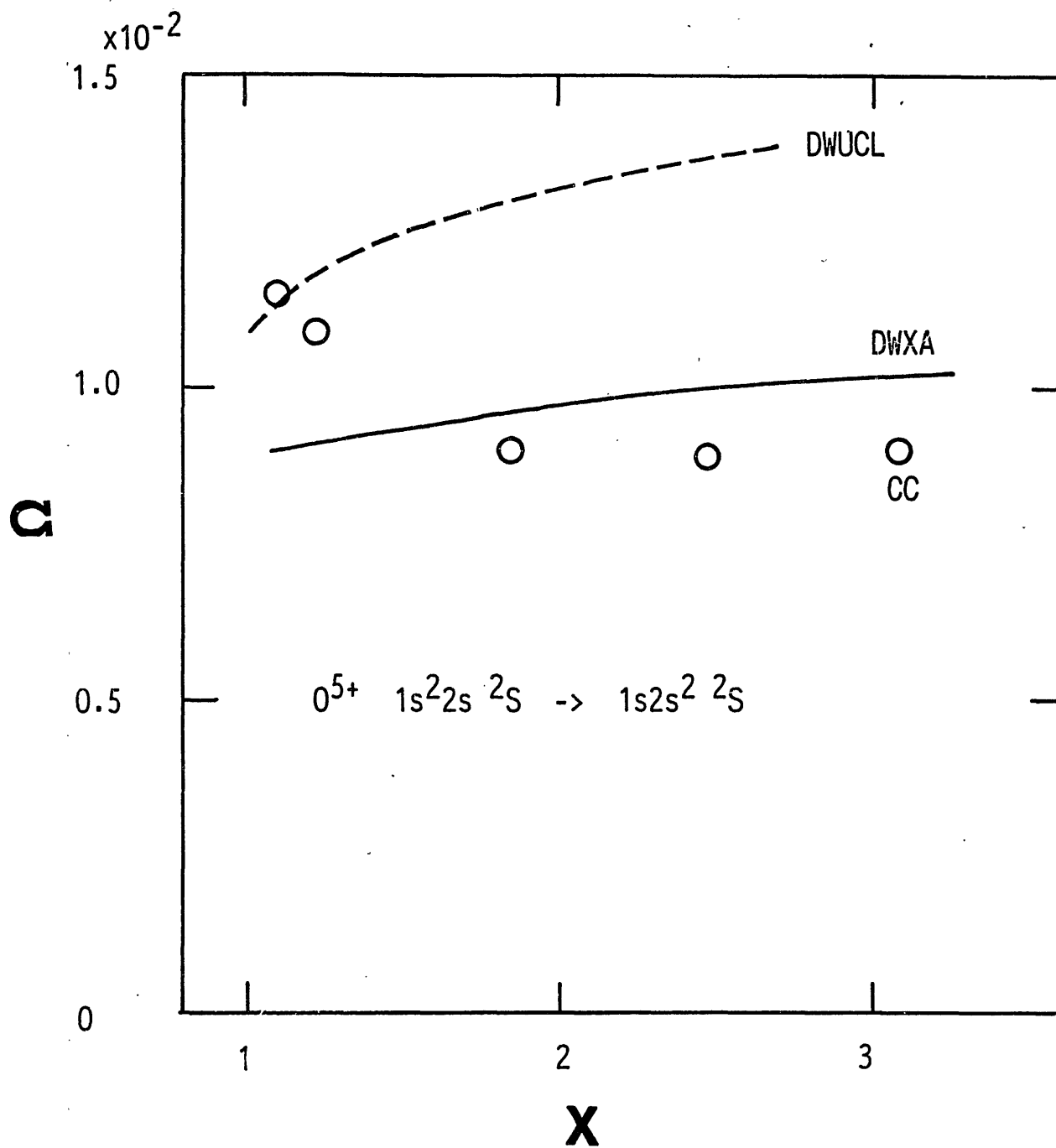


Fig. 1

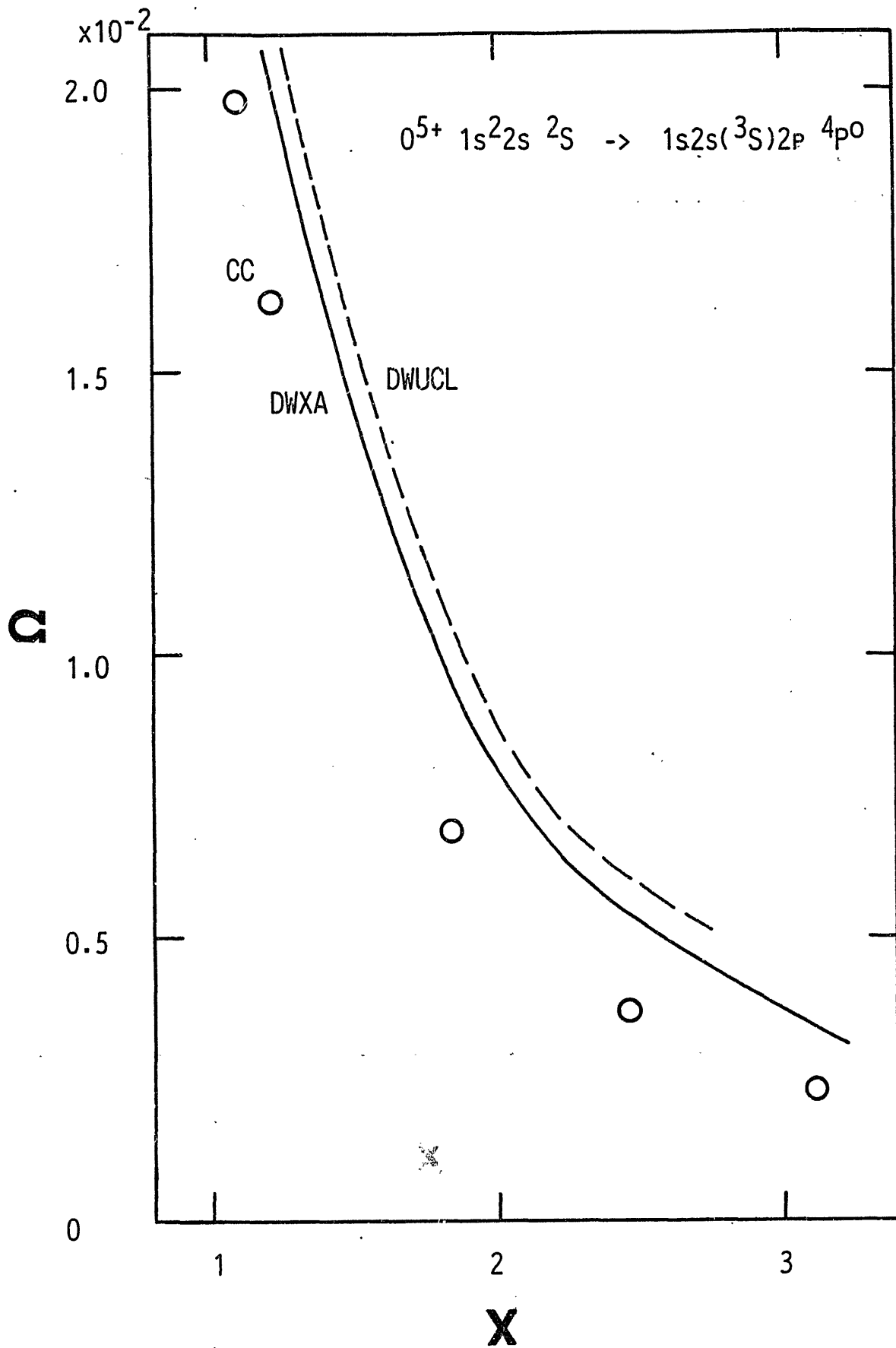


Fig. 2

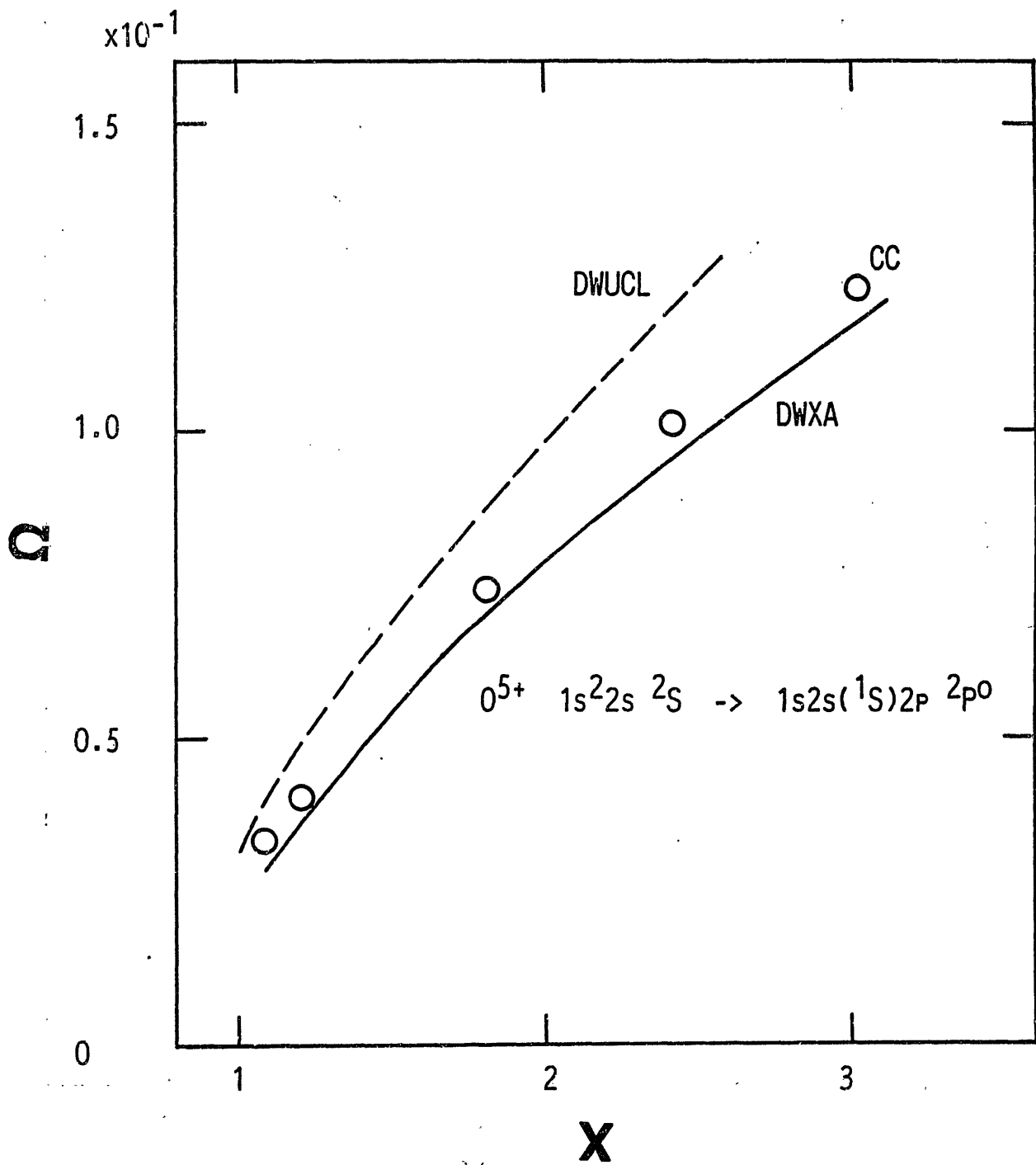


Fig. 3

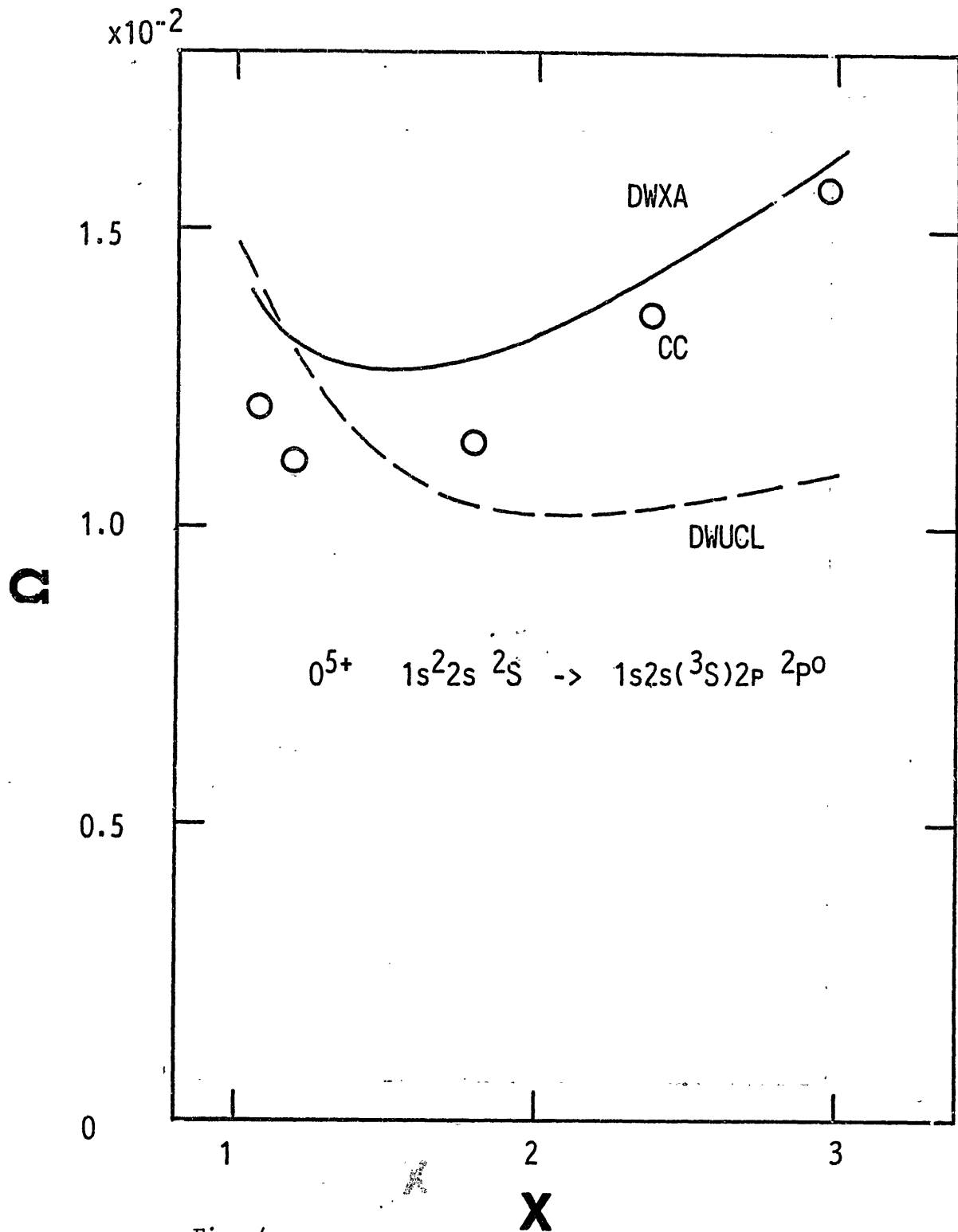


Fig. 4

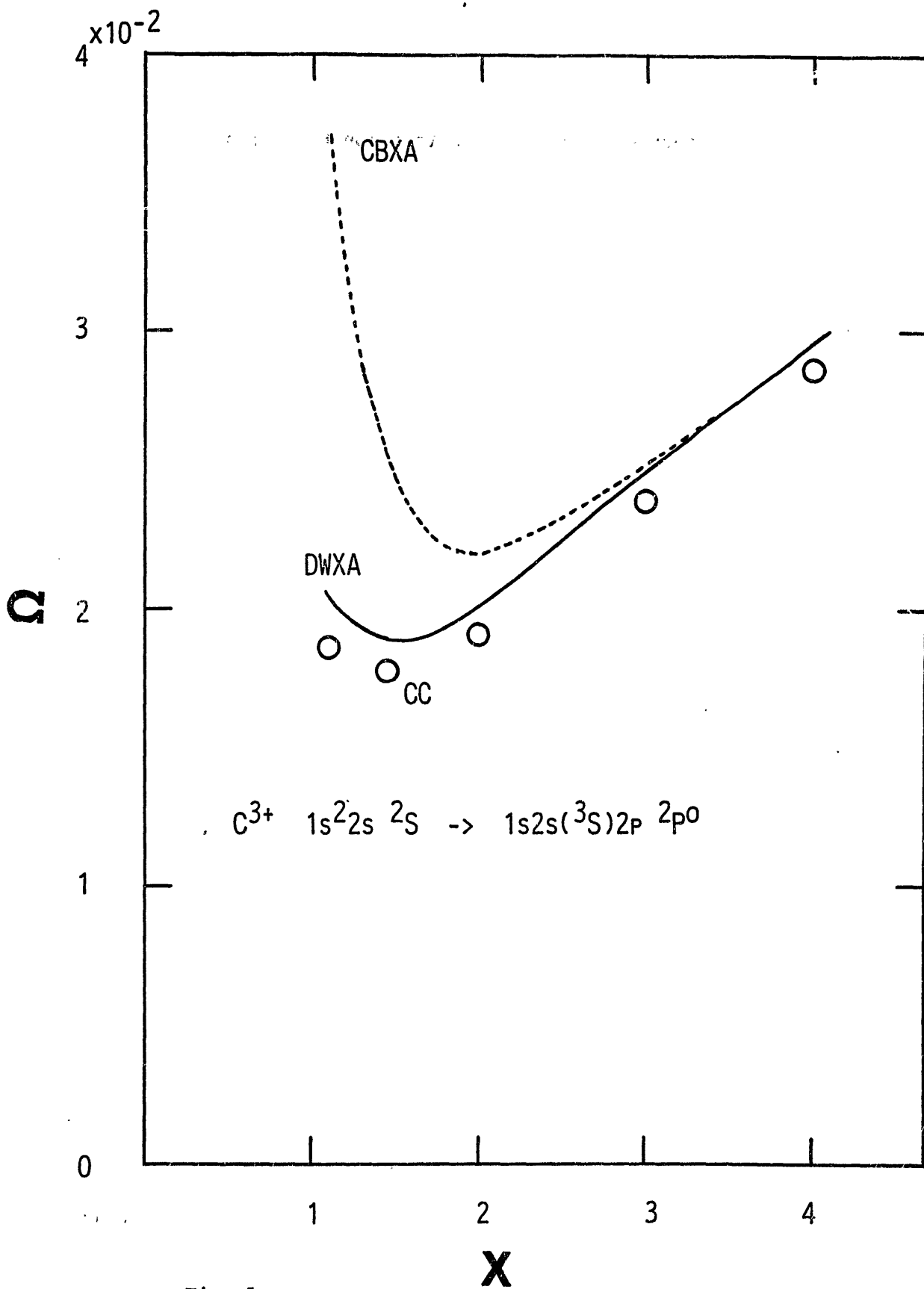


Fig. 5

## Resonance Effects in Electron Ion Excitation

Ronald J. W. Henry  
Department of Physics and Astronomy  
Louisiana State University, Baton Rouge, LA, USA

### 1. INTRODUCTION

Due to experimental difficulties encountered especially for multiply-ionized species, determination of collision strengths must rely primarily on calculations. Reviews of calculations include Seaton<sup>(1)</sup>, Henry<sup>(2)</sup> and Gallagher and Pradhan<sup>(3)</sup>.

Figure 1 summarizes the various ions on which calculations have been made. In addition to the light ions, the impetus for the field of electron-ion scattering has come from astrophysics as evidenced by the work on cosmically-abundant ions Ne, Fe, Si, Mg, S, and Ar. Also, tokamak plasmas have introduced data needs for Ti, Fe, and Mo. Experiments which yield direct values for integral cross sections or collision strengths are given by the open squares. Open circles represent ionization experiments from which cross sections for excitation have been deduced.

The reliability of the calculations may be judged by considering the effect of various physical approximations and comparing results with the various measurements. None of the measurements to date are at sufficient energy resolution to show explicit effects of resonances. Resonance effects have been considered theoretically for the ions listed in Figure 2.



## 2. DEFINITIONS

The collision strength  $\Omega(i,f)$  is related to the excitation cross section  $\sigma(i \rightarrow f)$  (measured in units of  $\pi a_0^2$ ) by:

$$\Omega(i,f) = \omega_i k_i^2 \sigma(i \rightarrow f) \quad (1)$$

where  $k_i^2$  is the energy (in Ry.) of the incident electron relative to the lower state  $i$ , and  $\omega_i$  is the statistical weight of the lower atomic state. We introduce the parameter  $x$ , the energy in threshold units defined by

$$x = k_i^2 / \Delta E_{if} \quad (2)$$

where  $\Delta E_{if}$  is the excitation energy (in Ry.) for the transition from level with energy  $E_i$  to level with energy  $E_f$ .

The rate parameter, or effective collision strength, is defined as

$$\gamma_{if}(T) = \int_0^{\infty} \Omega(i,f) \exp[-\Delta E_{if} x / (kT)] d[\Delta E_{if} x / (kT)] \quad (3)$$

and  $kT$  is in Ry and  $T$  is the electron temperature.

## 3. ESSENTIAL PHYSICS

The essential physics which should be considered for all calculations of electrons scattering from ions includes target state correlations, unitarization, exchange, channel coupling, resonances and relativistic mixing of target states. The best quantum mechanical description for the solutions of the collision problem is a converged close-coupling method. A discussion of the equations may be found in the review articles<sup>(1-3)</sup> and in Burke and Seaton<sup>(4)</sup>. Other approximate methods are also discussed in the various reviews.

For alkali-like systems, which have a single electron outside a closed core, target state correlations are not important. Various physical effects are well demonstrated in Figure 3 which gives  $\Omega(2s,2p)$  versus  $x$  for Be II. Curves B and C represent close-coupling calculations<sup>(5)</sup> in five-state and two-state approximations, respectively. Curve D is a distorted wave calculation<sup>(6)</sup>. Coulomb Born calculations<sup>(5)</sup> are given by curves E, F, and G for unitarized with exchange, unitarized without exchange, and non-unitarized without exchange, respectively. Measurements of Taylor et al.<sup>(7)</sup> of absolute collision strengths in a crossed-beam experiment to  $\pm 8\%$  are given by solid circles with the error bars. It is necessary to include both exchange, unitarization and channel coupling effects in order to obtain a reasonable estimate for the collision strength.

A small but perplexing disagreement exists between theory and experiment for Be II. At high energies the most accurate theoretical results are considered to be the two-state close-coupling results of Hayes et al.<sup>(5)</sup> and at intermediate energies the two-state plus three pseudo-state close-coupling results of Henry et al.<sup>(8)</sup> Theoretical results lie at least 18% above experimental results before cascade effects are taken into account. The shape of the experimental and theoretical collision strengths is in very good agreement.

The main type of resonance which dominates electron-ion scattering is the Feshbach or closed-channel resonance. An infinite series of resonances converge on to each of the states of the target ion due to the attractive Coulomb potential. When the initial and final states are more strongly coupled to the closed channel than to each other, then the resonance effects are large. One way of estimating the effect of resonances is to

use a Gailitis averaging method for the collision strength. Then the average collision strength is

$$\bar{\Omega}(i,j) = \Omega^>(i,j) + \sum_{i'} \frac{\Omega^>(i,i') \Omega^>(i',j)}{\sum_{i''} \Omega^>(i',i'')}$$

where the sum  $i'$  is over degenerate closed channels of the new threshold, and  $i''$  is summed over all open channels. Collision strengths  $\Omega^>$  are calculated above the new threshold and extrapolated to energies below threshold.

Figure 4 gives  $\bar{\Omega}(2p,3s)$  for C IV versus reduced temperature  $kT/IP$ , where  $IP$  is the ionization potential. The effect of resonances on  $2 \rightarrow 3$  transitions in lithium-like ions has been discussed by Bhadra and Henry<sup>(9)</sup>. Closed channels which couple strongly are  $3p$  and  $3d$ . The effect on  $\Omega(2s,2p)$  is less than 4% for C IV.

In general, resonance effects produce significant enhancement in collision strengths for most forbidden and semiforbidden transitions and are less important for optically allowed transitions. This is demonstrated in Figure 5 which gives effective collision strengths for spin-allowed and for spin-changing transitions between  $n = 2$  states of C III [Berrington<sup>(10)</sup>].

Target wave functions for lithiumlike ions may be represented to sufficient accuracy by single configuration, Hartree-Fock functions. However, for many systems, consideration of configuration mixing in the description of the target ion must be given. It follows from the variational principle used in the formulation of the scattering problem, that the error in the collision strengths is directly related to the first

order error in the target wave functions. Thus, target wave functions must be chosen carefully. A figure of merit for collision strengths is probably provided by the accuracy of oscillator strengths obtained with the same target wave functions. This is correct at least at very high energies where the collision strength is directly proportional to the oscillator strength.

Accuracy of the target wavefunctions can also play a crucial role in the positions of the resonances. Shifts in the resonance positions in the threshold region can cause significant differences in the collision strengths. Figure 6 gives<sup>(11)</sup>  $\Omega(3s^2\ ^1S, 3s3p\ ^3P^0)$  for Al II between the  $3s3p\ ^3P^0$  and  $3s3p\ ^1P^0$  thresholds. The large structure at about 0.4 Ry is the sum of four resonances:  $[3s3p(^1P^0)3p]\ ^2D, ^2S$  and  $[3s3p(^1P^0)3d]\ ^2F^0, ^2P^0$ . The  $^2F^0$  resonance is dominant and has a width of 0.031 Ry. Fig. 6 is an example of the  $[3s3p(^1P^0)n\ell]$  resonance series converging to the  $^1P^0$  threshold.

Figure 7 gives the effective collision strength for the transitions  $1^1S - 2^1S$  and  $1^1S - 2^1P^0$  in O VII as a function of electron temperature in K. Solid and dashed lines represent 11-state and 5-state calculations by Tayal and Kingston<sup>(12)</sup>, and the crosses are distorted wave results of Pradhan et al<sup>(13)</sup>. A group of resonances  $1s3\ell n\ell'$ , converging to the  $n = 3$  complex, which are not present in the 5-state calculation, makes a significant contribution to  $\Omega(1^1S, 2^1S)$ .

As the nuclear charge of the target ion increases, relativistic effects become important, especially for  $Z > 20$ . Figure 8 shows the effects of intermediate coupling on the collision strength  $\Omega(2s^2\ ^1S_0, 2s2p\ ^3P^0_1)$  for Fe XXIII. Calculations are by Robb<sup>(14)</sup> and Henry

and Bhadra<sup>(16)</sup> in a six-state close coupling approximation which includes the states  $2s^2(^1S)$ ,  $2s2p(^3P^0, ^1P^0)$ , and  $2p^2(^3P, ^1D, ^1S)$ . Curve A gives results of Robb in which intermediate coupling effects are included, whereas curve B represents calculations by Henry and Bhadra in which there is no mixing of levels. The spin-orbit term mixes the  $2s2p\ ^3P_1^0$  and  $2s2p\ ^1P_1^0$  configurations and so the dipole allowed transition  $2s^2\ ^1S - 2s2p\ ^1P_1^0$ , which has a collision strength  $\sim 0.5$ , dominates. Note also that the asymptotic slope of  $x^{-2}$  given by the dashed line in Fig. 8 is not reached for the unmixed results until  $x \sim 70$ .

An example of a complicated low-energy resonance structure is shown in Figure 9 for  $\Omega(2s^2\ ^1S_0, 2s2p\ ^3P_1^0)$  in Ca XVII. The solid curve represents a calculation by Dufton et al.<sup>(17)</sup> and the dashed line represents the background in the LS-approximation. One mitigating feature for higher-Z ions is that the energy range of importance to a plasma may be sufficiently above the ionization threshold that resonance effects may not be important. For Be-like ions for example, the electron temperature for maximum abundance of various ions is at  $0.5\ \Delta E(2s^2\ ^1S, 2s2p\ ^1P_1)$  for C III but at  $8\ \Delta E$  for Ca XVII.

#### ACKNOWLEDGEMENT

Research is supported in part by the U. S. Department of Energy, Division of Chemical Sciences.

## REFERENCES

1. M. J. Seaton, *Adv. Atom. Molec. Phys.* 11, 83 (1975).
2. R. J. W. Henry, *Phys. Reports* 68, 1 (1981).
3. J. Gallagher and A. N. Pradhan, JILA Report (1985).
4. P. G. Burke and M. J. Seaton, *Methods in Comp. Phys. B* 10, 1 (1971).
5. M. A. Hayes, D. W. Norcross, J. B. Mann and W. D. Robb, *J. Phys. B* 10, L429 (1977).
6. J. V. Kennedy, V. P. Myerscough, and M. R. C. McDowell, *J. Phys. B* 11, 1303 (1978).
7. P. O. Taylor, R. A. Phaneuf and G. H. Dunn, *Phys. Rev. A* 22, 435 (1980).
8. R. J. W. Henry, W. L. van Wyngaarden and J. J. Matese, *Phys. Rev. A* 17, 798 (1978).
9. K. Bhadra and R. J. W. Henry, *Phys. Rev. A* 26, 1848 (1982).
10. K. A. Berrington, *J. Phys. B* 18, L395 (1985).
11. S. S. Tayal, P. G. Burke and A. E. Kingston, *J. Phys. B* 17, 3847 (1984).
12. S. S. Tayal and A. E. Kingston, *J. Phys. B* 17, 1385 (1984).
13. A. K. Pradhan, D. W. Norcross and D. G. Hummer, *Astrophys. J.* 246, 1031 (1981).
14. W. D. Robb, quoted in Ref. 15.
15. A. L. Merts, J. B. Mann, W. D. Robb, N. H. Magee and M. F. Argo, Los Alamos Scientific Laboratory Report No. LA-8267-MS, Los Alamos, NM (1980).
16. R. J. W. Henry and K. Bhadra, quoted in Ref. 15.
17. P. L. Dufton, A. E. Kingston and N. S. Scott, *J. Phys. B* 16, 3053 (1983).

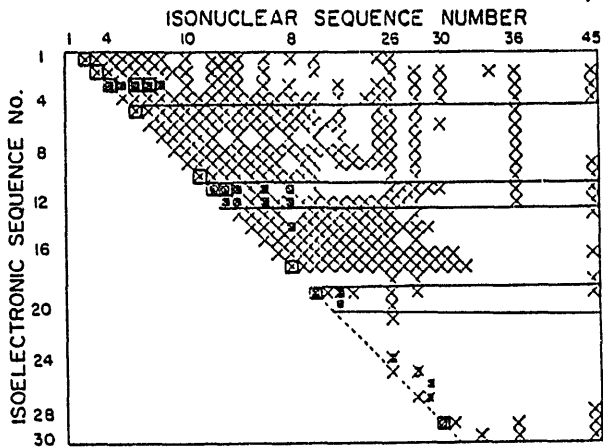


Fig. 1. Calculations and measurements

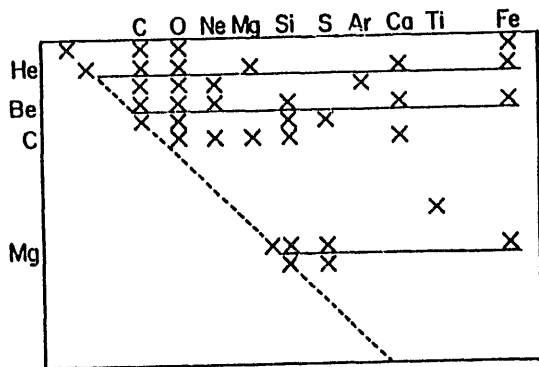


Fig. 2. Resonance calculations

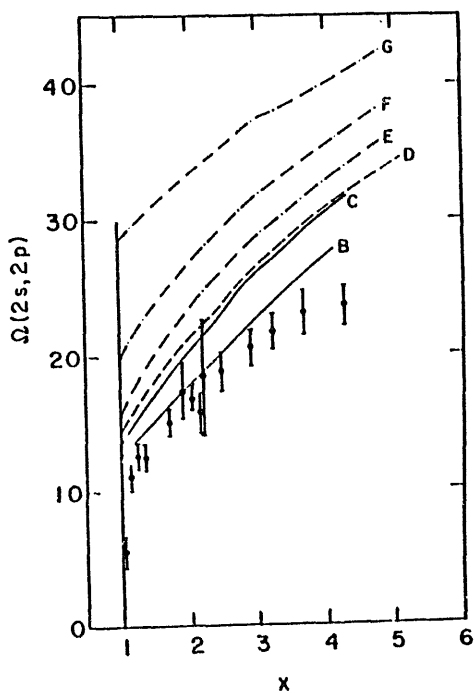


Fig. 3.  $\bar{\Omega}(2s, 2p)$  for Be II

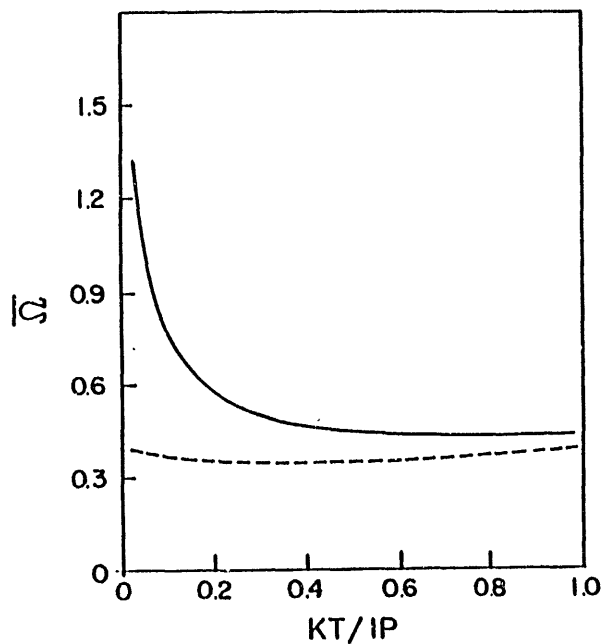


Fig. 4.  $\bar{\Omega}(2p, 3s)$  for C IV

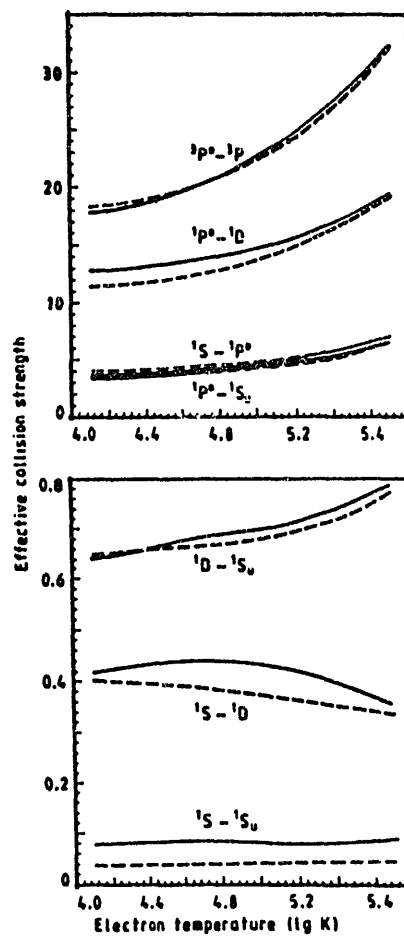


Fig. 5a. Spin-allowed C III

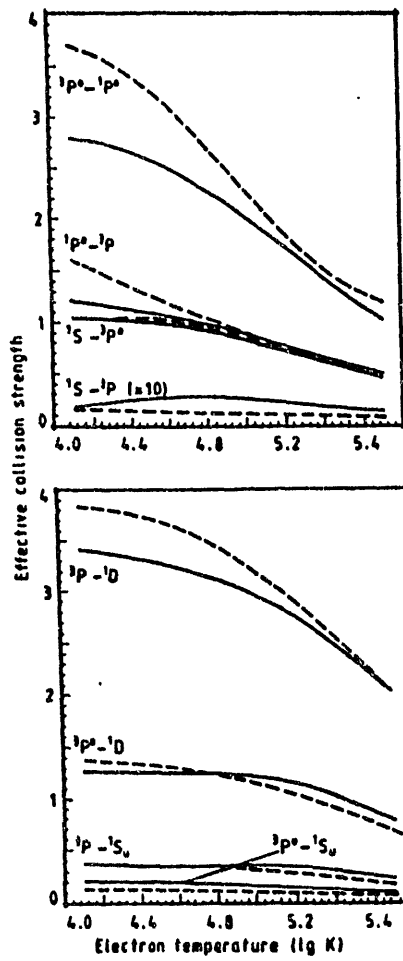


Fig. 5b. Spin-changing C III

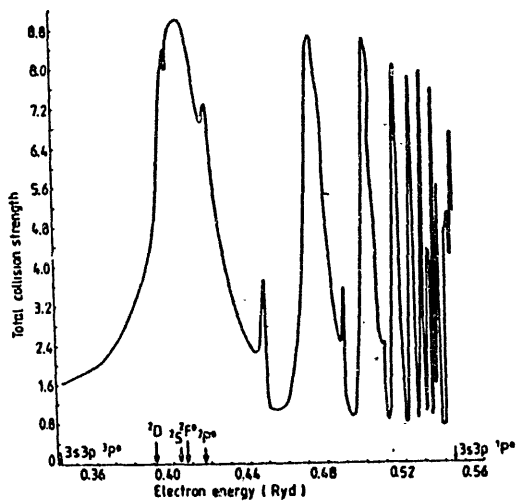


Fig. 6.  $\Omega(1S, 3P^0)$  for Al II

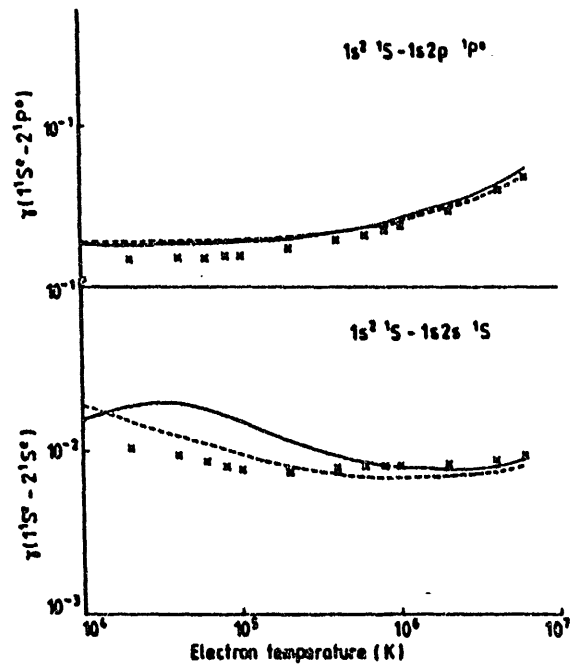


Fig. 7.  $\gamma$  for O VII

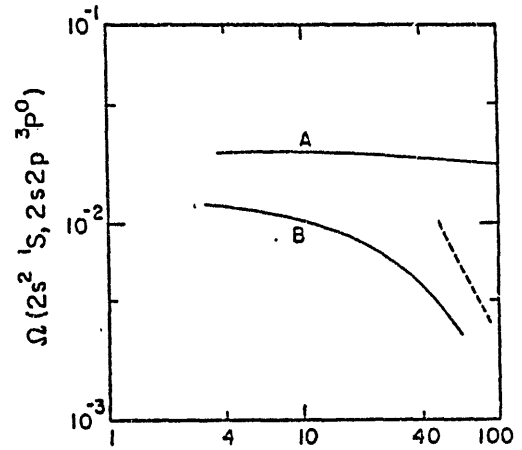


Fig. 8.  $\Omega(1S_0, 3P_1^0)$  for Fe XX III

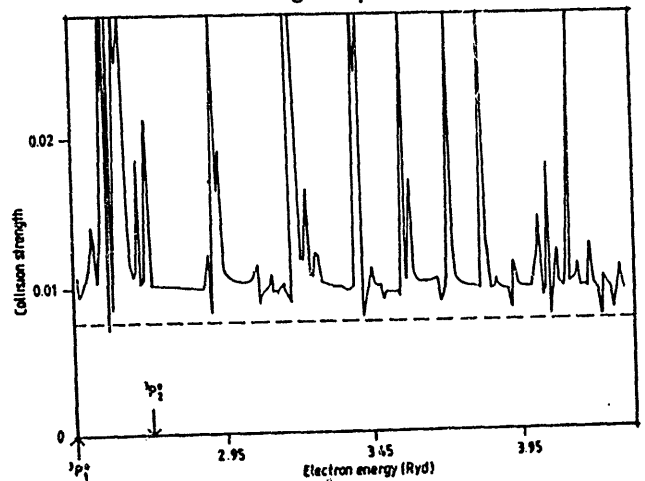


Fig. 9.  $\Omega(1S_0, 3P_1^0)$  for Ca XV II

## Cross Sections for Electron Impact Excitation of O IV

Shinobu Nakazaki

Department of Applied Physics, Faculty of Engineering,  
Miyazaki University, Miyazaki 889-21, Japan

Cross sections for allowed transitions of  $n=3$  terms in O IV are calculated using a two-state close-coupling approximation. Configuration interaction target wave functions which give accurate oscillator strengths are used in the calculation.

The intensities of emission lines of O IV and O V were measured in the JIPPT-IIU tokamak plasma by Kato et al.<sup>1</sup> The disagreement between the experimental results and the calculated results for O IV was noticed. So far, some excitation rate coefficients have been calculated for O IV. Hayes<sup>2</sup> performed a large close-coupling calculation for the excitation of O IV. Cross sections for the excitation of the principal quantum number  $n=2$  terms from the ground state and metastable states were obtained in her calculation. She used configuration interaction functions to describe the target. The close-coupling is the most elaborate method which has been used for the calculation of cross sections so far. Thus, her results are considered to be accurate cross sections. For the transitions included the  $n=3$  terms of O IV, Mann only calculated using a distorted-wave approximation

for the transitions which the lower state is the ground state. Reliable excitation cross sections for the transitions of  $n=3$  terms for allowed transitions are desired presently to solve the coupled equations which give the population density. We calculate oscillator strengths and collision strengths for allowed transitions included the  $n=3$  terms in O IV.

The excitation cross section  $\sigma(i-j)$  (measured in unit of  $\pi a_0^2$ ) is related to the collision strength  $\Omega(i,j)$  by

$$\sigma(i-j) = \Omega(i,j)/k_i^2 w_i, \quad (1)$$

where  $k_i^2$  is the energy (in Ryd) of the incident electron with respect to the lower state  $i$ , and  $w_i$  is the statistical weight of the lower atomic state for LS coupling.

The target wave functions are represented as configuration interactions in terms of orbitals  $1s, 2s, 2p, 3s, 3p$  and  $3d$ . The radial part of each orbital is expanded in the form

$$P_{nl}(r) = \sum_j C_j r^{I_j} \exp(-\xi_j r). \quad (2)$$

The values we use for  $C_j$  and  $\xi_j$  were provided by Clementi and Roetti<sup>3</sup> for the orbitals  $1s, 2s$  and  $2p$ . The orbitals  $3s, 3p$  and  $3d$  are optimized on  $2s^2 3s^2 S, 2s^2 3p^2 P$  and  $2s^2 3d^2 D$  states, respectively, by using the program CIV3 of Hibbert<sup>4</sup>. The oscillator strengths in the dipole length ( $f_l$ ) and dipole velocity ( $f_v$ ) approximations are obtained also using the program. The parameters of  $3s, 3p$  and  $3d$  orbitals are listed Table 1. Table 2 gives some of the oscillator strengths and excitation energies obtained in the present calculation. Theoretical accurate oscillator strengths of Saraph<sup>5</sup> are shown in the table. Experimental results for the oscillator strengths and the excitation energies are also given. Present results for the

oscillator strengths are in good agreement with those of Saraph, and are within error of experimental results of Buchet et al.<sup>6</sup> The difference between the oscillator strengths in the dipole length and dipole velocity approximations is an indication of accuracy of the wave function. Table 2 shows that the present target wave functions are enough for obtaining accurate collision strengths in the  $e + O IV$  scattering problem.

A two-state close-coupling method is used to obtain the collision strengths. The integro-differential equations are solved using a noniterative integral equation method NIEM of Henry et al.<sup>7</sup>

Fig. 1(a) gives collision strengths for the transition  $2s^2 2p^2 P^0 - 2s^2 3d^2 D$  as a function of  $X$ , the energy in threshold unit. So far, there is only the data of Mann<sup>8</sup> who obtained using the distorted wave approximation. The present excitation energy is listed with the experimental result and the Mann's result in Fig. 1(a). Fig. 1(b) shows collision strengths for the transition  $2s^2 2p^2 P^0 - 2s 2p(3P^0) 3p^2 D$ . It is seen from Figs. 1(a) and 1(b) that the agreement between the distorted-wave results of Mann and the present close-coupling results is very good for all the range of the incident energy.

For the transitions which the lower states are the excited states there is no collision strength so far. Figs. 1(c) and Fig. 1(d) show present collision strengths for the transitions  $2s 2p^2 4P - 2s 2p(3P^0) 3s^4 P^0$  and  $2s 2p^2 4P - 2s 2p(3P^0) 3d^4 D$ , respectively.

The collision strengths obtained for various transitions in

the present calculations are fitted to the following form

$$\Omega(X) = d_1 + d_2/X + d_3/X^2 + d_4 \ln X, \quad (4)$$

where the coefficients are determined by the least-squares method. The coefficients yield a fit to within 3% for the calculated collision strengths. The results are readily integrated over a Maxwellian velocity distribution to provide the excitation rate coefficients as

$$R = D [ d_1 \exp(-y)/y + d_3 \exp(-y) + (d_2 - d_3 y + d_4/y) \int_1^\infty dz \exp(-zy)/z ] \text{ cm}^3 \text{ s}^{-1}, \quad (5)$$

where  $D = 8.010 \times 10^{-8} y/w_i (kT)^{1/2}$ ,  $y = 13.60 E_{ij}/kT$ , with  $E_{ij}$  in Ryd and  $kT$  in eV.

The collision strengths for various transitions included the  $n=3$  terms are obtained by using the two-state close-coupling approximation. Resonance effects are not considered in the present calculations. However, it has been known that the effect of resonances on the allowed transition is not so much important. It is thought that the present collision strengths are useful for estimating the level populations.

#### References

1. T. Kato, K. Masai and K. Sato, Phys. Letters **108A**, 259(1985).
2. M. A. Hayes, J. Phys. B: At. Mol. Phys. **16**, 285(1983).
3. E. Clementi and C. Roetti, Atomic Data Nucl. Data Tables, **14**, 177(1974).
4. A. Hibbert, Comput. Comm. **9**, 141(1975).
5. H. E. Saraph, J. Phys. B: At. Mol. Phys. **13**, 3129(1980).
6. J. P. Buchet, M. C. Poulizac and M. Dreutta, J. Opt. Soc. Am. **66**, 842(1976).

7. R. J. W. Henry, S. P. Rountree and E. R. Smith, Comput. Phys.

Comm. **23**, 233(1981).

8. J. Mann(private communication).

Table 1. Values of parameters of the atomic orbitals for O IV.

Orbitals	$C_j$	$I_j$	$\xi_j$
3s	5.572404	1	6.12633
	-8.834521	2	2.38915
	2.908073	3	1.59003
3p	8.269277	2	2.81296
	-1.539654	3	1.40175
3d	1.471239	3	1.42912

Table 2. Oscillator strengths and excitation energies (in Ryd) in O IV.

Transitions	Oscillator strengths			Excitation energies	
	Present	Saraph <sup>A</sup>	Exp <sup>B</sup>	Present	Exp <sup>C</sup>
$2s^2 2p^2 \ ^2P^o - 2s^2 3s \ ^2S$	$f_l$ 0.031	0.030	$0.029 \pm 0.003$	3.232	3.258
	$f_v$ 0.032				
$- 2s^2 3d \ ^2D$	0.495	0.491	$0.53 \pm 0.05$	3.818	3.822
	0.460				
$- 2s2p(^3P^o)3p \ ^2D$	0.124	0.126	$0.116 \pm 0.011$	4.418	4.399
	0.125				
$2s2p^2 \ ^4P - 2s2p(^3P^o)3s \ ^4P^o$	0.108	0.112	$0.10 \pm 0.01$	3.363	3.348
	0.107				
$- 2s2p(^3P^o)3d \ ^4D^o$	0.716	0.729	$0.72 \pm 0.07$	3.938	3.902
	0.648				
$- 2s2p(^3P^o)3d \ ^4P^o$	0.234	0.243	$0.24 \pm 0.02$	3.970	3.941
	0.188				

A, Saraph(1980).

B, Beam-foil experiment Buchet et al.(1976).

C, Moore(1949).

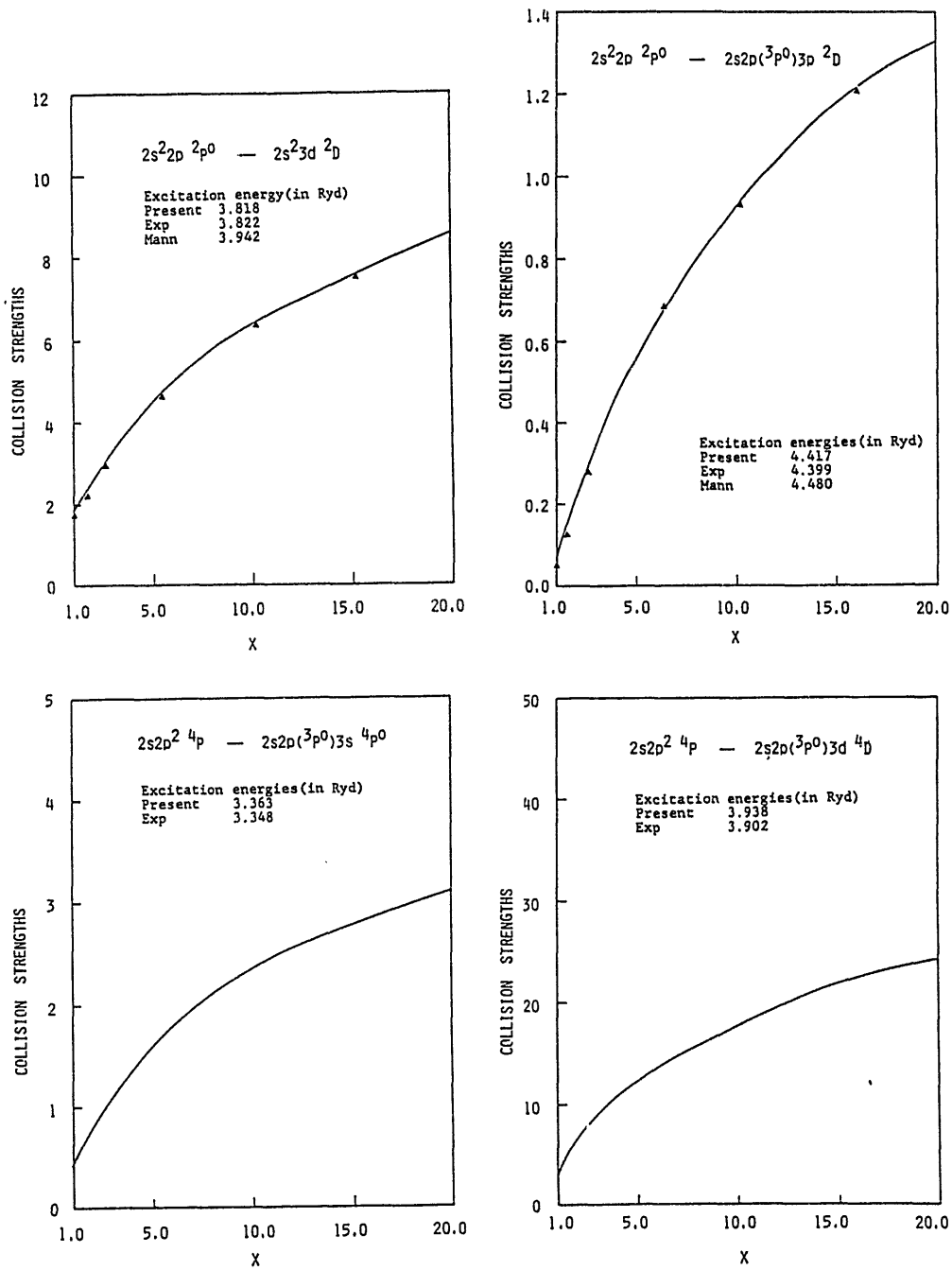


Fig. 1. Collision strengths for the transitions in O IV as a function of X (the incident energy in threshold unit): —, present two-state close-coupling results; ▲, distorted-wave results of Mann.

Decrease and disappearance of the resonance contribution to the excitation cross section of ions in dense plasma

Takashi Fujimoto

Department of Engineering Science, Kyoto University, Kyoto 606, Japan

Takako Kato

Institute of Plasma Physics, Nagoya University, Nagoya 464, Japan

Taking the excitation  $1s \rightarrow 2s$  of a hydrogen-like ion as an example, the authors have examined the effect of plasma electrons on the resonance contribution  $1s \rightarrow 3p n\ell \rightarrow 2s$  to the excitation cross section, where  $3p n\ell$  stands for the doubly excited ion produced by dielectronic capture of the  $1s$  ion. They adopt an approximation method in which all the dielectronic capture into the doubly excited levels lying higher than a certain critical level is lost from the doubly excited levels through the ladderlike excitation-  
"ionization". The part of the resonance contribution corresponding to these levels accordingly disappears. They apply the same procedure to obtain the effect on the resonance contributions from  $1s \rightarrow 3s n\ell \rightarrow 2s$  and  $1s \rightarrow 3d n\ell \rightarrow 2s$ . It is found that for  $Ne^{9+}$  ion taken as an example the plasma electron effect is appreciable for higher densities than  $10^{19} \text{ cm}^{-3}$ .

## I. Introduction

The importance of the resonance contribution to the excitation cross section has been recognized for more than ten years.<sup>1</sup> Resonances in the continuum states caused by the doubly excited rydberg-series states contribute to the excitation cross section. A number of theoretical investigations have been carried out on various excitation cross sections. In all these studies the process is treated as an electron-ion two-body collision process. In what follows we consider an excitation cross section of a hydrogen-like ion for the purpose of illustration. In this example the resonance contribution may be interpreted as follows: Dielectronic capture into a doubly excited state:  $1s + e \rightarrow 3l' n l''$ , followed by autoionization to the excited state:  $3l' n l'' \rightarrow 2l + e$ , constitute an effective excitation.

Suppose this ion is immersed in a plasma and is subjected to electron collisions. Then it is possible that the doubly excited ion,  $3l' n l''$  in the above example, suffers an electron collision before it autoionizes or decays radiatively. It is known<sup>2,3</sup> that the most probable inelastic electron collision on a singly excited rydberg state  $n l''$  is the excitation to the adjacent higher-lying level  $(n+1)l'''$ . It would be reasonable to assume that a similar excitation process takes place in the present example;  $3l' n l'' + e \rightarrow 3l' (n+1)l'''$  is the most probable inelastic collision process. The latter ion is further excited:  $3l' (n+1)l''' + e \rightarrow 3l' (n+2)l'''' + e \rightarrow \dots$ , and finally "ionized":  $3l' m l^{(k)} + e \rightarrow 3l' + 2e$  ( $m, k \gg 1$ ). This series of processes may be called the ladder-like excitation-"ionization". As its consequence, the doubly excited ion  $3l' n l''$  is lost before it autoionizes to produce the  $2l$  ion. Therefore, it is expected that in a dense plasma the resonance contribution to the excitation cross section of  $1s \rightarrow 2s$  may decrease and eventually disappear.

In the recent papers,<sup>4,5</sup> the present authors have proposed the dielectronic capture-ladderlike excitation mechanism: an example is  $1s + e \rightarrow 2\ell n\ell'$ , followed by  $2\ell n\ell' + e \rightarrow 2\ell(n+1)\ell'' + e \rightarrow \dots \rightarrow 2\ell m\ell^{(k)} + e \rightarrow 2\ell + 2e$  ( $m, k \gg 1$ ). This mechanism results in an effective increase in the excitation rate coefficient of  $1s \rightarrow 2\ell$ . They carried out a collisional-radiative calculation on the system of helium-like ion with 60 doubly excited levels and the  $1s$  and  $2\ell$  hydrogen-like levels. They obtained an increase in the effective excitation rate coefficient for  $1s \rightarrow 2\ell$  in dense plasmas as a function of electron density. In their study they further approximated this increase in the rate coefficient as an extrapolation of the excitation cross section below the threshold energy.<sup>5</sup> In the present paper we treat the decrease in the resonance contribution on the basis of the same approximation.

## II. Resonance of excitation cross section

### II.1. Resonance excitation

Although the resonance contribution is small to the excitation cross section of a hydrogen-like ion, we take the excitation  $1s \rightarrow 2s$  in this study for the purpose of illustration. Figure 1 shows the relevant schematic energy-level diagram; we take a series of processes of dielectronic capture  $1s + e \rightarrow 3p n\ell$  followed by autoionization  $3p n\ell \rightarrow 2s + e$  as an example of the resonance contribution to  $1s \rightarrow 2s$ . Since we consider processes in a dense plasma we assume that the collisional population mixing within the levels having same  $n$  takes place so rapidly that the statistical population distribution is established among them. We use only the principal quantum number to designate the state of the running electron disregarding different  $\ell$  or the singlet and triplet systems in the L-S coupling scheme. This approximation is justified by the detailed collisional

radiative model calculation,<sup>5</sup>

First, we evaluate the resonance contribution  $1s \rightarrow 3p n \rightarrow 2s$  in the limit of low density. We estimate the dielectronic capture rate coefficient,  $r_d(1s, 3p n)$ , or the autoionization probability,  $A_a(3p n, 1s)$ , on the basis of the threshold value of the excitation cross section of  $1s \rightarrow 3p$  in the infinite- $z$  approximation by Golden et al.<sup>6</sup> The autoionization probability to the final state,  $A_a(3p n, 2s)$ , is estimated similarly. In estimating the branching ratio of  $A_a(3p n, 2s)$  leading to the excitation to  $2s$  we include the stabilizing radiative decay  $3p n \rightarrow 1s n$  and the decay  $3p n \rightarrow 2s n$ . These transition probabilities are given the values of the corresponding hydrogen-like transitions. We also include the radiative decay of the running electron  $3p n \rightarrow 3p n'$  ( $n' < n$ ), Its probability is given by the approximation for a hydrogen-like level  $n$ . By multiplying the cross section  $1s \rightarrow 3p$  by the above branching ratio we obtain the excitation cross section  $1s \rightarrow 3p n \rightarrow 2s$  as a function of energy; the result is understood to correspond to the cross section averaged over resonances. Figure 2 shows the result for  $Ne^{9+}$  taken as an example. In this figure also shown are the resonance contributions from  $1s \rightarrow 3s n \rightarrow 2s$  and  $1s \rightarrow 3d n \rightarrow 2s$ ; The contributions from the  $3s n$  and  $3d n$  have been calculated in a similar procedure. The decrease in the resonance cross section near the series limit is due to a decrease in the branching ratio of  $A_a(3l n, 2s)$  in comparison with the stabilizing radiative decay. This figure also includes the direct excitation cross section  $1s \rightarrow 2s$  as given by Golden et al. and the cross section for  $1s \rightarrow 3p$ .

## II.2. The effect of electron collisions

We consider the effect of the electron collisions on these cross sections. In ref. 5 an approximation is proposed; that is, the doubly

excited levels  $2s_m$  are grouped into the higher-lying levels and the lower-lying ones; the critical level between these two groups,  $2s m_G$  (the generalized Griem's critical level<sup>2,3</sup>) is defined such that the sum of the autoionization probability and the radiative decay probabilities from this level is equal to the total excitation rate from this level, the dominant contribution to it being  $2s_m + e \rightarrow 2s(m+1) + e$ . It is justified (except in certain circumstances) to assume that the higher-lying levels than  $2s m_G$  are in a flow of the ladder-like excitation-"ionization" so that all the dielectronic capture into these levels contributes to the excitation  $1s \rightarrow 2s$ , whereas the dielectronic capture into the lower-lying levels than  $2s m_G$  is lost by autoionization or radiative decay and does not contribute to the excitation. On the basis of the relationship between the excitation cross section  $1s \rightarrow 2s$  and the autoionization probability  $A_a(2s n, 1s)$ , we can approximate the above effect of dielectronic-capture ladder-like excitation-"ionization" by an extrapolation of the excitation cross section  $1s \rightarrow 2s$  down to the energy of the critical level  $2s m_G$ .

In estimating the effect of electron collisions on the  $3p n$  levels we adopt the similar approximation; we calculate the critical level  $3p n_G$  by comparing the autoionization and radiative decay probabilities with the collisional excitation rates as a function of electron density. We regard that the dielectronic capture into the higher-lying levels than  $3p n_G$  is lost from autoionization  $3p n \rightarrow 2s$  and that the resonance cross section coming from these levels disappears. In Fig. 2 we give the energy of the critical level, or the upper limit to the resonance cross section of  $1s \rightarrow 3p n \rightarrow 2s$ . The similar upper limit is given to the other cross sections, and these are connected by thick lines. The disappearance is appreciable in dense plasmas of  $n_e \gtrsim 10^{19} \text{ cm}^{-3}$ . This figure is for an example of electron temperature of  $1 \times 10^6 \text{ K}$ , and the temperature dependence of the

above effect is quite small. This is because the temperature dependence stems only from the excitation rate coefficient which is weakly temperature dependent. (see Fig. 3 of ref. 5)

As mentioned earlier, the effect of the inelastic electron collisions on the doubly excited ions  $2s_m$  that have been produced by the dielectronic capture is to increase the excitation rate coefficient  $1s \rightarrow 2s$ , or effectively to extrapolate the excitation cross section to the critical doubly excited level. Thus the disappearance of the resonance cross section, e.g., of  $1s \rightarrow 3p n \rightarrow 2s$ , corresponds to the extrapolation of the excitation cross section,  $1s \rightarrow 3p$ , to the energy of the critical level  $3p n_c$ . In Fig. 2, the cross section is extrapolated below its threshold energy down to the critical level. Also shown is the similar extrapolation of the cross section  $1s \rightarrow 2s$ ; this is taken from ref. 5,

It is noted that the lowering of the "ionization potential" takes place at much higher energy than that of the critical level; e.g., at  $n_e = 10^{22} \text{ cm}^{-3}$  the lowering is about 18 eV, while the critical energy is about 100eV down from the original ionization limit. Therefore, the above treatment is little affected by the lowering. For the validity range see ref. 5.

In the present example of the excitation cross section of a hydrogen-like ion, the contribution from the resonance to the excitation cross section is rather small; about 30 % for  $1s \rightarrow 2s$  as seen in Fig. 2 and 15 % for  $1s \rightarrow 2p$ . In some cases the resonance contribution is quite important; sometimes it is larger than the direct or potential excitation cross section by an order. The above-mentioned plasma effect is also valid in such cases, resulting in a strong density dependence of the excitation rate coefficient.

## References

1. D.E. Osterbrock, *J. Phys. B* 3, 149 (1970); A.R.G. Jackson, *J. Phys. B* 6, 2325 (1973); W. Eissner and M.J. Seaton, *J. Phys. B* 7, 2533 (1974); L.P. Presnyakov and A.M. Urnov, *J. Phys. B* 8, 1280 (1975).
2. H.R. Griem, *Phys. Rev.* 131, 1170 (1963).
3. T. Fujimoto, *J. Phys. Soc. Japan* 47, 273 (1979).
4. T. Fujimoto and T. Kato, *Phys. Rev. Letters* 48, 1022 (1982).
5. T. Fujimoto and T. Kato, *Phys. Rev. A* 32, 1663 (1985).
6. L.B. Golden, R.E.H. Clark, S.J. Goett and D.H. Sampson, *Astrophys. J.* (suppl.) 45, 603 (1981).

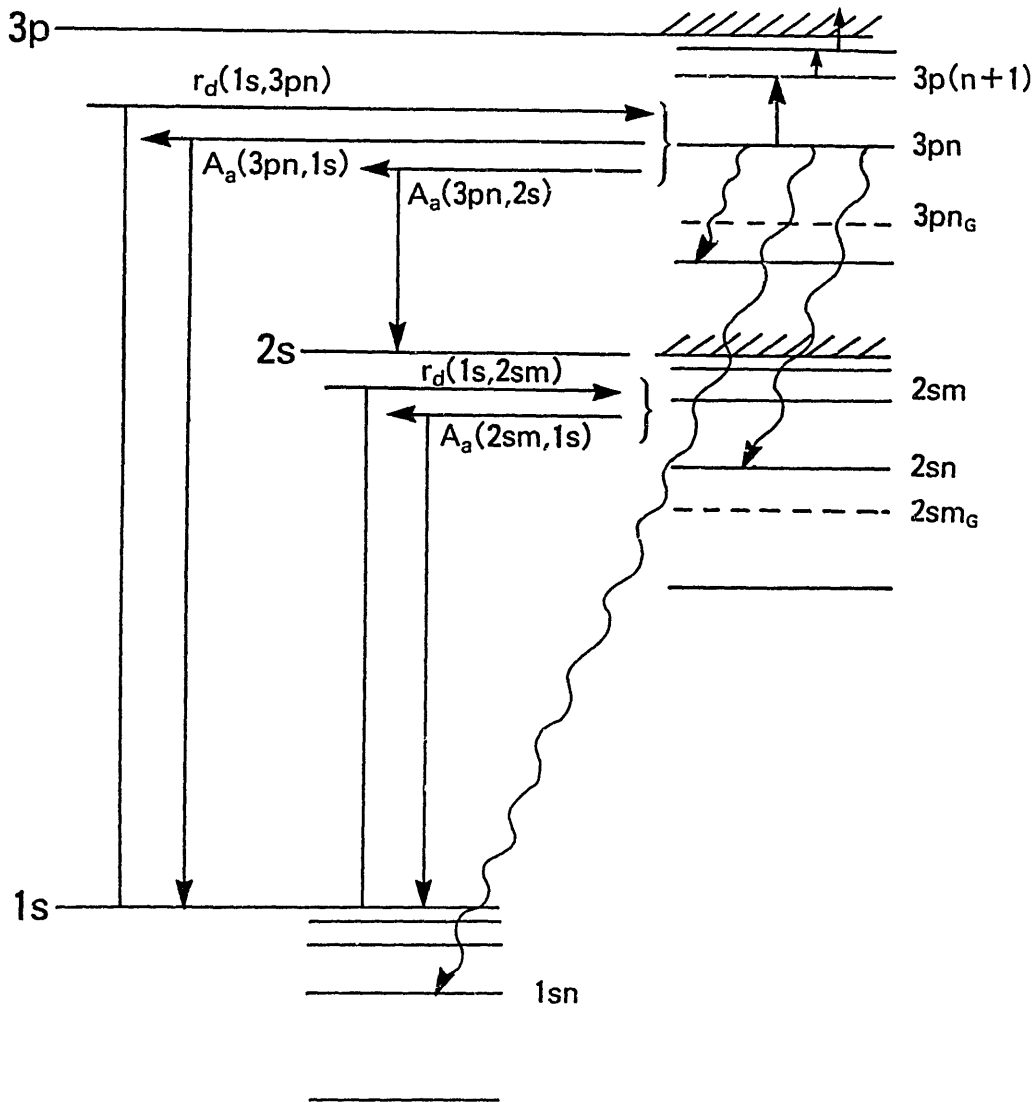


Fig. 1. Schematic energy-level diagram showing the dominant atomic processes of the doubly excited ions in plasma.  $3p n_G$  and  $2sm_G$  are the critical level (the generalized Griem's critical level) between the higher-lying levels and the lower-lying ones. The doubly excited ions produced by dielectronic capture into the higher-lying levels undergo the ladderlike excitation-"ionization" by the plasma electrons.

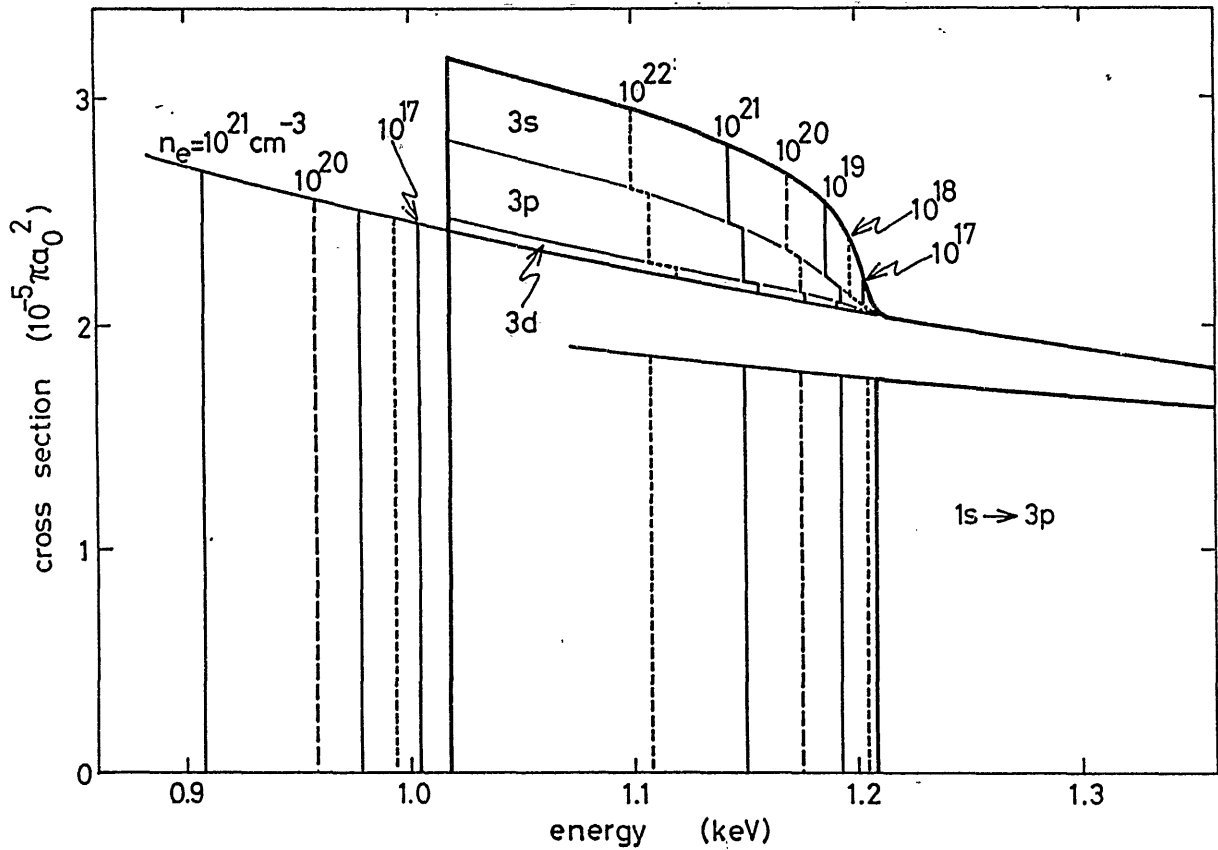


Fig. 2. The resonance contributions from the doubly excited levels to the excitation cross section  $1s \rightarrow 2s$  of a hydrogen-like neon. The energy of the critical level is indicated with the thick lines, and the part of the resonance cross section at higher energies than the critical energy disappears. Instead, the excitation threshold of the excitation cross section,  $1s \rightarrow 3p$  in this figure, is lowered to the critical level and the cross section is extrapolated to this energy. The electron temperature is  $1 \times 10^6$  K.



$$\sigma_{i-d-f}^{DR} = \frac{4\pi}{(k_c a_0)^2} V_a(i \rightarrow d) \omega(d \rightarrow f) \cdot \tilde{\delta} \cdot (\pi a_0^2) \quad (2a)$$

$$\sigma_{i-d-j}^{RE} = \frac{4\pi}{(k_c a_0)^2} V_a(i \rightarrow d) \xi(d \rightarrow j) \cdot \tilde{\delta} \cdot (\pi a_0^2) \quad (2b)$$

$$\sigma_{i-d'-f}^{EF} = \frac{4\pi}{(k_c a_0)^2} V_e(i \rightarrow d') \omega(d' \rightarrow f) \cdot \tilde{\theta} \cdot (\pi a_0^2) \quad (2c)$$

$$\sigma_{i-d'-j}^{AI} = \frac{4\pi}{(k_c a_0)^2} V_e(i \rightarrow d') \xi(d' \rightarrow j) \cdot \tilde{\theta} \cdot (\pi a_0^2) \quad (2d)$$

In (2),  $V_a$  is the simultaneous excitation-capture probability and  $V_e$  is the collisional excitation probability of inner-shell electrons.  $\omega(d \rightarrow f)$  is a partial fluorescence yield defined by

$$\omega(d \rightarrow f) = A_r(d \rightarrow f) / \Gamma(d), \quad \Gamma(d) = \Gamma_r(d) + \Gamma_a(d) \quad (3)$$

and  $\xi(d \rightarrow j)$  is a partial Auger yield

$$\xi(d \rightarrow j) = A_a(d \rightarrow j) / \Gamma(d), \quad (4)$$

where  $A_r$  and  $A_a$  are the radiative and Auger probabilities, respectively. Note the complementarity

$$\left. \begin{aligned} \sum_f \omega(d \rightarrow f) &= \omega(d) \\ \sum_j \xi(d \rightarrow j) &= \xi(d) \end{aligned} \right\} \omega(d) + \xi(d) = 1. \quad (5)$$

Also used in (2) are

$$\tilde{\delta}(E_i - E_d) = \frac{\Gamma(d)/2}{(E_i - E_d)^2 + \Gamma^2(d)/4}$$

$$\tilde{\theta}(E_i - E_d) = \begin{cases} 1 & \text{for } E_i > E_d \\ 0 & \text{for } E_i < E_d \end{cases}$$

Evidently, the correlation between the pairs DR/RE and EF/AI is effected by  $\omega / \xi$  of (5), so that the information derived from RE and AI can be

directly transferred to that for DR and EF, or vice versa. The correlation among the four processes in (1) is made complete by the quantum defect theory (QDT) relation

$$V_a(i \rightarrow d) \longrightarrow [V_e(i \rightarrow d')] \text{ analytic continuation} \quad (6)$$

where one of the bound orbitals in  $d$ , say  $d_2$  is analytically continued across the threshold to a positive energy orbital in  $d'$ , say  $c_2$ . QDT provides an explicit prescription to carry this out. For an energy-normalized continuum function we have<sup>2</sup>

$$\begin{aligned} V_a(d_1 d_2; c_1 t_2) &= \frac{z^2}{(n^*)^3} V_e(d_1 c_2; c_1 t_2) \Big|_{e_{c_2} \rightarrow e_{d_2}} \\ A_r(b' ; b) &= \frac{z^2}{(n^*)^3} A_r(c' ; b) \Big|_{e_{c'} \rightarrow e_b} \end{aligned} \quad (7)$$

where  $d_1$ ,  $d_2$ ,  $t_1$  and  $b$  are bound orbitals and  $c$ ,  $c'$  and  $c_2$  are continuum states.

The correlation between the resonant processes in e-I collision can be extended to a similar set of processes in ion-atom collisions, where charge exchange and excitations are taking place simultaneously. This is summarized in Figure 1b, where, for example, resonant-transfer-excitation with radiative decay (RTEX) is equivalent to DR in the e-I system, etc. ISEA implies an inner-shell excitation followed by an Auger decay. The entire e-I/I-A correlation can be established<sup>1</sup> in impulse approximation, and may be summarized in a 'resonance cube'. Such a unified picture is important not only in correlating our understanding of the various resonant processes, but also providing atomic data which are mutually complementary. For fusion plasma modelling and diagnostics, a large quantity of atomic data on reaction rates, energy levels, and field effects, etc is needed, and the intercorrelation of the processes should improve the data supply and accuracy of the data themselves as more checks are now available, both experimentally and theoretically.

Now we consider some of the latest results on DR and AI:

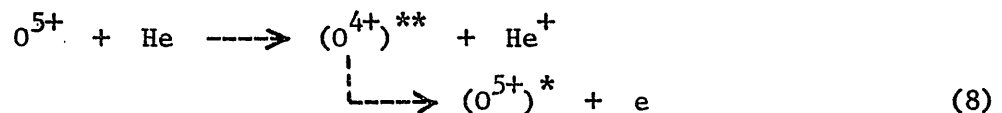
(1) DR study of  $e + Mg^+ (3s + k_c \rightarrow 3pnl, \Delta n_t = 0)$ . Dunn et al<sup>3</sup> carried out a detailed experimental study of the process, including the effect of external electric field on  $\sigma^{DR}$ . Current theoretical estimate<sup>4,5</sup> which includes the field-induced enhancement is in good agreement with experi-

ment in so far as the total energy-integrated cross section is concerned. There is however a serious discrepancy in the detailed distribution of the cross section as a function of the field strength parameter  $n_F$ . A recent study<sup>6</sup> of this problem, incorporating possible field-induced shift of the high Rydberg state quantum numbers due to a sudden rotation of the electric field, failed to explain the data.

(2) AI of positive ions. Much work has been done both experimentally and theoretically, mainly by the ORNL group<sup>7</sup> using low Z ion beam. Since the Auger yields  $\xi$  for low Z ions are nearly equal to unity, the study reduces to that of collisional excitation of inner-shell electrons.

The overall agreement between theory and experiment is good, considering the theoretical difficulty of generating reliable excitation cross sections. Large enhancement in the cross sections is often found due to the AI mode, but some of the finer details are yet to be worked out.

(3) DR and RS with  $\Delta n_t \neq 0$  excitations via I-A collisions. Presently, no direct measurement of the DR cross section is available, in which  $\Delta n_t \neq 0$  excitation of the core electrons is involved. On the other hand, RTEA in I-A collision was shown<sup>8</sup> to be closely related to DR, in the impulse approximation. Recent data on Ca and Nb ions<sup>9</sup> showed a striking dependence on the DR cross section<sup>10</sup>. More recently, this idea was extended<sup>11</sup> to RTEA, which corresponds to RE in e-I collision. The experiment was to examine the Auger electrons emitted in the reaction



The particular states analyzed in detail were  $O^{4+}(1s2s2p^2, {}^3D \text{ and } {}^1D)^{**}$ . The Auger peak ratio was found to be<sup>12</sup>

$$\begin{aligned}
 \sigma_{\text{peak}}^{\text{RE}}({}^3D) / \sigma_{\text{peak}}^{\text{RE}}({}^1D) &\approx 4.3 + 1 \quad \text{experiment} \\
 &\approx 6.6 + 1 \quad \text{theory}
 \end{aligned} \quad (9)$$

Also detected were the decay modes of  $O^{5+}$  resonance state,  $O^{5+}(1s2s2p)^{**} \longrightarrow O^{6+}(1s^2) + e$ , which corresponds to AI in e-I collision. The cross section ratio was estimated to be

$$\begin{aligned}
 \sigma^{\text{AI}}(1s2s^2 \ 2S) / \sigma^{\text{AI}}(1s2s2p \ 2P) &\approx 0.25 \quad \text{experiment} \\
 &\approx 0.22 \quad \text{theory}
 \end{aligned} \quad (10)$$

It is important to note that, unlike in all the earlier experiments, the resolution of the zero-degree Auger spectrometer used in ref. 11 was so high that the individual resonance states were isolated and their Auger decay spectra identified.

The unified resonance picture presented here<sup>1</sup> should be useful in future research activities with a new generation of highly charged ion sources.

The work reported here was supported in part by a DOE grant.

#### References

1. Y. Hahn, Comments on Atom. & Molec. Phys. 13, 103 (1983) and (1986)
2. Y. Hahn, Adv. Atom. & Molec. Phys. 21, 123 (1985), and NATO workshop, lecture note, Brussel 1985 (F. Brouillard, ed.)
3. A. Muller et al, Phys. Rev. Lett. 56, 127 (1986)
4. K. LaGattuta, I. Nasser and Y. Hahn, Phys. Rev. A33, 2782 (1986)
5. D. G. Griffin, M. S. Pindzola and C. Bottcher, Phys. Rev. A33, 3124 (1986)
6. Y. Hahn and I. Nasser, to be published.
7. M. S. Pindzola et al, ORNL/TM-9436 (1985)
8. J. A. Tanis et al, Phys. Rev. Lett. 49, 1325 and 53 2551 (1984)
9. J. A. Tanis, private communications
10. G. Omar and Y. Hahn, Phys. Rev. A (to be published); Y. Hahn, J. Gau and M. Dube, to be published.
11. J. K. Swenson et al, ORNL preprint, 1986; A. Itoh et al, J. Phys. B18 4581 (1985)
12. Y. Hahn, Phys. Lett. A (to be published)

# RELATIVISTIC EFFECTS IN ELECTRON-ION COLLISIONS

Yong-Ki Kim

National Bureau of Standards, Gaithersburg, MD 20899, U.S.A.

## Abstract

Relativistic effects in electron-ion collision cross sections and anticipated changes in resonances caused by relativity are discussed. For moderate incident energies ( $< 50$  keV), relativity reduces cross sections. For heavy ions, resonances will be shifted in energy and are likely to be broadened or fragmented due to relativistic effects.

## I. Introduction

As fusion devices advance, atomic data for very hot plasmas are required for plasma modeling and diagnostics. In such plasmas, impurity ions would be stripped very much, and relevant plasma electron energies would reach from a few to tens of keV. Spectroscopic studies of the past decade made it clear that relativistic effects in highly charged ions significantly alter energy levels and other properties.<sup>1</sup> Electron-impact collision cross sections are expected to follow the same trend.<sup>2</sup>

Relativistic effects not only alter threshold energies for both excitation and ionization of target ions but also change their orbital sizes, thus affecting collision cross sections. As the nuclear charge  $Z$  of a target ion increases, a gradual shift from LS coupling to jj coupling splits energy levels into their fine structure components, making it essential to introduce intermediate coupling in describing the target ion.

Relativistic interaction of the incident electron with an ion can be divided into two categories; spin-orbit and other interactions with the ion nucleus, and electron-electron interaction with bound electrons of the ion. The former is a one-electron effect and mostly responsible for intermediate coupling, and the latter is known as the Møller scattering.<sup>3</sup> Since relativistic orbitals with low values of orbital angular momentum  $l$  penetrate deeper into the ion core, they are affected most by the one-electron part of the relativistic effects. These effects can easily be accounted for by using the Dirac Hamiltonian for the one-electron part of the colliding complex.

Of course, the leading part of electron-electron interaction is the familiar Coulomb interaction  $e^2/r_{ij}$ , but there are additional terms that come from the exchange of a virtual transverse photon, which is the Møller scattering, and those from the exchange of more than one virtual photon. These relativistic interelectronic terms, however, contribute significantly only for very energetic incident electrons,  $T > 50$  keV, where  $T$  is the incident electron energy. For  $T$  of the order of the electron rest mass, Møller scattering dominates and electron-impact excitation and ionization cross sections are greatly enhanced.<sup>4</sup> Møller scattering is the analogue of the Breit interaction in relativistic atomic structure theory.

It is clear that a fully relativistic formulation of electron-ion collisions is desirable to account for the relativistic effects in level structure of target ions as well as to include the relativistic interaction of an incident electron with the ion nuclei. Both effects are amplified further as  $Z$  increases, while Møller scattering will grow with the collision velocity and the number of bound electrons, but not necessarily with  $Z$ .

Among various nonrelativistic theories for electron-ion collisions, distorted-wave Born approximation<sup>5</sup> (DWBA) offers the best compromise between accuracy and computational simplicity. In collaboration with J. P. Desclaux, we have extended DWBA to use relativistic Hartree-Fock (referred to as Dirac-Fock) wave functions for the target ion and relativistic continuum orbitals calculated as a self-consistent orbital in the field of bound orbitals of the ion. The bound orbitals are kept frozen while the SCF process for the continuum orbitals is applied. This procedure is equivalent to a "continuum Hartree-Fock" approximation commonly used in nonrelativistic studies.

Our distorted-wave code can enforce full exchange as well as full orthogonality between the continuum and bound orbitals. Although we plan to eventually use multiconfiguration Dirac-Fock (MCDFF) wave functions for the target, configuration mixing among continuum orbitals--similar to the K-matrix formulation--will be excluded. Only the Coulomb interaction is included in our calculation at present, though Møller scattering will be included in the near future.

To highlight the qualitative behavior of cross sections obtained using relativistic wave functions, we studied electron-impact excitation cross sections of Li-like ions. Results on Ni<sup>25+</sup> and Xe<sup>51+</sup> are presented below, with more details to be reported elsewhere.<sup>6</sup>

## II. Results

As is true in nonrelativistic cases, it is convenient to present cross sections in terms of collision strengths,  $\Omega$ :

$$\sigma = [\pi a_0^2 / (2J_i + 1)] \Omega / (T/R), \quad (1)$$

where  $a_0$  is the Bohr radius,  $J_i$  is the angular momentum of the initial target state, and  $R$  is the rydberg energy. The collision strength is an analog of the line strength in transition probabilities; it is basically interaction matrix element squared and summed over degeneracies, thus directly representing the quality of wave functions and collision theory used. Our definition of the relativistic collision strength agrees with that used by Hagelstein,<sup>7</sup> and in the nonrelativistic limit, it reduces to the nonrelativistic one commonly used.<sup>8,9</sup>

In Figs. 1 and 2, we present nonrelativistic collision strengths for the  $2S \rightarrow 2P_{1/2}$  excitation as curve A, and their relativistic counterparts as curve B. The nonrelativistic results were obtained by making the speed of light very large. Relativistic collision strengths for the  $2S \rightarrow 2P_{3/2}$  excitation were divided by 2 and plotted as curve C. If there were no spin-orbit splitting, curves B and C should coincide, and if there were no relativistic effects, curves A, B, and C should all coincide.

The difference between A and B represents mainly atomic structure effects, such as changes in target orbital sizes. The difference between curves B and C is due to intermediate coupling--a departure from the 2:1 ratio expected from LS coupling--though it is difficult to clearly separate atomic structure effects from intermediate coupling effects. As expected, these differences grow as the nuclear charge  $Z$  increases. Note that, both in Figs. 1 and 2, the difference between curves B and C is larger than that between curves A and B, indicating that intermediate coupling effects are greater than atomic structure effects.

Fig. 1. Excitations of Ni<sup>25+</sup>

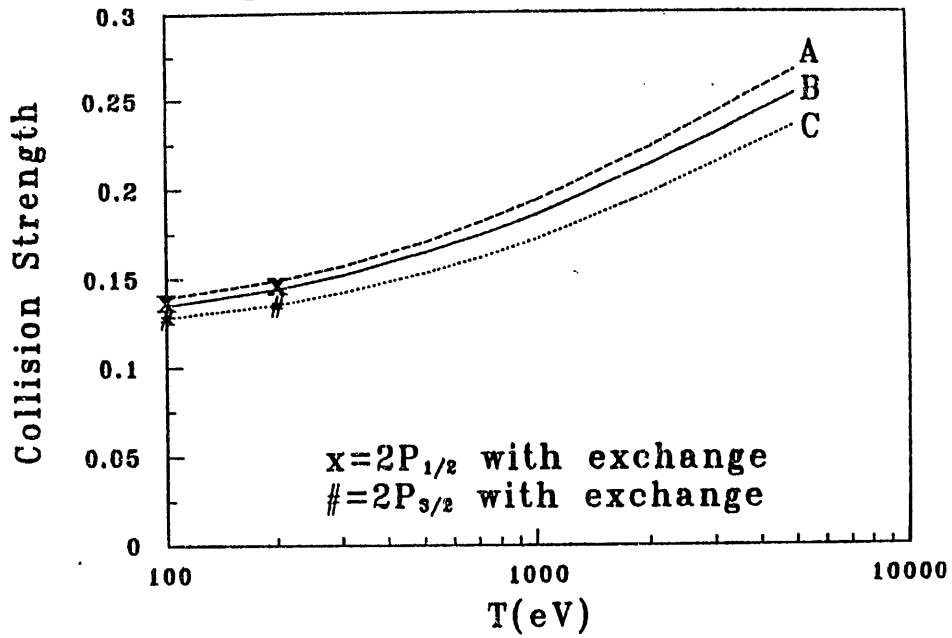
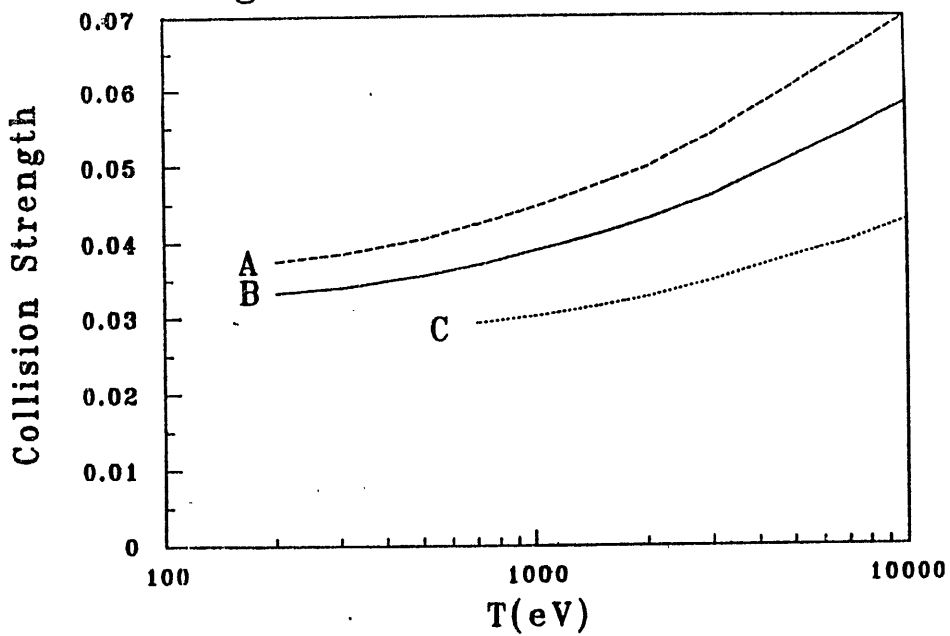


Fig. 2. Excitations of Xe<sup>51+</sup>



The departure of cross section ratios between fine structure levels from those predicted by LS coupling in  $n=3$  levels of  $\text{Ni}^{25+}$ , i.e.,  $3P_{1/2}$  versus  $3P_{3/2}$  and  $3D_{3/2}$  versus  $3D_{5/2}$ , is almost the same in relative magnitudes as those shown in Fig. 1.

Results in Figs. 1 and 2 and other relativistic cross sections we have calculated clearly show that electron-ion excitation cross sections tend to become smaller than corresponding nonrelativistic results, as long as the incident energy remains modest, i.e.,  $T < 50$  keV. This is to be expected since (a) atomic structure effects tend to shrink orbital sizes for inner orbitals thus reducing geometrical cross sections, (b) intermediate coupling affects energy levels more than orbital sizes, and (c) collision cross sections do not directly involve excitation energies [see Eq. (1)] unlike transition probabilities such as dipole oscillator strengths.

Although our codes can enforce full exchange between the incident and bound electrons as well as enforce orthogonality between them, we found that these options seriously affect cross sections only near the neutral end of an isoelectronic series and near excitation thresholds, where DWBA is unreliable. One can see in Fig. 1 that requiring exchange between the incident and bound electrons in distorted-wave calculations does not significantly alter collision strength even near the threshold. In this example, we used configuration-average exchange, i.e., the distorted waves were averaged over all allowed angular momenta  $J$  of the colliding system.

Another source of difficulty is the large number of partial waves needed for high  $T$ . For example, at  $T = 5$  keV, less than 50% of cross sections comes from partial waves of  $\ell < 50$ . Hence, a dependable method must be developed to

estimate contributions from higher partial waves. We found that results from distorted, Coulomb, and plane partial waves were significantly different only for  $\ell < 10$ . Therefore, we used the difference between plane-wave Born cross sections with and without partial-wave expansion to supplement cross sections for partial waves with high  $\ell$  ( $> 50$ ) which were not directly calculated with the distorted-wave code.

### III. Relativistic Effects in Resonances

Relativistic effects will certainly change resonances that appear in the course of electron-ion collisions for the same reasons that cross sections are affected. For instance, relativistic structure effects will shift resonance positions because doubly excited and inner-shell excited states will appear at energies different from those predicted by nonrelativistic calculations. In addition, fine-structure levels with different J's will spread due to intermediate coupling, as the nuclear charge of a target ion increases resulting in broadened resonances for intermediate Z and split ones for high Z.

Another serious consequence of relativistic effects is that excitation and ionization thresholds change so much for heavy ions (e.g., curve C in Fig. 2) that some resonances will be shifted below the relevant threshold and disappear, or new ones (not expected from nonrelativistic calculations) may appear when some excited levels are pushed above such a threshold.

For example, levels from the  $2p3s$  configuration of a Be-like ion lie above the first ionization potential for low Z, because this configuration is a doubly excited one. For high Z, however, levels from the  $2p_{1/2}3s$  configuration dive below the first ionization potential because the latter involves

one-electron  $j$ 's lower than the levels from the  $2s3p_{3/2}$  configuration; the latter is a typical, singly excited configuration. The  $2p_{3/2}3s$  configuration remains above the first ionization potential. The shifted levels will no longer appear as resonances.

#### IV. Conclusion

As we move toward high-temperature plasma devices, electron-impact cross sections for high  $T$  and ions with high ionicity are needed for diagnostics and plasma modeling. This will, in turn, require relativistic cross sections using relativistic wave functions both for continuum and bound electrons. For moderate incident energies ( $T < 50$  keV), relativistic cross sections are likely to be smaller than their nonrelativistic counterparts, mostly due to reduced orbital sizes. For very high incident energies, Møller scattering is expected to increase cross sections. Changes in energy levels and thresholds due to relativity are expected to affect resonances in highly charged, heavy ions. Relativistic effects are likely to broaden or split resonance widths and shift their positions, some below relevant ionization thresholds (these will not be resonances any more) and some above them, which will become resonances unexpected in nonrelativistic calculations.

#### Acknowledgment

The author is greatly indebted to Dr. J. P. Desclaux, whose computer codes were essential in obtaining relativistic wave functions for the present study. This work was supported in part by the Office of Magnetic Fusion Energy of the U.S. Department of Energy.

### References and Footnote

- <sup>1</sup>Y.-K. Kim and J. P. Desclaux, Phys. Rev. Lett. 36, 139 (1976).
- <sup>2</sup>Y.-K. Kim and K. T. Cheng, Phys. Rev. A18, 36 (1978).
- <sup>3</sup>C. Møller, Ann. Physik 14, 531 (1932).
- <sup>4</sup>Y.-K. Kim, Radiat. Res. 64, 205 (1975).
- <sup>5</sup>S. M. Younger in Electron Impact Ionization, edited by T. D. Märk and G. H. Dunn (Springer-Verlag, Wien, 1985), p. 1.
- <sup>6</sup>Y.-K. Kim and J. P. Desclaux, to be published.
- <sup>7</sup>P. L. Hagelstein, Phys. Rev. A34, 874 (1986), *ibid.*, A34, 924 (1986).
- <sup>8</sup>J. B. Mann, At. Data Nucl. Data Tables 29, 407 (1983).
- <sup>9</sup>For some open-shell configurations, matching relativistic and nonrelativistic spectroscopic terms may not be straightforward. For collision applications, however, such distinction is unimportant. See, for instance, C. P. Wood and N. C. Pyper, Mol. Phys. 41, 149 (1980).

# ENERGY LEVELS AND TRANSITION PROBABILITIES FOR MULTIPLY CHARGED IONS

Takashi Kagawa and Shuji Kiyokawa  
Department of Physics, Nara Women's University,  
Nara 630, Japan

Abstract: Atomic structure theory for multiply charged ions related to fusion study is reviewed. Firstly, two important effects, namely, electron correlation effects and relativistic effects on energy levels and transition probabilities for ions are briefly discussed. Finally plasma effects on the structure of ions immersed in hot dense plasmas are investigated with the finite temperature Dirac-Hartree-Fock  $X\alpha$  (FTDHF- $X\alpha$ ) method.

## 1. INTRODUCTION

In the theoretical treatments of structures for multiply charged ions, the electron correlation effects and the relativistic effects must be taken into account adequately. When ions are immersed in plasmas, plasma effects on their energy levels and wavefunctions depending on the electron temperature and density must also be considered. Plasma effects in this case mean time-averaged effects by surrounding plasma particles, which cause the shield of the nuclear charge of ions.

In the x-ray spectra emitted from highly ionized ions in low density plasmas such as laboratory Tokamak or solar corona plasmas, little shift of the transition wavelengths is observed. The line intensities observed can be used to obtain the electron density and temperature for a plasma through theoretical analysis, where transition probabilities for transitions in isolated ions are used.

However, as the electron density for a plasma increases, the structures of ions changes with strong plasma effects by surrounding ions and electrons. Here we use the FTDHF- $X\alpha$  method to investigate the plasma effects, that is,

the shield of the nuclear charge of an ion due to the free plasma electrons, on the energy levels for ions immersed dense plasmas.

This article consists of general features of the atomic structure theory for an isolated atoms and the theoretical treatment of structure for ions immersed in hot dense plasmas with the FTDHF- $X\alpha$  method.

## 2. ATOMIC STRUCTURE THEORY FOR ISOLATED ATOMIC SYSTEMS

### (a) Electron correlation effects

The Hartree-Fock (HF) model is a standard model for many-electron systems and yields an average local potential due to motions of electrons. Using the HF energy, the electron correlation energy is defined in the non-relativistic framework as

$$E_{\text{corr.}} = E_{\text{exact}} - E_{\text{HF}}, \quad (1)$$

where  $E_{\text{exact}}$  is a nonrelativistic exact energy for the ground state of a system. The  $E_{\text{corr.}}$  is not an observable quantity but a useful indication what degree of correlated motions of electrons interacting each other under the nucleus Coulomb field are covered with the theory used. A lot of people have so far studied various precise methods beyond the HF model. Those are the CI method, correlated orbital method, many-body perturbation theory etc. and their modifications. These accurate theories naturally can give accurate wavefunctions. For example, if one calculates transition probabilities for transitions in atomic systems using the CI method, he will obtain agreement of the values between the velocity and length formulations for the transition probability when number of configurations for the upper and lower states is increased. Although coincidence of values for oscillator strength or transition probability between the two different formulations is not a necessary and sufficient condition for wavefunctions to be accurate, the degree of this coincidence is usually used to judge

accuracy of wavefunctions obtained.

As is well known, reliable excitation cross sections for ions in electron-ion collisions depends on accuracy of wavefunctions for target ions. As few experimental cross sections for multiply charged ions in electron-ion collisions have so far been reported, it is important in fusion research to accumulate more reliable theoretical cross sections for these collision systems by using accurate wavefunctions for target ions as far as possible.

(b) Relativistic effects

In the relativistic case, it is difficult to extract the electron correlation energy from a calculated total energy because the electron correlation energy is defined in the nonrelativistic theory, where the correction energy due to the relativistic effects are calculated separately using the first-order-perturbation theory.

The relativistic effects become much more important than the correlation effects when atomic number  $Z$  increases. Using hydrogenic wavefunctions, it is shown that relativistic effects on the energy have strong  $Z$  dependence: For example,  $E_{\text{spin-orbit}} \propto \alpha^2 Z^4$ ,  $E_{\text{spin-spin}} \propto \alpha^2 Z^3$ ,  $E_{\text{Lamb shift}} \propto \alpha^3 Z^4$ , etc.<sup>1)</sup> Relativistic total energies for a state in an atom are always lower than nonrelativistic ones.

Relativistic effects also appear in wavefunctions for atomic systems. Orbitals especially for inner shells obtained from the relativistic HF calculations are contracted compared with nonrelativistic HF ones. A crude but intelligible explanation for the shrinkage of orbitals due to the relativistic effects is that the Bohr radius  $a_0$  is in inverse proportion to electron mass, since electron mass  $m$  becomes large when its speed increases according to the relation of  $m = m_0 / \sqrt{1 - (v/c)^2}$ .

Another important relativistic effects on the energy levels and wavefunctions are the change of the coupling scheme from LS to jj-ones mainly due to the spin-orbit interaction. Wavefunctions for actual atoms or ions must be

expressed in intermediate coupling scheme. So the multiconfiguration Dirac-Fock (MCDF)<sup>2,3)</sup> or the multiconfiguration relativistic Hartree-Fock-Roothaan (MCRHFR)<sup>4)</sup>, namely, the expansion method, have been developed to introduce wavefunctions in intermediate coupling scheme into the theory.

At present, the relativistic atomic structure theory is still suffering from the disease so called Brown-Ravenhall<sup>5)</sup> (BR) problem or variational collapse. The spectra of the relativistic Hamiltonian for many-electron atoms, which consists of the Dirac one-electron Hamiltonian and the two-electron operators due to the Coulomb and the Breit interactions, is not bounded from below because not only positive-energy but also negative-energy solutions are obtained from the relativistic equation. This means that the variational principle cannot be applied to relativistic wave equations, since the lowest energy obtained by a variational calculation, in principle, drops into negative-energy continuum. Some methods to avoid the problem such as the projection operator method<sup>6)</sup> or general variation method<sup>7)</sup> are proposed but examined little until now. In spite of the BR problem, it has been known that relativistic calculations can successfully be applied to atomic systems: Calculated transition energies and oscillator strengths for multiply charged ions are in good agreement with experiment.

### 3. FTDHF- $X_\alpha$ THEORY FOR MULTIPLY CHARGED IONS IMMERSSED IN HOT DENSE PLASMAS

Recently, we have studied on the structures of ions immersed in hot dense plasmas by use of the finite temperature Dirac-Hartree-Fock- $X_\alpha$  (FTDHF- $X_\alpha$ ) method<sup>8)</sup> which yields energy levels, thermodynamic parameters such as free energies and chemical potential for an average ion. This method has also been investigated by Rozsnyai<sup>9)</sup>.

In this study, we consider plasmas which satisfy the following two assumptions: (1) Plasmas under consideration are in thermodynamic equilibrium and (2) correlation among

ions can be neglected, so that the ion-sphere model is valid for the plasmas.

In the ion-sphere model, each ion-sphere consists of an ion and free electrons, where charge neutrality in a sphere holds.

The total Hamiltonian for an ion in a sphere in the second quantized form is given by

$$\hat{H} = \sum h_{ij} a_i^\dagger a_j + \frac{1}{2} \sum v_{ijkl} a_i^\dagger a_j^\dagger a_l a_k, \quad (2)$$

where  $a_i^\dagger$  and  $a_i$  are the creation and annihilation operators for electrons in the  $i$ -th shell, respectively.

The thermodynamic potential  $\Omega$  for the system is written as

$$\Omega = \langle \hat{H} \rangle - \mu \langle \hat{N} \rangle - TS, \quad (3)$$

where

$$\hat{N} = \sum a_i^\dagger a_i, \quad (4)$$

and  $\mu$ ,  $T$  and  $S$  are the chemical potential, electron temperature and entropy.  $\langle \rangle$  denotes the grand canonical ensemble average.

We divide the total Hamiltonian into two parts, namely, the unperturbed  $\hat{H}_0$  and perturbing  $\hat{H}'$  ones. Here we assume the unperturbed Hamiltonian in the form,

$$\hat{H}_0 = \sum (\epsilon_i - \mu) a_i^\dagger a_i, \quad (5)$$

where  $\epsilon_i$  is a constant, so that  $\hat{H}'$  is given by

$$\hat{H}' = \hat{H} - \hat{H}_0. \quad (6)$$

Using the many-body perturbation theory,  $\Omega$  is expressed in the following form,

$$\Omega = \Omega_0 - T \sum_{n=1}^{\infty} \frac{(-1)^n}{n!} \int_0^{\beta} \langle \text{Tr}[\hat{H}_I(t_1) \cdots \hat{H}_I(t_n)] \rangle_0 dt_1 \cdots dt_n, \quad (7)$$

where  $\beta = 1/k_B T$  and  $k_B$  is the Boltzmann constant.  $\hat{H}_I(t)$  is an interacting Hamiltonian defined as

$$\hat{H}_I(t) = e^{\beta \hat{H}_0} \hat{H}_I e^{-\beta \hat{H}_0} \quad (8)$$

and

$$\hat{H}_I = \hat{H}' - \mu \hat{N} = \hat{H} - \mu \hat{N} - \hat{H}_0. \quad (9)$$

$\Omega_0$  in eq.(7) is given by

$$\Omega_0 = \sum_i (\epsilon_i - \mu) f_i + T \sum_i \{ f_i \ln f_i + (1-f_i) \ln (1-f_i) \}, \quad (10)$$

where  $f_i$  is the Fermi distribution function written as

$$f_i = 1 / \{ \exp[\beta(\epsilon_i - \mu)] + 1 \}. \quad (11)$$

We obtain an approximate  $\Omega$  in eq.(7) by truncating terms for  $n > 1$  in the following,

$$\Omega \approx \Omega_0 + \Omega_1, \quad (12)$$

where

$$\begin{aligned} \Omega_1 &= T \int \langle \hat{H}_I(t) \rangle dt \\ &= \sum_i (h_{ii} - \epsilon_i) f_i + \frac{1}{2} \sum (v_{ijij} - v_{ijji}) f_i f_j. \end{aligned} \quad (13)$$

Applying the variational principle to the approximate  $\Omega$  in eq. (12) with respect to wavefunctions for the unperturbed Hamiltonian  $\hat{H}_0$ , the finite temperature Dirac-Hartree-Fock (FTDHF) equation with the Kohn-Sham

approximation for the exchange potential  $V_x(r)$  is obtained as

$$[h_D(\vec{r}) + v_d(r) - v_x(r)]\phi_i = \epsilon_i\phi_i, \quad (14)$$

where

$$h_D(\vec{r}) = c \vec{\alpha} \vec{p} + \beta mc^2 - Ze^2/r, \quad (15)$$

$$v_d(r) = e^2 \int \{[\rho_{\text{bound}}(r) + \rho_{\text{free}}(r)]/|\vec{r} - \vec{r}'|\} d\vec{r}', \quad (16)$$

$$v_x(r) = (3e^2/2\pi) \{3\pi^2[\rho_{\text{bound}}(r) + \rho_{\text{free}}(r)]\}^{1/3}, \quad (17)$$

$$\rho_{\text{bound}}(r) = \sum_i (2j_i+1)f_i \{G_i^2(r)+F_i^2(r)\}, \quad (18)$$

$$\rho_{\text{free}}(r) = (8\pi/h^3) \int \frac{p^2 dp}{\exp[\beta(\epsilon-\mu)] + 1}, \quad (19)$$

and  $G_i(r)$  and  $F_i(r)$  are the large and small components of the radial part of a relativistic four-component orbital, respectively. The average number of bound electrons  $N$ , which is not an integer, is also obtained from the calculation of chemical potential  $\mu$  which is determined so that the sum of bound and free electrons becomes  $Z$ . The average charge state  $Q$  is obtained as  $Z-N$ .

Calculated average charge state for iron plasmas with electron temperatures of 50 eV and 100 eV as a function of ion density is shown in Figure. It is seen from the figure that the average charge state is almost twelve for the plasma with ion density of  $10^{22}/\text{cm}^3$ , near normal solid state density of iron. In this case, calculated Fermi distribution functions for 1s, 2s and 2p orbitals are almost unity so that these electrons form core.

For actual systems, we calculate the total energy for an ion having specific charge state and configuration using the FTDHF  $X\alpha$  equation in eq. (14), where the Fermi distribution functions are replaced by integer occupation

numbers for bound electrons. The chemical potential  $\mu$  in the expression of  $\rho_{\text{free}}(r)$  in eq. (19) is fixed in the calculations. These results will be used to analyze the x-ray spectra emitted from heavy elements in hot dense plasmas such as the laser-beam-inertia-confinement-fusion plasmas.

#### 4. SUMMARY

The present status of the atomic structure theory for multiply charged ions related to the fusion study is briefly presented. It is emphasized that the relativistic effects are much more important than the correlation effects in the theoretical treatment of the structure for ions as the atomic number increases, and that the plasma effects on energy levels and transition probabilities for ions are negligible if they are immersed in thin plasmas such as the laboratory-magnetic-confinement-fusion ones. The FTDHF-X $\alpha$  equation is derived to calculate charge states and energy levels for an average ion in hot dense plasmas, where the plasma effects as well as the relativistic effects are taken into account in the theory.

- 1) H.A. Bethe and E. E. Salpeter, Quantum Mechanics of One- and Two-Electron Atoms (Springer, Berlin, 1957), p-185.
- 2) I.P. Grant, B.J. McKenzie, P.H. Norrington, D.F. Mayers and N.C. Pyper, Comput. Phys. Commun. 21, 207 (1980).
- 3) J. P. Desclaux, Comput. Phys. Commun. 9, 31 (1975).
- 4) T. Kagawa, Phys. Rev. A22, 2340 (1980).
- 5) G.E. Brown and D.G. Ravenhall, Proc. R. Soc. London Ser. A208, 552 (1951).
- 6) J. Sucher, Phys. Rev. A22, 348 (1980).
- 7) T. Kagawa, Intern. J. Quant. Chem. 23, 973 (1983).
- 8) S. Kiyokawa and T. Kagawa, in preparation.
- 9) B.F. Rozsnyai, Phys. Rev. A5, 1137 (1972).

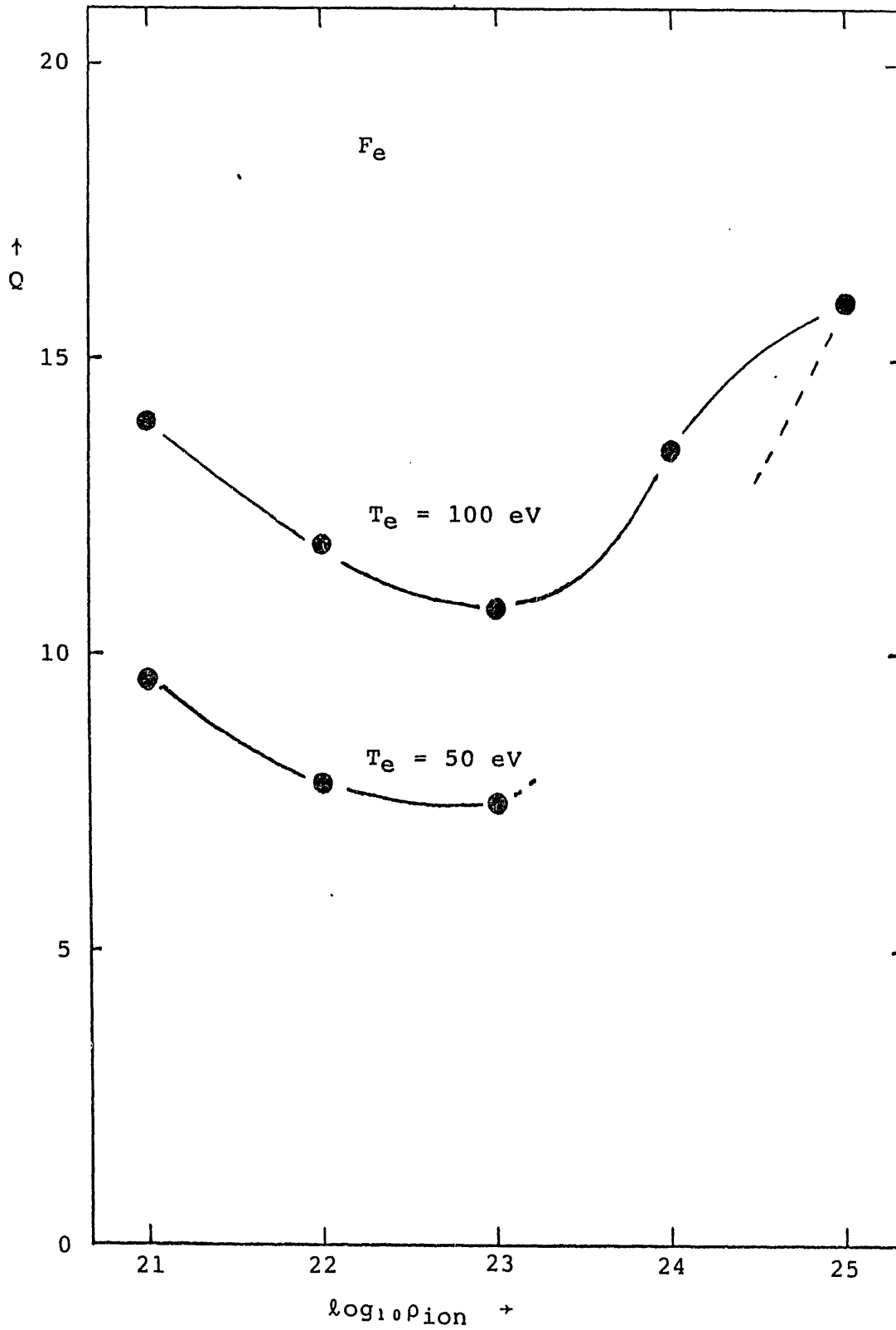


Figure. FTDHF-X charge state for iron plasmas as a function of ion density.

## TUNEABLE RESONANCES: DIELECTRONIC RECOMBINATION

Gordon H. Dunn

Joint Institute for Laboratory Astrophysics of the  
National Bureau of Standards and the University of Colorado  
Boulder, CO 80309-0440, USA

It was recognized very early by Burgess<sup>1</sup> that there are very many capture resonances that normally don't contribute to dielectronic recombination (DR). These are usually states with moderate to large angular momenta which don't contribute to DR because the autoionization rate falls off rapidly with  $\ell$ , the angular momentum quantum number.

To understand this, one must remember that the DR cross section for recombination to a state with a Rydberg electron described by quantum numbers  $n\ell$  behaves as

$$\sigma_{n\ell} = \sigma_0 2(2\ell + 1) \left( \frac{A_a(n, \ell) \cdot A_r(n, \ell)}{A_a(n, \ell) + A_r(n, \ell)} \right) \quad (1)$$

Here  $\sigma_0$  involves various constants and the statistical weights of the initial state and of the core of the product,  $2(2\ell+1)$  is the statistical weight of the final Rydberg state, and  $A_a(n, \ell)$  and  $A_r(n, \ell)$  are autoionization and radiative rates of respectively of the doubly excited state.

For DR into a Rydberg state characterized by  $n$ , we have  $\sigma_n = \sum_{\ell=0}^{n-1} \sigma_{n\ell}$ , and the total cross section for DR is  $\sigma = \sum_n \sigma_n$ . Now, if  $A_a \gg A_r$ , as is often the case, then the bracketed quantity in Eq. (1) becomes approximately just equal to  $A_r$ . Then  $\sigma_n$  diverges as  $n^4$ , since  $\sum_{\ell=0}^{n-1} 2(2\ell+1) = 2n^2$ . However,  $A_a \propto 1/n^3$ , i.e., electrons in very distant orbits don't "see" the core excited electron enough to make autoionization likely. Also,  $A_r$  is essentially

constant with  $n$ . Thus, at high enough  $n$ ,  $A_a < A_r$  and  $\sigma_n \propto 1/n^3$ . Similarly,  $A_a(n, l)$  decreases rapidly with  $l$  [for example,  $A_a \propto \exp(-al^2)$ , where  $a$  is a constant]. For a given (low to moderate)  $n$ , and for low  $l$ , again  $A_a \gg A_r$ , so that  $\sigma_{nl} \propto (2l+1) A_r$ , and for high  $l$ ,  $\sigma_{nl} \propto (2l+1)\exp(-al^2)$ , becoming negligible for  $l > l_c$  where  $A_a(n, l_c) \approx A_r$ . The value of  $l_c$  may typically lie in the range 7-10. Thus, though the number of resonances which could contribute to DR increases as  $2n^2$ , only  $l$ 's for  $l \lesssim l_c$  will contribute substantially, and states with  $l_g > l_c$  form a substantial reservoir of states which, if their autoionization rates were increased, could contribute to DR and enhance the cross section.

Burgess and Summers<sup>2</sup> treated the mixing of  $l$  states by collisions with electrons, showing an important dependence of DR rate coefficients upon electron density. Jacobs et al.<sup>3</sup> recognized that electric fields may also mix angular momenta and treated the effect of plasma microfields on DR rates. Thus, electric fields present in the collision region may mix states of different angular momentum. States in the "reservoir" referred to above with low  $A_a$  may become mixed with states of high  $A_a$ , thus leading to an effective  $A_a > A_r$ . The field is like a "knob" by which the participating numbers of resonances may be tuned in and out. Since  $A_r \propto Z^4$  for  $\Delta n \neq 0$ , then for highly charged ions  $A_r < A_a$  only for a few low values of  $n$ . The reservoir of "unused" resonances is non-existent for these low  $n$ , and consequently small or no field effects will be expected for ions of high enough charge or for situations where low  $n$  are observed for other reasons.

Subsequent to the work of Jacobs et al., the effects of fields have been investigated by others.<sup>4-13</sup> Some<sup>6-11</sup> have looked in detail at systems for which there are experimental measurements. Quite recently Harmin<sup>12</sup> and

Sakimoto<sup>13</sup> extended the ab initio theory for DR of Bell and Seaton<sup>14</sup> to include the effects of extrinsic fields.

A variety of experiments have been conducted recently using an assortment of somewhat complementary techniques.<sup>15</sup> The methods include colliding beams, resonance transfer and excitation (RTE), spectroscopic measurements of DR satellite to resonance line ratios, and time history observation and modelling of plasmas.

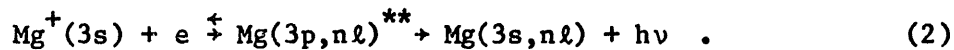
The line ratio experiments, the RTE measurements, and a few of the time behavior experiments deal with highly charged ions where -- as discussed above -- little effect of "tuning" should be in evidence. Reasonable agreement with theory is found. For the plasma experiments utilizing time history modelling and observation of ions of intermediate charge, comparison between experiment and theory gives very mixed results. Most authors conclude by emphasizing the probable importance of fields in determining the results, but have no way to reliably assess the impact in detail. Indeed, one may expect the "tuning" effect to be operable in these instances.

The merged beams apparatus at ORNL has been used to measure most of the DR cross sections/rates using colliding beams.<sup>16</sup> With this method there is a quite substantial electric field in the collision region due to the space charge of the high intensity electron beam. The field is not measureable nor otherwise readily assessable, but most of the DR data can be rationalized with theory by assuming an average electric field of about  $254 \text{ cm}^{-1}$ . However, there remain some interesting -- and perhaps important -- anomalies in this effort to rationalize the data. For example, for the Li-like ions, the cross sections seem to be of a magnitude which one would predict for a fully mixed collision complex, where "fully mixed" means that all  $\ell$  states are mixed into

a range where  $A_a > A_r$ . The data on Na-like ions are of a magnitude to suggest about 50% of full mixing.

The other<sup>17-19</sup> first generation beams experiments also have been at least approximately rationalized with theory if fields are taken into account. A second generation colliding beams experiment has now been completed and reported<sup>20</sup> which is deliberately designed and conducted to study the effects of fields on the DR process. The process under study is thus explicitly DRF dielectronic recombination in the presence of fields.

Crossed beams of electrons and ions are employed to study the process,



The product Rydberg atoms,  $\text{Mg}(3s, n\ell)$ , formed from DRF enter a wedge field Rydberg state analyzer and detector. The cross section for DRF can thus be measured as a function of the field index quantum number

$$n_F = \left( \frac{3.2 \times 10^8}{E} \right)^{1/4}, \quad (3)$$

the value of  $n$  which will classically just field ionize in a field  $E$  V cm<sup>-1</sup>.

The cross section can also be measured as a function of electron energy  $E_e$  for fixed  $n_f$  and all this can be measured for different fields  $E_c$  in the collision region.

The variation of the cross section at  $n_f = 33$  with  $E_c$  is very steep between about 2 V cm<sup>-1</sup> and 20 V cm<sup>-1</sup>, and levels out for fields significantly above or below these values. The measured shape of this variation with  $E_c$  agrees quite well with the theoretical<sup>9,11</sup> variation. At  $E_c = 7.2$  V cm<sup>-1</sup>, the total collision strength  $S = \int_{n_f} \sigma(n_f) dE_e$  agrees perfectly with theoretical values.<sup>9,11</sup> At  $E_c = 23.5$  V cm<sup>-1</sup>, the measured total strength is nearly 30% larger than calculated.

Similarly, at  $E_c = 7.2 \text{ V cm}^{-1}$  the collision strength as a function of  $n_f$  is in reasonable agreement with theory.<sup>9,11</sup> At  $E_c = 23.5 \text{ V cm}^{-1}$  the curve versus  $n_f$  is more strongly peaked and narrow. Though hypotheses concerning redistribution of Stark states in transit to the detector can lead to arbitrarily good agreement between theory and experiment for  $E_c = 23.5 \text{ V cm}^{-1}$ , it is likely that such hypotheses will also detract from the agreement at  $E_c = 7.2 \text{ V cm}^{-1}$ .

Thus, "tuning" the DR cross section with electric fields has been shown to be real, significant, and theoretically predictable. Some disagreements with theory at a detailed level persist. The anomaly concerning the Li-like and Na-like ions in the merged-beams experiments remains unsettled, and will probably remain unsettled until detailed field variation studies are conducted for these ions.

It is clear that further second generation beams experiments must allow for determination of fields in the interaction region and, if possible, variation of the field should be provided for. Carefully planned plasma experiments on ions of intermediate charge with controlled and determinable fields will be a challenge, but a challenge which needs to be met in unravelling how "tuning" occurs in the plasma environment.

#### References

1. A. Burgess, *Ann. D'Astrophysique* 28, 774 (1965).
2. A. Burgess and H. P. Summers, *Ap. J.* 157, 1007 (1969).
3. V. L. Jacobs, J. Davis, and P. C. Kepple, *Phys. Rev. Lett.* 37, 1390 (1976); V. L. Jacobs and J. Davis, *Phys. Rev. A* 19, 776 (1979).
4. A. K. Grigoriadi and O. I. Fison, *Sov. J. Plasma Phys.* 8, 440 (1982).

5. W. A. Huber and C. Bottcher, J. Phys. B 13, L399 (1980).
6. K. LaGattuta and Y. Hahn, Phys. Rev. Lett. 51, 558 (1983).
7. A. P. Hickman, J. Phys. B 17, L101 (1984).
8. D. C. Griffin, M. S. Pindzola, and C. Bottcher, Oak Ridge National Laboratory Report ORNL/TM-9478 (1985).
9. K. LaGattuta, I. Nasser, and Y. Hahn, Phys. Rev. A 33, 2782 (1986).
10. D. C. Griffin, M. S. Pindzola, and C. Bottcher, Phys. Rev. A 33, 3124 (1986).
11. C. Bottcher, D. C. Griffin, and M. S. Pindzola, Phys. Rev. A 34, 860 (1986).
12. D. Harmin, Phys. Rev. Lett. (1986).
13. K. Sakimoto, J. Phys. B (1986).
14. R. H. Bell and M. J. Seaton, J. Phys. B 18, 1589 (1985).
15. Experimental methods and data have been reviewed recently in: G. H. Dunn, in Physics of Electron-ion and Ion-ion Collisions, F. Brouillard and P. Defrance, eds. (Plenum, New York, 1986).
16. P. F. Dittner, S. Datz; P. D. Miller, C. D. Moak, P. H. Stelson, C. Bottcher, W. B. Dress, C. D. Alton, and N. Nesković, Phys. Rev. Lett. 51, 31 (1983); P. F. Dittner, S. Datz, P. D. Miller, P. L. Pepmiller, and C. M. Fou, Phys. Rev. A 33, 124 (1986).
17. D. S. Belić, G. H. Dunn, T. J. Morgan, D. W. Mueller, and C. Timmer, Phys. Rev. Lett. 50, 339 (1983).
18. J. B. A. Mitchell, C. T. Ng, J. L. Foraud, D. P. Levac, R. E. Mitchell, A. Sen, D. B. Miko, and J. W. McGowan, Phys. Rev. Lett 50, 335 (1983).
19. J. F. Williams, Phys. Rev. A 29, 2936 (1984).
20. A. Müller, D. S. Belić, B. D. DePaola, N. Djurić, G. H. Dunn, D. W. Mueller, and C. Timmer, Phys. Rev. Lett. 56, 127 (1986).

# EFFECTS OF ELECTRIC FIELDS ON DIELECTRONIC RECOMBINATION

--- MQDT treatment ---

Kazuhiro Sakimoto

The Institute of Space and Astronautical Science

Meguro-ku, Komaba, Tokyo 153, Japan

**Abstract.** A multichannel quantum defect theory of the Stark effect developed recently by the present author is applied to a dielectronic recombination (DR) process in an external electric field. Analytical formulae are derived for calculating the DR cross sections so that the effect of an applied electric field is correctly taken into account. Some model calculations are performed.

## 1. Introduction

Recently, it has been experimentally confirmed that an electric field (EF) significantly affects a dielectronic recombination (DR) process<sup>1</sup>. In this study, we provide an ab initio treatment of DR in an EF, and derive an analytical formula for calculating the DR cross section where effects of an EF on resonance states are correctly taken into account. For this purpose, we invoke a multichannel quantum defect theory (MQDT) of the Stark effect introduced by the present author<sup>2</sup> and a general theory of DR in vanishing fields developed by Bell and Seaton<sup>3</sup>.

## 2. MQDT treatment of the Stark effect for the bound state

Fano<sup>4</sup> suggested that a quantum defect theory (QDT) is useful in the study of an alkali metal perturbed by an EF. Harmin<sup>5</sup> applied Fano's idea to the photoabsorption of an alkali metal in an EF. Although Harmin's treatment was found to be very useful, his theory was developed only for an alkali metal with a closed-shell core. Recently, the present author has extended Harmin's theory so that it can treat a Rydberg atom with an ion core in an arbitrary state<sup>2</sup>. This method employs an approach somewhat different from that of Harmin, and is a natural extension of the MQDT<sup>6</sup> developed for a Rydberg atom in vanishing fields by Seaton and his co-workers.

When an electron moves far from an ion, i.e.,  $r \gg r_0$  ( $r$  being the relative distance between the electron and the ion, and  $r_0$  the ion radius), the interaction acting on the electron is

$$V = -1/r + Fz, \quad (1)$$

where  $F(>0)$  is the strength of an applied EF (parallel to the  $z$ -axis), and the ion is assumed to be singly ionized for simplicity. The Schroedinger equation of the electron motion in the potential (1) is separable in parabolic coordinates<sup>7</sup>,  $\xi = r(1+\cos \theta)$ ,  $\eta = r(1-\cos \theta)$ ,  $\phi = \phi$ , where ( $r$  &  $\theta$ ) indicate polar coordinates. The two linearly-independent solutions of the Schroedinger equation can be written in the form<sup>9</sup>,

$$\psi(\epsilon \beta m) = (2\pi \xi \eta)^{-1/2} f_{\epsilon \beta m}(\xi) g_{\epsilon \beta m}(\eta) \exp(im\phi), \quad (2)$$

$$\psi^I(\epsilon \beta m) = (2\pi \xi \eta)^{-1/2} f_{\epsilon \beta m}(\xi) g_{\epsilon \beta m}^I(\eta) \exp(im\phi), \quad (3)$$

where  $f$  and  $g$  (and  $g^I$ ) are the solutions of the two equations originating from the separation of the Schroedinger equation;  $\epsilon$  is the electron energy;  $\beta$  the separation constant (an effective Coulomb charge of the  $\xi$  motion); and  $m$  the magnetic quantum number. The solutions  $g$  and  $g^I$  are

regular and irregular at  $\eta = 0$ , respectively. The  $\xi$  motion is bound. Thus, the separation constant  $\beta$  is quantized, and has discrete values at a given energy. Channels in parabolic coordinates are specified by  $(\beta m)$  instead of  $(lm)$  in polar coordinates, where  $l$  is the orbital angular momentum quantum number.

Since short range interactions other than (1) are present at  $r < r_0$ , the wavefunction of the electron has the following form at  $r \gg r_0^2$ ,

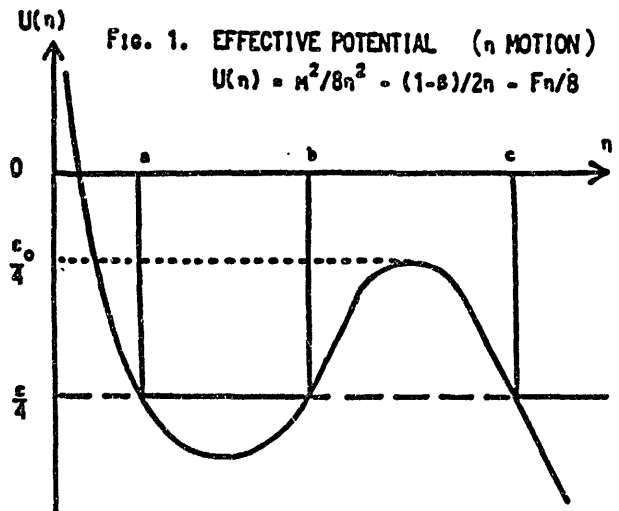
$$G(\delta' \beta' m'; \delta \beta m) = \psi(\epsilon \beta m) \delta_{\delta' \delta} \delta_{\beta' \beta} \delta_{m' m} + \psi^I(\epsilon' \beta' m') R_{\delta' \beta' m'; \delta \beta m}, \quad (4)$$

where  $\delta'$  and  $\delta$  indicate the ion state. The coefficient  $R$  is a reactance matrix defined in the parabolic-coordinates representation. This matrix is connected with the reactance matrix  $R^0$  defined in the  $(F=0)$  MQDT by the frame transformation,

$$R_{\delta' \beta' m'; \delta \beta m} = \sum_{\ell' \ell} U_{\beta' \ell'} R^0_{\delta' \ell' m'; \delta \ell m} U_{\beta \ell}, \quad (5)$$

where  $R^0$  is defined in polar coordinates, and the frame transformation matrix can be analytically given<sup>2,4,5</sup>.

Figure 1 shows the effective potential energy  $U(\eta) = m^2/8\eta^2 - (1-\beta)/2\eta - F\eta/8$  of the  $\eta$  motion. The energy eigenvalue  $\epsilon$  in the Stark problem is always continuous because the  $\eta$  motion is not bound. However, when  $\epsilon < \epsilon_0$  (fig.1), we can have quasibound states. The quasibound state satisfies the



condition that the wavefunction has only a small component that decreases with increasing  $\eta$  in the barrier region ( $b < \eta < c$ ). Thus, once we know the analytical properties of the functions  $g$  and  $g^I$  in the barrier region, we can easily derive the condition of the quasibound state.

Here, we employ an extended WKB method developed by Miller and Good<sup>8</sup> to see the analytical properties of  $g$  and  $g^I$ . With use of the extended WKB method, we find that  $g$  and  $g^I$  behave in the barrier region as follows<sup>2</sup>,

$$g \sim A \sin \Delta \exp(-\alpha \rho) + B \cos \Delta \exp(+\alpha \rho), \quad (6)$$

$$g^I \sim A \cos \Delta \exp(-\alpha \rho) - B \sin \Delta \exp(+\alpha \rho), \quad (7)$$

where  $A$  and  $B$  are non-zero constants,

$$\Delta = \int_a^b q(\eta) d\eta, \quad (8)$$

$$\alpha = \left[ \frac{1}{\pi} \left| \int_b^c q(\eta) d\eta \right| \right]^{1/2}, \quad (9)$$

with a local momentum of the  $\eta$  motion  $q(\eta)$ ,

$$q^2(\eta) = \epsilon/2 - m^2/4 \eta^2 + (1-\beta)/\eta + F\eta/4. \quad (10)$$

The new variable  $\rho$  is mapped from  $\eta$  by a one-to-one correspondence,

$$\int_{-2\alpha}^{\rho} (\rho'^2/4 - \alpha^2)^{1/2} d\rho' = \int_b^{\eta} q(\eta') d\eta'. \quad (11)$$

When  $\eta=b$ ,  $\rho=-2\alpha$ ; when  $\eta=c$ ,  $\rho=2\alpha$ ; and the variable  $\rho$  increases with  $\eta$ .

The function (4) contains an exponentially increasing component ( $\sim e^{+\alpha\rho}$ ) in the barrier region. We take a linear combination of (4) with respect to the channel ( $\gamma\beta m$ ), and impose the condition that only an exponentially decreasing component ( $\sim e^{-\alpha\rho}$ ) remains. Then, we have the condition of the quasibound state<sup>2</sup>,

$$\det \left| \cot \Delta_{\epsilon\beta m} \delta_{\gamma\gamma'} \delta_{\beta\beta'} \delta_{m'm} - R_{\gamma'\beta'm', \gamma\beta m} \right| = 0. \quad (11)$$

From this equation, we can calculate the Stark energy level of Rydberg atoms.

### 3. MQDT treatment of resonance scattering and DR in an EF

We apply the present MQDT to dynamical processes in an EF. In this study, we assume that the ion has only two states ( $\gamma=a, b$ ), and the incident energy of the electron  $\epsilon_*$  is less than the excitation energy.

Furthermore, we consider the case that  $\epsilon_* \gg Fd$ , where  $d$  is the distance within which the incident electron is accelerated by an EF in the collision region. Therefore, we neglect the EF effect on the free electron. Open channels are indicated by the angular momentum ( $lm$ ) of the incident electron (in polar coordinates). On the other hand, the EF effect on the resonance state is correctly taken into account. Thus, closed channels are indicated by  $(\beta m)$  in parabolic coordinates.

We give the boundary condition for the closed channel in the same way as that for the Stark bound state. Then, we can easily obtain a scattering S matrix<sup>2,9</sup>, in a matrix notation,

$$S = X_{oo} - X_{oc} [X_{cc} + \exp(-2i\Delta)]^{-1} X_{co}, \quad (12)$$

where  $\Delta_{\epsilon\beta m, \epsilon\beta m}$  is a diagonal matrix whose element is given by (8). The matrix  $X$  can be expressed in terms of the reactance matrix  $R^0_{\gamma' l' m', \gamma l m}$  defined in the ( $F=0$ ) MQDT,

$$X = (1 + iU^t R^0 U)(1 - iU^t R^0 U)^{-1}. \quad (13)$$

The matrix  $X$  and the frame transformation matrix  $U$  are partitioned into submatrices, the open-channel (indicated by the subscript "o") and the closed-channel ("c") parts. Since we neglect the EF effect on the free electron, the frame transformation matrix  $U$  has a form,

$$U_{oo} = 1, \quad U_{oc} = U_{co} = 0, \quad U_{cc} = (U_{\beta l}).$$

The second term in the S matrix (12) gives the resonance contribution. The expression (12) is very similar to the one for the S matrix<sup>6</sup> obtained in the ( $F=0$ ) MQDT. The calculation of (12) is straightforward when we have the vanishing-field reactance matrix  $R^0$ .

Recently, Bell and Seaton<sup>3</sup> provided an ab initio theory of the DR in vanishing fields by using the MQDT. Since we have the S matrix (12) at  $F \neq 0$  similar to the zero-field S matrix, the same procedure as that used by Bell and Seaton gives a scattering matrix  $\mathcal{S}$  where radiative decays of the reso-

nance state are taken into account<sup>9</sup>,

$$\mathcal{S} = X_{00} - X_{0c} e^{i\Lambda} [e^{i\Lambda} X_{cc} e^{i\Lambda} - \exp(\pi\nu^3 A - 2\pi i\nu)]^{-1} e^{i\Lambda} X_{c0}, \quad (14)$$

where  $A$  is a radiative transition probability of the excited ion. In (14), we have put

$$\Delta_{\epsilon\beta m} = \pi(\nu^{-n_1 - m - 1/2}) + \Lambda_{\epsilon\beta m}, \quad (15)$$

where an integer  $n_1$  is a Stark quantum number relating to the quantization of the separation constant  $\beta$ . It should be noted that in deriving (14), we require an assumption that the change in  $\Lambda$  with  $\nu \rightarrow \nu+1$  is negligible. To see the validity of this assumption, we expand  $\Delta$  to the first order of  $F$ ,

$$\Delta_{\epsilon\beta m} = \pi(\nu^{-n_1 - m - 1/2}) + \frac{3}{2}\pi F \nu^4 (\nu^{-2n_1 - m - 1}). \quad (16)$$

From this equation, the change in  $\Lambda$  can be estimated by

$$\Delta \Lambda_{\epsilon\beta m} \sim \frac{15}{2}\pi F \nu^5 \frac{\Delta\nu}{\nu}. \quad (17)$$

Therefore, we can say that the change in  $\Lambda$  is very small at  $F\nu^5 \ll 1$ , and still small for  $\nu \gg 1$  even if  $F\nu^5 \sim 1$ . Noticing (15), we have a simpler form for  $\mathcal{S}$ ,

$$\mathcal{S} = X_{00} - X_{0c} [X_{cc} + \exp(\pi\nu^3 A - 2i\Delta)]^{-1} X_{c0}. \quad (18)$$

From (14) or (18), the DR probability for an initial channel  $(lm)$  is given by

$$P(i) = 1 - \sum_{i'} |\mathcal{S}_{i',i}|^2, \quad (19)$$

where  $i$  and  $i'$  indicate the open channel  $(lm)$ . Furthermore, from (14), we can derive an analytical expression for the DR probability averaged over resonances<sup>9</sup>

$$\langle P(i) \rangle = \sum_{\alpha'\alpha} \frac{2\pi\nu^3 A Y_{\alpha i} Y_{\alpha' i}^* (N^\dagger N^*)_{\alpha\alpha'}}{2\pi\nu^3 A + 1 - \sum_{\alpha\alpha} \sum_{\alpha'\alpha'}^*}, \quad (20)$$

where  $Z_{\alpha\alpha}$  is a diagonal matrix obtained by the diagonalization of  $e^{i\Lambda} X_{cc} e^{i\Lambda}$

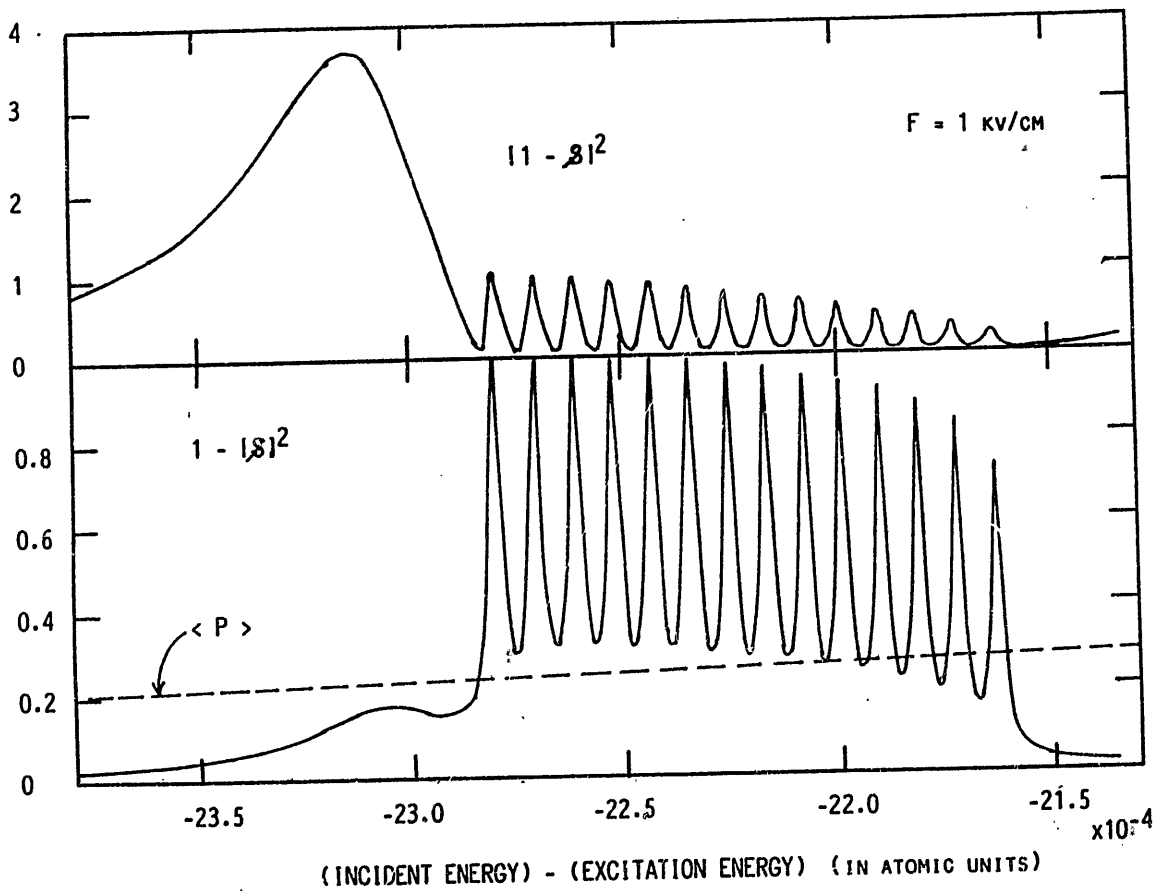
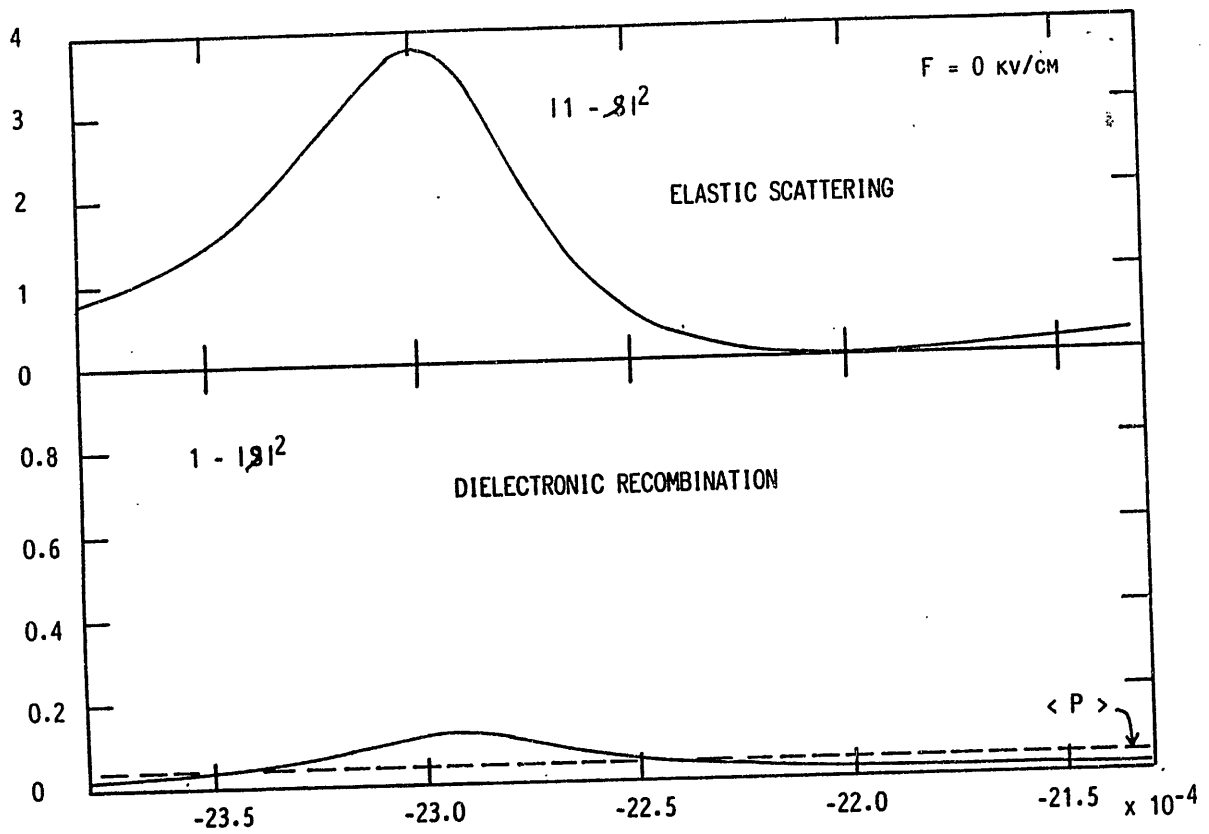


Fig. 2. Resonance profile of the elastic scattering and the dielectronic recombination

$$[e^{i\Lambda} X_{cc} e^{i\Lambda}] N = NZ, \quad (21)$$

and  $N$  is an orthogonal matrix. The subscript  $\alpha$  indicates the resonance channel in a diagonalized representation. The matrix  $Y = N^t [e^{i\Lambda} X_{co}]$  gives the coupling between the resonance and the continuum states. In (20), the overlapping resonances are taken into account. Thus, the interference term between the channels  $\alpha$  and  $\alpha'$  is present.

#### 4. Model calculations

To illustrate the EF effect, we have made some model calculations. For simplicity, we assume that  $R^0_{al'm',blm}$  is non zero only when  $l'=l=0$ . This means that only an s-wave electron can excite the ion and be trapped into an s state at  $F=0$ . We choose  $R^0_{aa}=0.5$ ,  $R^0_{ab}=R^0_{ba}=0.8$ ,  $R^0_{bb}=1.0$ , and  $A=2 \times 10^{-6}$  au.

Figure 2 shows the resonance profile of the elastic scattering ( $|1-\mathcal{S}|^2$ ) and the DR ( $1-|\mathcal{S}|^2$ ). The resonance peak shown in the upper figure corresponds to the 15s Rydberg state of the captured electron at  $F=0$ . When an EF is applied (the lower figure), the Rydberg states of the captured electron with  $l>0$  can have autoionizing properties because of the Stark mixing. Owing to this effect, there appear many sharp resonance peaks, and the averaged DR probability (indicated by the dotted line) is enhanced. It should be noted that the sharp resonances in the DR are overlapped.

Figure 3 shows the averaged DR probability as a function of the effective quantum number of the captured electron. As a field strength increases, the probability becomes larger. We find that the probability becomes a constant value as  $F$  or  $\nu$  increases. When  $F$  or  $\nu$  becomes large, we have the condition of the strong Stark mixing. When the Stark mixing is strong, we can show that the averaged DR probability (20) becomes an as-

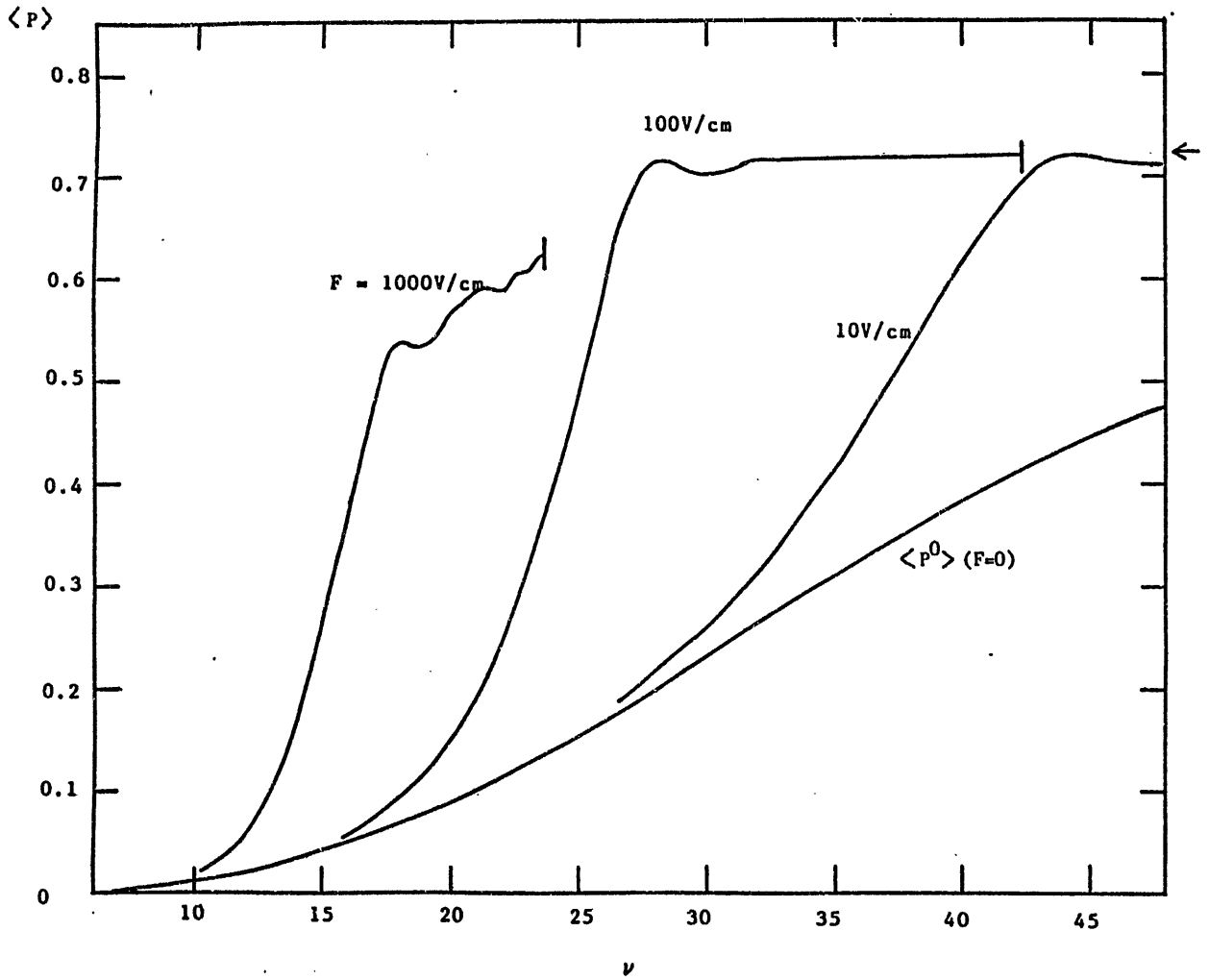


Fig. 3. Averaged DR probabilities as a function of the effective quantum number. The arrow indicates the asymptotic value  $\langle P \rangle_{\text{asyp}}$ . The vertical bar indicates the classical ionization limit.

ymptotic value  $\langle P \rangle_{\text{asympt}}$  which is independent of  $F$ .

We expect that the Stark mixing is strong when the Stark energy shift is larger than the shift due to the quantum defect of the ( $F=0$ ) resonance state. This gives the condition of the onset of the strong Stark mixing,  $F\nu^5 > 2|\mu^0|/3$ , where  $\mu^0$  is the quantum defect of the ( $F=0$ ) resonance state. Since the Stark mixing first occurs between the nearest levels, we can define the range of the quantum defect  $|\mu^0| < 0.5$ . Therefore, we can say that the Stark mixing is always strong when  $F\nu^5 > 1/3$ . This is a very useful finding. We have assumed  $F\nu^5 < 1$  to obtain an analytical expression for the matrix  $\mathcal{S}$ . However, the averaged DR probability is independent of  $F$  for  $F\nu^5 > 1/3$  because of the strong Stark mixing. Thus, we can conclude that the averaged DR probability (20) can be used for any field strengths.

## 5. Summary

In order to obtain an analytical expression for  $\mathcal{S}$  and  $\langle P \rangle$ , we have introduced the three assumptions:

- (I) The EF effect on the free electron is neglected. When this effect is taken into account, we have the following problems. Since the  $z$  axis is chosen along the field direction, an arbitrary direction of the incident electron must be expressed in parabolic coordinates. Furthermore, the free electron motion in an EF cannot be expressed in terms of the plane wave. Thus, the scattering boundary condition and the definition of the scattering matrix must be modified. These problems remain in a future work.
- (II) The tunneling effect through the barrier is neglected. This effect is important when the electron energy is nearly equal to the local maximum of the ( $\eta$ ) potential. In addition, the ionization limit depends on the channel ( $\beta m$ ). These effects can be included in the MQDT, as was done by

Harmin<sup>5</sup>.

(III) The change in  $\Lambda$  is neglected. However, we have found that this assumption does not matter when using the DR probability averaged over resonances.

Recently, Hahn and his coworkers<sup>10,11</sup> and Bottcher et al.<sup>12</sup> have studied the DR in an EF. Their calculations are based on the assumptions of the isolated resonances and the Stark mixing within the same  $n$  Rydberg manifold (i.e., only 1 mixing). The present theory is free from these assumptions, and the calculation is straightforward when we have the vanishing-field scattering information. It is very interesting to apply the present theory to a real system and to compare the experiments<sup>1</sup> and other calculations<sup>10-12</sup>.

#### References

1. A. Muller, D.S. Belic, B. D. DePaola, N. Djuric, G. H. Dunn, D. W. Mueller, and C. Timmer, Phys. Rev. Lett. 56, 127 (1986).
2. K. Sakimoto, J. Phys. B (1986), in press.
3. R. H. Bell and M. J. Seaton, J. Phys. B 18, 1589 (1985)
4. U. Fano, Phys. Rev. A24, 619 (1981).
5. D. A. Harmin, Phys. Rev. A26, 2656 (1982).
6. M. J. Seaton, Rep. Prog. Phys. 46, 167 (1983).
7. H. A. Bethe and E. E. Salpeter, Quantum Mechanics of One- and Two-Electron Atoms (New York, Plenum, 1977).
8. S. C. Miller and R. H. Good, Phys. Rev. 91, 174 (1953).
9. K. Sakimoto, J. Phys. B, to be published.
10. K. LaGattuta and Y. Hahn, Phys. Rev. Lett. 50, 668 (1983).
11. K. LaGattuta, I. Nasser, and Y. Hahn, Phys. Rev. A33, 2782 (1986).
12. C. Bottcher, D. C. Griffin, and M. S. Pindzola, Phys. Rev. A33, 3124 (1986); Phys. Rev. A34, 860 (1986).

Electron-Ion Collisional Rate Coefficients from  
Time-Dependent Plasmas

Hans R. Griem  
Laboratory for Plasma and Fusion Energy Studies  
University of Maryland  
College Park, Maryland 20742

Measurements of effective collisional electron-ion rate coefficients for ionization, dielectronic recombination and excitation performed using methods of quantitative spectroscopy are reviewed. These methods are based on the corona model for excitation and ionization, modified to account for two-step processes, etc., if necessary. Plasma parameters are determined using independent methods, mostly Thomson scattering of laser radiation for the electron temperature and density. A large number of ionization coefficients have been obtained with an expected accuracy approaching 30%. For dielectronic recombination, the number of measurements is much smaller and the expected accuracy is typically about a factor 2. For both processes, the highest ionic charge for which some measurements based on time-dependent radiation have been reported is  $\sim 30$ . For excitation, the number of rate coefficients obtained is intermediate to those for ionization and recombination, but the expected accuracy is not significantly better than that of recombination coefficients. The highest charge is  $\sim 15$  for such measurements of excitation rates.

## I. Introduction

Quantitative spectroscopy of plasmas containing multiply ionized atoms almost always requires a detailed analysis of level populations and charge state distributions, because such plasmas tend to be far from a state of local thermodynamic equilibrium<sup>1</sup> (LTE). Interest in non-LTE plasmas is increasing for a number of reasons. There is still much work to be done in understanding the spectra, especially at short wavelengths, from the solar corona and other more distant and frequently even more tenuous sources. With the development of high temperature laboratory plasmas with temperatures similar to those in stellar interiors, non-LTE spectroscopy has also become very important to plasma physicists<sup>2</sup>. They are concerned with the effects of radiation losses, mostly from high charge states of impurity ions, and with the opportunities offered for diagnostic measurements from line and continuum spectra. Another application of non-LTE quantitative spectroscopy is in the challenging search for short wavelength lasers<sup>3,4</sup> based on bound-bound transitions in highly ionized atoms. These not only must be out of LTE but must also have very large population densities or, rather, inversion densities, for significant gain from stimulated emission to occur.

A common need in these research areas is the requirement for a large number of realistic collisional rate coefficients for excitation and ionization and for de-excitation and recombination, which in case of ionization and recombination are not necessarily inverse processes in the sense of the principle of detailed balance. The corresponding cross sections are mostly obtained from electron-ion scattering theory<sup>5</sup>, actual

computations being based on a number of approximations whose validity must be checked by experiments designed to measure the cross section for the elementary process in question as directly as possible. Much progress has been made in this way in regard to ionization of (mostly) groundstate ions by electron collisions<sup>6</sup>, but excitation cross section measurements even for groundstate ions are still quite rare<sup>7</sup>. Experiments to determine cross sections for dielectronic recombination have succeeded only recently<sup>8</sup>, and theory and experiment could be reconciled only after consideration of electric field effects in the apparatus on the doubly excited states formed in the initial step of this recombination process.

This experience and various considerations for other processes point out the important role of plasma measurements in establishing a system of reliable and relevant rate coefficients. Although at least for recombination and ionization one may not be able to obtain the rate of any particular elementary process, one certainly measures effective rate coefficients that are appropriate sums or averages of elementary rate processes multiplied with relative probabilities, e.g., for an excited state formed by recombination to decay to the groundstate. Another advantage is the greater ease for plasma measurements to reach high charge states and also some excited states as targets. Returning to the subject of effective rate coefficients, one must always keep in mind that they tend to retain some density dependence, which must either be obtained from measurements in plasmas of different densities, or be gleaned from theoretical models. A frequently used compromise in such studies is to assume that the temperature dependence is according to some

relatively simple theoretical approximation.

A first review of the method for rate coefficient determinations from time-dependent plasmas and of early results was provided by Kunze<sup>9</sup>. The purpose of the present paper is to describe certain variations of the general method, which have been applied with some success, and to summarize experimental results from plasma measurements obtained since 1972. It is hoped that this mini-review will be useful to researchers in this particular sub-field of plasma spectroscopy, to atomic collision physicists, and to the much larger number of workers whose research depends on electron-ion collisional rate coefficients.

The next section describes the general methods used for the analysis of time-dependent plasma emissions in terms of collisional rate coefficients. The following sections are summaries of ionization, recombination, and excitation measurements. In a concluding section, some plasma measurements whose analysis is not relying on the transient nature of the emissions are mentioned, and an attempt is made to summarize any conclusions reached so far.

## II. General Method

The theoretical model used for the deduction of effective collisional rate coefficients is based on the set of rate equations for the densities of ions in charge state  $i$ ,

$$\frac{dN_i}{dt} = (S_{i-1}N_{i-1} + \alpha_{i+1}N_{i+1})N_e - (S_i + \alpha_i)N_iN_e + Q_i \quad (1)$$

and, in many cases, on the coronal relation for resonance line intensities,

$$I = \frac{h\nu}{4\pi} \int X N_i N_e d\ell \quad (2)$$

An implicit assumption is that almost all ions are in their ground states or in a small number of low-lying states, often of the same configuration as the actual ground state, which are statistically populated and have total density  $N_i$ . The ionization, recombination and excitation coefficients,  $S$ ,  $\alpha$  and  $X$ , are then appropriate averages of the coefficients for these states. Also,  $h\nu$  is the photon-energy and the integral in Eq. (2) is along the line of sight. In cases where several emission lines originate from the excited level, Eq. (2) must be multiplied by the ratio of transition probabilities of the line to the sum of the transition probabilities of all lines from this level. The required relative transition probabilities are usually taken from atomic structure calculations<sup>10</sup>, but can and should for complex spectra be checked by measuring the intensities of all the lines.

The source term  $Q_i$  in Eq. (1) accounts for the transport of ions into and out of the volume element being observed. Since most experiments were analyzed assuming a homogeneous plasma of some average electron density  $N_e$  and temperature  $T_e$ , and because frequently the ions to be studied were a small minority in hydrogen (or helium) carrier plasmas, it was simply assumed that the ions were compressed or lost with the fully ionized hydrogen plasma which in turn had provided almost all of the electrons. These considerations suggest a source term

$$Q_i = (N_i/N_e) \frac{dN_e}{dt}, \quad (3a)$$

a relation which was and is indeed used for most of the experiments. It was found invalid, however, for heavy impurity ions, like argon<sup>11</sup>, because the heavy ions were not as strongly compressed as hydrogen. For experiments with pure gases, or whenever a substantial fraction of the electrons is not from the hydrogen, the source term must be modified. In pure gases, or in cases where the product of relative impurity concentration and average charge is not much below 1, Eq. (3a) must be replaced by<sup>12</sup>

$$Q_i = \frac{N_i}{N_e} \frac{dN_e}{dt} - N_i \sum_{i'} (S_{i'} - \sigma_{i'}) N_{i'}. \quad (3b)$$

The additional term corrects for the change in electron density not caused by transport, but the basic assumption in both cases is that electrons and ions have the same flow velocity and that the hydrogen is fully ionized.

In long-lived plasmas, e.g., in tokamaks, these simple source terms must be replaced by considering directly the flow velocity term and impurity ion diffusion. Assuming cylindrical geometry, the corresponding source term is<sup>13</sup>

$$Q_i = - \frac{1}{r} \frac{d}{dr} (r\Gamma_i) , \quad (3c)$$

where  $\Gamma_i$  is the radial flux of ion  $i$ . This radial flux may be written

$$\Gamma_i = - \left[ D(r) \frac{dN_i}{dr} + v(r)N_i \right] , \quad (4)$$

where  $D$  is the diffusion coefficient of the ions in the hydrogen background plasma and  $v$  the radial velocity. One normally assumes  $v(r) \sim -r$  and  $D(r) = D(0)$ , determining the two remaining constants as to obtain agreement of measured time- and space-resolved relative impurity concentrations from laser blow-off impurity injection experiments with the theoretical model.

The magnitudes of typical diffusion coefficients,  $D \approx 10^4 \text{ cm}^2/\text{sec}$ , are such that the corresponding time scale, namely  $\gtrsim 100 \text{ } \mu\text{sec}$  for typical pinch experiments with plasma radii  $r_p \gtrsim 1 \text{ cm}$ , is too long for diffusion to be important in most of the pinch experiments. This had of course been assumed all along. Another comment concerning typical pinch experiments concerns the relatively large ion gyroradii and mean free paths. The ions therefore sample a large volume, a fact which justifies the use of radially averaged electron temperatures and densities in the modelling of ionization and recombination. However, for excitation, i.e., in Eq.

(2), it is usually better to use radially resolved  $T(r)$ , i.e.,  $X(r)$ , and  $N_e(r)$  values in order to determine line intensities from the model<sup>14</sup>. This is suggested by the short radiative life times and therefore small differences between the spatial positions of excitation and line emission.

### III. Ionization Coefficients

Especially in pinch experiments, the temperature often rises so rapidly that the actual ionization lags behind the corona equilibrium ionization. For the same reason, ionization coefficients are then usually much larger than recombination coefficients. Measuring time histories of lines from successive charge states and electron temperatures and densities from Thomson scattering or interferometry as input for Eqs. (1) and (2), assuming  $X \sim T^{-1/2} \exp(-\Delta E/k_B T)$  with  $\Delta E$  the excitation energy, then allows a determination of the ionization coefficients  $S_i$ . In the analysis of most of these experiments, the rate equations were first solved using approximate values of the  $S_i$  as originally proposed by Lotz<sup>15</sup> and conveniently parameterized by Kunze<sup>16</sup>. (This analytical formula<sup>16</sup> is used in most of the plasma investigations. It agrees with Lotz's value to  $\sim 15\%$ .) Then these  $S_i$  were multiplied by factors of order 1 to obtain a more satisfactory fit between measured and calculated time histories.

For relatively low charge states, such improved  $S_i$  values would be subject to large systematic errors, because the plasmas are far from homogeneous at early times. This fact can be gleaned from the often substantial differences between end- and side-on observations. However, around the peak of the magnetic field pulse, the plasmas emitting lines from high charge states are reasonably homogeneous and the source term in Eq. (1) is relatively small. The fit to the line time histories in regard to time of peak and to pulse width is then quite sensitive to the factors applied to the initial values for  $S_i$ , variation by  $\sim 20\%$  leading

to noticeable differences in time histories. Adding some error in the electron density, one would thus expect 25 - 30% accuracy in the measured rate coefficients.

That this accuracy can be reached, or even be exceeded, is indicated by the  $\sim 10\%$  agreement obtained<sup>17</sup> for the hydrogen-like ions BV and CVI for  $k_B T/E_i \approx 0.7$  and  $0.5$ ,  $E_i$  being the ionization energy, and  $N_e \approx 3 \times 10^{16} \text{ cm}^{-3}$ . For these ions more recent calculations (see Ref. 17) are within  $\sim 10\%$  of the Lotz values, and the excellent agreement is therefore even more noteworthy.

For the helium-like ions BIV, CV and NVI at  $k_B T/E_i$  between  $0.4$  and  $0.6$  and with  $N_e \approx 1.3 - 2.6 \times 10^{16} \text{ cm}^{-3}$  similar agreement was reached<sup>17</sup> after allowing for ionization from the  $n = 2$  triplet levels which contributes from 35 to 50% of the effective ionization coefficient. These corrections add some uncertainty and differ in detail from earlier determinations of CV effective ionization coefficients<sup>18</sup> and BIV and CV effective ionization coefficients<sup>19</sup> at lower densities. Nevertheless, in all cases experimental and calculated values are within  $\sim 25\%$ , i.e., there may be no significant deviations between plasma experiments and collision theory. However, derived groundstate coefficients<sup>17-19</sup> are about 25% below theoretical values and about 20% below values deduced from crossed-beam measurements<sup>20</sup> for BIV and CV. For NVI, the deduced value<sup>17</sup> is less than 2/3 of the crossed-beam result<sup>20</sup> which, however, does not seem to fit the iso-electronic trend.

Definitely larger than expected errors of the transient plasma method are the experiment-theory deviations found for low and medium Z lithium-like ions. From the beginning of theta pinch experiments for

such ions<sup>16</sup>, namely CIV, NV and OVI, measured coefficients were only ~ 60% of the Lotz values. Although especially for the earlier members of the isoelectronic sequence ionization from the 2P level is about as important as from the 2S groundstate, the theoretical correction<sup>17</sup> to the effective ionization coefficient to obtain the coefficient for the groundstate is  $\lesssim 10\%$ , because for the  $k_B T/E_i$  values in these experiments calculated ionization coefficients for 2P are only slightly larger than those for 2S. Also, more recent ab-initio calculations give ~ 20% smaller ionization coefficients than the Lotz formula. Nevertheless, even after these reductions in the theoretical values, more recent measurements<sup>17</sup> for NV, OVI, FVII and NeVIII for  $k_B T/E_i \approx 1.1 - 0.9$  and  $N_e \approx 0.8 - 2.2 \times 10^{16} \text{ cm}^{-3}$  still only gave 0.76 - 0.54 of the new theoretical values. On the other hand, these measurements and an experiment<sup>23</sup> on NV do agree within experimental errors with semiclassical (ECIP) calculations by Burgess, an observation consistent with conclusions in a review<sup>24</sup> of all methods to determine ionization coefficients.

Two other pinch experiments<sup>25,26</sup> resulted in ionization coefficients for NV and OVI which exceed the Lotz values by factors 1.3 - 2.3. In one of these theta pinches, the effective ionization coefficient for NeVIII was found<sup>27</sup> with ~ 0.7 the Lotz value, for  $k_B T/E_i \approx 0.95$ . A possible mechanism for enhanced ionization<sup>25</sup>, especially at relatively low temperatures and high densities, is excitation followed by ionization. Inclusion of this two-step process in the analysis of similar measurements<sup>28</sup> of effective ionization rates for TiIX, NeVI, NeVII and OVI at  $k_B T/E_i = 0.3 - 0.4$  indeed resulted in much improved agreement, the

enhancement over the groundstate Lotz ionization rate being as much as a factor  $\sim 2$ .

In favor of the relatively high values for NV and OVI, even without two-step processes, are rate coefficients derived from crossed-beam measurements<sup>6,20</sup> which are larger than the low density plasma results by factors  $\lesssim 2$  and are therefore in  $\sim 20\%$  agreement with ab-initio theoretical values. A continuation of pinch experiments<sup>29</sup> to AlXI and SiXII gave effective ionization coefficients agreeing with theory to within the somewhat larger experimental errors,  $\sim 30\%$  and  $50\%$ , respectively. Measurements<sup>13</sup> on a time-dependent tokamak plasma,  $k_B T/E_1 \approx 0.5$  and  $N_e \approx 3 \times 10^{13} \text{ cm}^{-3}$  (see following section) yielded effective ionization rates for the lithium-like ion TiXX exceeding the Lotz value and calculations of Younger<sup>30</sup> by factors 1.2 - 1.4, which is barely significant in view of the sensitivity of the fit and other experimental errors. As suggested in Ref. 29, plasma experiments and atomic collision theory therefore indeed seem to agree for higher members of the lithium-like sequence.

Effective ionization coefficients for beryllium-like ions from plasma measurements are very difficult to compare with calculations or with crossed-beam measurements<sup>6,20</sup> of groundstate ionization because of the low-lying  $2p^3P$  metastable levels and other excited levels which may have significant populations in pinch experiments. Still, at not too small  $k_B T/E_1$ , the ionization coefficients for the various  $n = 2$  levels are probably not too different so that the average coefficient from the measurement should not differ too much from that for the groundstate. Another interesting complication<sup>29</sup> may arise through the inner-shell

ionization of the corresponding boron-like ion which would cause an early rise of Be-like line intensities. Ignoring this possibility, one finds<sup>29</sup> for AlX and SiXI at  $k_B T/E_1 \approx 0.6 - 0.5$  and  $N_e \approx 3 \times 10^{16} \text{ cm}^{-3}$  experimental values  $\sim 0.8 - 0.65$  of the Lotz values, similarly to the original results<sup>16</sup> for OV and NeVII and a later result<sup>27</sup> of a factor  $\sim 0.4$  for NeVII at  $k_B T/E_1 \approx 2$ . If comparisons are made with ab-initio calculations<sup>21</sup>, the factor would be  $\sim 0.9 - 0.7$ , whereas comparison with the semiclassical ECIP calculations gives  $\sim 1.55 - 1.35$ . As for Li-like ions, the differences between various plasma measurements seem somewhat larger than estimated experimental errors. For NIV the factor found<sup>23</sup> relative to the Lotz value was  $\sim 1.5$  at  $k_B T/E_1 \approx 0.8$  and  $N_e \approx 3 \times 10^{15} \text{ cm}^{-3}$ . This relatively large value may again be in parts the result of early-time plasma dynamics or of two-step processes. As a matter of fact, for NeVII and  $k_B T/E_1 \approx 0.27$  and  $N_e \approx 3 \times 10^{16} \text{ cm}^{-3}$ , the Lotz groundstate ionization coefficient may have to be increased<sup>28</sup> by a factor 1.6 to allow for excitation-ionization, still leaving the measured value in this case a factor 1.3 above such corrected Lotz value. For higher members of the isoelectronic sequence tokamak observations<sup>13</sup> for TiXIX agreed with the Lotz value and also with ab-initio calculations<sup>30</sup> to within the  $\sim 20\%$  estimated accuracy. As in most other plasma experiments,  $k_B T/E_1$  values ( $\sim 0.6$ ) were too small for innershell excitation followed by autoionization to be important. However, in contrast to the pinch experiments, ionization from excited states should be negligible.

Crossed-beam results<sup>6,20</sup> for 50-50 mixtures of groundstate and metastable ions of NIV and OV indicate also for this sequence larger ionization coefficients than obtained in most plasma experiments. For

example, the results of Refs. 16 and 23 would seem to bracket the crossed-beam results. For boron-like ions and ions with more bound electrons, there are additional complications connected with the presence of various states in the groundstate configurations which for low members of the sequences would be statistically populated but not necessarily for high members observed in high temperature and low density tokamaks. Measurements<sup>29</sup> for B-, C-, and N-like ions of aluminum and silicon gave effective ionization coefficients of  $\sim 0.5 - 0.7$  the Lotz values, which in these cases are within 10% of the results of Ref. 21 for  $k_B T/E_i$  ranging from 0.7 to 0.6. For  $k_B T/E_i \approx 2.5$ , as small a value as 0.15 was found<sup>27</sup> for NeVI. For NeVI at  $k_B T/E_i \approx 0.35$ , on the other hand, good agreement<sup>28</sup> was obtained with a Lotz value corrected for excitation-ionization. The B- and C-like ions of titanium, TiXVIII and XVII, were found<sup>13</sup> to have effective ionization coefficients under tokamak conditions which are  $\sim 20\%$  larger than the Lotz values.

Measurements<sup>31</sup> in a theta pinch of the O-, F-, Ne-, and Na-like ions of argon, i.e., of ArXI - VIII, again showed the pattern of effective rate coefficients falling below the Lotz values and theory<sup>30</sup> by factors 0.4 - 0.8. (An earlier pinch experiment<sup>32</sup> had given a factor  $\sim 0.6$  for ArVIII.) Another pinch measurement<sup>14</sup> of Cl-, Ar-, and K-like ions of iron, i.e., of FeXII, XI, and X, resulted in ionization coefficients about equal to the Lotz value (FeXII,  $k_B T/E_i \approx 0.6$ ), or smaller by factors 0.7 (FeXI,  $k_B T/E_i \approx 0.7$ ) and 0.5 (FeX,  $k_B T/E_i \approx 0.75$ ). No direct comparisons seem to be available here, although it may be noted that crossed-beam measurements<sup>33</sup> for the Na-like ions MgII, AlIII and SiIV also fall well below the Lotz values for near-threshold energies. The

increases in cross sections due to innershell excitation followed by autoionization are evidently not important for the  $k_B T/E_i$  values in the plasma measurements. As a by-product of excitation rate measurements, ionization coefficients for Fe X, IX and VIII had been obtained earlier under slightly different plasma conditions<sup>34</sup>, all having  $\sim 0.5$  times the Lotz value.

Ionization rate coefficients for the krypton ions KrIX, X, XI and XII, which have an even more complex level structure, were deduced from measurements on a theta pinch plasma with 10% krypton in hydrogen<sup>35</sup>. In this case, it was necessary to first analyze the spectra in order to obtain lines ascribable to specific ions, using atomic structure codes<sup>10</sup> and estimated relative line intensities as a guide. (In one case, line intensity ratios differed by a factor  $\sim 5$  from such simple estimates, possibly because the corona model needs modifications at the relatively high densities,  $N_e \lesssim 10^{16} \text{ cm}^{-3}$ .) The factors multiplying the Lotz values of the ionization coefficients in the simulations were chosen to 2.5, 0.15, 3.0 and 2.0 for the various ions to obtain a best fit. The ions KrX and XI showed the same time history, which is reflected in the very large difference between the ionization coefficients obtained for KrX and XI. This unusual time behavior could also be explained<sup>35</sup> by a significant rate of double ionization for KrIX. Finally, similar to the interpretation<sup>28</sup> of the relatively large ionization coefficients found for the ions TiIX, NeVI, NeVII and OVI, ionization from excited states may also have been important.

To summarize, most of the plasma experiments should yield effective ionization rate coefficients to  $\sim 30\%$  accuracy even for very highly

charged ions. However, there may be a systematic error for low charge states, which could be somewhat larger than 30%. It would be responsible for the trend<sup>9,24</sup> toward small effective rate coefficients from such plasma measurements. A possible source of such error<sup>26</sup> is the diffusion of ions into the hot annulus existing especially in reverse bias field theta pinches. Such transport would lead to an extended line emission pulse from the annulus, which often gives most of the emission.

#### IV. Recombination Coefficients

Because of the short duration of pinch plasmas, time histories of spectral lines are usually insensitive to recombination coefficients used in the simulations. However, by operating at higher density and lower temperature than normally encountered, it was possible<sup>36</sup> to measure time histories of FeIX, X and XI lines whose decaying portions were sensitive to the actual values of recombination coefficients. Ionization coefficients for the simulation were obtained from comparisons with measurements at higher temperatures, using the theoretical temperature scaling.

The original analysis of the experiment was subsequently improved<sup>14</sup> by including the radial temperature variation in the line intensity calculations. Effective recombination coefficients obtained are then almost equal to the calculated value<sup>37</sup> of the dielectronic recombination coefficient in case of FeIX and about 0.4 times or 0.6 times these values for FeX and XI. The FeIX value is about twice as large as the coefficient deduced originally<sup>36</sup>, while those for FeX and XI are about half the original values. The measurements were taken at  $N_e \approx 3 \times 10^{16} \text{ cm}^{-3}$ , whereas the calculations<sup>37</sup> were for coronal densities,  $\sim 10^{10} \text{ cm}^{-3}$ . The expected reduction of dielectronic recombination coefficients at high densities therefore appears to be less pronounced than one might expect.

More slowly ionizing theta pinch plasmas, in which recombination is therefore relatively more important, can also be produced<sup>31,38</sup> by omitting the usual reversed bias magnetic field, thus reducing the temperature and increasing the density. One of these experiments was devoted to CV and CVI, and the effective recombination coefficients were

obtained using an analysis very similar to that used for FeIX, X and XI in Ref. 36. Because of the relatively high excitation energies, radiative recombination is not negligible for the carbon ions and was therefore subtracted from the measured rate. (These corrections were  $\sim 3\%$  and  $\sim 30\%$ , respectively, for CV and CVI.) The remaining recombination rates were then found to be about twice the calculated rates<sup>39,40</sup> for CV and  $\sim 30\%$  larger than these rates for CVI, but only 0.6 times a more recently calculated value. As in the experiment on iron ions, it is again surprising that the dielectronic rates seem not to be significantly reduced by high density effects on the doubly excited states produced in the initial capture process.

In continuation of this work, (mostly) dielectronic recombination coefficients were determined for ArVIII - XII ions as well. The fit between measured and simulated time histories was quite sensitive, variations of the rate coefficients by 30% resulting in noticeably poorer agreement. Agreement well within the experimental errors was obtained with detailed calculations<sup>41</sup> for ArVIII, whereas similar calculations<sup>42</sup> for ArIX are about a factor 3 below the measured values. Comparison for these ions and for ArX, XI and XIII with calculations from Ref. 41 shows considerable variations. For ArVIII and XII, the measured coefficients are larger by a factor  $\sim 1.5$ , for ArX and XI by factors 3 - 2. The corresponding factor for the neon-like ion ArIX is 25 - 30, to be contrasted with the factor 3 in the comparison with Ref. 42. Since it is not clear why the experiment would give larger recombination coefficients than calculations for lower densities, charge exchange recombination was considered as well but found to be only  $\sim 1\%$  of the observed ionization

rate.

Higher charge states can be investigated in tokamak plasmas by a very similar method. These plasmas reach much higher temperatures, which are naturally modulated by sawtooth oscillations. The corresponding line intensity variations of MoXXXI and XXXII ions were directly used by Breton et al.<sup>43</sup> to infer effective recombination coefficients, adopting ionization coefficients of Lotz<sup>15</sup> and recombination coefficients of Burgess<sup>39</sup> as a reference in a 0-dimensional rate equation model and neglecting transport. The observed time histories were found to be consistent with 1 - 1.5 the Lotz values and 0.5 - 1 the Burgess values.

This method can be refined<sup>13</sup> by using a 1-D model with transport for the simulations (see Sect. II) and by considering cross correlations between line histories and x-ray intensities as modulated by the sawtooth oscillations. As demonstrated in Ref. 13, sensitive comparison between measured and simulated cross correlations was possible for four titanium ions, TiXVII - XX. Also, any systematic errors from uncertainties in impurity transport could be assessed more realistically. While ~ 20% accuracy was estimated for ionization coefficients, recombination coefficients could be claimed only to have ~ 60% accuracy. Actual best fit values were found to be 0.8 - 1.2 of coefficients calculated according to Burgess<sup>39</sup>.

No crossed or merged beams measurements<sup>8</sup> are available for the ions studied in transient plasmas. The experience so far suggests that measured effective dielectronic recombination coefficients from transient plasmas are generally accurate to within a factor ~ 2.

## V. Excitation Coefficients

An important assumption for the interpretation of most of the experiments described in the preceding sections was the assumed  $T^{-1/2} \exp(-\Delta E/k_B T)$  dependence of excitation rates on temperature,  $\Delta E$  being the excitation energy. This assumption corresponds to an energy-independent collision strength<sup>5</sup> (or constant Gaunt factor) and is of course very approximate, but probably not a source of major error as long as  $k_B T/\Delta E$  is not changing by factors  $\gtrsim 2$ . Other simplifying assumptions for the analysis, i.e., the corona relation for absolute line intensities, Eq. (2), or its modifications using suitable branching ratios, are frequently more restrictive, as is the requirement for absolute rather than relative intensity measurements and the need for absolute densities of the target ions. In spite of these difficulties, early measurements as reviewed by Kunze<sup>9</sup> were quite useful in revealing that effective Gaunt factors for collision-induced electric dipole transitions were often larger than 0.2, that collision-induced singlet-triplet transitions had comparable rates, and that other than electric dipole transitions also had significant excitation rates in case of multiply ionized atoms.

Since these early measurements, which were mostly concerned with helium-, lithium-, and beryllium-like ions, refined measurements and analysis have not only been performed for these ionic systems but also for ions with more bound electrons. Because of the presence of metastable levels, modifications of the corona model are especially important for He- and Be-like ions, which have therefore received special attention. A long-standing problem, e.g., has been the ratio of intercombina-

tion to resonance line ratios in He-like ions, in particular its electron density and temperature dependence. These experiments are particularly simple, because only relative intensity measurements of two neighboring lines are required and target ion concentrations need not be known, except when corrections for radiative transfer must be made. The experimental line intensity ratios for CV<sup>44</sup> vary from 2.0 - 6.1, or from 2.2 - 9.6 after allowing for radiative transfer, as the electron density increases from  $0.8 \times 10^{15}$  to  $1.5 \times 10^{16} \text{ cm}^{-3}$ . Agreement with theory<sup>45</sup> is within 20%, except at the highest density and lowest temperature. The latter deviations could be resolved if the temperature dependence of the ratio of singlet and triplet excitation rates were actually weaker than calculated.

A more recent experimental study<sup>46</sup> for of the BIV resonance to intercombination line ratio R at  $N_e = 1.5 \times 10^{16} \text{ cm}^{-3}$  and  $k_B T = 175 \text{ eV}$  gives  $R = 106 \pm 30$ , to be compared with  $R = 124$  based on the calculations of Ref. 45. A very important cause of the reduced intensity of the intercombination line is ionization from the triplet levels, which was allowed for according to Gabriel and Jordan<sup>47</sup> in their study of modified corona models. Also relative intensities of the resonance lines from the  $n = 2, 3$  and 4 levels were found to be in good agreement with calculated values<sup>48</sup>. However, absolute line intensities were a factor  $\sim 4$  below expectations based on constant B to H gas fill ratios and BIV relative abundances inferred from the ionization (and recombination) rate equations. This again suggests that added impurities are not necessarily swept up by the implosion<sup>11</sup>.

It is therefore worthwhile to remember that rate coefficients by the transient plasma method can also be measured in pure gases. As a matter of fact, an experiment<sup>32</sup> on the Na-like ArVIII ions, done both with argon seeded hydrogen and pure argon fill, gave the first indication of changes in the mixture ratio during the compression. The pure argon results for the 3s-3p, 3d, 4s, 4p, 4d and 4f excitation rates were found to agree with Coulomb-Born calculations to well within a factor of 1.5. For  $n = 5$ , the agreement was less satisfactory, possibly because of collisional coupling or cascading not included in the modified corona model.

A recent experiment<sup>49</sup> in pure neon on the Li-like NeVIII ions yielded effective excitation coefficients for all  $n = 3$  and 4 levels which were assigned to 2s and 2p as initial states according to relative values of theoretical rate coefficients<sup>5</sup> from 5-state close-coupling calculations for the  $n = 3$  states and from Coulomb-Born calculations for the  $n = 4$  states. The sum of 2s and 2p populations was taken from the fitting to measured time histories and from the measured electron density, using quasi-neutrality of the plasma. Absolute line intensities were measured, using the branching ratio method, and corrected for selfabsorption according to a method first used for He-like lines<sup>50</sup>. The absolute values of all  $n = 3$  excitation rate coefficients thus obtained at  $k_B T = 75$  eV agreed to within a factor  $\sim 1.5$  with calculated values. For 4s and 4p the agreement was better or similar, while a factor 3 discrepancy occurred for 4d.

It is also interesting to note that these results are consistent with results obtained at higher temperatures, up to  $\sim 260$  eV, in neon-seeded hydrogen<sup>51</sup> or helium<sup>52</sup> plasmas. (Helium was used to reduce

absorption losses between plasma and spectrograph.) The new experimental value for 4f excitation<sup>49</sup> is consistent with a result obtained in neon-seeded hydrogen<sup>53</sup> at  $k_B T = 125 - 260$  eV. These favorable experimental comparisons make it more difficult to understand why the  $B_2H_6$  seed used in the measurement<sup>46</sup> of excitation coefficients for BIV evidently did not appear in the initial fill gas mixture ratio. Possibly dissociation in the preheater phase and wall effects were responsible for the de-mixing in this case rather than the theta pinch mechanism acting in the case of argon<sup>11</sup>.

In any case, for most important states of Li-like ions, plasma measurements seem to give very satisfactory results. Because of the low-lying metastable  $2^3P$  level of beryllium-like ions, the interpretation of relative and absolute line intensity measurements for such ions is more involved and critically dependent on accurate transition probabilities for branching ratios required in the appropriate modifications of Eq. (2). A very complete experimental study<sup>54</sup> of NeVII at  $k_B T \lesssim 80$  eV and  $N_e \lesssim 2 \times 10^{16} \text{ cm}^{-3}$ , using 5% neon in helium or hydrogen, resulted in very satisfactory agreement with theory for  $n = 3$  excitations except for the  $2s^2 \ ^1S - 2s3p \ ^1P$  transition, for which the theoretical excitation coefficient was found to be too low by a factor  $\sim 2$ . Also, from a consideration of branching ratios, the theoretical A value for the  $2p^2 \ ^3P - 2s3p \ ^3P$  transition seemed a factor  $\sim 6$  too high. For  $n = 2$  levels no satisfactory agreement could be obtained. A reduction in the measured intensity of the intercombination line  $2s^2 \ ^1S - 2s2p \ ^3P$  would be needed to reconcile these differences. For a discussion of earlier experiments on Be-like ions, the reader is referred to Kunze's review<sup>9</sup>, where the required

modifications to the corona model are also discussed.

One of the experimental problems in the determination of absolute excitation coefficients, the measurement of absolute target ion densities in seeded plasmas, which are preferable otherwise to avoid selfabsorption, can be solved in special cases by observing forbidden lines (fine-structure transitions) between levels of the ground configurations. These levels are almost certainly statistically populated at densities typical of theta pinches, and the corresponding magnetic dipole transition probabilities can be calculated easily and accurately. This method was used for FeX<sup>55</sup> which emits the red coronal line, whose absolute intensity thus gave the FeX groundstate densities, the upper fine structure level population directly and that of the lower level by using statistical weights. This not only allowed the determination of excitation coefficients for FeX, but from various measurements<sup>56,57</sup> of relative excitation coefficients for neighboring iron ions, also of absolute excitation coefficients<sup>58</sup> for FeVIII, IX and XI. With one exception, the results agreed with theory to within a factor 2. Smaller deviations are probably not significant.

The same method has been applied to a tokamak plasma to measure<sup>59</sup> excitation coefficients for CuXIII and CuXVII, with an estimated uncertainty of  $\pm 70\%$ , and to Al-like lines of iron, nickel, copper and zinc<sup>60</sup>. The major source of error is in the XUV intensity calibrations.

A more general method for target ion density measurements<sup>61</sup> in theta pinches is based on a comparison of electron density measurements in pure hydrogen plasma and plasma injected with  $\sim 1\%$  of the element of interest, e.g., by a titanium gun. (A similar iron gun was used in the work of

Ref. 55.) As always, the distribution over charge states is inferred from time histories, and quasi-neutrality is invoked to relate the change in electron density to ion density.

A common purpose of many of the excitation coefficient measurements was to investigate energy losses due to impurity radiation at known impurity concentrations. A corresponding experiment<sup>62</sup> based on the methods of Ref. 55 gave radiative powers, summed over all important lines of FeVII - XI in a ~ 1% iron-seeded plasma at  $k_B T \approx 45$  eV to within a factor of 2. Agreement with various calculations<sup>63-65</sup> is within or close to this factor.

## VI. Summary

The transient plasma method has yielded effective ionization rate coefficients for a large number of multiply ionized atoms of simple and complex atomic structure and with ionic charges up to  $\sim 30$ . Depending on the ion, the plasma density, temperature, and the plasma homogeneity, the accuracy of such measurements may reach  $\sim 30\%$ . For early members of the Li, Be, B, etc., isoelectronic sequences measured coefficients tend to be smaller than calculated values, but for higher charge states and near threshold ionization they are in agreement within estimated errors.

Dielectronic recombination rate coefficients have only been obtained for a much smaller number of ions and at relatively high densities. Their estimated accuracy is not much better than a factor  $\sim 2$ , and they tend to agree with theory before any corrections for collisional ionization of the intermediate doubly-excited states of the recombining ion, or for  $\ell$ -changing collisions.

The data for collisional excitation are again quite numerous, reaching from He-like ions to ions with complex structure, say, Cl- or Ar-like. The accuracy of absolute measurements is rarely much better than a factor  $\sim 2$  and agreement with calculations is usually found to be within these limits. Relative excitation rates for states of a given ion can be measured with substantially better accuracy, although definite conclusions regarding theoretical approximations may be constrained by the quality of the corona model used for the interpretation of the relative line intensity measurements.

Other plasma measurements not using the time-dependence of line intensities have also contributed to the determination of effective collisional rate coefficients, especially in case of dielectronic recombination. Assuming corona equilibrium to exist in the center of a tokamak, one can measure ratios of ionization and recombination rate coefficients. Using theoretical values for the ionization coefficients, dielectronic recombination coefficients were determined in this way for FeXV - XIX<sup>66</sup>. Another method involves high resolution measurements of dielectronic satellite lines, whose relative intensities with respect to the main line are essentially given by the ratio of the corresponding contribution to the dielectronic recombination coefficient and the excitation coefficient of the main line. Such determinations have been made for CaXIX<sup>67</sup>, FeXXV<sup>68</sup>, TiXXI<sup>69</sup> and for TiXXII<sup>70</sup>.

## References

1. H. R. Griem, "Plasma Spectroscopy," McGraw-Hill (New York, 1964); Univ. Microfilms Internatl. 212000007559, Ann Arbor, Mich.).
2. C. DeMichelis and M. Mattioli, Rep. Prog. Phys. 47, 1233 (1984).
3. R. W. Waynant and R. C. Elton, Proc. IEEE 64, 110 (1976).
4. P. L. Hagelstein, in "Atomic Physics 9," edited by R. S. van Dyck, Jr., and E. N. Fortson (World Scientific, Singapore, 1985), p. 382.
5. R. J. W. Henry, Phys. Rep. 68, 1 (1981).
6. D. H. Crandall, Physica Scripta 23, 153 (1981); see also Oak Ridge Natl. Lab. Rep. ORNL/TM-9501 (1985).
7. D. H. Crandall, in "Atomic Physics of Highly Ionized Atoms," edited by R. Marrus (Plenum, 1983), p. 399.
8. G. H. Dunn (review), JILA preprint (1986).
9. H.-J. Kunze, Space Science Reviews 13, 565 (1972).
10. R. D. Cowan, "The Theory of Atomic Structure and Spectra," Univ. of Calif. Press (Berkeley, 1981).
11. R. J. Comisso and H.-J. Kunze, Phys. Fluids 18, 392 (1975).
12. P. Grewe, Ph.D. Dissertation, Bochum University (1981), unpublished.
13. J. S. Wang, H. R. Griem, R. Hess, W. L. Rowan, and T. Kochanski, Phys. Rev. A 33, 4293 (1986).
14. R. L. Brooks, R. U. Datla, A. D. Krumbein, and H. R. Griem, Phys. Rev. A 21, 1387 (1980).
15. W. Lotz, Astrophys. J. Suppl. 14, 207 (1967).
16. H.-J. Kunze, Phys. Rev. A 3, 937 (1971).
17. P. Greve, M. Kato, H.-J. Kunze, and R. S. Hornady, Phys. Rev. A 24, 429 (1981).
18. H.-J. Kunze, A. H. Gabriel, and H. R. Griem, Phys. Rev. 165, 267 (1968).
19. R. U. Datla, L. J. Nugent, and H. R. Griem, Phys. Rev. A 14, 979 (1976).

20. D. H. Crandall, R. A. Phaneuf, and D. C. Gregory, Oak Ridge Natl. Lab. Rep. No. ORNL/TM-7020 (1979, unpublished); D. H. Crandall, R. A. Phaneuf, D. C. Gregory, A. M. Howald, D. W. Mueller, T. J. Morgan, G. H. Dunn, D. C. Griffin, and R. J. W. Henry, Phys. Rev. A (in press).
21. L. B. Golden and D. H. Sampson, J. Phys. B: At. Mol. Phys. 10, 2229 (1977); B. Golden, D. H. Sampson, and K. Omidvar, *ibid* 11, 5 (1978); D. H. Sampson and L. B. Golden, *ibid* 11, 541 (1978); D. L. Moores, L. B. Golden, and D. H. Sampson, *ibid* 13, 385 (1980).
22. S. M. Younger, Phys. Rev. A 23, 1138 (1981); 24, 1272 (1981).
23. R. Brown, W. M. Deuchars, D. E. Kidd, H. P. Summers, and L. Wood, J. Phys. B: At. Mol. Phys. 16, 2053 (1983).
24. A. Burgess, H. P. Summers, D. M. Cochrane, and R. W. P. McWhirter, Mon. Not. R. Astron. Soc. 179, 275 (1977).
25. E. Kallne and L. A. Jones, J. Phys. B: At. Mol. Phys. 10, 3637 (1977).
26. W. L. Rowan and J. R. Roberts, Phys. Rev. A 19, 90 (1979).
27. L. A. Jones, E. Kallne, and D. B. Thomson, J. Phys. B: At. Mol. Phys. 10, 187 (1977).
28. R. U. Datla and J. R. Roberts, Phys. Rev. A 28, 2201 (1983).
29. P. Greve, Physica Scripta 26, 451 (1982).
30. S. M. Younger, Phys. Rev. A 22, 11 (1980); 24, 1278 (1981).
31. H. C. Meng, P. Greve, H.-J. Kunze, and T. Schmidt, Phys. Rev. A 31, 3276 (1985).
32. R. U. Datla, H.-J. Kunze, and D. Petrinì, Phys. Rev. A 6, 38 (1972).
33. D. H. Crandall, R. A. Phaneuf, R. A. Falk, D. S. Belic, and G. H. Dunn, Phys. Rev. A 25, 143 (1982).
34. R. U. Datla, M. Blaha, and H.-J. Kunze, Phys. Rev. A 12, 1076 (1975).
35. L. A. Jones and E. Kallne, J. Quant. Spectrosc. Radiat. Transfer 30, 317 (1983).
36. R. L. Brooks, R. U. Datla, and H. R. Griem, Phys. Rev. Lett. 41, 107 (1978).
37. V. L. Jacobs, J. Davis, P. C. Kepple, and M. Blaha, Astrophys. J. 211, 605 (1977).

38. H. C. Meng, H.-J. Kunze, and T. Schmidt, Phys. Lett. 105A, 221 (1984).
39. A. Burgess, Astrophys. J. 141, 1588 (1965).
40. J. M. Shull and M. van Steenberg, Astrophys. J. Suppl. 48, 95 (1982).
41. K. J. LaGattuta and Y. Hahn, Phys. Rev. A 30, 316 (1984).
42. Y. Hahn, J. N. Gan, R. Luddy, and J. A. Retter, J. Quant. Spectrosc. Radiat. Transfer 23, 65 (1980).
43. C. Breton, C. DeMichelis, M. Finkenthal, and M. Mattoli, Phys. Rev. Lett. 41, 110 (1978).
44. H.-J. Kunze, Phys. Rev. A 24, 1096 (1981).
45. A. K. Pradhan, D. W. Norcross, and D. G. Hummer, Astrophys. J. 246, 1031 (1981).
46. K.-H. Kolk, R. König and H.-J. Kunze, Phys. Rev. A 33, 747 (1986).
47. A. H. Gabriel and C. Jordan, in "Case Studies in Atomic Collision Physics," edited by E. W. McDaniel and M. R. C. McDowell (North-Holland, Amsterdam, 1972), Vol. 2, Ch. 4.
48. D. H. Sampson, S. J. Goett, and R. E. H. Clark, At. Data Nucl. Data Tables 29, 467 (1983).
49. C. C. Chang, P. Greve, K.-H. Kolk, and H.-J. Kunze, Physica Scripta 29, 132 (1984).
50. R. C. Elton and W. W. Köppendorfer, Phys. Rev. 60, 194 (1967).
51. H.-J. Kunze and W. D. Johnston III, Phys. Rev. A 3, 1384 (1971).
52. G. N. Haddad and R. W. P. McWhirter, J. Phys. B: At. Mol. Phys. B 6, 715 (1973).
53. H.-J. Kunze, Phys. Rev. A 4, 111 (1971).
54. J. Lang, J. Phys. B: At. Mol. Phys. 16, 3907 (1983).
55. J. S. Wang and H. R. Griem, Phys. Rev. A 27, 2249 (1983).
56. R. U. Datla, M. Blaha, and H.-J. Kunze, Phys. Rev. A 12, 1076 (1975).
57. J. S. Wang, A. Marotta, and R. U. Datla, Astrophys. J. 279, 460 (1984).

58. J. S. Wang, R. U. Datla, and H. R. Griem, Phys. Rev. A 29, 1558 (1984).
59. R. U. Datla, J. R. Roberts, W. L. Rowan, and J. B. Mann, Phys. Rev. A (in press).
60. R. U. Datla, J. R. Roberts, R. D. Durst, W. L. Hodge, C. C. Klepper, W. L. Rowan, and J. B. Mann (private communications).
61. R. U. Datla, Phys. Rev. A 31, 2764 (1985).
62. Z. Y. Zhu, J. S. Wang, E. J. Iglesias, K. C. Maffei, and H. R. Griem, Nucl. Fusion 23, 1686 (1983).
63. D. E. Post, R. V. Jensen, C. B. Tarter, W. H. Grassberger, and W. W. Lokke, At. Data Nucl. Data Tables 20, 397 (1977).
64. J. Davis, V. L. Jacobs, P. C. Kepple, and M. Blaha, J. Quant. Spectrosc. Radiat. Transfer 17, 139 (1977).
65. S. Uchikawa, H. R. Griem, and D. Duchs, "Calculation of Impurity Radiation from Non-Corona Equilibrium Plasmas, Max-Planck-Institut fur Plasmaphysik, Rep. IPP-6/99 (1980).
66. R. C. Isler, E. C. Crume, and D. E. Arnarius, Phys. Rev. A 26, 2105 (1982).
67. B. N. Chichkov, M. A. Mazing, A. P. Shevelko, and A. M. Urnov, Phys. Lett. 83A, 401 (1981).
68. F. Bely-Dubau, M. Bitter, J. Dubau, P. Faucher, A. H. Gabriel, K. W. Hill, S. von Goeler, N. Sauthoff, and S. Volonte, Phys. Lett. 93A, 189 (1983).
69. F. Bely-Dubau, P. Faucher, L. Steenman-Clark, M. Bitter, S. von Goeler, K. W. Hill, C. Camhy-Val, and J. Dubau, Phys. Rev. A 26, 3459 (1982).
70. M. Bitter, S. von Goeler, S. Cohen, K. W. Hill, S. Sesnic, F. Tenney, J. Timberlake, U. I. Safronova, L. A. Vainshtein, J. Dubau, M. Loulergue, F. Bely-Dubau, and L. Steenman-Clark, Phys. Rev. A 29, 661 (1984).

## EVALUATION AND ASSESSMENT OF ATOMIC DATA FOR PLASMA MODELLING

T. Kawamura and T. Ono\*

Institute of Plasma Physics, Nagoya University, Nagoya 464, Japan

### Abstract

The characteristic points and atomic data needs in plasma modellings are discussed laying emphasis on tokamak plasma modelling. As an example evaluation and assessment for rate coefficient formulas available for impurity transport modelling are presented, and the remarkable dependence of the radial impurity distribution on the difference between the two dielectronic recombination rate coefficient formulas presented by the different authors is pointed out. It is concluded that considerably accurate atomic data are needed in order to draw out reliable values of anomalous impurity transport coefficients from the comparison of the results from plasma modellings with those from experiments.

---

\* Permanent Address: Department of Physics, Nagoya University, Nagoya 464, Japan.

## 1. Introduction

Recently plasma modelling studies draw attention to fusion scientists. Plasma modelling is quoted to theoretical or computational work on the basis of an appropriate plasma model in a real device for fusion study. The plasma which should be treated in modelling work is different from the ideal plasma which was treated in the traditional plasma theory.

The characteristic points in plasma modellings are as follows: (1) Plasma is spatially bounded. (2) The structure of a plasma is affected by the existence of a vessel wall. (3) The plasma structure is subject to the transport processes in an inhomogeneous plasma. (4) There exist a large number of neutral fuel particles ( $H^0$ ,  $D^0$ ,  $T^0$ ). (5) Impurities originating from the first wall influence energy balance and structure of the plasma. (6) A lot of elementary processes such as atomic and molecular processes and plasma-surface interaction processes contribute in determining the physical nature of a plasma.

The first objective of modelling study is analysis of experimental results. Generally an inhomogeneous and spatially finite hot plasma confined in a magnetic field includes microscopic electromagnetic fluctuations due to non-linear instabilities. Such fluctuations promote the anomalous transport across the magnetic fields and the confinement times of fuel particles and impurities are greatly ruled by these anomalous fluctuations. The characteristics of such anomalous phenomena are subject to the device structure concerned. Then, in order to develop a fusion machine it is necessary to know a scaling law from the experimental results with various devices. We can obtain universal knowledge on anomalous phenomena by comparing the results from plasma modellings and experiments.

Secondly plasma modelling is necessary for design studies of a new device. In this case plasma modelling is devoted to determine the design parameters of a device with which desired plasma parameters should be attained.

Here we restrict our discussion to tokamak plasma modelling for the following reasons. (1)At present only the tokamak can realize a plasma with the conditions nearest to the fusion break-even. (2)The treatment of boundary plasma is very important for tokamak modelling. Recently the study on a boundary plasma has been one of the key issues of tokamak researches, because particle and energy balances in a tokamak plasma are controlled through its boundary plasma. (3)In a boundary plasma atomic and molecular processes and plasma surface interaction processes play a key role. However, at present their data are not so reliable for modelling of a boundary plasma in rather a low temperature.

In this note we will make an assessment of atomic data available for plasma modelling laying emphasis on boundary plasma modelling.

## 2. Data Needs for Tokamak Modelling

For modelling various kinds of data in a broad range of plasma conditions are needed. Generally a tokamak plasma can be divided into two parts, main plasma and boundary plasma. In the main plasma near the torus center the condition over the break-even in which the plasma density is  $10^{14} \text{ cm}^{-3}$  and the ion temperature is 10 keV should be attained. A tokamak plasma is scraped by solid limiter or magnetic separatrix. The latter constitutes a part of a magnetic divertor system. Outside the scraping surface the magnetic field lines are connected to the solid surface. This region of a tokamak plasma is called a scrape-off layer (SOL). In this region the confinement times of

particles and energy are very short, and plasma density and temperature become, for example, as low as  $10^{12} - 10^{13} \text{ cm}^{-3}$  and 1 - 30 eV. In front of limiter sides or a divertor neutralizer plate we frequently have a rather high density ( $10^{14} \text{ cm}^{-3}$ ) and low temperature (1 - 10 eV) plasma due to predominant recycling of neutrals and radiation loss by hydrogen ionization and recombination radiation. The plasma in the peripheral region inside the scraping surface and the plasma in SOL constitute a boundary plasma in a tokamak where the direct influence of the first wall is predominant. For tokamak plasma modelling, as seen above, we need the data in the ranges of plasma densities  $10^{11} - 10^{14} \text{ cm}^{-3}$  and of plasma temperature 1 eV - 10 keV. The latter corresponds to an enormously wide range of reaction energy for the atomic processes.

At present almost all tokamak modelling works are based on fluid equations of multi-components which include electrons, fuel ions and ionized impurities in different charge states, as well as on Monte Carlo procedures for neutrals. Then, numerical data for an atomic process should be expressed by a reaction rate coefficient  $\langle\sigma v\rangle$ , which is determined by averaging the cross section over a Maxwellian velocity distribution of particles and is a function of plasma temperature and, in some cases, also a function of electron density. Therefore we have to construct an appropriate rate coefficient formula on the basis of experimental or theoretical results on an elementary process, if we have no available formula for the rate coefficient of the process concerned.

For description of tokamak plasma using multi-component fluid equations we need a lot of rate coefficients including ionization, recombination and charge exchange for fuel particles and impurities, and these rate coefficients should be expressed by analytical formulas with numerical coefficients for computer calculations. If we want to calculate a plasma structure over all regions of

main plasma and boundary plasma, we need rate coefficients formulas with considerable accuracy in a broad range of temperature. In order to obtain the temperature distributions self-consistently we have to include a radiation cooling term in modelling equations in addition to heat conduction and convection terms. The radiation cooling term consists of the summation of cooling rates due to ions in many charge states and knowledge of electron impact excitation of these ions is needed for determining these rates.

A comprehensive review on data base needed for tokamak modelling has been presented recently<sup>1)</sup>. Therefore in what follows we restrict our discussion to impurity transport modelling and assess presently available rate coefficient formulas for ionization and recombination of impurities.

### 3. Rate Coefficient Formulas Available for Modelling

The electron impact ionization processes consist of direct ionization and autoionization. The convenient semi-empirical formula of Lotz<sup>2)</sup> is widely used as a total rate for electron impact ionization. This expression was derived by fitting to the experimental cross sections existing at that time. Also used in fusion plasmas is the formula of Post et al.<sup>3)</sup> which was obtained by combining various expressions and adopting an appropriate Gaunt factor. As for direct ionization, Summers<sup>4)</sup> developed a semiclassical rate coefficient formula based on the Exchange-Classical-Impact-Parameter method. Recently, Golden and Sampson<sup>5)</sup> derived an expression from their cross section calculations using Coulomb-Born with exchange approximation. Quite recently, Arnaud and Rothenflug<sup>6)</sup> have calculated fitting parameters of the rate coefficient formula based on the theoretical cross section expression proposed by Younger<sup>7)</sup> which was developed in the distorted wave approximation for specific values of  $Z$ . Comparison of the rates of Lotz, Arnaud and Rothenflug, and Post

et al. shows that there is a good agreement among them for ionic charges  $\geq +9$  and that the rates of Post et al. fall a few orders of magnitudes below the others for  $Te < 10$  eV and for ionic charges  $\leq +8$ . Among autoionization processes, excitation-autoionization is the strongest one. Concerning excitation-autoionization, there is no reliable empirical or theoretical rate coefficient formula for lack in experimental and theoretical data. Mewe et al.<sup>8)</sup> proposed a rate formula. Recently, Arnaud and Rothenflug have calculated fitting parameters of the rate formula using experimental and theoretical data for isoelectronic sequences.

The recombination processes consist of radiative and dielectronic ones. As for radiative recombination, the rates towards hydrogenic ions of Seaton<sup>9)</sup> are used frequently which are based on an expansion of the Gaunt factor. In the case of recombination towards non-hydrogenic ions, Aldrovandi and Pequignot<sup>10)</sup> fitted their calculated results with a simple empirical formula. For Fe ions, Woods et al.<sup>11)</sup> derived parameter values of this formula using theoretical calculations for photoionization cross sections. Their rates for  $Fe^{+24} - Fe^{+23}$  and  $Fe^{+23} - Fe^{+22}$  are pointed out to be in error and corrected by Arnaud and Rothenflug. As for dielectronic recombination, Burgess<sup>11)</sup> developed a general theoretical formula. This expression was then modified for  $\Delta n=0$  transitions by Mertz et al.<sup>12)</sup> based on their calculations for Fe ions. The modified one is widely used by fusion scientists. Aldrovandi and Pequignot calculated rate coefficients based on the Burgess formula and fitted the results with their formula. For He to Ni ions, Shull and Van Steenberg<sup>13)</sup> calculated rates and expressed the results by the same formula. With the same formula Woods et al. fitted rate coefficient calculations for Fe ions by Jacobs et al.<sup>14)</sup> in which autoionization from doubly excited states to excited states were taken into account. Our comparative study of the rates for Fe

ions of Shull and Van Steenberg and of Post et al. who used the modified Burgess formula shows that the rates of Shull and Van Steenberg are smaller than those of Post et al. by a factor of 2-3 on the average, as can be expected from Fig. 1 where these two rates for  $\text{Fe}^{+13}$  are shown.

#### 4. Effects of Atomic Data on Modelling

As an example of data assessment we report the results obtained from impurity transport analysis using a one-dimensional tokamak model<sup>15)</sup> in which the anomalous diffusion and convection in hot hydrogen plasma in a steady state are assumed. For the diffusion constant across the magnetic field  $D_k$  of an ionization state  $k$  ( $k=1$  for neutrals) we adopt  $D_k = D_k^{\text{nc}} + D_A$  where  $D_k^{\text{nc}}$  is the neoclassical term and  $D_A$  is the phenomenological anomalous diffusion constant. The radial convection velocity  $V_k$  is taken as  $V_k = V_k^E + (r/a)V_A$  where  $V_k^E$  is the radial inward velocity due to the pinch effect caused by the tokamak plasma current,  $(r/a)V_A$  is the phenomenological anomalous convection velocity,  $r$  and  $a$  are the radius from the torus center and the minor plasma radius respectively. Here we treat  $D_A$  and  $V_A$  as free parameters which are given identical values for all charge states of the impurity ions, and we assume the stationary density and temperature profiles of hydrogen plasma.

We calculated impurity distributions using the different sets of rate coefficients in our computer code and checked the sensitivity of atomic data to modelling results. We here report the effects of different dielectronic recombination rate coefficient formulas because the dielectronic recombination has a leading effect on the recombination processes in the region of electron temperature concerned.

As a standard case we used ionization and recombination rate coefficients which are prepared by Post et al.<sup>3)</sup>, where ionization rate coefficients are

electron impact ionization rates estimated by them and the recombination rate coefficients are the sum of the radiative recombination rates given by Seaton and the dielectronic recombination rates in the Burgess scheme. Here we have used another dielectric recombination rate formula given by Shull and Van Steenberg<sup>13</sup>), and have compared the calculated results of impurity (Fe) distributions using the above two different subroutines for dielectric recombination rate coefficients. In the following we refer to the computation using the standard data as Case A and to the one as Case B when only the dielectric recombination rate coefficients are replaced by the ones given by Shull and Van Steenberg.

We present the results of our computations, for example, for the case when  $D_A = 5 \cdot 10^3 \text{ cm}^3 \text{ sec}^{-1}$  and  $V_A = 300 \text{ cm sec}^{-1}$  in Fig. 2 and Fig. 3. Fig. 2(a) shows the results with the use of the standard data ( the dielectronic recombination rate coefficients in the form of Bugess ) while Fig. 2(b) shows the ones in which only the dielectronic recombination rate coefficients are replaced by the ones given by Shull and Van Steenberg. In Fig. 3(a) and Fig. 3(b) we illustrate the differences of the FeXVI and FeXVII distributions for the two cases respectively. From these results we can deduce remarkable dependence of the radial impurity distributions on the difference between the two dielectronic recombination rate coefficient formulas.

In Fig. 4 we plot the full width at half maximum of the radial ion distributions for the k-th ionization state,  $d_k$ , versus different  $D_A$  values (  $V_A = 0$  is assumed ) to clarify the difference between the two cases. These results show the fact that the change of  $d_k$  in the wide range of  $D_A$  values is buried under the change due to the different dielectronic recombination rate formulas. The peak spacing between the radial distributions of different charge states,  $l_{kk}$ , should be related to convection velocity. In Fig. 5 we

illustrate the relation between the spacing  $l_{IX, XIV}$  and  $V_A$  ( $D_A = 0$  is assumed) in the above two cases with the different dielectronic recombination rate coefficient formulas. This shows that the discrepancy of the spacing  $l_{IX, XIV}$  due to the different dielectronic recombination formulas becomes larger for large  $V_A$  values.

Our analysis shows that considerably accurate atomic data are needed in order to draw out reliable values of the anomalous impurity transport coefficients from the plasma modelling researches.

## 5. Discussion

As described in Section 3, there is still today no accurate rate coefficient formula for the atomic processes taking place in the broad ranges of plasma density and temperature of fusion plasmas. Evident effect of the difference between the two atomic data sets on our plasma modelling has been exemplified through the impurity transport analysis. From these, the following statements may be inferred in connection with the atomic data:

- (1) We need the data with the accuracy of the order for all the processes that are supposed to take place in a plasma concerned.
- (2) For such processes as are order-estimated to influence the plasma structure, we need the data with the accuracy of about 50 % at least for a reliable modelling.
- (3) The atomic data required in modellings should be constructed in the form of rate coefficient formulas for fuel and impurity elements in the ranges of plasma density  $10^{11} - 10^{14} \text{ cm}^{-3}$  and of temperature 1 eV - 10 keV.
- (4) For developing fusion machines, knowledge on atomic processes is so indispensable that the studies in this field should also be promoted with the same order of weight as that given to the work on plasma devices.

## References

- 1) D.E. Post and C.E. Singer, J. Nucl. Mater. 128&129(1984) 78.
- 2) W. Lotz, Report IPP 1/62(1967), 1/76(1968).
- 3) D.E. Post, R.V. Jensen, C.B. Tarter, W.H. Grasberger and W.A. Lokke, Atomic Data and Nuclear Data Tables, 20(1977) 397.
- 4) H.P. Summers, Appleton Lab. AL-R-5 (1974).
- 5) L.B. Golden and D.H. Sampson, J. Phys. B 10(1977) 2229.
- 6) M. Arnaud and R. Rothenflug, Astron. Astrophys. Suppl. Ser., 60(1985)425.
- 7) S.M. Younger, J. Quant. Spectrosc. Radiat. Transfer, 26(1981)329.
- 8) R. Mewe, J. Schrijver and J. Sylwester, Astron. Astrophys. Suppl. Ser. 40(1980) 323.
- 9) M. J. Seaton, M.N.R.A.S., 119(1959)81.
- 10) S.M. V. Aldrovandi and D. Pequignot, Astron. Astrophys., 25(1973)137.
- 11) A. Burgess, Astrophys. J., 141(1965)1588.
- 12) A.L. Mertz, R.D. Cowan and N.H. Magee, Jr., LA-6220-MS, Los Alamos(1976).
- 13) J.M. Shull and M. Van Steenberg, Astrophys. J. Suppl. Ser. 48(1982)95.
- 14) V.L. Jacobs, J. Davis, P.C. Kepple and M. Blaha, Astrophys. J., 211(1977)605.
- 15) T. Amano, J. Mizuno and M. Kako, Research Report of Institute of Plasma Physics, Nagoya, IPPJ-616 (1982).

## Figure Captions

- Fig. 1 Dielectronic recombination rates  $\alpha_d$  for  $\text{Fe}^{+13}$  versus electron temperature  $T_e$ .  $\alpha_d(\text{S \& V.S})$  stands for the rate calculated with the use of the rate coefficient formula by Shull and Van Steenberg<sup>13)</sup>.  $\alpha_d(\text{B-M})$  is the rate derived from the formula by Post et al.<sup>3)</sup>.
- Fig. 2 a) The radial distributions of Fe  $k$  ( $k=X \sim \text{XVIII}$ ) with the use of the standard data<sup>3)</sup> in which the dielectronic recombination rate coefficients are given in the form of Burgess. (case A)  
b) The same results using the data in which only the dielectronic recombination rate coefficients are replaced by the ones given by Shull and Van Steenberg<sup>13)</sup>. (case B)
- Fig. 3 The comparison of the FeXVI distributions for cases A and B shown in Fig. 2 (a) and the same result for FeXVII (b).
- Fig. 4 The full width at half maximum of the radial distributions for FeXV versus anomalous diffusion constant  $D_A$  ( $V_A = 0$ ).  $\odot$  stands for case A and  $\triangle$  for case B as defined in Fig. 2.
- Fig. 5 The radial spacing between the peaks of the distributions for FeIX and FeXIV versus anomalous convection velocity constant  $V_A$  ( $D_A = 0$ ).  $\odot$  corresponds to case A and  $\triangle$  to case B.

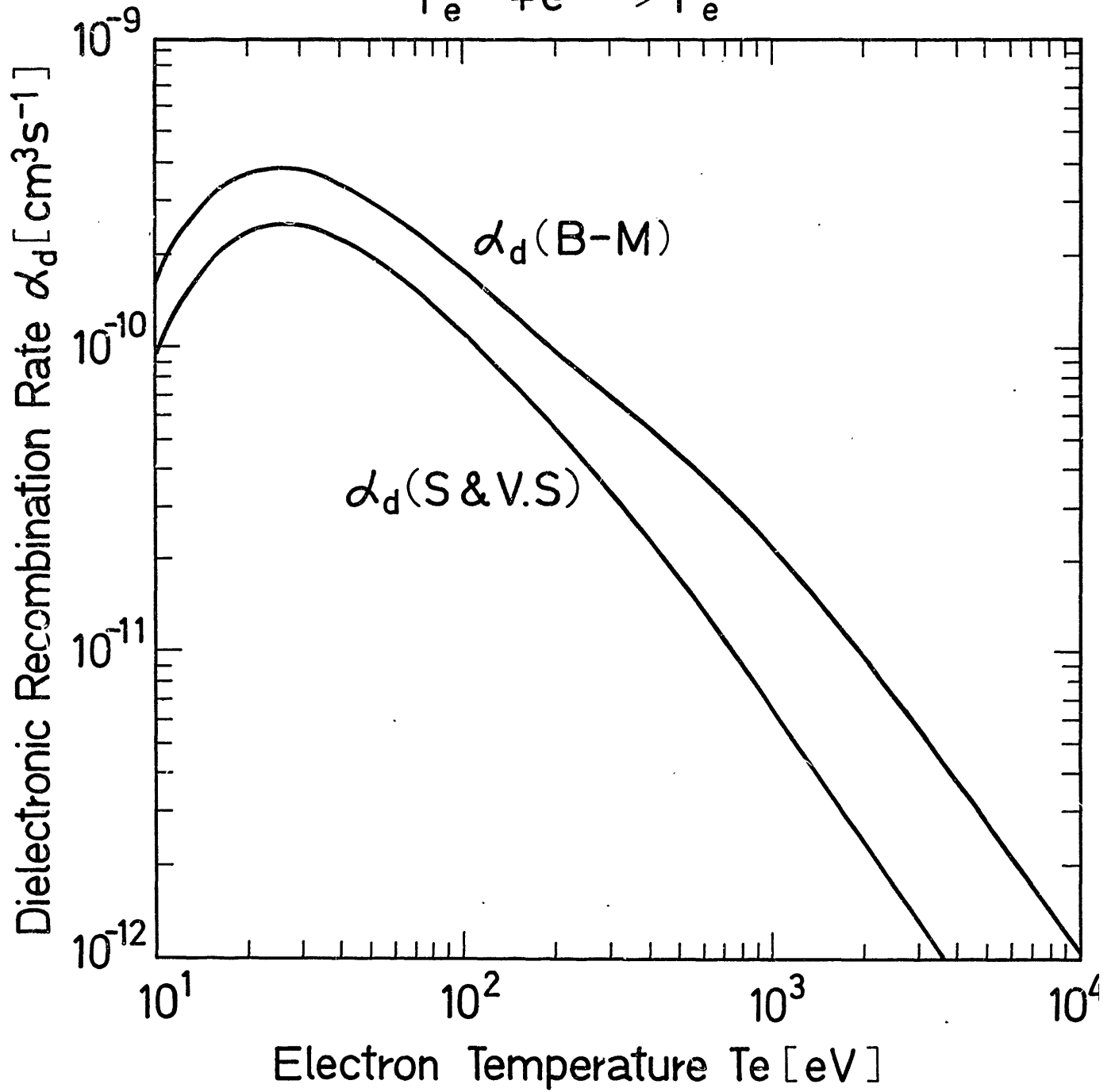
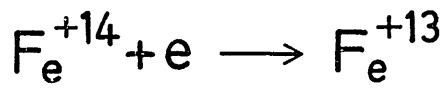
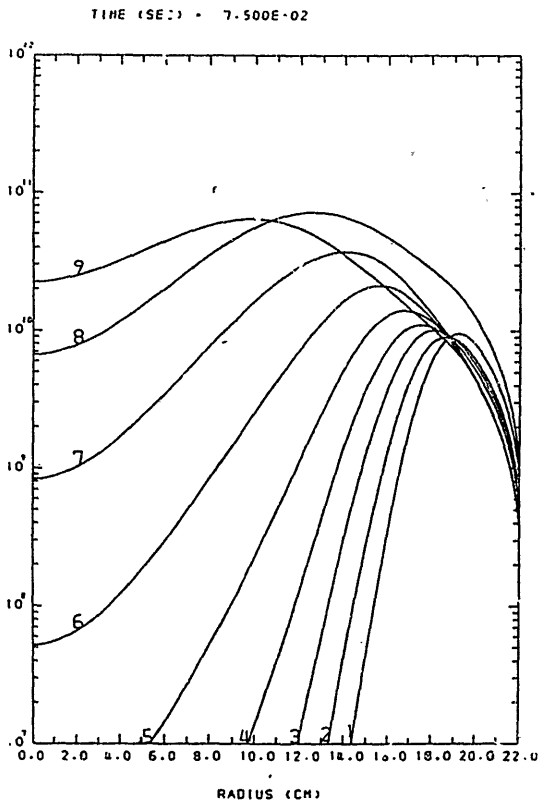
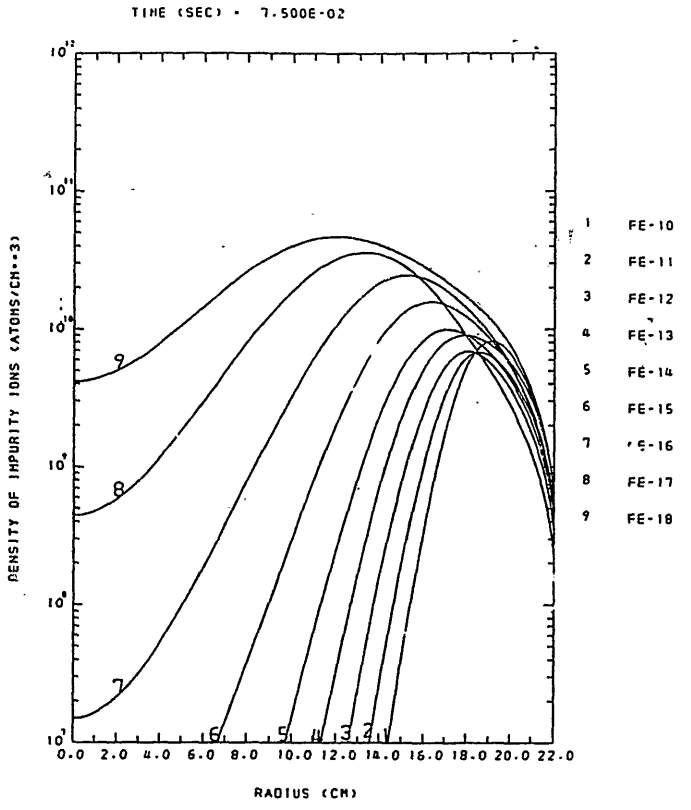


Fig.1

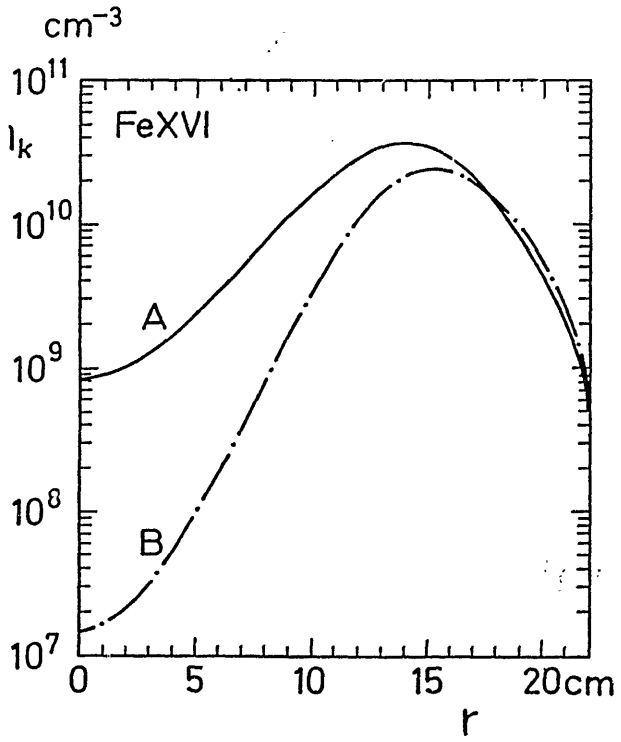


(a)

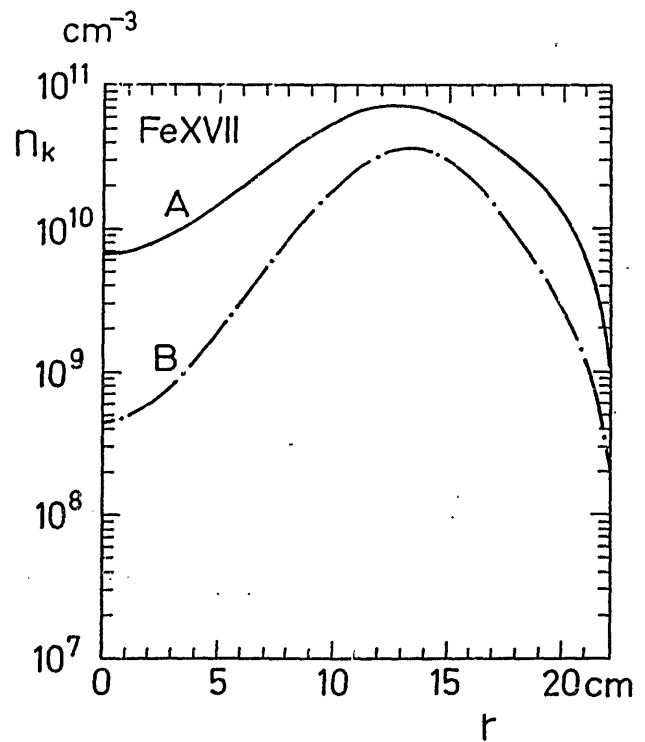


(b)

Fig.2



(a)



(b)

Fig.3

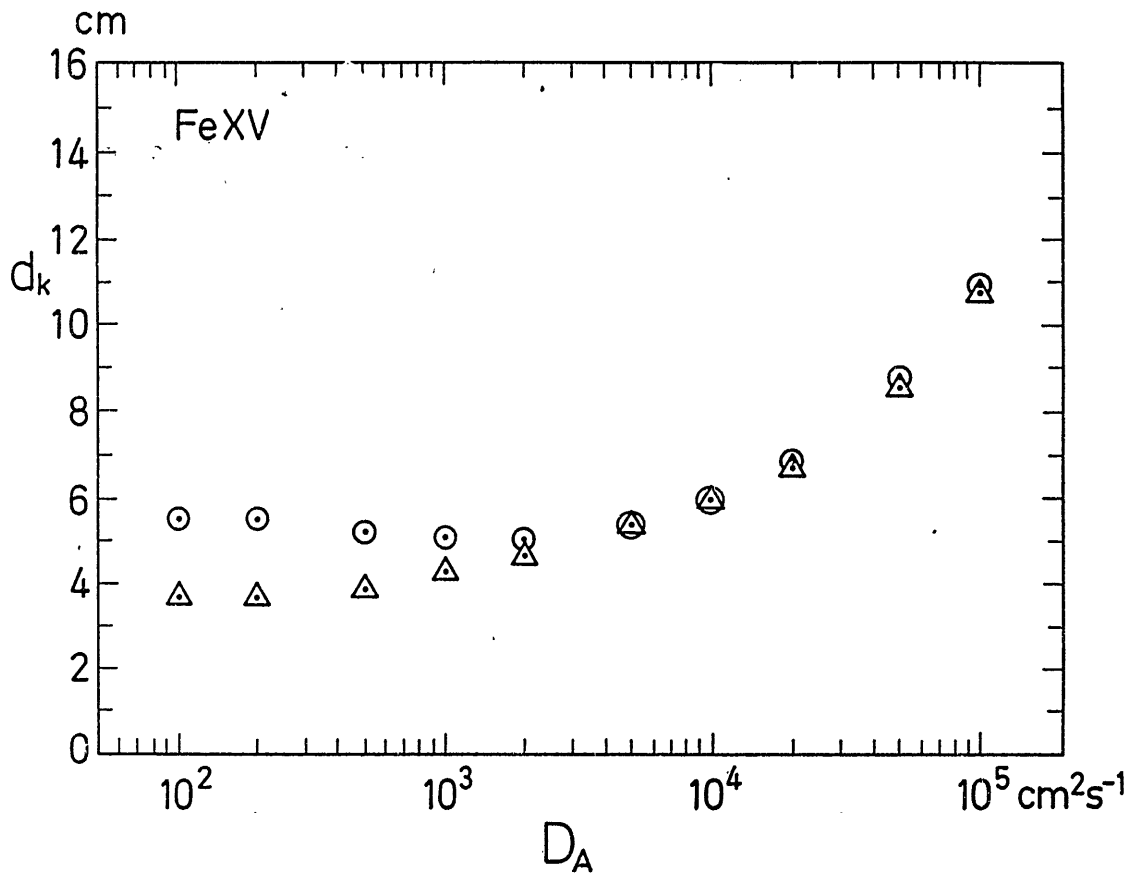


Fig. 4

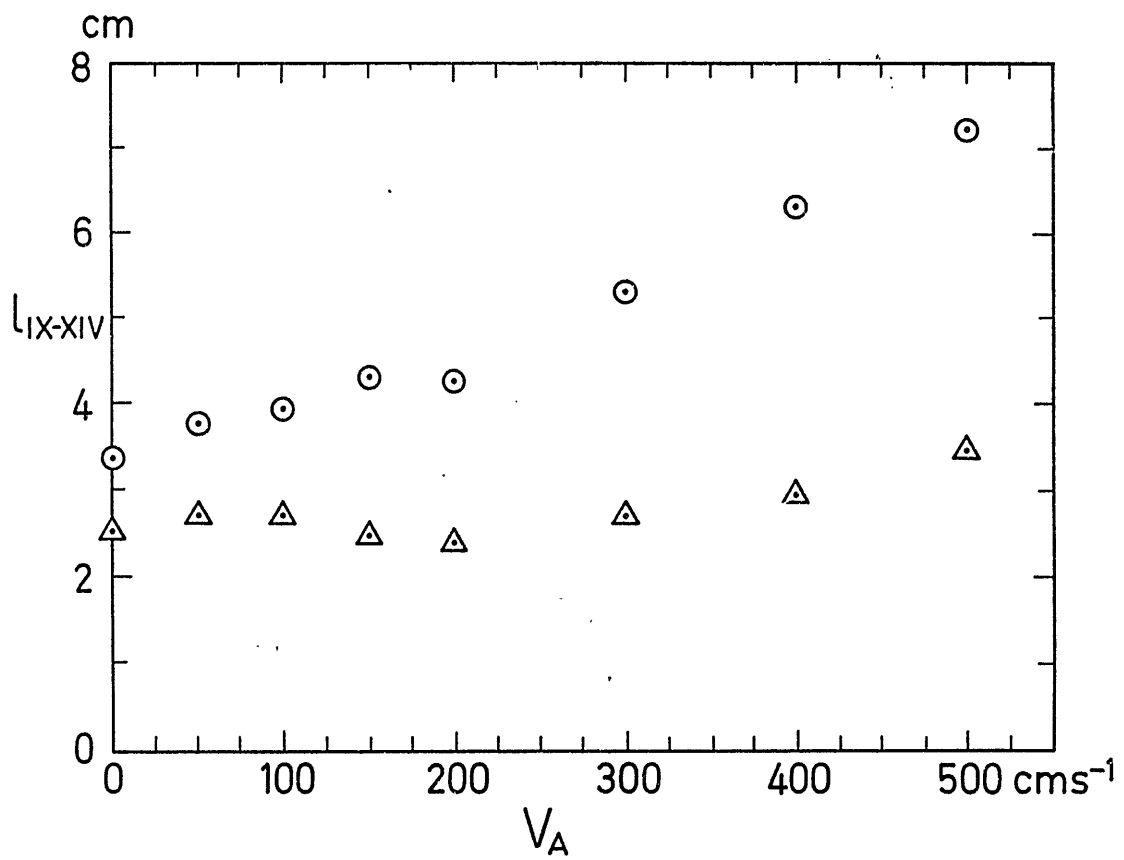


Fig. 5

PROGRAM

Joint Workshop of U.S.- Japan Fusion Collaboration Program  
" Resonance effects in electron - ion collisions :  
A new contribution of A & M processes to fusion "

September 1-2, 1986  
Institute of Plasma Physics, Nagoya University  
Nagoya 464

September 1

- 9:30 - 10:00 Registration  
10:00 - 12:00 Introduction  
A. Miyahara (IPP)  
J.R. Martinez (DOE)  
G.H. Dunn (JILA, Co-chairperson)  
H. Tawara (IPP, Co-chairperson)
- session  
chairman  
T.Oda
- Y. Sugie (JAERI) (30 min.)  
Diagnostics of JT - 60 and impurity measurements  
s. Morita (IPP) (15 min.)  
X-ray spectroscopy of highly ionized atoms  
M. Nakai (ILE, Osaka Univ.) (30 min.)  
Spectroscopic measurement of non-local transport in  
laser produced plasma
- 12:00 - 13:00 lunch
- 13:00 - 15:00 R. Phaneuf (ORNL) (30 min.)  
Indirect mechanisms in electron impact ionization of  
multiply charged ions  
H. Suzuki (Sophia Univ.) (30 min.)  
Recent activities of electron - ion collision experiments  
in IPP/Nagoya and Sophia University  
Y. Itikawa (ISAS) (30 min.)  
Distorted -wave-method calculation of innershell excitation
- 15:00 - 15:30 coffee break
- 15:30 - 17:30 R. Henry (Louisiana State Univ.) (30 min.)  
Resonance effects in electron-ion excitations  
T.Kagawa S. Nakazaki (Miyazaki Univ.) (15 min.)  
Cross sections for electron excitation of  $O^{3+}$   
T. Fujimoto (Kyoto Univ.) (30 min.)  
Decrease and disappearance of the resonance contribution  
to the excitation cross section of ions in plasma  
Y. Hahn (Univ. Connecticut) (15 min.)  
Resonance effects in electron capture and ionization

September 2

- 9:00 - 10:30 Y. Kim (NBS) (30 min.)  
R. Henry Relativistic effects in electron-ion excitation  
T. Kagawa (Nara Women's Univ.) (30 min.)  
Energy levels and transition probabilities of multiply  
charged ions
- 10:30 - 11:00 coffee break
- 11:00 - 12:30 G. Dunn (JILA) (30 min.)  
T. Fujimoto Tuneable resonances : dielectronic recombination  
K. Sakimoto (ISAS) (30 min.)  
Effects of electric fields on dielectronic recombination
- 12:30 - 13:30 lunch
- 13:30 - 15:00 H. Griem (Univ. Maryland) (30 min.)  
R. Phaneuf Collisional rate coefficients for highly charged ions  
from transient plasmas  
T. Kawamura (IPP) (30 min.)  
Evaluation and assessment of atomic data and surface  
interaction data for boundary plasma modelling
- 15:00 - 17:00 Discussion on future U.S.- Japan collaboration  
H. Tawara

Please note that 5-10 min. discussion time is reserved after each talk.

LIST OF PARTICIPANTS

US - JAPAN WORKSHOP  
RESONANCE EFFECTS IN ELECTRON - ION COLLISIONS -- A NEW CONTRIBUTION  
OF A AND M PROCESSES TO FUSION  
IPP, Nagoya University, JAPAN  
September 1-2, 1986

US PARTICIPANTS

Gordon H. Dunn  
JILA, Campus Box 440  
University of Colorado  
Boulder, Colorado 80309-0440

H. R. Griem  
Dept. of Physics and Astronomy  
University of Maryland  
College Park, Maryland 20742

Yukap Hahn  
Dept. of Physics  
University of Connecticut  
Storrs, CT 06268

R. J. W. Henry  
College of Basic Sciences  
Room 338 Chopin Hall  
Louisiana State University

Yong-Ki Kim  
Physics A261  
National Bureau of Standards  
Gaithersburg, Maryland 20899

J. V. Martinez  
Fundamental Interactions Branch  
Division of Chemical Sciences  
Office of Basic Energy Sciences  
U.S. Department of Energy  
Washington, D.C. 20545

Ronald Phaneuf  
Physics Division  
Bldg. 6603  
PO Box X  
Oak Ridge National Laboratory  
Oak Ridge, TN 37830

JAPANESE PARTICIPANTS

A. Danjo  
Dept. of Physics  
Niigata University  
Niigata 950-21

T. Fujimoto  
Dept. of Applied Physics  
Kyoto University  
Kyoto 606

J. Fujita  
IPP, Nagoya University  
Nagoya 464

T. Hirayama  
Sophia University  
Chiyoda-ku, Tokyo 102

A. Howald  
IPP Nagoya University  
Nagoya 464

K. Ida  
IPP, Nagoya University  
Nagoya 464

Y. Itikawa  
Institute of Space and Aeronautical  
Komaba, Tokyo 153

T. Kagawa  
Dept. of Physics  
Nara Women's University  
Nara 630

T. Kato  
IPP, Nagoya University  
Nagoya 464

T. Kawamura  
IPP, Nagoya University  
Nagoya 464

K. Kawatsura  
Japan Atomic Energy Research Institute  
Tokai-mura, Ibaraki 319-11

A. Miyahara  
IPP, Nagoya University  
Nagoya 464

S. Morita  
IPP, Nagoya University  
Nagoya 464

M. Nakai  
Institute of Laser Engineering  
Osaka University  
Suita, Osaka 565

S. Nakazaki  
Dept. of Applied Physics  
Miyazaki University  
Miyazaki 880

H. Narumi  
Kure Women's College  
Kure, Hiroshima 737

T. Oda  
Hiroshima University  
Higashi-Hiroshima  
Hiroshima 724

T. Ohgo  
Fukuoka Univ. Education  
Manakata, Fukuoka 811-01

S. Ohtani  
IPP, Nagoya University  
Nagoya 464

T. Ono  
Department of Physics  
Nagoya University  
Nagoya 464

M. Otsuka  
IPP, Nagoya University  
Nagoya 464

K. Sakimoto  
Institute of Space and Aeronautical  
Science  
Komaba, Tokyo 153

K. Sato  
IPP, Nagoya University  
Nagoya 464

T. Sugie  
Critical Plasma Diagnostics Dept.  
Japan Atomic Energy Research Institute  
Naka-machi  
Ibaraki 311-02

H. Suzuki  
Dept. of Physics  
Sophia University  
Chiyoda-ku, Tokyo 102

H. Tawara  
IPP, Nagoya University  
Nagoya 464

K. Wakiya  
Dept. of Physics  
Sophia University  
Chiyoda-ku, Tokyo 102

I. Yamada  
IPP, Nagoya University  
Nagoya 464

M. Yoshino  
Shibaura Inst. Tech.  
Ohmiya, Saitama 330

## LIST OF IPPJ-AM REPORTS

- IPPJ-AM-1\* "Cross Sections for Charge Transfer of Hydrogen Beams in Gases and Vapors in the Energy Range 10 eV–10 keV"  
H. Tawara (1977) [Published in Atomic Data and Nuclear Data Tables 22, 491 (1978)]
- IPPJ-AM-2\* "Ionization and Excitation of Ions by Electron Impact –Review of Empirical Formulae–"  
T. Kato (1977)
- IPPJ-AM-3 "Grotrian Diagrams of Highly Ionized Iron FeVIII-FeXXVI"  
K. Mori, M. Otsuka and T. Kato (1977) [Published in Atomic Data and Nuclear Data Tables 23, 196 (1979)]
- IPPJ-AM-4 "Atomic Processes in Hot Plasmas and X-Ray Emission"  
T. Kato (1978)
- IPPJ-AM-5\* "Charge Transfer between a Proton and a Heavy Metal Atom"  
S. Hiraide, Y. Kigoshi and M. Matsuzawa (1978)
- IPPJ-AM-6\* "Free-Free Transition in a Plasma –Review of Cross Sections and Spectra–"  
T. Kato and H. Narumi (1978)
- IPPJ-AM-7\* "Bibliography on Electron Collisions with Atomic Positive Ions: 1940 Through 1977"  
K. Takayanagi and T. Iwai (1978)
- IPPJ-AM-8 "Semi-Empirical Cross Sections and Rate Coefficients for Excitation and Ionization by Electron Collision and Photoionization of Helium"  
T. Fujimoto (1978)
- IPPJ-AM-9 "Charge Changing Cross Sections for Heavy-Particle Collisions in the Energy Range from 0.1 eV to 10 MeV I. Incidence of He, Li, Be, B and Their Ions"  
Kazuhiko Okuno (1978)
- IPPJ-AM-10 "Charge Changing Cross Sections for Heavy-Particle Collisions in the Energy Range from 0.1 eV to 10 MeV II. Incidence of C, N, O and Their Ions"  
Kazuhiko Okuno (1978)
- IPPJ-AM-11 "Charge Changing Cross Sections for Heavy-Particle Collisions in the Energy Range from 0.1 eV to 10 MeV III. Incidence of F, Ne, Na and Their Ions"  
Kazuhiko Okuno (1978)
- IPPJ-AM-12\* "Electron Impact Excitation of Positive Ions Calculated in the Coulomb-Born Approximation –A Data List and Comparative Survey–"  
S. Nakazaki and T. Hashino (1979)
- IPPJ-AM-13 "Atomic Processes in Fusion Plasmas – Proceedings of the Nagoya Seminar on Atomic Processes in Fusion Plasmas Sept. 5-7, 1979"  
Ed. by Y. Itikawa and T. Kato (1979)
- IPPJ-AM-14 "Energy Dependence of Sputtering Yields of Monatomic Solids"  
N. Matsunami, Y. Yamamura, Y. Itikawa, N. Itoh, Y. Kazumata, S. Miyagawa, K. Morita and R. Shimizu (1980)

- IPPJ-AM-15 "Cross Sections for Charge Transfer Collisions Involving Hydrogen Atoms"  
Y. Kaneko, T. Arikawa, Y. Itikawa, T. Iwai, T. Kato, M. Matsuzawa, Y. Nakai,  
K. Okubo, H. Ryufuku, H. Tawara and T. Watanabe (1980)
- IPPJ-AM-16 "Two-Centre Coulomb Phaseshifts and Radial Functions"  
H. Nakamura and H. Takagi (1980)
- IPPJ-AM-17 "Empirical Formulas for Ionization Cross Section of Atomic Ions for Elec-  
tron Collisions –Critical Review with Compilation of Experimental Data–"  
Y. Itikawa and T. Kato (1981)
- IPPJ-AM-18 "Data on the Backscattering Coefficients of Light Ions from Solids"  
T. Tabata, R. Ito, Y. Itikawa, N. Itoh and K. Morita (1981) [Published in  
Atomic Data and Nuclear Data Tables 28, 493 (1983)]
- IPPJ-AM-19 "Recommended Values of Transport Cross Sections for Elastic Collision and  
Total Collision Cross Section for Electrons in Atomic and Molecular Gases"  
M. Hayashi (1981)
- IPPJ-AM-20 "Electron Capture and Loss Cross Sections for Collisions between Heavy  
Ions and Hydrogen Molecules"  
Y. Kaneko, Y. Itikawa, T. Iwai, T. Kato, Y. Nakai, K. Okuno and H. Tawara  
(1981)
- IPPJ-AM-21 "Surface Data for Fusion Devices – Proceedings of the U.S.–Japan Work-  
shop on Surface Data Review Dec. 14-18, 1981"  
Ed. by N. Itoh and E.W. Thomas (1982)
- IPPJ-AM-22 "Desorption and Related Phenomena Relevant to Fusion Devices"  
Ed. by A. Koma (1982)
- IPPJ-AM-23 "Dielectronic Recombination of Hydrogenic Ions"  
T. Fujimoto, T. Kato and Y. Nakamura (1982)
- IPPJ-AM-24 "Bibliography on Electron Collisions with Atomic Positive Ions: 1978  
Through 1982 (Supplement to IPPJ-AM-7)"  
Y. Itikawa (1982) [Published in Atomic Data and Nuclear Data Tables 31,  
215 (1984)]
- IPPJ-AM-25 "Bibliography on Ionization and Charge Transfer Processes in Ion-Ion  
Collision"  
H. Tawara (1983)
- IPPJ-AM-26 "Angular Dependence of Sputtering Yields of Monatomic Solids"  
Y. Yamamura, Y. Itikawa and N. Itoh (1983)
- IPPJ-AM-27 "Recommended Data on Excitation of Carbon and Oxygen Ions by Electron  
Collisions"  
Y. Itikawa, S. Hara, T. Kato, S. Nakazaki, M.S. Pindzola and D.H. Crandall  
(1983) [Published in Atomic Data and Nuclear Data Tables 33, 149 (1985)]
- IPPJ-AM-28 "Electron Capture and Loss Cross Sections for Collisions Between Heavy  
Ions and Hydrogen Molecules (Up-dated version of IPPJ-AM-20)  
H. Tawara, T. Kato and Y. Nakai (1983) [Published in Atomic Data and  
Nuclear Data Tables 32, 235 (1985)]

- IPPJ-AM-29 "Bibliography on Atomic Processes in Hot Dense Plasmas"  
T. Kato, J. Hama, T. Kagawa, S. Karashima, N. Miyanaga, H. Tawara,  
N. Yamaguchi, K. Yamamoto and K. Yonei (1983)
- IPPJ-AM-30 "Cross Sections for Charge Transfers of Highly Ionized Ions in Hydrogen  
Atoms (Up-dated version of IPPJ-AM-15)"  
H. Tawara, T. Kato and Y. Nakai (1983) [Published in Atomic Data and  
Nuclear Data Tables 32, 235 (1985)]
- IPPJ-AM-31 "Atomic Processes in Hot Dense Plasmas"  
T. Kagawa, T. Kato, T. Watanabe and S. Karashima (1983)
- IPPJ-AM-32 "Energy Dependence of the Yields of Ion-Induced Sputtering of Monatomic  
Solids"  
N. Matsunami, Y. Yamamura, Y. Itikawa, N. Itoh, Y. Kazumata, S. Miyagawa,  
K. Morita, R. Shimizu and H. Tawara (1983) [Published in Atomic Data and  
Nuclear Data Tables 31, 1 (1984)]
- IPPJ-AM-33 "Proceedings on Symposium on Atomic Collision Data for Diagnostics and  
Modelling of Fusion Plasmas, Aug. 29 – 30, 1983"  
Ed. by H. Tawara (1983)
- IPPJ-AM-34 "Dependence of the Backscattering Coefficients of Light Ions upon Angle of  
Incidence"  
T. Tabata, R. Ito, Y. Itikawa, N. Itoh, K. Morita and H. Tawara (1984)
- IPPJ-AM-35 "Proceedings of Workshop on Synergistic Effects in Surface Phenomena  
Related to Plasma-Wall Interactions, May 21 – 23, 1984"  
Ed. by N. Itoh, K. Kamada and H. Tawara (1984) [Published in Radiation  
Effects 89, 1 (1985)]
- IPPJ-AM-36 "Equilibrium Charge State Distributions of Ions ( $Z_1 \geq 4$ ) after Passage  
through Foils – Compilation of Data after 1972"  
K. Shima, T. Mikumo and H. Tawara (1985) [Published in Atomic Data and  
Nuclear Data Tables 34, 357 (1986)]
- IPPJ-AM-37 "Ionization Cross Sections of Atoms and Ions by Electron Impact"  
H. Tawara, T. Kato and M. Ohnishi (1985)
- IPPJ-AM-38 "Rate Coefficients for the Electron-Impact Excitations of C-like Ions"  
Y. Itikawa (1985)
- IPPJ-AM-39 "Proceedings of the Japan-U.S. Workshop on Impurity and Particle Control,  
Theory and Modeling, Mar. 12 – 16, 1984"  
Ed. by T. Kawamura (1985)
- IPPJ-AM-40 "Low-Energy Sputterings with the Monte Carlo Program ACAT"  
Y. Yamamura and Y. Mizuno (1985)
- IPPJ-AM-41 "Data on the Backscattering Coefficients of Light Ions from Solids (a  
Revision)"  
R. Ito, T. Tabata, N. Itoh, K. Morita, T. Kato and H. Tawara (1985)

- IPPJ-AM-42 "Stopping Power Theories for Charged Particles in Inertial Confinement Fusion Plasmas (Emphasis on Hot and Dense Matters)"  
S. Karashima, T. Watanabe, T. Kato and H. Tawara (1985)
- IPPJ-AM-43 "The Collected Papers of Nice Project/IPP, Nagoya"  
Ed. by H. Tawara (1985)
- IPPJ-AM-44 "Tokamak Plasma Modelling and Atomic Processes"  
Ed. by T. Kawamura (1986)
- IPPJ-AM-45 Bibliography of Electron Transfer in Ion-Atom Collisions  
H. Tawara, N. Shimakura, N. Toshima and T. Watanabe (1986)
- IPPJ-AM-46 "Atomic Data Involving Hydrogens Relevant to Edge Plasmas"  
H. Tawara, Y. Itikawa, Y. Itoh, T. Kato, H. Nishimura, S. Ohtani, H. Takagi, K. Takayanagi and M. Yoshino (1986)
- IPPJ-AM-47 "Resonance Effects in Electron-Ion Collisions"  
Ed. by H. Tawara and G. H. Dunn (1986)

---

Available upon request to Research Information Center, Institute of Plasma Physics, Nagoya University, Nagoya 464, Japan, except for the reports noted with\*.